

The effect of alkali hydroxides and equilibration time on Al uptake by calcium silicate hydrates (C-S-H)

Présentée le 16 juillet 2021

Faculté de l'environnement naturel, architectural et construit
Groupe Ludwig
Programme doctoral en génie civil et environnement

pour l'obtention du grade de Docteur ès Sciences

par

Sonya BARZGAR

Acceptée sur proposition du jury

Prof. A. J. Wüest, président du jury
Prof. C. Ludwig, Prof. B. Lothenbach, directeurs de thèse
Prof. J. Skibsted, rapporteur
Dr C. Cau Dit Coumes, rapporteuse
Dr D. Kulik, rapporteur

Acknowledgements

I would also like to express my deepest appreciation to my thesis director, Prof. Christian Ludwig, for his continuous support, wealth of knowledge, constant encouragement and amicable attitude. I highly benefited from his inspiring supervision during my PhD. His generosity in offering time for scientific discussions and professional advisory has been key in achieving the outcomes of this thesis.

I would like to thank my co-advisor, Prof. Barbara Lothenbach, for her support throughout my PhD studies. Her established knowledge about cement and particularly the thermodynamics has always lighted the way for me. Her follow up on the workflow of my thesis has fruited towards fulfilling the milestones of this thesis.

A particular acknowledgement goes to Dr. Mohamed Tarik for providing a solid knowhow on ICP-MS and ICP-OES measurements, and for exchanging scientific ideas on various occasions.

I am also very thankful to Prof. Karen Scrivener for organizing knowledge-sharing events and for the valuable discussions during these 4 years.

I am extremely grateful to Prof. Alfred Johny Wüest, Prof. Jørgen Skibsted, Dr. Céline Cau-Dit-Coumes and Dr. Dmitrii Kulik for acting as my examination committee. A special thanks goes to Dr. Kulik for great scientific discussions about cement thermodynamics.

Special thanks goes to my colleagues at Empa and PSI and particularly to technicians: Luigi Brunetti, Boris Ingold, Beatrice Fischer and Albert Schuler for their help in the lab.

Last but not least, my warmest appreciation goes to my husband, Ata, for his love, encouragement and support. I would like to thank my parents and my sister for unconditional love and support at every stage of my life. This thesis is dedicated to my family who have always been there for me.

Sonya Barzgar

Zürich, 14 May 2021

Abstract

Cement production accounts for approximately 8% of man-made CO₂ emissions. Lowering these CO₂ emissions is currently one of the most important and urgent research topics within the cement community. To reduce these emissions, the Portland cement (PC) is partially replaced by supplementary cementitious materials (SCM) such as blast furnace slag, fly ash or silica fumes. Reaction of these SCM with PC during hydration leads to the formation of additional calcium silicate hydrates (C-S-H), which is the single most important phase in cements based on silica-rich SCM. The high Al₂O₃ and SiO₂ content of the SCM results in C-S-H compositions with more Si and Al than in PC, which affects the stability and durability of such cements. Therefore, it is crucial to determine the role of Al on C-S-H properties to predict the formed hydrate phase assemblages and their effect on durability.

Al sorption isotherms including very low Al concentrations have been determined for C-S-H with Ca/Si ratios from 0.6 to 1.4. The solubility, structure and composition of calcium silicate hydrates incorporating aluminum “C-A-S-H” as a function of different parameters such as Ca/Si ratio, equilibration time, Al and alkali contents were investigated. Elemental measurements were performed with ICP-MS and ICP-OES. The presence of secondary phases was investigated by using TGA and XRD and the structure of C-A-S-H was investigated by FTIR.

High alkali hydroxide concentrations led to an increased Al(OH)₄⁻ formation in solution, which reduced the Al uptake in C-S-H. Increasing the pH values and/or decreasing the Ca/Si in C-S-H increased not only the Al concentrations but also in parallel the Si concentrations in solution. This comparable behavior of Al and Si towards changes in pH, pointed towards the uptake of Al within the silica chain both at low and high Ca/Si ratios. A higher Al uptake in C-S-H was observed at higher Ca/Si ratios, which indicated a stabilizing effect of Ca in the interlayer on Al uptake.

The effect of equilibration time on Al uptake in C-S-H was investigated using equilibration times from 7 days up to 3 years. Lower Al concentrations were measured in the solution after longer equilibration times. In addition, a decrease in the content of secondary phases was observed by TGA indicating a higher uptake of Al in C-S-H. Little further decrease in Al concentrations was observed after 2 years and longer at low Ca/Si ratios. At high Ca/Si ratios no significant change in solution concentrations was observed after more than 3 months, while the destabilization of secondary phases continued up to 1 year, indicating that a (meta)stable equilibrium was reached faster at higher Ca/Si ratios.

In addition to the C-A-S-H phase, the formation of secondary phases such as strätlingite, katoite and Al(OH)₃ was observed at Al/Si ≥ 0.03, which limited the Al uptake in C-S-H. More secondary phases were observed at higher Al concentrations and/or lower pH values. At low Al/Si ratios, a more significant decrease of Al concentrations with time was observed indicating a slower equilibration than at higher Al concentrations.

The Al sorption isotherms showed a linear trend between the Al in solution and Al in C-A-S-H from Al/Si of 0.001 up to 0.2. The linear trend pointed towards an Al uptake on one or several types of sorption sites, with a high sorption capacity, which would be consistent with an Al uptake in the bridging position of the silica chains suggested based on NMR studies.

Keywords

Cement, supplementary cementitious materials, C-A-S-H, alkali hydroxide, Ca/Si ratio, equilibration time, Al concentration.

Résumé

La production de ciment représente environ 8% des émissions de CO₂ d'origine humaine. La réduction de ces émissions est actuellement l'un des sujets de recherche les plus importants et urgents dans la communauté du ciment. Pour réduire ces émissions, le ciment Portland (PC) est partiellement remplacé par des matériaux cimentaires supplémentaires (SCM) tels que le laitier de haut fourneau, les cendres volantes ou les fumées de silice. La réaction de SCM avec PC pendant l'hydratation conduit à une formation supplémentaire de silicate de calcium hydraté (C-S-H), qui est la phase la plus importante dans les ciments à base de SCM riches en silice. La teneur élevée en Al₂O₃ et en SiO₂ des SCM donne des compositions en C-S-H avec plus de Si et Al qu'en PC, ce qui affecte la stabilité et la durabilité de ces ciments. Par conséquent, il est crucial de déterminer le rôle d'aluminium sur les propriétés de C-S-H pour prédire les assemblages de phase hydratée formés et leurs effets sur la durabilité.

Des isothermes de sorption d'Al, contenant très faibles concentrations d'Al, ont été déterminés pour C-S-H avec des rapports Ca/Si de 0,6 à 1,4. La solubilité, la structure et la composition de silicate de calcium hydraté incorporant de l'aluminium "C-A-S-H" en fonction de différents paramètres tels que le rapport Ca/Si, le temps d'équilibrage, l'Al et les teneurs en alcali ont été étudiés. L'analyse élémentaire (de Al, Ca, Na et Si) a été effectuée avec ICP-MS et ICP-OES. La présence de phases secondaires a été mesurée en utilisant TGA et XRD et la structure de C-A-S-H par FTIR.

Des concentrations élevées d'hydroxyde alcalin ont entraîné une augmentation de la formation d'Al(OH)₄⁻ en solution, ce qui a réduit l'absorption d'aluminium dans le C-S-H. L'augmentation des valeurs de pH et/ou la diminution de Ca/Si dans le C-S-H ont causé une augmentation non seulement de concentrations d'aluminium, mais aussi de concentrations de Si dans la solution. Ce comportement comparable d'aluminium et du silicium à l'égard des changements de pH a mené à l'absorption d'aluminium dans la chaîne de silice à des rapports Ca/Si faibles et élevés. On a observé une absorption d'aluminium plus élevée chez C-S-H à des rapports Ca/Si plus élevés, ce qui indique un effet stabilisateur de Ca dans l'interlayer sur l'absorption d'aluminium.

L'effet du temps d'équilibrage sur l'absorption d'aluminium dans le C-S-H a été étudié en utilisant des temps d'équilibrage allant de 7 jours à 3 ans. Des concentrations d'aluminium plus faibles ont été mesurées dans la solution après des temps d'équilibrage plus longs. De plus, une diminution de la teneur en phases secondaires a été observée par TGA, ce qui indique une plus grande absorption d'aluminium dans le C-S-H. Une faible diminution des concentrations d'aluminium a été observée après deux ans et plus à de faibles ratios Ca/Si. À des rapports Ca/Si élevés, aucun changement significatif des concentrations en solution n'a été observé après plus de trois mois, tandis que la déstabilisation des phases secondaires s'est poursuivie jusqu'à un an, ce qui indique qu'un équilibre (méta)stable a été atteint plus rapidement à des rapports Ca/Si plus élevés.

En plus de la phase C-A-S-H, la formation de phases secondaires telles que strätlingite, katoite et $\text{Al}(\text{OH})_3$ a été observée à $\text{Al}/\text{Si} \geq 0.03$, ce qui a limité l'absorption d'aluminium dans C-S-H. D'autres phases secondaires ont été observées à des concentrations d'aluminium plus élevées et/ou à des pH plus faibles. À de faibles rapports Al/Si , on a observé une diminution plus importante des concentrations d'aluminium avec le temps, ce qui indique un équilibre plus lent qu'à des concentrations d'aluminium plus élevées.

Les isothermes de sorption d'aluminium ont montré une tendance linéaire entre Al en solution et Al en C-A-S-H d'un rapport Al/Si de 0.001 jusqu'à 0.2. La tendance linéaire indiquait une absorption d'aluminium, principalement, sur un ou plusieurs types de sites de sorption, avec une capacité de sorption élevée, ce qui serait cohérent avec une absorption d'aluminium dans la position de pontage des chaînes de silice suggérée sur la base d'études NMR.

Mots-clés

Ciment, matériaux cimentaires supplémentaires, C-A-S-H, hydroxyde alcalin, rapport Ca/Si , temps d'équilibrage, concentration en Al.

Contents

Acknowledgements.....	i
Abstract	ii
Résumé.....	iv
List of Figures	ix
List of Tables	xii
List of Equations.....	xiii
List of Appendices	xiii
List of Abbreviations	xiv
Chapter 1 Introduction	1
1.1 CO ₂ emissions from cement production.....	1
1.2 Cement hydration	2
1.2.1 Portland cement	2
1.2.2 Blended cement.....	2
1.3 Calcium silicate hydrate (C-S-H).....	3
1.4 Aluminum uptake in C-S-H (C-A-S-H)	3
1.4.1 ²⁷ Al MAS NMR	4
1.4.2 Molecular modeling.....	5
1.4.3 Thermodynamic modeling.....	5
1.4.4 C-A-S-H with different Ca/Si ratio and alkali concentration	6
1.4.5 C-A-S-H with different equilibration times	6
1.4.6 C-A-S-H with different Al concentrations	7
1.5 Objectives of the thesis.....	7
1.6 Thesis outline	8
1.7 Journal Papers.....	9

Chapter 2	Materials and methods	10
2.1	Synthesis	10
2.1.1	Long-term experiment	10
2.1.2	Short-term experiment	11
2.2	Drying	11
2.3	Analysis	11
2.3.1	ICP-MS and ICP-OES	11
2.3.2	pH measurement	11
2.3.3	Zeta potential measurement	12
2.3.4	TGA	12
2.3.5	XRD	12
2.3.6	FTIR	12
2.3.7	Thermodynamic modeling	12
2.3.8	Al uptake in C-S-H	13
Chapter 3	The effect of alkali hydroxides on C-A-S-H	15
3.1	The effect of pH on Al sorption isotherm	15
3.2	The Al speciation at different pH values	18
3.3	Zeta potential at different pH values	19
3.4	The effect of pH on aqueous phase composition	20
3.5	The effect of pH on solid phase composition	23
3.6	Conclusions	24
Chapter 4	The effect of Ca/Si ratio on C-A-S-H	25
4.1	The effect of Ca/Si ratio on Al sorption isotherm	25
4.2	The effect of Ca/Si ratio on solid phase composition	27
4.3	Conclusions	29
Chapter 5	The effect of equilibration time on C-A-S-H	31
5.1	The effect of time on secondary phases' composition	31
5.2	The effect of time on C-A-S-H structure	35
5.3	The effect of time on Al uptake in C-S-H	40
5.4	The effect of NaOH, Ca/Si ratio and time on Al sorption isotherm	42
5.5	The effect of time on aqueous phase composition	45
5.6	The effect of time on C-A-S-H solubility	47
5.7	Conclusions	48

Chapter 6	The effect of Al concentration on C-A-S-H	50
6.1	C-A-S-H without NaOH	50
6.1.1	The effect of Al concentration on secondary phases	50
6.1.2	The effect of Al concentration on C-A-S-H structure	54
6.2	C-A-S-H with 1 M NaOH	55
6.2.1	The effect of Al concentration on secondary phases	55
6.2.2	The effect of Al concentration on C-A-S-H structure	57
6.3	C-A-S-H with different NaOH concentrations	58
6.3.1	The effect of NaOH concentration on Al sorption isotherm	58
6.3.2	The effect of NaOH concentration on secondary phases	60
6.3.3	The effect of NaOH concentration on C-A-S-H structure	62
6.4	Conclusions	62
Chapter 7	Concluding remarks	64
7.1	Achieved results	64
7.2	Future development	67
Appendices		68
References		105
Curriculum Vitae		113

List of Figures

Figure 1. Predicted evolution of Portland cement production with time [5].	1
Figure 2. A ternary $\text{CaO-SiO}_2\text{-Al}_2\text{O}_3$ diagram of cement hydrates; Reproduced from [25].	3
Figure 3. Schematic structure of C-A-S-H. Dark grey circle: calcium ion; light grey circle: ions in the interlayer (water or alkali) and red triangle: Al in the bridging position; Adapted from [34].	4
Figure 4. ^{27}Al MAS NMR spectra of C-A-S-H. Spectra are composed of five distinct resonance contributions labeled δ_{Al1} and δ_{Al2} (two IV-coordinated aluminum), δ_{Al3} (one V-coordinated aluminum), δ_{Al4} and δ_{Al5} (two VI-coordinated aluminum); Reproduced from [39].	5
Figure 5. The CSHQ solid solution model versus the literature C-S-H solubility data [32,48–52] (scattered points), shown as function of Ca/Si in the solid in linear scale (A) and \log_{10} scale (B); Reproduced from [47].	6
Figure 6. The effect of pH value on Al uptake in C-S-H after 3 months equilibration for Ca/Si ratios of a) 0.6; b) 0.8; c) 1.0; d) 1.2 and e) 1.4 in the absence of NaOH and in the presence of 0.1, 0.5 and 1 M NaOH. (The lines serve as eye-guides only and the errors are smaller than the symbols' size).	18
Figure 7. The effect of pH value on the calculated Al speciation in equilibrium with microcrystalline $\text{Al}(\text{OH})_3$.	19
Figure 8. Zeta potential measurements for C-S-H samples in the absence of alkali hydroxide (circles; [27]), the effect of 0 to 0.15 M KOH (squares; [37]), and in the presence of 0.1 M NaOH (triangles; this study).	20
Figure 9. The effect of pH value on aqueous phase composition after 3 months equilibration for Ca/Si ratios of a) 0.6; b) 0.8; c) 1.0; d) 1.2 and e) 1.4. (The points represent the experimental data and the lines are the calculated values using the CSHQ solid solution model [47]). (The errors are smaller than the symbols' size).	23
Figure 10. The TGA results for Al/Si ratio of 0.03 and Ca/Si ratio of 0.8 with different NaOH concentrations.	24
Figure 11. The effect of target Ca/Si ratio on Al uptake in C-S-H after 3 months equilibration for samples a) without NaOH (The data at Ca/Si = 0.6 were below the detection limit); b) 0.1 M NaOH; c) 0.5 M NaOH and d) 1 M NaOH. (The lines serve as eye-guides only and the errors are smaller than the symbols' size).	27
Figure 12. The TGA results for samples with different target Ca/Si ratios at a) Al/Si ratio of 0.1 without NaOH and b) Al/Si ratio of 0.03 with 1 M NaOH.	29

Figure 13. The XRD pattern for samples at Al/Si ratio of 0.03 with 1 M NaOH and different target Ca/Si ratios.....	29
Figure 14. TGA of C-A-S-H after different equilibration times for Ca/Si = 0.8 and 1 M NaOH. (*: signals assigned to an unidentified calcium sodium aluminate silicate hydrate (C-N-A-S-H) phase [34]).....	32
Figure 15. The effect of equilibration time on the composition of secondary phases in the absence of NaOH for a) Ca/Si = 0.8 & Al/Si = 0.1; b) Ca/Si = 0.8 & Al/Si = 0.2 and c) Ca/Si = 1.4 & Al/Si = 0.1.	34
Figure 16. The XRD pattern of C-A-S-H as a function of equilibration time in the absence of NaOH for Ca/Si = 0.8 and Al/Si = 0.1 (C: C-A-S-H, K: katoite, A: Al(OH) ₃ , S: strätlingite).	35
Figure 17. The FTIR spectra for C-A-S-H samples without alkali at Ca/Si = 0.8 for 2 years equilibration and different Al/Si ratios; a) transmittance (T) vs. wavelength (W) and b) 2 nd derivative of the transmittance d ² T/dW ² vs. wavelength.	37
Figure 18. The FTIR spectra for C-A-S-H samples without alkali at Ca/Si = 0.8 and Al/Si = 0.2 after different equilibration times: a) transmittance (T) vs. wavelength (W) and b) 2 nd derivative of the transmittance d ² T/dW ² vs. wavelength.	38
Figure 19. The FTIR spectra for C-A-S-H samples in the presence of 1 M NaOH for Al/Si = 0.03 and different equilibration times: a) transmittance (T) vs. wavelength (W) for Ca/Si = 0.8; b) 2 nd derivative of the transmittance d ² T/dW ² vs. wavelength for Ca/Si = 0.8; c) transmittance (T) vs. wavelength (W) for Ca/Si = 1.2 and d) 2 nd derivative of the transmittance d ² T/dW ² vs. wavelength for Ca/Si = 1.2.	40
Figure 20. The effect of equilibration time on the Al concentrations in solution for Ca/Si ratios of 0.8 and 1.2 in the presence of 1 M NaOH. (The errors are smaller than the symbols' size).	41
Figure 21. The Al sorption isotherm on C-A-S-H for Ca/Si = 0.8 recorded after different equilibration times for a) 0.1 M NaOH; b) 0.5 M NaOH and c) 1 M NaOH. The darkness of colors indicates an increase in equilibration time; 3 months indicated by the lightest and 3 years represented by the darkest symbols. (The lines serve as eye-guides only and the errors are smaller than the symbols' size).	42
Figure 22. The effect of equilibration time on Al uptake in C-S-H for Ca/Si ratios of a) 0.6; b) 0.8; c) 1.0; d) 1.2 and e) 1.4 at 0, 0.1, 0.5 and 1 M NaOH. The 3 months samples are indicated by the empty and 1 year represented by the full symbols. (The lines serve as eye-guides only and the errors are smaller than the symbols' size).....	45
Figure 23. The effect of pH value and equilibration time on measured Ca (a,c) and Si (b,d) concentrations (symbols) and on the calculated solubility of C-S-H (using the CSHQ model [47]), portlandite and amorphous SiO ₂ for Ca/Si ratios of a,b) 0.8 and c,d) 1.2 at 0, 0.1, 0.5 and 1 M NaOH. (*: outlier Ca concentrations for Ca/Si = 0.8 after 1 year equilibration). (The errors are smaller than the symbols' size).....	47

Figure 24. The effect of equilibration time on C-A-S-H solubility product with Al/Si = 0.03 and 1 M NaOH. The Ca concentrations are below the detection limit for Ca/Si = 0.8 after 14, 28 and 56 days of equilibration. (*: higher value due to the outlier Ca concentration for Ca/Si = 0.8 after 1 year equilibration).....	48
Figure 25. The effect of a) Al content at 3 months equilibration and b) equilibration time on secondary phases' content in the absence of NaOH for Ca/Si = 0.8.....	51
Figure 26. The Al fraction in solution, C-A-S-H and secondary phases vs measured Al concentration for target Ca/Si = 0.8 in the absence of NaOH after 3 months (empty symbols) and 12 months (filled symbols) equilibration. (The lines serve as eye-guides only).	54
Figure 27. The FTIR spectra for C-A-S-H samples in the absence of NaOH at target Ca/Si = 0.8 for a) 12 months equilibration with different Al/Si ratios and b) different equilibration times with target Al/Si ratios of 0.03 and 0.2.	55
Figure 28. The effect of a) Al content at 3 months equilibration and b) equilibration time on secondary phases' content in the presence of 1 M NaOH for target Ca/Si = 0.8. (The samples at target Al/Si = 0.2 were analyzed after 15 months instead of 12 months).	56
Figure 29. The Al fraction in solution, C-A-S-H and secondary phases vs measured Al concentration for target Ca/Si = 0.8 in the presence of 1 M NaOH after 3 months (empty symbols) and 15 months (filled symbols) equilibration. (The lines serve as eye-guides only and the errors are smaller than the symbols' size).	57
Figure 30. The FTIR spectra for C-A-S-H samples in the presence of 1 M NaOH at target Ca/Si = 0.8 for a) 15 months equilibration with different Al/Si ratios and b) different equilibration times with target Al/Si ratios of 0.03 and 0.2.	58
Figure 31. The Al sorption isotherm on C-A-S-H for target Ca/Si = 0.8 recorded after different equilibration times. The 3 months samples are indicated by empty and 1 year represented by full symbols. The samples at target Al/Si \geq 0.05 were analyzed after 15 months instead of 1 year. The lines indicate the slope of the increase; slopes \leq 1 indicate sorption; slopes $>$ 1 indicate precipitation of an additional solid. (The errors are smaller than the symbols' size).	59
Figure 32. The pH dependence of Al sorption on C-A-S-H for target Ca/Si = 0.8. (The errors are smaller than the symbols' size).	60
Figure 33. The effect of NaOH concentration on secondary phases' content for target Ca/Si = 0.8 with target Al/Si ratios of 0.03 and 0.2 after 3 months equilibration. The darkness of colors indicates an increase in NaOH concentration; 0 M NaOH is indicated by the dashed lines with light colors and 1 M NaOH represented by the solid lines with dark colors. (The lines serve as eye-guides only).	61
Figure 34. The Al fraction in C-A-S-H for target Ca/Si = 0.8 in the absence of NaOH and presence of 0.1, 0.5 and 1 M NaOH after 1 year equilibration. Samples at target	

Al/Si ≥ 0.05 were analyzed after 15 months instead of 1 year. (The errors are smaller than the symbols' size).	61
Figure 35. The FTIR spectra for C-A-S-H samples in the absence of NaOH and presence of 1 M NaOH for target Ca/Si = 0.8 with target Al/Si ratios of 0.03 and 0.2 after 3 months equilibration. The samples without NaOH are represented by dashed lines with light colors and those with 1 M NaOH are shown by solid lines with dark colors.	62
Figure 36. A schematic image representing the changes in the structure of C-A-S-H with NaOH addition. Grey circle: calcium ion; blue circle: sodium ion and red triangle: Al in the bridging position.	65
Figure 37. The effect of synthesis method (sorption: empty symbols vs co-precipitation: filled symbols) after different equilibration times for a) Ca/Si = 0.8 and b) Ca/Si = 1.2. (The Ca concentrations in sorption method are below the detection limit for Ca/Si = 0.8).	66
Figure 38. The quantified effect of Si on m/z 27.	100
Figure 39. The effect of pH value and equilibration time on measured Ca (a,c,e) and Si (b,d,f) concentrations (symbols) and on the calculated solubility of C-S-H (using the CSHQ model [47]), portlandite and amorphous SiO ₂ for Ca/Si ratios of a,b) 0.6; c,d) 1.0 and e,f) 14.	103
Figure 40. The Al fraction in C-A-S-H for target Ca/Si = 0.8 in the absence of NaOH and presence of 0.1, 0.5 and 1 M NaOH after 3 months equilibration.	104

List of Tables

Table 1. The Ca/Si, Al/Si molar ratios and NaOH concentrations used to prepare C-A-S-H at 20 °C for long-term experiments. (*: samples at Ca/Si ratio of 0.8 were analyzed also at Al/Si = 0.2 and after 24 and 36 months).	10
Table 2. The Ca/Si, Al/Si molar ratios and NaOH concentrations used to prepare C-A-S-H at 20 °C for short-term experiments.	11
Table 3. Assignment of FTIR spectra for C-A-S-H samples.	36
Table 4. The fraction of Al in solution, C-A-S-H and different secondary phases at different NaOH concentrations and equilibration times for target Ca/Si = 0.8.	52
Table 5. Mixing proportions used for preparing the C-A-S-H samples (in g per 171 mL solution) at 20 °C in long-term experiments. (Remark: for Ca/Si = 0.8 samples, 4 g of solid was suspended in 180 mL solution).	68
Table 6. Mixing proportions used for preparing the C-A-S-H samples (in g per 171 mL solution) at 20 °C in short-term experiments.	69

Table 7. The solid phase composition after different equilibration times at 20 °C. The Ca/Si and Al/Si ratios were calculated from massbalance.	69
Table 8. Aqueous concentrations after different equilibration times at 20 °C.	76
Table 9. The calculated saturation indexes (SI) values for strätlingite, microcrystalline Al(OH) ₃ , katoite, CSHQ, amorphous silica, portlandite, Ca-gismondine, chabazite and OH-sodalite.	84
Table 10. The calculated molar Al/Si and Ca/Si ratios in C-A-S-H and the corresponding errors.	91
Table 11. The calculated K _d values and the corresponding errors.	98
Table 12. Optimized parameters used for the ICP-MS and ICP-OES analysis.	100

List of Equations

Eq.1	12
Eq.2	13
Eq.3	13
Eq.4	13
Eq.5	13
Eq.6	14

List of Appendices

Appendix A. Mixing proportions used for preparing the C-A-S-H samples.	68
Appendix B. The solid phase composition of C-A-S-H.	69
Appendix C. Elemental concentrations in aqueous solution.	76
Appendix D. Saturation Indexes for different solid phases.	84
Appendix E. The error calculations for solid phase composition.	91
Appendix F. Further details about ICP-MS and ICP-OES measurements discussed in chapter 2.	100
Appendix G. The effect of equilibration time on Ca and Si concentrations for Ca/Si ratios of 0.6, 1.0 and 1.4 discussed in section 5.5 of chapter 5.	101

Appendix H. The Al fraction in C-A-S-H for Ca/Si = 0.8 after 3 months equilibration discussed in section 6.3.2 of chapter 6.	104
--	-----

List of Abbreviations

DFT	Density Functional Theory
DNP	Dynamic Nuclear Polarization
FTIR	Fourier Transform Infrared Spectroscopy
IAP	Ion Activity Product
IC	Ion Chromatography
ICP-OES	Inductively Coupled Plasma Optical Emission Spectrometry
ICP-MS	Inductively Coupled Plasma Mass Spectrometry
K_d	Distribution Coefficient
K_{so}	Solubility product
NMR	Nuclear Magnetic Resonance
SI	Saturation Index
TGA	Thermogravimetric Analysis
TMS	Trimethylsilylation
XANES	X-Ray Adsorption Near Edge Spectroscopy
XRD	X-Ray Diffraction

Chemical Abbreviations

Al_2O_3	Aluminum Oxide
$Al(OH)_3$	Microcrystalline Aluminum Hydroxide
CaO	Calcium Oxide
$Ca(OH)_2$	Calcium Hydroxide
$CaCO_3$	Calcium Carbonate or Limestone

CO_2	Calcium Dioxide
$2\text{CaO}\cdot\text{Al}_2\text{O}_3\cdot\text{SiO}_2\cdot 8\text{H}_2\text{O}$	Strätlingite
$3\text{CaO}\cdot\text{Al}_2\text{O}_3\cdot 6\text{H}_2\text{O}$	Katoite
$\text{CaAl}_2\text{Si}_2\text{O}_8\cdot 4.5\text{H}_2\text{O}$	Ca-Gismondine
$\text{CaAl}_2\text{Si}_4\text{O}_{12}\cdot 6\text{H}_2\text{O}$	Chabazite
$\text{Ca}_8\text{Al}_6\text{Si}_6\text{O}_{24}(\text{OH})_2\cdot 2\text{H}_2\text{O}$	OH-Sodalite
CA	Calcium Aluminate
C_3A	Tricalcium Aluminate
C_3S	Tricalcium Silicate or Alite
C_2S	Dicalcium Silicate or Belite
C_4AF	Tetracalcium Aluminoferrite
CH	Portlandite
C-S-H	Calcium Silicate Hydrate
C-A-S-H	Calcium Aluminate Silicate Hydrate
C-N-A-S-H	Calcium Sodium Aluminate Silicate Hydrate
KOH	Potassium Hydroxide
NaAlO_2	Sodium Aluminate
NaOH	Sodium Hydroxide
SCM	Supplementary Cementitious Materials
SiO_2	Silica

Chapter 1 Introduction

1.1 CO₂ emissions from cement production

Concrete is one of the world's most affordable, reliable, durable and readily available construction materials and is the second most consumed material after water, however, the construction industry has suffered from an image of being environmentally unfriendly [1,2]. An environmentally sustainable concrete production is achieved by utilizing the inherently environmentally beneficial properties of concrete, e.g. the high compressive strength, good durability and the high thermal capacity. Concrete consists of cement as binder, sand and stones as the aggregates and water as a hydration medium [3]. Since concrete consists of a number of different constituents, the environmental impact of concrete is a complex mechanism governed by the impacts from each of these constituents. The cement production is associated with high energy consumption and carbon dioxide (CO₂) emissions. Thus, the sustainability of concrete as a material is strongly influenced by the cement industry [4]. The worldwide demand for cement production is increasing continuously and Portland cement (PC) clinker production recently exceeding 4 billion tons annually, as shown in Figure 1 [5]. The projections suggest that a 50% increase in annual production of cement should be expected by 2050. This massive scale of production results in ~8% of the global CO₂ emissions due to its high kiln temperature and decomposition of limestone (CaCO₃) in raw materials [1,2,6,7]. About 40% of CO₂ emissions of cement production come from the combustion of fuels while approximately 60% result from the calcination process, i.e. the transformation of limestone into calcium oxide (CaO) ($\text{CaCO}_3 \rightarrow \text{CaO} + \text{CO}_2$) [8]. Decomposition of limestone in the process of manufacturing PC clinker results in the production of approximately 0.5 tonne of CO₂ per tonne of clinker produced [8].

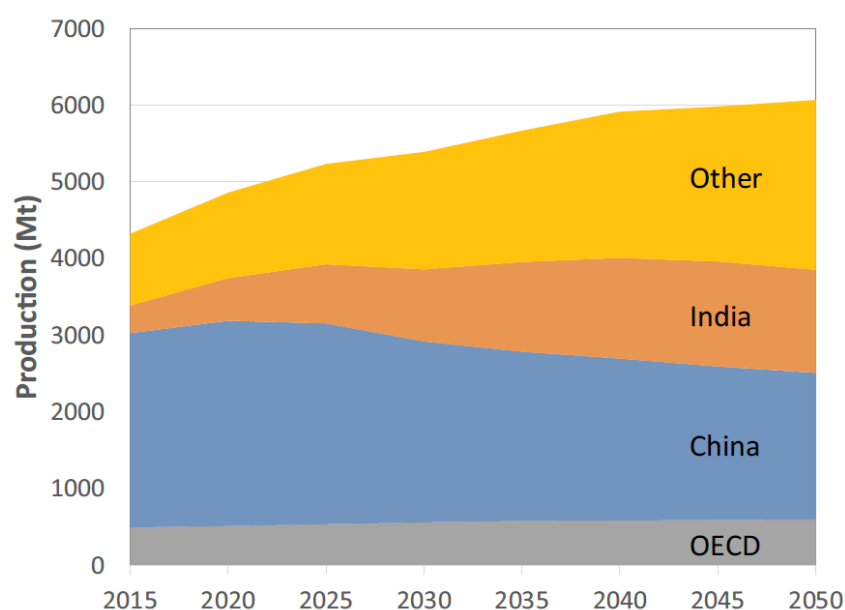


Figure 1. Predicted evolution of Portland cement production with time [5].

Improving the sustainability of cement production by reducing these CO₂ emissions is currently one of the most important and urgent research topics within the cement community [2,9]. Using 'carbon capture and storage (CCS)' technologies in cement production for reducing the CO₂ emissions is becoming attractive, although it is not cost-effective. A report from the World Business Council for Sustainable Development (WBCSD) introduced CCS as the main strategy to reduce 56% of the planned CO₂ emissions by 2050, but estimated that it would require between US\$ 321 to 592 billion investment to capture that fraction of CO₂ from the cement industry [10]. Another approach focuses on replacing Portland cement in the concrete composition using cements based on alkali activated binders, often called geopolymers. However, there are some doubts regarding their long-term durability [9]. Furthermore, the use of wastes as fuel can be also an opportunity to reduce CO₂ intensity with expanding the use of biomass and alternative less-carbon intensive fuels. It is expected that the worldwide use of alternative fuels grow from 3% in 2006 to about 37% in 2050 and leads to 15% of the targeted overall reduction in CO₂ emissions [5].

A very well-established strategy to reduce the content of clinker is partial replacement of Portland cement with supplementary cementitious materials (SCM) such as blast furnace slags, by-products from steel production, fly ash from coal combustion, or calcined clays [8,11,12]. The reaction of Portland cement with SCM, which have different chemical compositions leads to changes in the amount and composition of the hydrates [11]. This is relevant for the stability of construction materials as well as for oil well cement such as stabilized filter ashes [13,14].

1.2 Cement hydration

1.2.1 Portland cement

Portland cement is obtained by heating limestone and clay or other calcium carbonate and silicate mixtures at high temperatures (1500 °C) in a rotating kiln. In this process limestone breaks down to calcium oxide and carbon dioxide [4,8,15]. The heating at a high temperature transforms the minerals into hard nodules called clinker. The clinker is mixed with gypsum (calcium sulfate) and ground to a uniform final product [3] which consists of the following major compounds:

- Tricalcium silicate, Alite or C₃S (3CaO·SiO₂)
- Dicalcium silicate, Belite or C₂S (2CaO·SiO₂)
- Tricalcium aluminate, C₃A (3CaO·Al₂O₃)
- Tetracalcium aluminoferrite, C₄AF (4CaO·Al₂O₃·Fe₂O₃)

In the presence of water, the clinker phase dissolves in water and solid hydration products are formed. C₃S and C₂S react to the large prismatic crystals of calcium hydroxide (Ca(OH)₂) and very small needle-like crystals of calcium silicate hydrates (C-S-H). The reaction of C₃A and C₄AF leads in the presence of calcium sulfate to the formation of ettringite and/or monosulfate [3].

1.2.2 Blended cement

Blended cements are produced by substituting a part of clinker with SCM such as fly ash, calcined clay, slag, silica fume, volcanic ash and by-products from steel production, in various proportions, at the grinding stage of cement production [3,11,16]. The addition of SCM results in cement that is now widely considered superior to common cement and aids in expanded production capacity, reducing the amount of energy used and CO₂ emissions during the calcination process [8,15]. SCM have lower lime and higher silica (SiO₂) and aluminum oxide (Al₂O₃) contents than a regular Portland cement [11].

1.3 Calcium silicate hydrate (C-S-H)

Calcium silicate hydrate is the main hydration product of Portland cements which results from the silicate phase hydration and contributes significantly to the compressive strength and other mechanical properties of cement based materials [9,11,17]. The high Al_2O_3 and SiO_2 content of the SCM leads to C-S-H compositions with more silicon and aluminum than in Portland cements as shown in Figure 2. In the presence of SCM, C-S-H has different compositions with lower Ca/Si ratio and higher Al/Si ratio compared to the C-S-H in Portland cements. The Ca/Si molar ratio of the C-S-H present in Portland cement is in the range of 1.5-1.9 [18,19], however, in SCM blends it is in the range of 0.6-1.9 [20–22]. The high amount of silica in SCM, e.g. if using fly ashes or silica fumes, lowers the Ca/Si ratio of C-S-H and modifies the structure of C-S-H phases. These low Ca/Si C-S-H phases have different space filling properties and are able to take up more aluminum and alkalis, but less chloride and sulfates. All of these changes can be critical for the performance of concrete in terms of mechanical properties and durability [23,24].

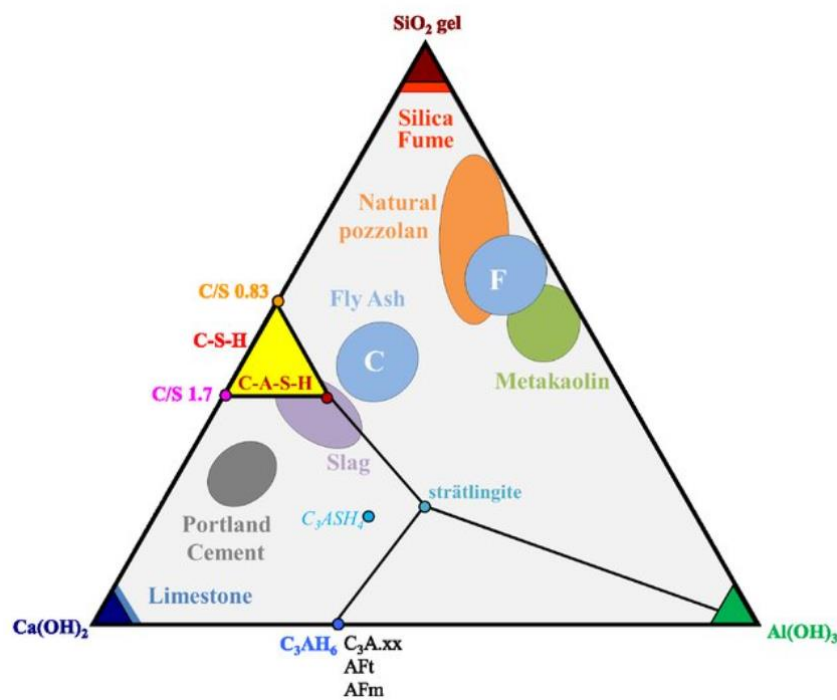


Figure 2. A ternary $\text{CaO-SiO}_2\text{-Al}_2\text{O}_3$ diagram of cement hydrates; Reproduced from [25].

1.4 Aluminum uptake in C-S-H (C-A-S-H)

If aluminum is dissolved in the solution, C-S-H is able to incorporate aluminum [26,27] resulting in what is generally named as calcium aluminate silicate hydrate (C-A-S-H). The C-A-S-H structure consists of calcium oxide polyhedra sheets flanked with “dreierketten” – tetrahedral (alumino) silicate chains – on both sides and water as well as counter-ions (e.g., Ca^{2+} and OH^-) in an interlayer between two such layers [26–29]. Two of these silica tetrahedra are linked to the calcium oxide layer and called pairing tetrahedra, while the third one, the bridging tetrahedron, links the two pairing tetrahedra [28–30]. The interlayer containing water, calcium, alkalis and other ions connects a number of sheets together. The incorporation of Al as tetrahedral AlO_4 occurs into the bridging sites of silica tetrahedral chains. The schematic structure of C-A-S-H is shown in Figure 3. The silica chain length varies with the Ca/Si ratio. At Ca/Si ratio of 0.66, the calcium ions are absent in the interlayer and the dimers in the silicate chains are connected together in long chains by bridging tetrahedra [7,30]. At Ca/Si ratios in range of 0.6-0.8, long silicate tetrahedral chains occur, in which repeating

units of one bridging site are connected to two paired silicate tetrahedral sites on either side [29–32]. At Ca/Si ratios above 1.0, a higher Ca content in the interlayer results in shorter silica tetrahedral chains and more vacancies in the bridging sites of the silica chains occur [29–31,33].

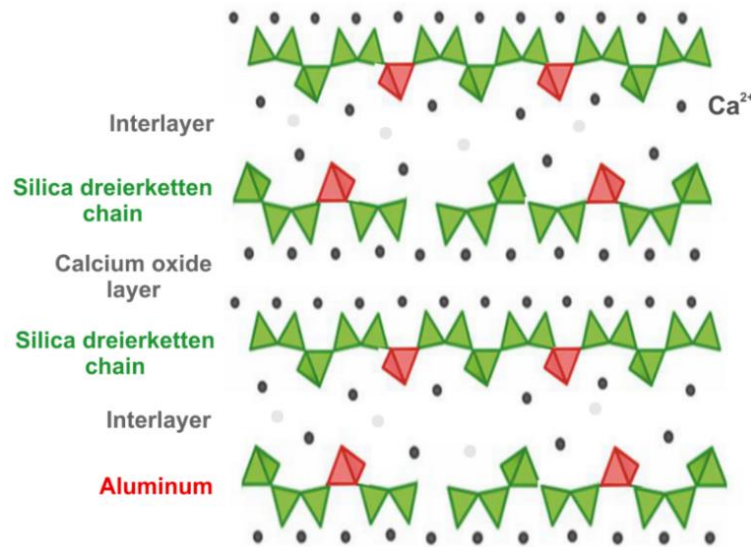


Figure 3. Schematic structure of C-A-S-H. Dark grey circle: calcium ion; light grey circle: ions in the interlayer (water or alkali) and red triangle: Al in the bridging position; Adapted from [34].

Our knowledge about the structure and aluminum uptake of low Ca/Si C-S-H and their impact on hydration is still insufficient. The solubility of C-S-H with different Ca/Si, Al/Si and alkali/Si ratios has been measured systematically in previous studies [23,27,35–38]. These experimental data comprised a unique dataset for the effect of aluminum on C-S-H solubility and were helpful to gain an overview of the relations between solid and aqueous phase composition. The comparison of different datasets, however, revealed also major differences in the aluminum uptake observed, depending on the reaction time and/or synthesis method used, as discussed in more details in [19]. The experimental investigation on uptake of aluminum by C-S-H showed a strong dependency of the Al uptake in C-S-H on the aqueous Al concentrations [19,27,34,37,38]. The data available, however, revealed also the dependency of aluminum uptake on the alkali concentration, Ca/Si ratios and reaction time [19,23,34,37,38]. In most available studies, the concentrations have been measured by Ion Chromatography (IC) with a relatively high limit of detection of 0.04 mmol/L Al, which is only slightly below the aluminum concentrations of 0.01 to 0.05 mmol/L, at which secondary phases such as microcrystalline aluminum hydroxide ($\text{Al}(\text{OH})_3$), strätlingite ($2\text{CaO} \cdot \text{Al}_2\text{O}_3 \cdot \text{SiO}_2 \cdot 8\text{H}_2\text{O}$) and katoite ($3\text{CaO} \cdot \text{Al}_2\text{O}_3 \cdot 6\text{H}_2\text{O}$) start to precipitate [23]. Thus, very limited information is available on the effect of aluminum concentrations on the different binding sites in C-S-H structure, and on how the different possible aluminum binding sites influence each other; the information which proved to be crucial for the development of chemical thermodynamic models.

1.4.1 ²⁷Al MAS NMR

Solid-state Nuclear Magnetic Resonance (NMR) spectroscopy is one of the most important techniques which provides information about the local silicate and aluminate structures and their nearest neighbors. Figure 4 illustrates the ²⁷Al MAS NMR spectra for C-A-S-H phases at different Ca/Si ratios [39] and indicates the substitution of aluminum mainly as fore-fold coordinated Al^{IV} within the silicate chains for C-S-H with low Ca/Si ratios [40], while five-fold Al^V and octahedrally coordinated Al^{VI} are also present at high Ca/Si ratios [38,39]. In fact, four-fold coordinated Al^{IV} is the dominant environment in low Ca/Si C-S-H, where Al substitutes Si in the bridging sites of the dreierketten chain. Al^{IV} has been reported to be in the bridging sites

either without charge balance or are charge balanced by interlayer Ca^{2+} , Na^+ , or H^+ [41]. At Ca/Si ratios above 1, a second Al^{IV} species is present, which has been assigned to aluminum in bridging position charge-balanced by calcium cations [33,38,39,41]. Increasing the Ca/Si ratio decreases the fraction of Al^{IV} , and Al^{VI} species become dominant [38,39]. Also, a lower fraction of hexa-coordinated Al^{VI} species has been observed, while their content do not change with increasing the Ca/Si ratio of C-S-H [38,39].

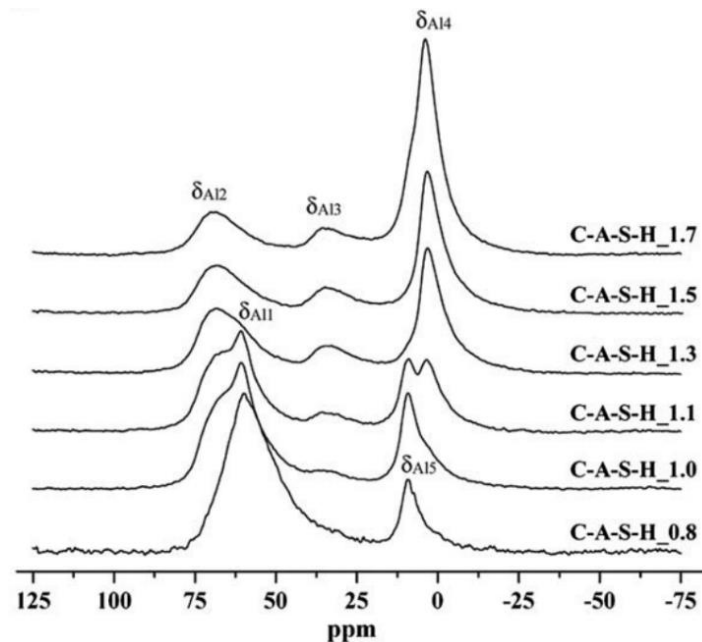


Figure 4. ^{27}Al MAS NMR spectra of C-A-S-H. Spectra are composed of five distinct resonance contributions labeled δ_{AlI} and δ_{AlII} (two IV-coordinated aluminum), δ_{AlIII} (one V-coordinated aluminum), δ_{AlIV} and δ_{AlV} (two VI-coordinated aluminum); Reproduced from [39].

1.4.2 Molecular modelling

Classical molecular dynamics simulations on aluminum binding in C-S-H indicated the possible substitutions of Al^{IV} in the silicate chain both in the bridging and pairing sites [42], while a strong preference of Al^{IV} uptake in the bridging position has been illustrated in [43,44]. A recent study was able to determine the atomic level structure of C-A-S-H at $\text{Ca/Si} \geq 1.0$ by combining the Density Functional Theory (DFT) computational methods with Dynamic Nuclear Polarization (DNP)-enhanced solid-state NMR experiments [45]. The investigation indicated the presence of four-, five-, and six-coordinated aluminates at bridging tetrahedral sites. At low Ca/Si ratios, tetrahedral Al^{IV} species are favored, however, at $\text{Ca/Si} \geq 1.2$, Al^{V} and octahedral Al^{VI} species predominate as they show a higher stability compared to Al^{IV} species [45].

1.4.3 Thermodynamic modelling

The C-S-H system has long been investigated and various thermodynamic models have been developed based on the solubility data using different C-S-H compositions, solid-solution between end-members with different Ca/Si ratios or the sorption of calcium and silica on C-S-H phases [19,46]. The CSHQ solid solution model [47] has been developed based on the experimental data for alkali-free C-S-H [32,48–52] as shown in Figure 5. Such models need to be extended to account for the uptake of aluminum, alkalis or other ions by adding them to the respective building units. Furthermore, the model should cover the changes at high pH values and the uptake of alkalis in C-S-H as discussed in [34].

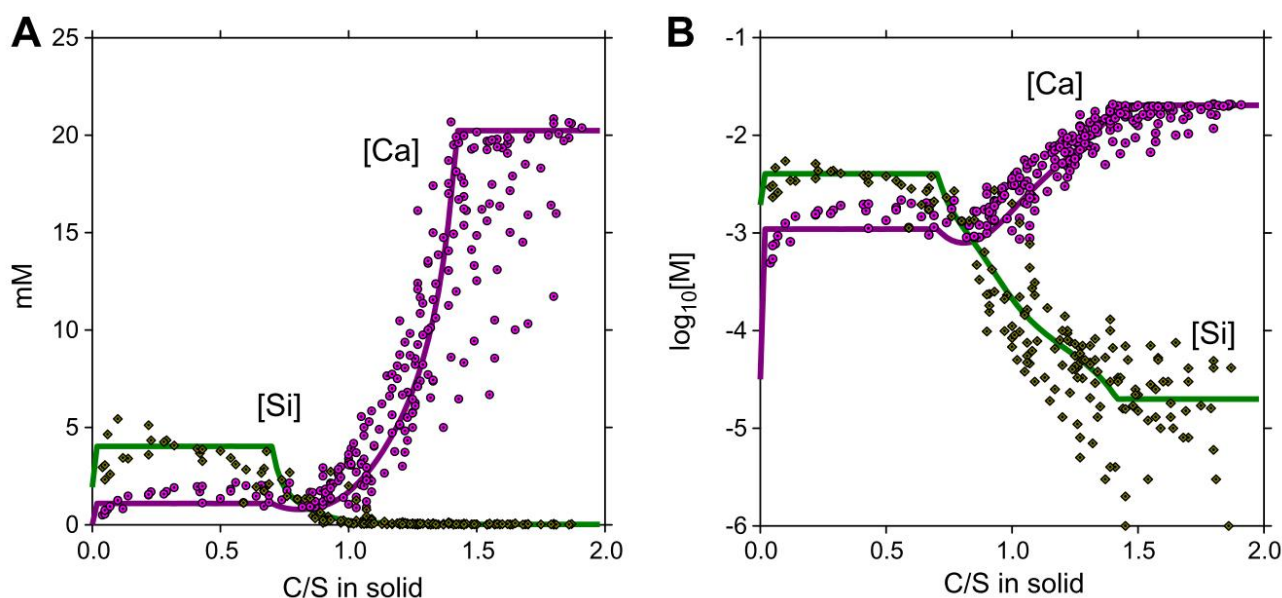


Figure 5. The CSHQ solid solution model versus the literature C-S-H solubility data [32,48–52] (scattered points), shown as function of Ca/Si in the solid in linear scale (A) and \log_{10} scale (B); Reproduced from [47].

1.4.4 C-A-S-H with different Ca/Si ratio and alkali concentration

The experimental investigations on the relations between the composition of the aqueous and solid phase indicated a clear relation between Al concentrations in the aqueous solution and Al uptake in C-S-H at Ca/Si > 1.0, both in short- and long-term experiments [23,27,38]. At low Ca/Si ratios and in short-term experiments, an increase of aluminum uptake in C-S-H has been observed with adding Al to the pre-synthesized C-S-H [27,38]. However, in long-term experiments in which calcium, silicon and aluminum have been added simultaneously [23], the aluminum concentrations in solution were very low, although the observed aluminum binding in C-S-H remained high. The high affinity of aluminum uptake at low Ca/Si and possibly an irreversibility of the binding is in agreement with ab-initio calculations which predicted the strong stabilization of the C-S-H structure by substituting silicon with aluminum in the bridging position [44].

The composition of C-S-H depends on the dissolved calcium, silicon and hydroxide concentrations in the aqueous solution. At low Ca/Si ratios, dreierketten chain length is longer and Al is mainly taken up as tetrahedral Al^{IV} in the bridging position [39,53]. However, at higher Ca/Si ratios Al is taken up as five-fold coordinated and octahedrally coordinated aluminum into the bridging position [45]. The solubility of C-S-H with different Ca/Si ratios and alkali concentrations has been measured systematically [23,34,36,37,54]. However, there is a lack of information on the effect of different alkali concentrations on C-A-S-H structure and its thermodynamic stability.

1.4.5 C-A-S-H with different equilibration times

The data available in the literature point towards a possible dependency of C-S-H solubility [32] and of aluminum uptake on the reaction time [19,23,34,37,38]. The solubility of C-S-H has been observed to depend also on the synthesis methods, indicating the possible existence of several metastable C-S-H phases after short equilibration times [32]. The incorporation of Al in C-S-H investigated after 1 day equilibration for C-A-S-H with a Ca/Si = 0.66 [55] and 5 days equilibration for C-A-S-H with Ca/Si ratios of 0.7 and 0.95 [38] showed a linear increase of Al uptake in C-S-H with the amount of Al present. No precipitation of secondary phases such as strätlingite, katoite and $Al(OH)_3$ was reported [19]. After equilibration times of 6 months and longer, in addition to C-A-S-H, also the precipitation of strätlingite, katoite and $Al(OH)_3$ has been observed,

which lowers the aluminum concentration in the aqueous solution and thus an increase of Al uptake in C-S-H [19,29,36]. Further analysis revealed that the content of katoite, which had precipitated in the first months in addition to C-A-S-H phases, decreased with equilibration time, indicating an increasing Al uptake in C-S-H with time [37] pointing towards a restructuring of C-A-S-H with decreasing aqueous Al concentrations.

1.4.6 C-A-S-H with different Al concentrations

A number of studies investigated the effect of varying Al/Si ratios on the structure of C-A-S-H gel [33,39,56]. The experimental investigations on the uptake of aluminum by C-S-H showed a strong dependency of the Al uptake in C-S-H on the aqueous Al concentrations [19,27,34,37,38,47]. Moreover, the precipitation of katoite and strätlingite at high concentrations of aluminum limits the Al concentration in solution and thus the Al uptake in C-S-H [37,55]. Faucon et al. [33] showed that the amount of aluminum present in the C-A-S-H is proportional to the aluminum concentration in the equilibrium solution. According to data available in literature, the quantity of aluminum incorporated in C-S-H increases with increasing the Al concentrations in solution [30,55]. Very little information is available on the relation between Al concentration in solution and Al uptake in C-S-H as well as the composition of C-A-S-H gels at different Al/Si ratios. Such information on both the aqueous and solid composition is needed to further develop thermodynamic models, used for calculating the speciation of C-A-S-H phases in hydrating cements.

1.5 Objectives of the thesis

The thesis aims at investigating the effect of aluminum uptake in the C-S-H structure in depth by combining the solubility measurements using Inductively Coupled Plasma Mass Spectrometry (ICP-MS) and Inductively Coupled Plasma Optical Emission Spectrometry (ICP-OES), capable of determining very low dissolved aluminum concentrations. This thesis was embedded in a large project, in which dedicated NMR spectroscopic investigations as well as an extended C-A-S-H thermodynamic solid solution model based on the NMR results are being conducted in parallel. This thesis focused mainly on sorption isotherm experiment to optimize the measurements of low aluminum concentrations (below 0.04 mmol/L) with ICP-MS and ICP-OES in the absence and presence of alkali hydroxides. Measurements of “sorption isotherms” in batch experiments at different Ca/Si ratios helped in quantifying the relations between Ca/Si ratios and occupancies of different Al sites. Furthermore, the sorption isotherm experiments at different equilibration times determined the dependency of Al uptake in C-S-H on different reaction times. These data are required for the further development of more structurally consistent thermodynamic models of C-A-S-H. In order to further develop the implementation of new cements with lower CO₂ emissions, an in-depth knowledge about the differences in short- and long-term thermodynamic stability, chemical evolution, and mechanical properties of C-A-S-H phases is needed.

Analysis of the available data and models representing the effects of aluminum on C-S-H revealed some important knowledge gaps, which hinder a more in-depth understanding of the effects of SCMs on cement composition, stability and durability:

- The difference in binding positions for aluminum in the structure of C-A-S-H and how their occupancy varies as a function of Ca/Si ratio, aluminum concentration, pH value and time.
- Effects of synthesis methods (co-precipitation versus addition of aluminum to pre-synthesized C-S-H) and effect of short- and long-term equilibration time on the amount of aluminum in C-S-H.
- Effect of aluminum concentration on the amount of Al taken up in C-S-H.

- Optimization of the measurement of very low Al concentrations (below 0.04 mmol/L) with ICP-MS and ICP-OES in the absence and presence of alkali hydroxides in order to be able to measure Al uptake over a large range of aluminum concentrations.

In this study, the effect of different aluminum concentrations, alkali hydroxide concentrations, Ca/Si ratios and equilibration times on the aluminum uptake in C-S-H was investigated. The experiments were performed by synthesizing the C-A-S-H samples containing different Al/Si ratios, Ca/Si ratios and alkali hydroxide contents. Short- and long-term sorption isotherms were recorded in order to perform a kinetic study at different ages of C-A-S-H samples. Samples were filtrated after different equilibration times from 7 days to 56 days in short-term experiments and from 3 months to 3 years in long-term experiments. The elemental concentrations of different ions such as Ca, Si, Al and Na in the solution were determined by ICP-MS and ICP-OES. The detection limit (DL) for Al in ICP-OES and ICP-MS was 4×10^{-5} mmol/L. The solid samples were analyzed with Thermogravimetric Analysis (TGA) and X-Ray Diffraction (XRD) to check for the presence of secondary phases in the solid phase. Fourier Transform Infrared Spectroscopy (FTIR) technique was used to investigate the structure of C-A-S-H phase. Moreover, the measured concentrations were compared with the calculated solubility of C-S-H using the Gibbs Free Energy Minimization program GEM-Selektor version 3.7 [47,57].

1.6 Thesis outline

This dissertation is composed of eight chapters which are organized as follows:

- Chapter 1: Introduction – This chapter provides a broad overview of Al uptake in C-S-H and the topics comprising the thesis.
- Chapter 2: Materials and methods – This chapter provides information regarding the synthesis of C-A-S-H, analytical techniques for solid and solution phases and thermodynamic modelling.
- Chapter 3: The effect of alkali hydroxides on C-A-S-H – This chapter presents the experimental results of C-A-S-H structure synthesized at different sodium hydroxide (NaOH) concentrations (published in the Journal of Colloid and Interface Science [58]).
- Chapter 4: The effect of Ca/Si ratio on C-A-S-H – This chapter presents our work on the investigation of Al uptake in C-S-H at a broad range of Ca/Si ratios (published in the Journal of Colloid and Interface Science [58]).
- Chapter 5: The effect of equilibration time on C-A-S-H – This chapter provides our improved kinetic study of C-A-S-H after short- and long-term equilibration times (published in the Cement and Concrete Research [59]).
- Chapter 6: The effect of Al concentration on C-A-S-H – This chapter presents the investigation of solid and solution phases at different Al/Si ratios from low to high Al contents (journal paper in progress).
- Chapter 7: Concluding remarks – This chapter summarizes the thesis outcome and sketches the outlook for future research.
- Appendices – The appendices include the supplementary information for chapters 2, 3, 4, 5 and 6.

1.7 Journal Papers

- S. Barzgar, M. Tarik, B. Lothenbach and C. Ludwig, "The effect of sodium hydroxide on Al uptake by calcium silicate hydrates (C-S-H)", *J. Colloid Interface Sci.*, (2020) 572, 246–256.

Doctoral candidate's contribution: Investigation, Writing – Original Draft, Measurement, Modelling, Formal analysis, Methodology.

- S. Barzgar, M. Tarik, C. Ludwig and B. Lothenbach, "The effect of equilibration time on Al uptake in C-S-H", *Cem. Concr. Res.*, (2021) 144, 106438.

Doctoral candidate's contribution: Methodology, Writing – Original Draft, Modelling, Visualization, Formal analysis, Investigation, Measurement,.

- S. Barzgar, Y. Yan, M. Tarik, C. Ludwig and B. Lothenbach, "The effect of Al concentration on Al uptake in C-S-H", to be further adapted and complemented for submission.

Doctoral candidate's contribution: Methodology, Formal analysis, Investigation, Measurement, Modelling, Writing – Original Draft, Visualization.

Chapter 2 Materials and methods

2.1 Synthesis

All samples were synthesized in a nitrogen filled glovebox to minimize carbonation and were stored in 200 mL PE-HD containers placed on a horizontal shaker moving at 100 rpm and equilibrated at 20 °C. After different equilibration times, the solid and liquid phases were separated by vacuum filtration using nylon filters (pore size: 0.45 µm) and analyzed.

2.1.1 Long-term experiment

All synthesis were done at room temperature following a one-step protocol in which a total 3.8 g of calcium oxide (CaO), silica fume (SiO₂, Aerosil 200, Evonik) and calcium aluminate (CA: CaO·Al₂O₃) were added into 171 mL of Milli-Q water or NaOH solutions (liquid/solid = 45 (mL/g)) to obtain C-A-S-H with different compositions (Table 1). CaO with 96% purity was obtained by burning calcium carbonate (CaCO₃, Merck, pro analysis) at 1000°C for 12 hours. CA was synthesized from CaCO₃ and Al₂O₃ (Sigma Aldrich). The mixture was heated at 800 °C for 1 hour, at 1000 °C for 4 hours and at 1400 °C for 8 hours. Then, it was cooled down with a rate of 600 °C/h. The molar ratios of CaO, SiO₂ and CA were varied in order to obtain C-A-S-H with Ca/Si ranging from 0.6 to 1.4, and Al/Si from 0 to 0.2, as indicated in Table 1. 0.5 M NaOH corresponds to the pH value generally observed in the pore solution of cement [60,61]. In addition, NaOH concentrations of 0, 0.1 and 1 M were selected to cover the different range of pH values relevant for hydrated cements and in order to investigate the effect of pH values on Al uptake in C-S-H [19]. The samples were prepared with four replicates and the analysis of solid and solution phases were performed after 3 months, 1 year, 2 and 3 years. All experimental details on samples are compiled in Appendix A.

Table 1. The Ca/Si, Al/Si molar ratios and NaOH concentrations used to prepare C-A-S-H at 20 °C for long-term experiments. (*: samples at Ca/Si ratio of 0.8 were analyzed also at Al/Si = 0.2 and after 24 and 36 months).

Molar Ca/Si	Molar Al/Si	NaOH (mol/L)	Equilibration time (months)
0.6, 0.8, 1.0, 1.2 and 1.4	0	0, 0.1, 0.5 and 1	3 and 12*
	0.001		
	0.003		
	0.01		
	0.03		
	0.05		
	0.1		
	0.2*		

2.1.2 Short-term experiment

In short-term experiments, C-S-H samples with Ca/Si ratios of 0.8 and 1.2 containing 1 M NaOH were synthesized and equilibrated for 1 month. Afterwards, 0.086 and 0.073 g of sodium aluminate (NaAlO_2), corresponding to an Al/Si molar ratio of 0.03, was added to the pre-equilibrated C-S-H samples with Ca/Si ratios of 0.8 and 1.2, respectively. The details of C-A-S-H samples in short-term experiments are shown in Table 2. The composition of solution and solid phases of C-S-H samples containing Al (C-A-S-H) was measured after 7, 14, 28 and 56 days (up to 3 months).

Table 2. The Ca/Si, Al/Si molar ratios and NaOH concentrations used to prepare C-A-S-H at 20 °C for short-term experiments.

Molar Ca/Si	Molar Al/Si	NaOH (mol/L)	Equilibration time (days)
0.8 and 1.2	0.03	1	7, 14, 28 and 56

2.2 Drying

After filtrating the samples inside the glove box, the solids were washed first with a 50%-50% (volumetric) water-ethanol solution to avoid the precipitation of alkali during drying, and then with pure ethanol in order to remove the free water. The samples were then dried in the freeze dryer for one week and then stored until analysis (at least 1 week) in nitrogen filled desiccators in the presence of saturated $\text{CaCl}_2 \cdot 2\text{H}_2\text{O}$ solution, which generates a relative humidity of 30%, following the procedure described by [34,36].

2.3 Analysis

2.3.1 ICP-MS and ICP-OES

The elemental concentrations of Na, Ca, Si and Al in the filtrates were determined with ICP-MS and ICP-OES. The different liquid samples were first acidified to contain 1% HNO_3 (using Suprapur HNO_3 , Merck). Samples containing NaOH were diluted using 1% HNO_3 to have Na concentrations below 230 mg/L and 1500 mg/L for the ICP-MS and ICP-OES analysis, respectively. With this dilution, the maximum Si and Ca concentrations were below 1 mg/L in ICP-MS. Multi-standard solutions and blank solution (1% HNO_3), containing Al, Ca and Si, were prepared in the range from 0 to 200 $\mu\text{g/L}$ and from 0 to 20 mg/L for ICP-MS and ICP-OES, respectively. In alkali-free samples, the standard solutions were prepared containing Al, Ca and Si. However, in samples containing NaOH, 230 mg/L and 1500 mg/L of Na were added to the standard solutions for the ICP-MS and ICP-OES analysis, respectively. The goal of this procedure was to minimize the matrix effect and ascertain that all samples including the standard solutions have the same Na concentration. The measurements were carried out on ICP-MS (7700x, Agilent) and/or ICP-OES (Spectro Arcos). Further details regarding the operating parameters used in ICP-MS and ICP-OES are listed in Appendix F.

2.3.2 pH measurement

To measure the hydroxide concentration, pH measurements were made at room temperature with a Knick pH meter (pH-Meter 766) equipped with a Knick SE100 electrode. To minimize the alkali error, the pH electrode was calibrated against 0.1, 0.2, 0.5 and 1 M NaOH concentrations [62].

2.3.3 Zeta potential measurement

The zeta potential was measured with an acoustophoresis electroacoustic method using a Zeta Probe from Colloid Dynamics, which is based on the frequency-dependent electroacoustic effect. The zeta potential is calculated from the frequency-dependent mobility using the O'Brien Equation [63]. The calibration was made with potassium tungstosilicates, KSiW. To have the C-S-H particles in a homogeneous suspension, magnetic stirrer was used at 450 rpm during 10 minutes. A first measurement of zeta potential was made on unfiltered C-A-S-H samples. Then, the second measurement was carried out on the filtrated solutions to determine any interferences due to ions present in the solution considered as background and thus deducted from the initial measurement. The zeta potential is measured close to the interface between the stern layer and the diffusive layer giving the effective charge of the particle surface in the suspension.

2.3.4 TGA

TGA data were acquired with a TGA/SDTA851e Mettler Toledo device using approximately 30 mg of sample. The weight loss of the samples was recorded from 30 °C up to 980 °C with a heating rate of 20 °C/min under N₂ atmosphere. The amount of strätlingite, Al(OH)₃, katoite, portlandite (CH) and CaCO₃ were quantified based on the measured weight loss between 150-240, 240-300, 300-350, 350-450 and 600-900, respectively, using the tangential method and the theoretical weight loss of solids [64].

2.3.5 XRD

PANalytical X'Pert Pro MDF diffractometer equipped with an X'Celerator detector was used to record the X-ray powder diffraction patterns. Diffraction patterns were collected in increments from 5° to 70° 2θ at a conventional step size of 0.017° 2θ and a step measurement time of 460 s. The presence of different phases was determined with X'Pert HighScore Plus. The quantification of the amounts of the phases was carried out with calcium fluoride as an external standard.

2.3.6 FTIR

FTIR spectra were recorded in the range of 400-4300 cm⁻¹ on a Bruker Tensor 27 spectrometer with a resolution of 4 cm⁻¹ by transmittance on small amounts of powder. To make the comparison easier, the spectra were corrected for background and scaled to the maximum of Si-O bonds. The second derivative of FTIR spectra was used in order to identify the different bands and differentiate the wavenumbers [65].

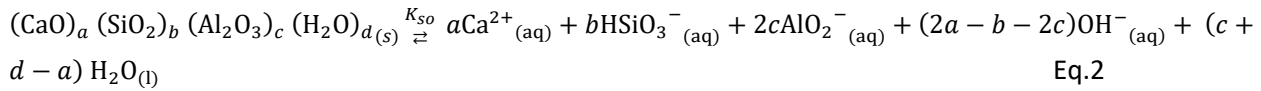
2.3.7 Thermodynamic modelling

Thermodynamic modelling was performed with GEM-Selektor software [57], version 3.7. The PSI-Nagra chemical thermodynamic database [66] was used as a source of the standard thermodynamic data for aqueous species, portlandite and amorphous SiO₂. The standard thermodynamic data for microcrystalline Al(OH)₃, strätlingite, C-S-H and katoite were taken from the Cemdata18 chemical database [67]. The CSHQ thermodynamic solid solution model was used in order to model the stability and composition of the C-S-H system [47]. The activity coefficients of aqueous species γ_i were calculated using the extended Debye-Hückel equation (Eq.1) with common ion-size parameter $a_i = 3.31 \text{ \AA}$ for NaOH solutions [68] and common third parameter b_y according to:

$$\log \gamma_i = \frac{-A_y z_i^2 \sqrt{I}}{1 + B_y a_i \sqrt{I}} + b_y I \quad \text{Eq.1}$$

where z_i denotes the charge of species i , I the effective molal ionic strength, b_y is a semi-empirical parameter (~ 0.098 for NaOH electrolyte at 25 °C), and A_y and B_y are P, T -dependent coefficients. This activity correction is applicable up to ~ 1 M ionic strength [69].

The solubility products (K_{so}) for C-A-S-H were calculated from the generalized dissolution reaction shown in Eq.2:



where a, b, c and d are the respective stoichiometric coefficients for CaO, SiO₂, Al₂O₃ and H₂O in C-A-S-H [36]. At equilibrium, this reaction implies the following relationship for K_{so} at Ca/Si = 0.8 and Al/Si = 0.03 (Eq.3):

$$K_{so} = \{Ca^{2+}_{(aq)}\}^{0.777} \cdot \{HSiO_3^{-}_{(aq)}\}^{0.971} \cdot \{AlO_2^{-}_{(aq)}\}^{0.029} \cdot \{OH^{-}_{(aq)}\}^{0.554} \cdot \{H_2O_{(l)}\}^{1.02} \quad \text{Eq.3}$$

And for Ca/Si = 1.2 and Al/Si = 0.03 (Eq.4):

$$K_{so} = \{Ca^{2+}_{(aq)}\}^{1.165} \cdot \{HSiO_3^{-}_{(aq)}\}^{0.971} \cdot \{AlO_2^{-}_{(aq)}\}^{0.029} \cdot \{OH^{-}_{(aq)}\}^{1.33} \cdot \{H_2O_{(l)}\}^{1.19} \quad \text{Eq.4}$$

Activities of $Ca^{2+}_{(aq)}$, $HSiO_3^{-}_{(aq)}$, $AlO_2^{-}_{(aq)}$, $OH^{-}_{(aq)}$ and $H_2O_{(l)}$ species were calculated with GEM-Selektor v3.7 using the measured concentrations of Ca, Si, Al and OH⁻ in the supernatants.

The saturation index (SI) of different solids was calculated according to Eq.5 using the elemental concentrations of Al, Ca, Si and Na:

$$SI = \log \left(\frac{IAP}{K_{so}} \right) \quad \text{Eq.5}$$

The ion activity product (IAP) was calculated based on the measured concentrations in solution. A positive saturation index (> 0) indicates that the solution is oversaturated with respect to this solid phase and that this phase could possibly precipitate. A negative value indicates undersaturation. The SI calculation was used to verify the solid phase composition found experimentally.

2.3.8 Al uptake in C-S-H

The elemental composition in C-A-S-H was calculated by mass balance. The amount of Al, Ca, Si and Na in secondary phases and the fraction of Al, Ca, Si and Na in solution were subtracted from the initial quantities in order to calculate the effective C-A-S-H composition as detailed in [37,58,59]. For example, for calculation of molar Al/Si ratio in C-A-S-H, the mass of Al in secondary phases containing Al (strätlingite, Al(OH)₃, katoite) and the mass of Al in solution were subtracted from the initial mass of Al in CaO·Al₂O₃ used in synthesis. The same method was followed to calculate the mass of Si in C-A-S-H. Then, the molar Al/Si ratio was calculated using the molar quantity of Al and Si in C-A-S-H. The measurements and quantifications are also detailed in Appendix B. The measurements' error were taken into account in the calculation of elemental compositions in C-A-S-H. The errors of concentrations in the aqueous solution are less than 2%. However, 10% error was

considered in the quantification of different secondary phases with TGA. Thus, the errors in Al/Si and Ca/Si ratios in C-A-S-H were calculated using the 10% error in the content of different secondary phases in solid which are compiled in Table 10 in Appendix E.

The uptake of Al into C-S-H phases can be expressed in terms of a K_d value (distribution coefficient), which is defined as the ratio of the quantity of aluminum adsorbed per unit mass of solid to the quantity of aluminum remaining in solution at equilibrium. The K_d values were calculated according to Eq.6:

$$K_d = \frac{C_{s,eq}}{C_{l,eq}} \quad (\text{m}^3 \text{ kg}^{-1}) \quad \text{Eq.6}$$

where $C_{s,eq}$ is the equilibrium Al concentration sorbed on C-A-S-H phases [mol.kg^{-1}] and $C_{l,eq}$ is the equilibrium concentration in solution [mol.m^{-3}]. The errors of K_d values are mainly less than 1% as compiled in detail in Table 11 in Appendix E.

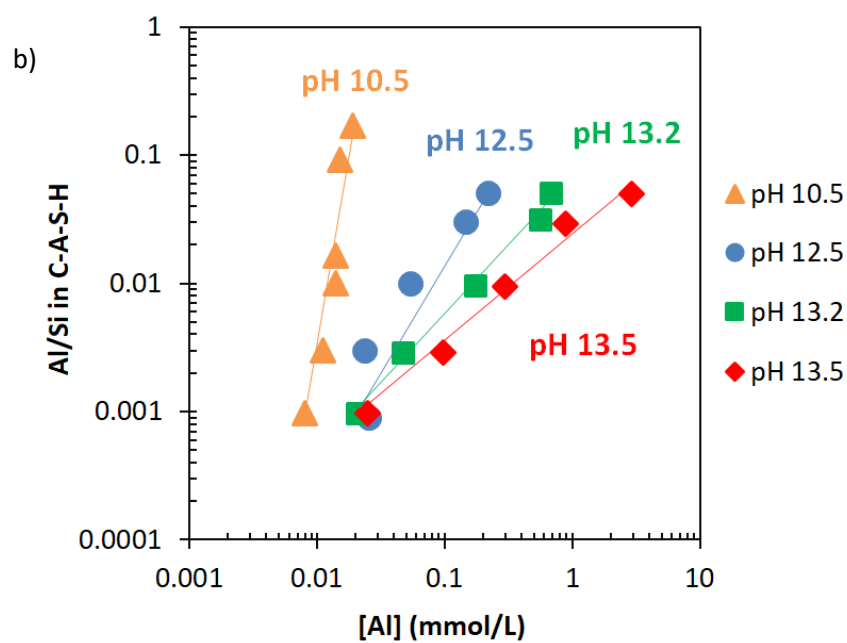
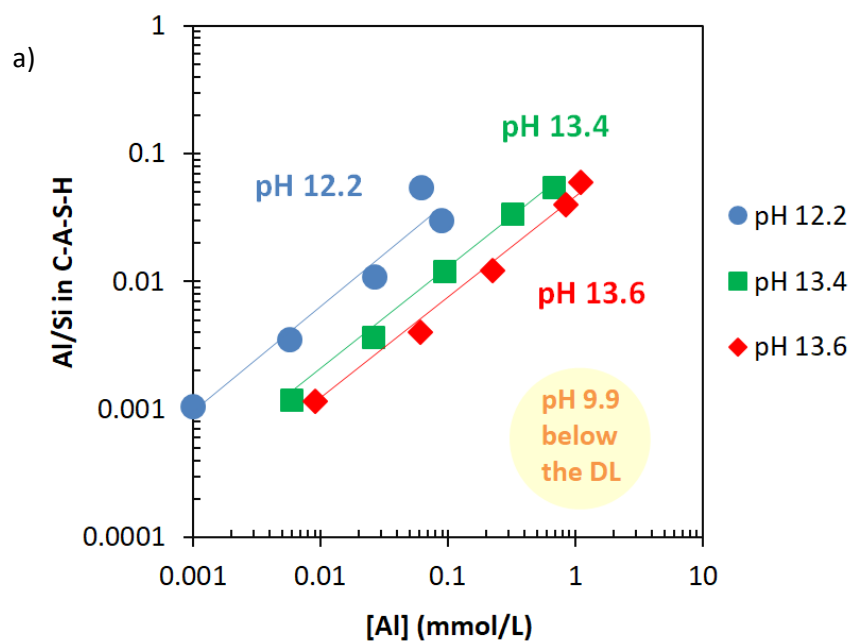
Chapter 3 The effect of alkali hydroxides on C-A-S-H

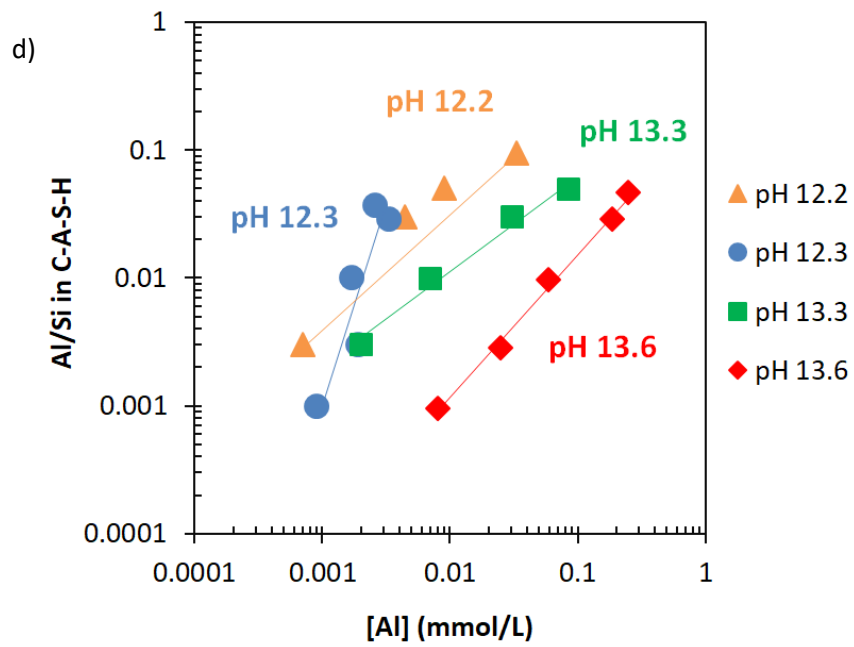
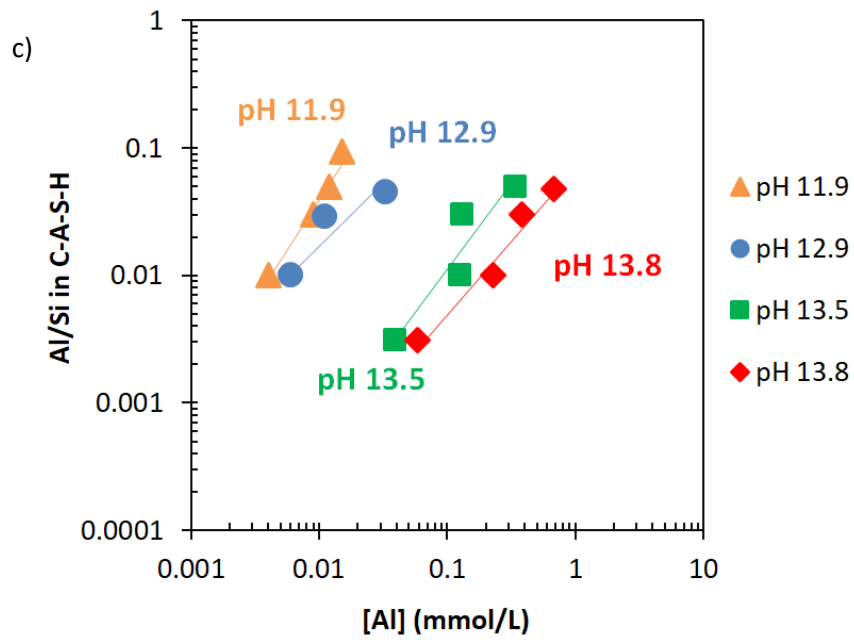
This chapter investigates the effect of different sodium hydroxide concentrations (pH values) on the aluminum uptake in C-S-H which has been published in the Journal of Colloid and Interface Science and the information regarding the contribution of the author of this PhD thesis can be found in section 1.7. The analysis were performed on C-A-S-H samples containing different Al/Si ratios, Ca/Si ratios and NaOH contents filtrated after 3 months equilibration.

3.1 The effect of pH on Al sorption isotherm

Figure 6 shows the molar Al/Si in C-A-S-H obtained from mass balance calculations against the measured Al concentrations in aqueous solution. The aluminum uptake in C-S-H increases with the dissolved aluminum concentrations at Ca/Si ratios of a) 0.6; b) 0.8; c) 1.0; d) 1.2 and e) 1.4. A similar relation between aluminum uptake in C-S-H and dissolved aluminum in the solution has also been reported in [55] albeit at much higher aluminum concentrations (0.5 mmol/L to 3.5 mmol/L for Ca/Si = 0.95) and in [37] at similar concentrations (0.021 mmol/L to 0.37 mmol/L for Ca/Si = 1.0). This clear relation between aluminum concentrations and Al/Si ratio in C-A-S-H indicates either a surface sorption of aluminum on the C-S-H [27] or the uptake in the C-S-H structure, which might be described by a solid solution model [70,71].

The addition of alkali hydroxide increases the pH value, which is a key parameter in the system. The pH increases from 10.5-12.0 for the alkali-free C-A-S-H up to 13.6 in the systems containing sodium hydroxide. Increasing the pH values leads to higher dissolved Al concentrations preventing the precipitation of secondary phases such as aluminum hydroxide. The sorption isotherms in Figure 6 show that in fact the presence of alkali hydroxide leads to much higher dissolved Al concentrations as the addition of NaOH increases the pH value and destabilizes the solubility of strätlingite and aluminum hydroxide. At all Ca/Si ratios investigated (0.6, 0.8, 1.0, 1.2 and 1.4, see Figure 6) this effect of the pH value on the dissolved Al concentration is clearly visible.





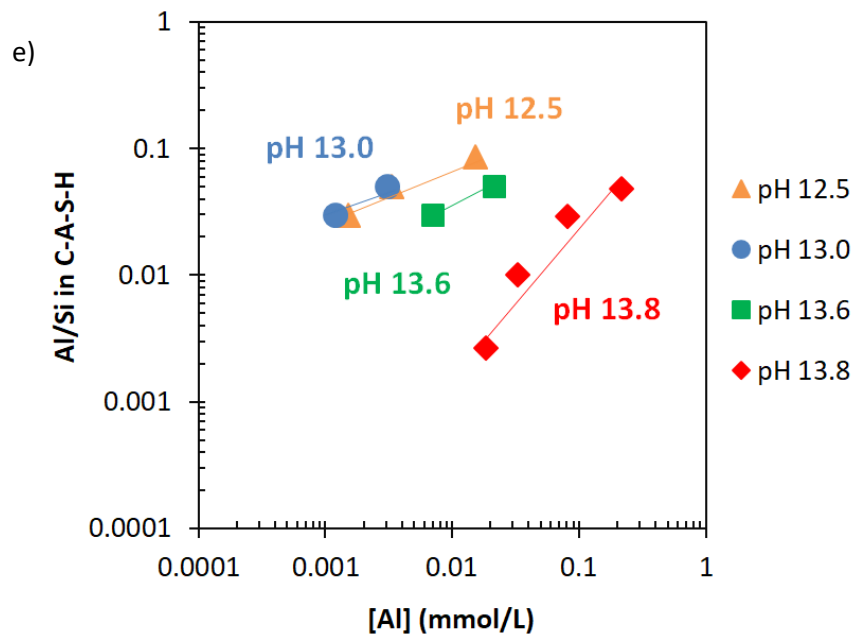


Figure 6. The effect of pH value on Al uptake in C-S-H after 3 months equilibration for Ca/Si ratios of a) 0.6; b) 0.8; c) 1.0; d) 1.2 and e) 1.4 in the absence of NaOH and in the presence of 0.1, 0.5 and 1 M NaOH. (The lines serve as eye-guides only and the errors are smaller than the symbols' size).

3.2 The Al speciation at different pH values

Figure 7 illustrates the strong dependence of dissolved aluminum concentrations in equilibrium with solid $\text{Al}(\text{OH})_3$. A similar graph is obtained for the aluminum hydroxide species in equilibrium with gibbsite as shown e.g. in [72]. 100 times higher dissolved Al concentrations can be reached at pH 13.5 than at pH 11.5 before aluminum hydroxide precipitation occurs. At the same aluminum concentrations, less aluminum uptake in C-S-H is observed in the presence of alkali hydroxide. This suppression of aluminum uptake is stronger at higher pH values. This could be related to i) the increase of the fraction of the thermodynamically stable aqueous aluminum hydroxide complex ($\text{Al}(\text{OH})_4^-$) in solution and/or ii) the increase of the negative surface charge of C-S-H due to the pH increase, i.e. the interaction of the negatively charged complex ($\text{Al}(\text{OH})_4^-$) in solution with the negatively charged surface will lower the tendency for aluminum incorporation. The speciation of aqueous aluminum depends on the pH values as shown in Figure 7, where negatively charged $[\text{Al}(\text{OH})_4^-]$ dominates the speciation at $\text{pH} > 7$ [73]. The fraction of the $\text{Al}(\text{OH})_4^-$ species increases with the pH values, which lowers the tendency of Al to be sorbed by C-S-H. Furthermore, the formation of a $\text{NaAl}(\text{OH})_4$ complex could be possible at higher pH values and at high concentrations of sodium [74] which could contribute to stabilize aluminate ions in the solution and decrease its uptake by C-S-H. Lower aluminum uptake in C-S-H at high NaOH concentrations could also be related to the decrease of the occurrence of filled bridging position with increasing pH value. Si NMR measurements have shown shorter silica chain length at higher pH values [23].

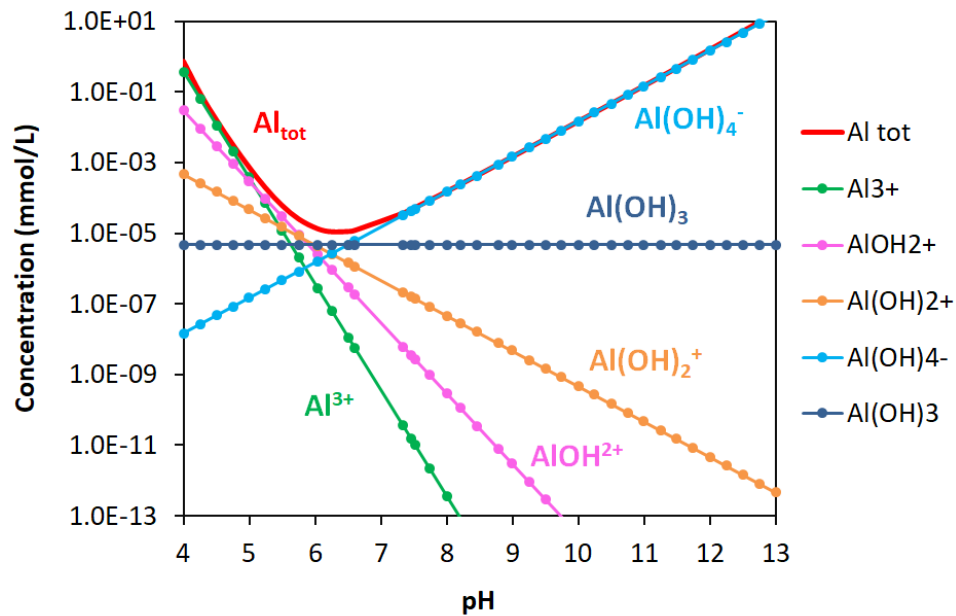


Figure 7. The effect of pH value on the calculated Al speciation in equilibrium with microcrystalline $\text{Al}(\text{OH})_3$.

3.3 Zeta potential at different pH values

Zeta potential measurements are shown in Figure 8. The zeta potential measures the charge of a particle not directly at the surface but in some distance; such that ions near the surface and even some in the diffuse layer, contribute to the measured charge [73,75]. The zeta potential measurements of C-S-H show a negative charge for low Ca/Si C-S-H and thus at low calcium concentrations. At higher calcium concentrations, the measured zeta potential increases from negative values to positive values, as the calcium accumulates near the surface of C-S-H as discussed in detail in [27]. As the increase of calcium concentrations at higher Ca/Si ratios in C-S-H is also accompanied by an increase of the pH value, this charge reversal can also be observed as a function of pH value as shown by the circles in Figure 8, which represents measured zeta potentials on C-S-H with Ca/Si = 0.66 to 1.51, in the absence of any alkali hydroxide [27].

However, an increase of the pH value at constant Ca/Si has the opposite effect. It lowers the measured zeta potential to more negative values as illustrated by the squares in Figure 8, where the measured zeta potential decreases from -0.5 mV for Ca/Si = 1.0 and no alkali to -18.4 mV in the presence of 0.15 M potassium hydroxide (KOH) as reported by [37]. This effect is also visible in the difference between the zeta potential values measured in the absence of alkali (blue circles) and those in the presence of 0.1 M NaOH (red triangles); for Ca/Si ratio of 1.0, the measured zeta potential decreases from 1 mV in the absence of NaOH to -14 mV in the presence of 0.1 M NaOH. This is related to an increased deprotonation of the silanol sites at higher pH values, in agreement with the trends predicted by molecular modelling [76].

Measurements of the zeta potential in 0.1 M NaOH of C-S-H with Ca/Si ratios from 0.6 to 1.6 (red triangles) confirms the effect of pH values on the measured zeta potential, all data are significantly lower than in the absence of NaOH indicating a more negative C-S-H surface at higher pH values. Even at higher pH values an increase of the Ca/Si ratio of C-S-H increases the zeta potential from -27 mV to -3 mV (from full triangles to empty ones) as the calcium concentrations increase with the Ca/Si ratio in C-S-H. Thus, also in the presence of 0.1 M NaOH increasing the Ca/Si ratio decreases the negative charge near the C-S-H particles which leads to an increase in the measured zeta potentials. The measured zeta potential is in addition influenced by the

concentration of Na^+ cations, which can also be present near the surface of C-S-H. As Ca^{2+} and Na^+ cations compete to compensate the negative charge [19], at high NaOH concentration Na^+ can replace some of the Ca^{2+} near the C-S-H surface, thus lowering the measured zeta potential. At higher alkali hydroxide concentrations (0.5 and 1 M NaOH), however, the zeta potential measurements are strongly affected by the increase in ionic strength which moves the distance where the zeta potential is measured, such that the experimental values show a very high scatter and a reliable measurement is not possible (data not shown). The different shading of the triangles and circles correspond to the different Ca/Si ratios; for each Ca/Si at 0.1 M NaOH several measurements are available corresponding to the different Al/Si ratios from 0 to 0.2. The different experiments are also the reason for the slight difference in the zeta potential values for Ca/Si = 0.6 from 11.9 mV to 12.2 mV.

The zeta potential measurements illustrate that higher pH values at constant Ca/Si result in a more negatively charged C-S-H surface due to the deprotonation of the silanol sites. Together, the more negative surface charge and the increasing predominance of aqueous $\text{Al}(\text{OH})_4^-$ complexes suppresses Al uptake by C-S-H at high pH values as discussed above and as visible in the data shown in Figure 7.

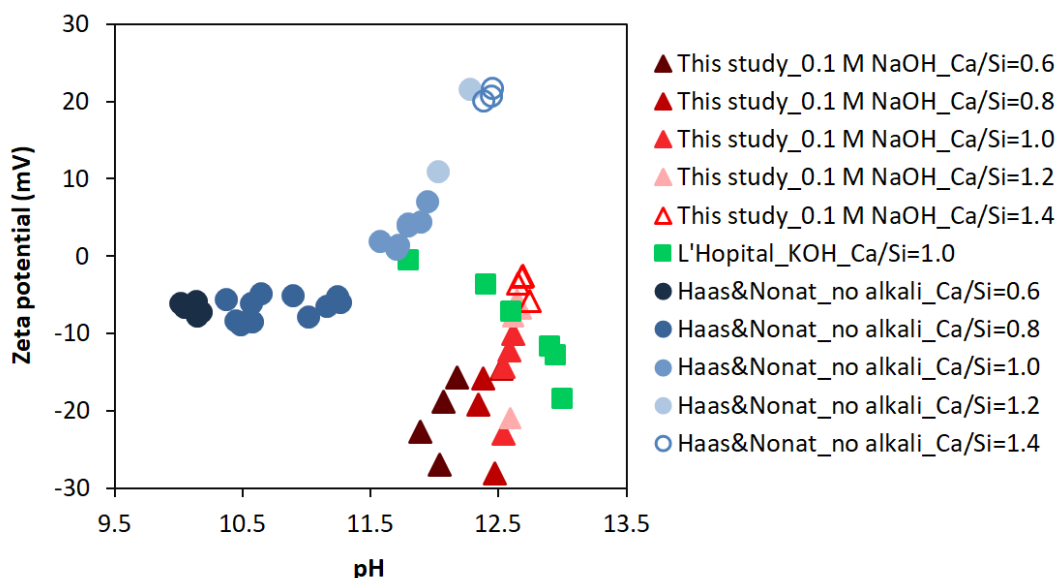


Figure 8. Zeta potential measurements for C-S-H samples in the absence of alkali hydroxide (circles; [27]), the effect of 0 to 0.15 M KOH (squares; [37]), and in the presence of 0.1 M NaOH (triangles; this study).

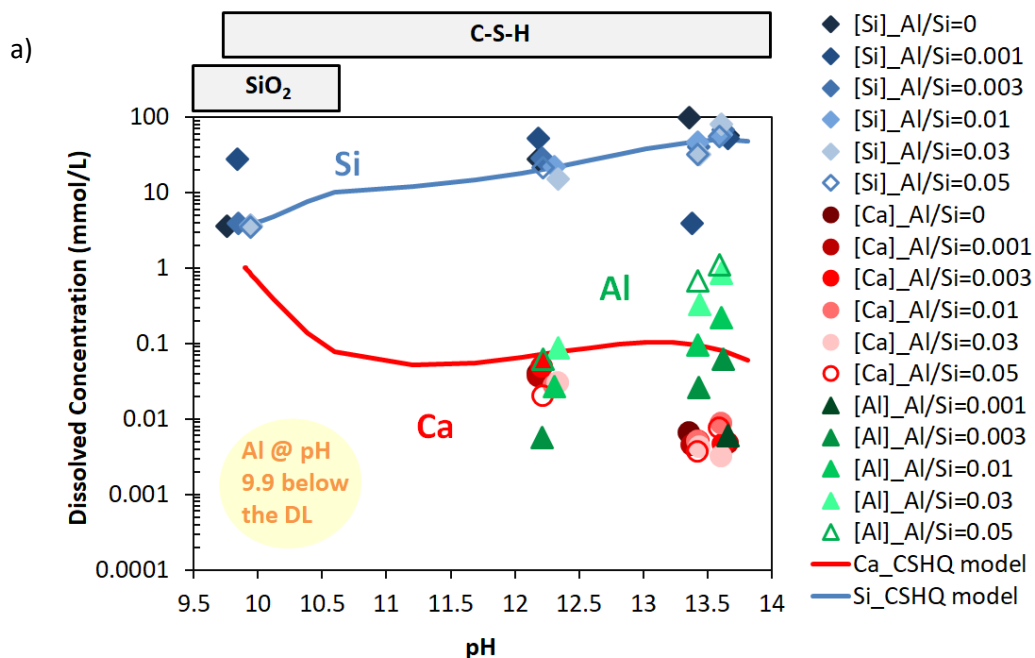
3.4 The effect of pH on aqueous phase composition

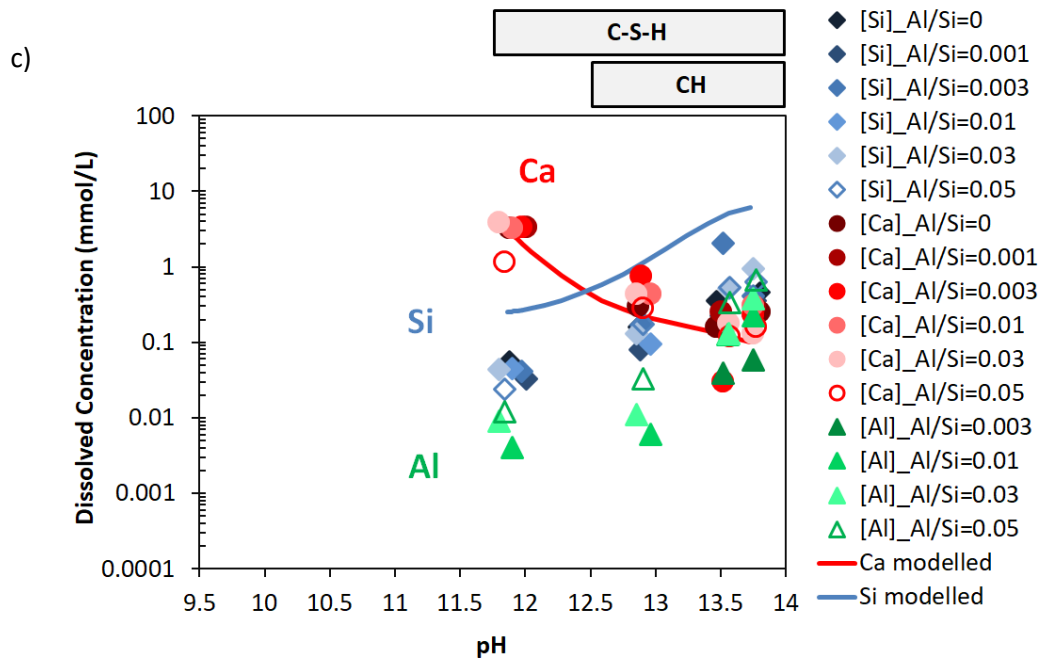
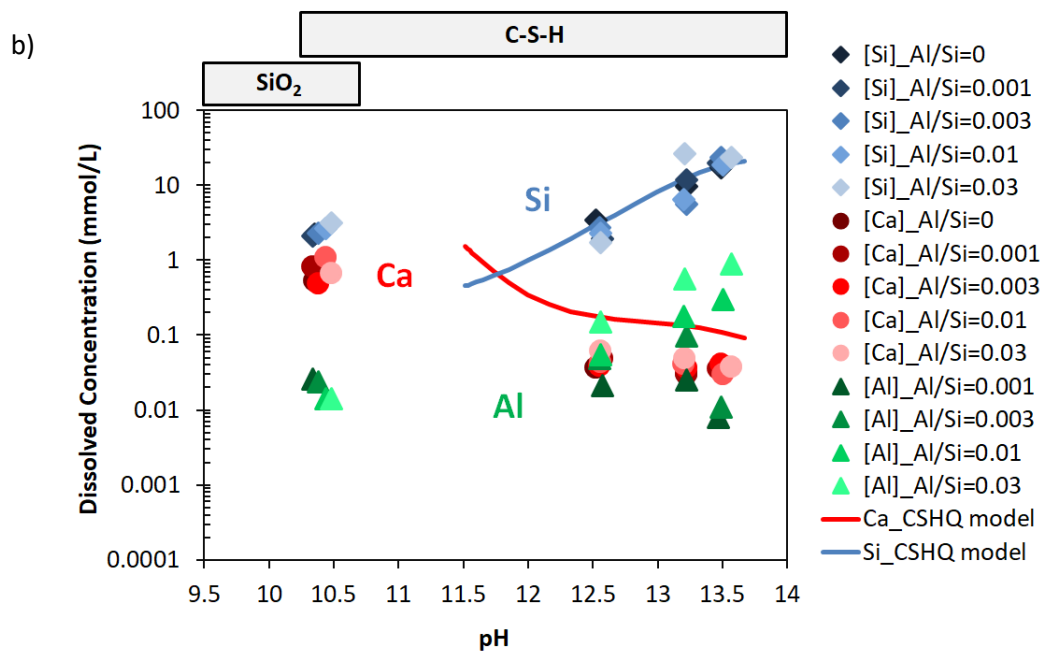
Figure 9 shows the effect of sodium hydroxide on the aqueous phase composition at five different Ca/Si ratios of a) 0.6; b) 0.8; c) 1.0; d) 1.2 and e) 1.4. The measured dissolved Ca and Si concentrations in Figure 9 are compared to thermodynamic predictions using the CSHQ solid solution model for C-S-H [47,67]. The CSHQ model was used as it is able to model the entire Ca/Si range investigated instead of the CNASH model developed by [70,71] as the CNASH model concentrates on low Ca/Si.

The alkali-free C-S-H are the data points at pH of 10, 10.5, 11.9, 12 and 12.2 for Ca/Si ratios of 0.6, 0.8, 1.0, 1.2 and 1.4, respectively. A comparison of the alkali-free C-S-H in Figure 9a-e illustrates that the Ca concentrations increase with increasing Ca/Si and the Si concentrations decrease; both these trends as well as the measured concentrations agree well with other solubility measurements of C-S-H published in literature as summarized in [19,46].

Higher pH values increase the concentrations of silica and aluminum in solution, while the calcium concentrations decrease. The same trend has been observed for C-S-H and C-A-S-H systems in the presence of different quantities of sodium and potassium hydroxide [23,37,77,78]. Increasing the pH values leads to a decrease in Ca concentrations in the solution; this decreasing trend in calcium concentrations agrees well with the modelling predictions although the model overestimates somewhat the measured calcium concentrations at low Ca/Si ratios and underestimates them at Ca/Si = 1.2. At Ca/Si = 1.4, the calcium concentrations above pH of 12.5 are determined by the solubility of portlandite as shown in Figure 9e. In contrast to the calcium, the silica concentrations increase with the pH values. At low Ca/Si ratios, this behavior is dominated by the increase of the amorphous silica solubility with pH. At intermediate Ca/Si ratios, the increase of dissolved Si is related to the decrease of the dissolved Ca concentration and the common ion effect with respect to C-S-H.

The measured Al concentrations increase with the amount of Al present in the system as visible in Figure 9a-e, where the different symbols represent samples with different Al/Si ratios from 0.001 to 0.05. The formation of $\text{SiO}(\text{OH})_3^-$, $\text{SiO}_2(\text{OH})_2^{2-}$ and $\text{Al}(\text{OH})_4^-$ complexes at high pH values increases the silicon and aluminum concentrations as illustrated for aluminum in Figure 7. This simultaneous increase of Si, Al and hydroxide concentrations with pH value lowers the calcium concentrations due to the common ion effect with C-S-H, katoite and/or portlandite. Increasing the pH values increases the Al concentrations in the aqueous solution at all Ca/Si ratios similarly to the Si concentrations, which could indicate a comparable uptake mechanism for Si and Al in C-S-H both at high and low Ca/Si. In fact, an uptake of Al^{IV} in the silica chain as observed at low Ca/Si ratios, can be expected to result in similar trends of Si and Al concentrations upon variation of pH values and Ca/Si ratios. These results tentatively indicate that also six-fold coordinated Al^{VI} , the dominant Al species at high Ca/Si ratios, could be associated with the silica chain [19,38,39,45], in agreement with recent findings from molecular modelling [45] and with the observed increase of the silica chain length in the presence of Al [23].





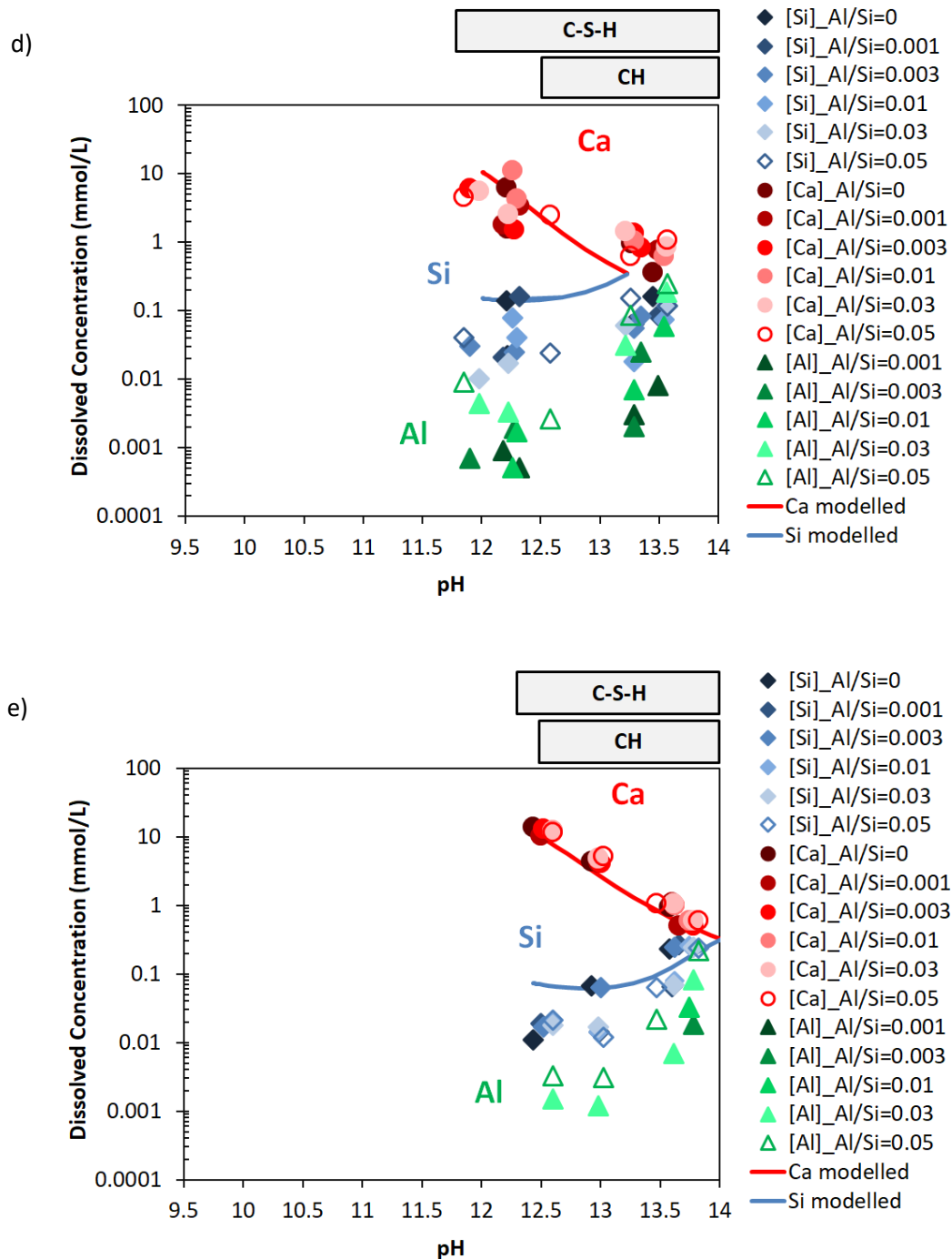


Figure 9. The effect of pH value on aqueous phase composition after 3 months equilibration for Ca/Si ratios of a) 0.6; b) 0.8; c) 1.0; d) 1.2 and e) 1.4. (The points represent the experimental data and the lines are the calculated values using the CSHQ solid solution model [47]). (The errors are smaller than the symbols' size).

3.5 The effect of pH on solid phase composition

Figure 10 shows the TGA results for samples at Ca/Si ratio of 0.8 and Al/Si ratio of 0.03 with different NaOH concentrations. For the sample without NaOH, the presence of a low amount of $\text{Al}(\text{OH})_3$ and katoite is observed. However, at higher NaOH concentrations (0.1, 0.5 and 1 M) no secondary phases are present, in agreement with Figure 7 which illustrates that the presence of NaOH increases the pH values and destabilizes

aluminum hydroxide. At higher alkali hydroxide concentrations, more Al is present in solution due to the preferred formation of $\text{Al}(\text{OH})_4^-$ complex which leads to the less secondary phases and less Al in C-S-H.

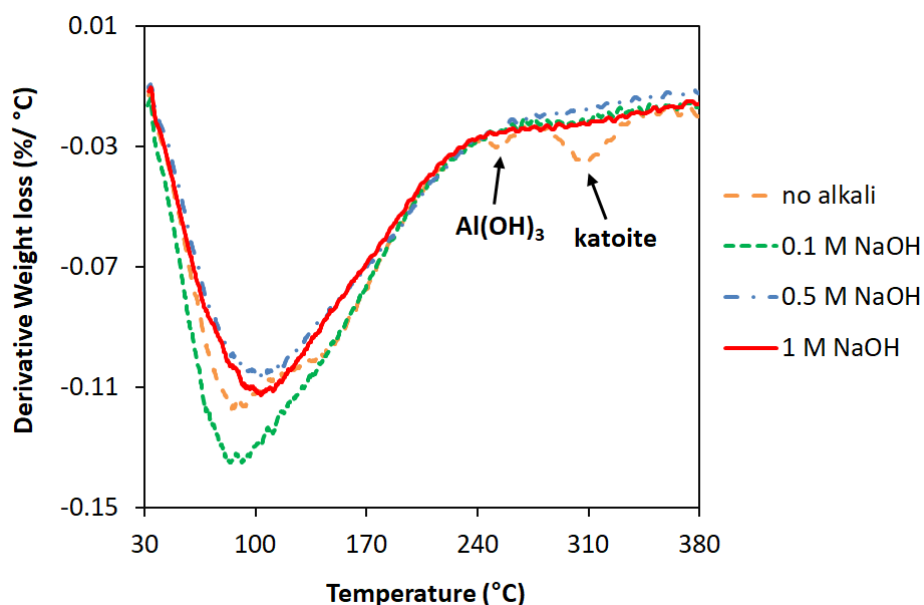


Figure 10. The TGA results for Al/Si ratio of 0.03 and Ca/Si ratio of 0.8 with different NaOH concentrations.

3.6 Conclusions

The sorption isotherm experiments indicated that aluminum uptake in C-S-H increases with the aluminum concentrations in solution. In the absence of alkali hydroxide, however, the maximum Al concentrations in solution were limited to approximately < 0.03 mmol/L by the precipitation of $\text{Al}(\text{OH})_3$ and katoite, which limits the maximum molar Al/Si to ≈ 0.1 .

The presence of sodium hydroxide increased the pH value, which prevented aluminum hydroxide formation, and led thus to much higher dissolved Al concentration of up to 2 mmol/L. The increase of the Al uptake in C-S-H, however, was limited as alkalinity suppresses Al uptake in C-S-H. Zeta potential measurements and molecular modelling [76] indicated that at higher pH values the C-S-H surface is more negatively charged due to increased deprotonation of the silanol sites, which suppresses Al uptake, as the main hydroxide complex of aluminum above pH of 7, $\text{Al}(\text{OH})_4^-$, is also negatively charged. In addition, the fraction of the $\text{Al}(\text{OH})_4^-$ aqueous complex increased also with the pH values, which further lowers the tendency of Al to be sorbed by C-S-H.

Increasing the pH values and/or decreasing the Ca/Si ratios in C-S-H increased not only the Al concentrations but also in parallel the Si concentrations in solution. This similar behavior of Al and Si towards changes in pH pointed toward the uptake of aluminum within the silica chain both at high and low Ca/Si. This agrees well with solid state Si NMR results indicating that at low Ca/Si C-S-H Al^{IV} is present in the bridging sites of the silica chain. The results tentatively indicated that also six-fold coordinated Al^{VI} , the dominant Al species at high Ca/Si, could be present within the silica chain in agreement with recent molecular modelling studies [45].

Chapter 4 The effect of Ca/Si ratio on C-A-S-H

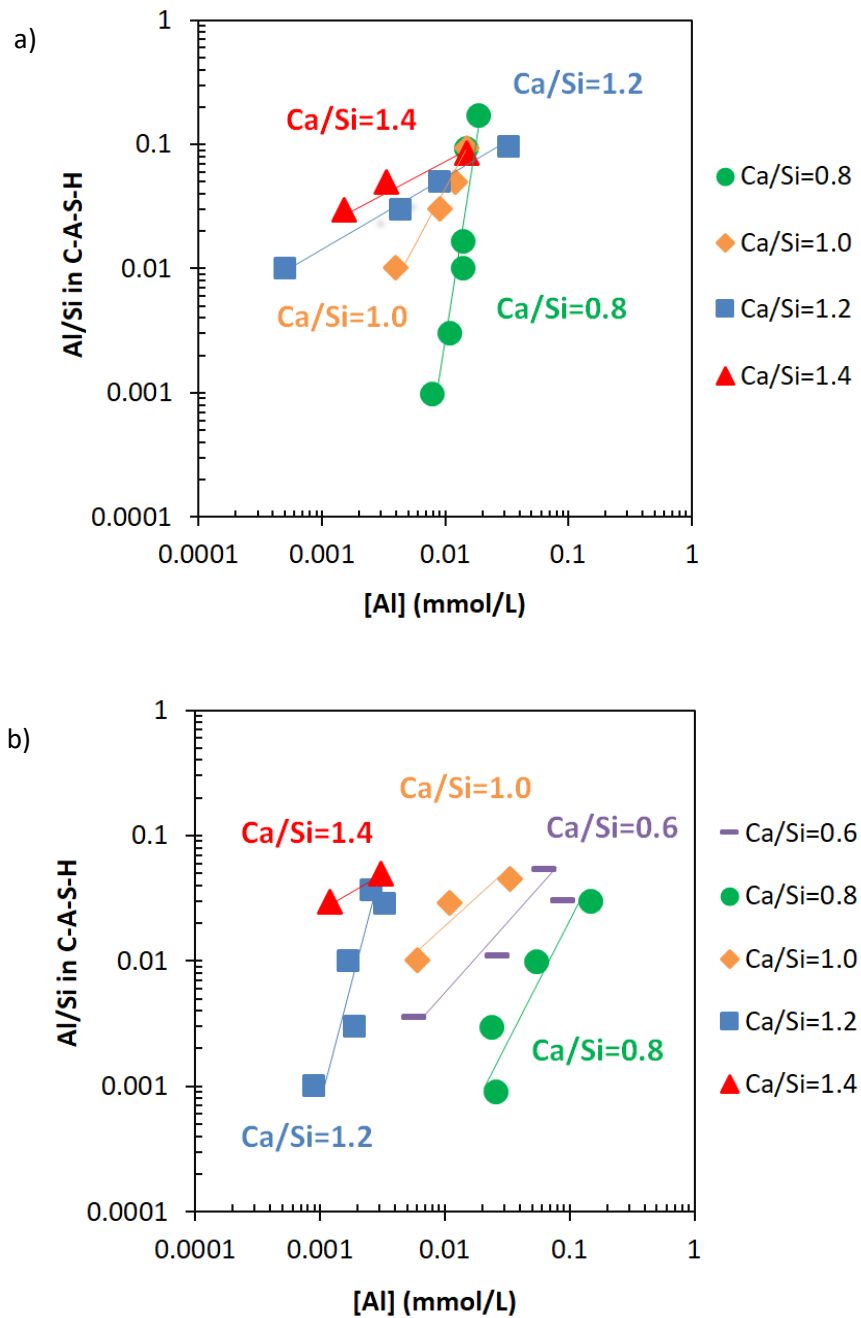
This chapter illustrates how different Ca/Si ratios affect the uptake of Al in C-S-H at different NaOH concentrations and Al/Si ratios using the equilibration time of 3 months. This chapter has been published in the Journal of Colloid and Interface Science and the information regarding the contribution of the author of this PhD thesis can be found in section 1.7.

4.1 The effect of Ca/Si ratio on Al sorption isotherm

The Ca/Si ratio in C-S-H affects not only the aluminum concentration in aqueous solution but also the amount of Al taken up in C-S-H. Figure 11 shows the effect of target Ca/Si ratio on Al uptake in C-S-H for different systems: a) in the absence of sodium hydroxide; b) in the presence of 0.1 M NaOH; c) in the presence of 0.5 M NaOH and d) in the presence of 1 M NaOH. Figure 11a shows that in the absence of alkali hydroxide, the maximum aluminum concentrations in solution are < 0.03 mmol/L, limited by the precipitation of $\text{Al}(\text{OH})_3$ and katoite, which restrains the maximum molar Al/Si to ≈ 0.1 . Figure 11a also indicates that at higher Ca/Si ratios more Al is taken up in C-S-H for the samples without alkali hydroxide, in particular at very low Al concentrations. For a given Al concentration, the Al uptake in C-S-H is increasing in a row from Ca/Si = 0.8 to Ca/Si = 1.4. In contrast, the uptake is similar at Al concentrations above 0.01 mmol/L. In addition, a different uptake regime is observed at high and at low Ca/Si ratios. The slope of the line between dissolved Al concentrations and Al in C-A-S-H is much steeper for samples at target Ca/Si ratio of 0.8 compared to those at target Ca/Si of 1.0 and above. A comparable difference between the Al uptake by low Ca/Si and high Ca/Si C-S-H is also observed in 0.1 M NaOH (Figure 11b). At low aluminum concentrations (< 0.01 mmol/L), increasing the Ca/Si ratios leads to an increase of the Al uptake in C-S-H. This might be related to the presence of different Al environments at low and high Ca/Si ratios. ^{27}Al MAS NMR have indicated that in low Ca/Si C-S-H four-fold coordinated Al^{IV} is the dominant environment, while at high Ca/Si ratios six-fold coordinated Al^{VI} is dominant [19,23,33,38,39,41]. The position of six-fold coordinated Al^{VI} has been suggested to be present in the bridging site [45]. However, how these different Al environments in C-S-H affect the Al uptake is presently not well investigated. Possibly, the presence of more calcium in the interlayer at higher Ca/Si ratios and the resulting apparent positive charge on the C-S-H surface could ease the uptake of $\text{Al}(\text{OH})_4^-$. Such a stabilizing effect of Ca on Al uptake would be consistent with a recent X-ray Adsorption Near Edge Spectroscopy (XANES) study, where an ordering of the Ca in the interlayer was observed in the presence of Al [29]. However, in addition also kinetic restraints could be important, and the equilibration time could be different at low Ca/Si and high Ca/Si.

Figure 11d shows the effect of target Ca/Si ratio on Al uptake in C-S-H for samples with 1 M NaOH. Increasing the Ca/Si ratio leads to a decrease in Al concentrations in solution and an increase in Al uptake in C-S-H as

also observed for the samples without NaOH. At Al concentration of 0.01 mmol/L, Al/Si of 0.003 is observed for low Ca/Si C-S-H, which increases to Al/Si = 0.05 at Ca/Si = 1.2. However, little difference is observed between the Ca/Si ratios of 0.6 and 0.8 and between Ca/Si ratios of 1.2 and 1.4 for samples with 1 M NaOH. Moreover, the uptake of Al in C-S-H in samples at Ca/Si ratio of 0.6 (for 0.1 M and 1M NaOH) do not show the same trend compared to the case of Ca/Si = 0.8. The reason for this behavior cannot be explained. Both at 0.5 M NaOH (Figure 11c) and at 1 M NaOH (Figure 11d) the slope has a comparable steepness independent of the Ca/Si ratio in contrast to the observation at lower pH values. The reason for this different behavior is presently unknown but points towards different binding sites for Al in C-S-H. Further detailed studies of Al binding in C-S-H by spectroscopic methods at different Al concentrations and pH values are needed, which is presently carried out in parallel projects [29].



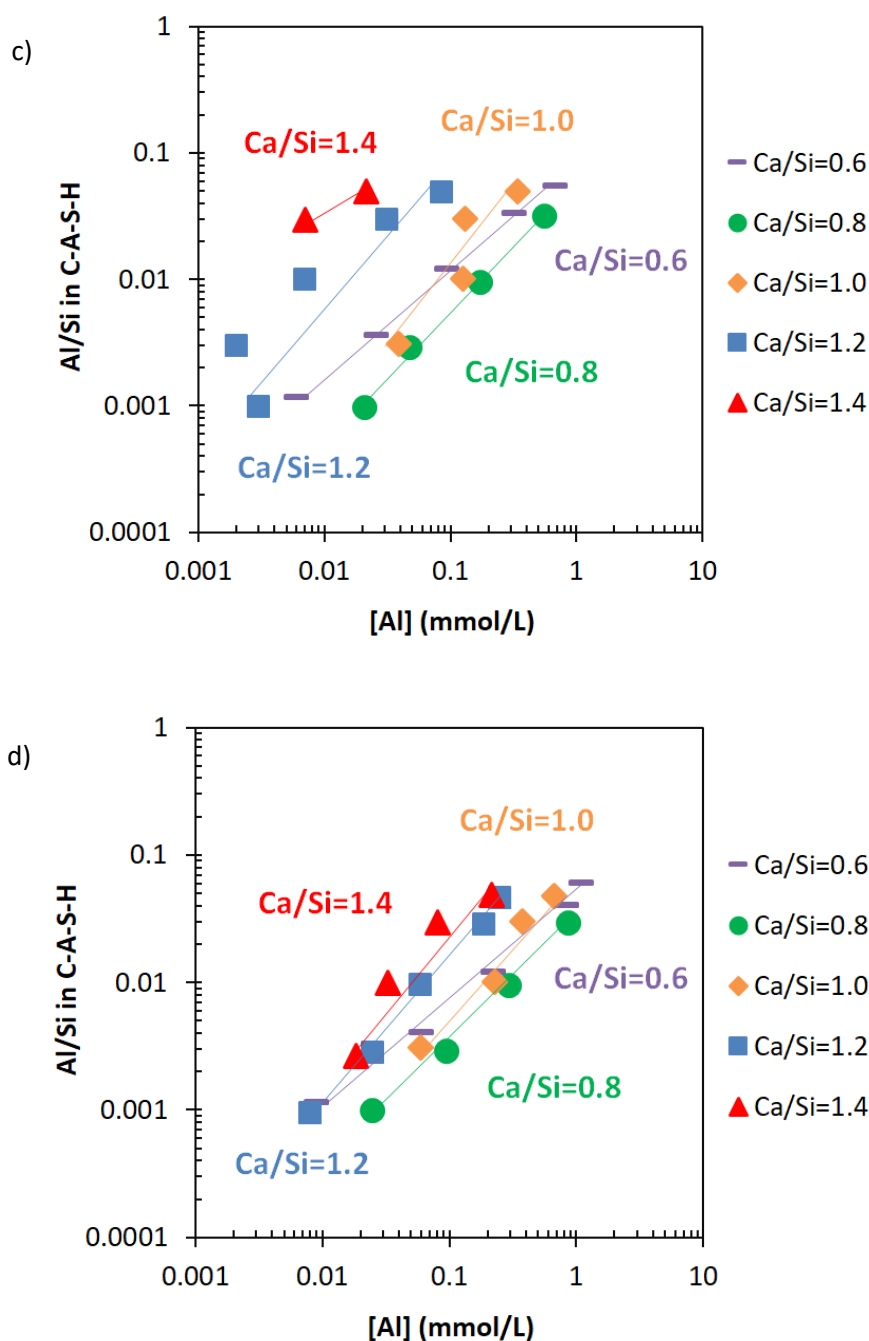


Figure 11. The effect of target Ca/Si ratio on Al uptake in C-S-H after 3 months equilibration for samples a) without NaOH (The data at Ca/Si = 0.6 were below the detection limit); b) 0.1 M NaOH; c) 0.5 M NaOH and d) 1 M NaOH. (The lines serve as eye-guides only and the errors are smaller than the symbols' size).

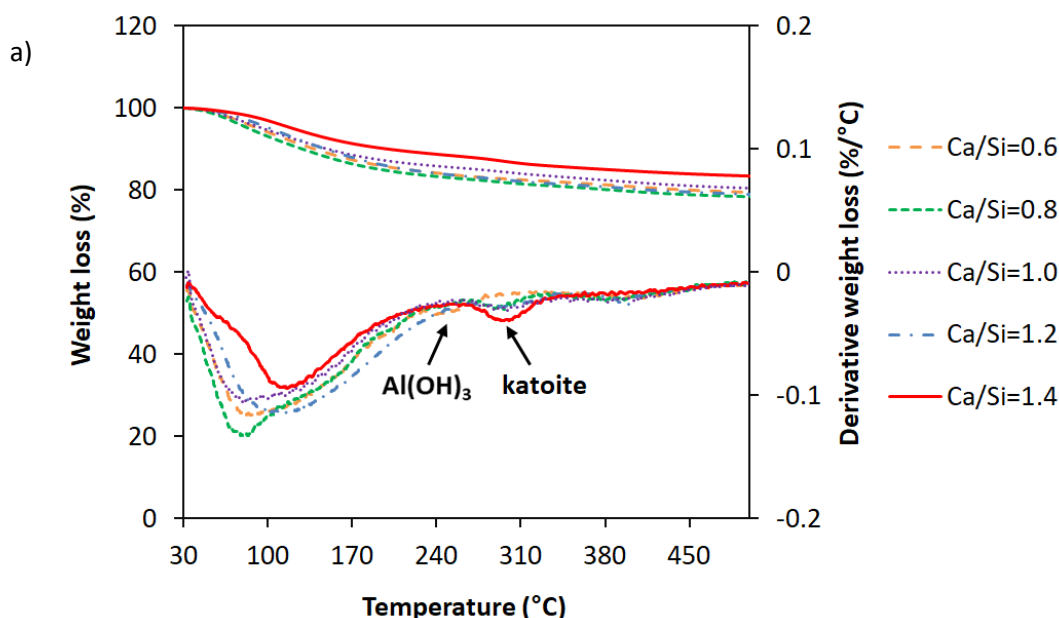
4.2 The effect of Ca/Si ratio on solid phase composition

Figure 12 illustrates the effect of target Ca/Si ratio on the phases present for samples with a) Al/Si = 0.1 and without NaOH and b) Al/Si = 0.03 and 1 M NaOH. The addition of aluminum in the absence of NaOH leads to near saturation with respect to microcrystalline $\text{Al}(\text{OH})_3$ and katoite at higher Al concentrations at target Ca/Si ratio of 0.6 and 0.8, but the solution remains undersaturated at higher Ca/Si ratios. All solutions are undersaturated with respect to katoite, although katoite has been observed in some of the samples. A similar observation (presence of katoite although the solutions were clearly understaturated) has been made by [37]

and has been related to a kinetically very slow dissolution of katoite which has formed early in the experiments. In the absence of NaOH (Figure 12a), the presence of 1.16 wt% and 0.14 wt% $\text{Al}(\text{OH})_3$ has been observed for target Ca/Si ratios of 0.6 and 0.8, respectively, while katoite was present at target Ca/Si ≥ 0.8 . The presence of 1.4 wt%, 0.95 wt%, 0.7 wt% and 1.9 wt% of katoite has been observed for target Ca/Si ratios of 0.8, 1.0, 1.2 and 1.4, respectively.

In the presence of 1 M NaOH and at high Ca/Si ratios, the presence of high amount of portlandite is observed. Due to the high pH value in 1 M NaOH solutions, portlandite is observed at target Ca/Si = 1.2 (0.9 wt%) and at target Ca/Si = 1.4 (4 wt%) (Figure 12b). In the absence of NaOH, no portlandite is observed at target Ca/Si = 1.2 and 1.4 in agreement with earlier observations [23,46]. The formation of portlandite at high NaOH concentrations and high Ca/Si ratios also explains the decrease in the dissolved calcium concentrations at increasing pH values shown in Figure 9. At Ca/Si ratios of 0.6 and 0.8 (Figure 12b), the presence of additional very broad TGA signals in the range of 250 °C to 450 °C is observed, which was tentatively assigned to the thermal decomposition of C-N-A-S-H [35] and the presence of a minor amount of portlandite.

From the measured aqueous concentrations, calculation of saturation indexes (SI) was used as an independent method to verify the presence of secondary phases in the solid samples. The SI values for different secondary phases such as portlandite, amorphous silica, microcrystalline aluminum hydroxide, strätlingite and katoite are compiled in Appendix D. All the solutions are near saturation with respect to C-S-H (the calculated SI are generally in the range of ± 0.5). In the absence of NaOH, the solution is also saturated with respect to amorphous SiO_2 at low Ca/Si (Ca/Si = 0.6) (note that amorphous silica might be present at low Ca/Si and in the absence of NaOH but cannot be detected by TGA [34]) but in all cases significantly undersaturated with respect to portlandite, in agreement with the TGA data. The presence of NaOH leads to undersaturation with respect to amorphous SiO_2 (even at Ca/Si = 0.6) and stabilizes portlandite at Ca/Si = 1.2 and 1.4, again in agreements with the TGA data.



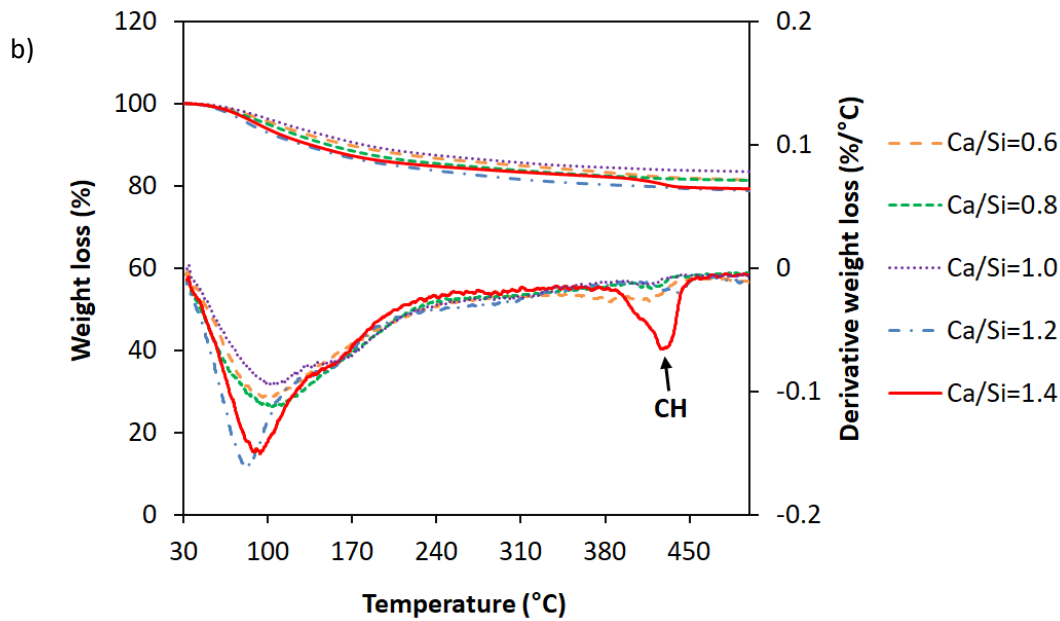


Figure 12. The TGA results for samples with different target Ca/Si ratios at a) Al/Si ratio of 0.1 without NaOH and b) Al/Si ratio of 0.03 with 1 M NaOH.

Figure 13 shows the XRD pattern for samples at Al/Si ratio of 0.03 with 1 M NaOH at different target Ca/Si ratios. At higher Ca/Si ratios, the presence of significant amount of portlandite is observed; in agreement with our observation in Figure 12. However, at low Ca/Si ratios a small amount of portlandite is also visible. The TGA results in Figure 12 also indicated the presence of very low amount of portlandite at target Ca/Si ratio of 0.6. As it is mentioned before, this can be due to non-equilibrium condition of system.

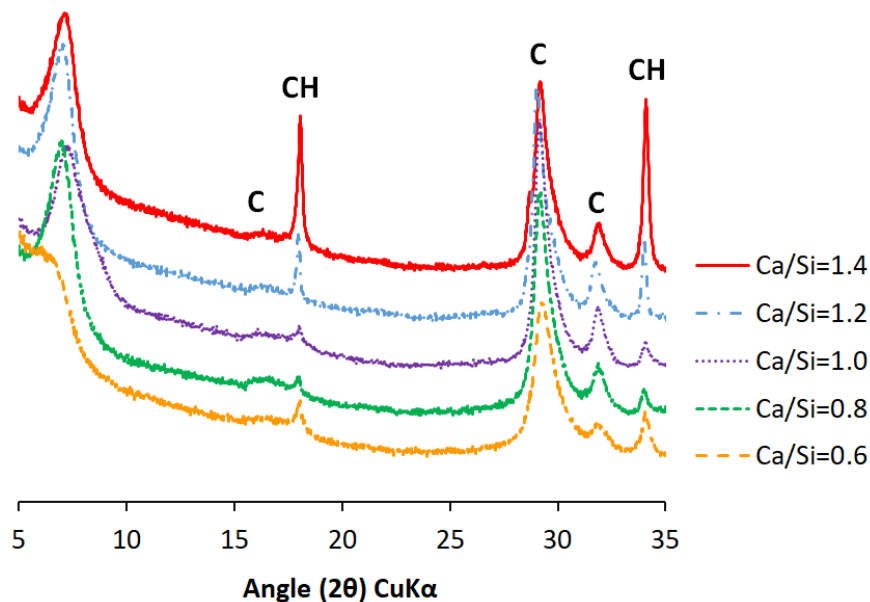


Figure 13. The XRD pattern for samples at Al/Si ratio of 0.03 with 1 M NaOH and different target Ca/Si ratios.

4.3 Conclusions

The aluminum uptake in C-S-H is influenced by the Ca/Si ratios. Increasing the Ca/Si ratio increased the Al uptake in C-S-H, while the dissolved Al concentrations decreased such that at constant Al concentration in

the solution more Al is taken up in C-S-H at higher Ca/Si ratios. This could be related to a stabilization of aluminum in the C-S-H interlayer in the presence of calcium in agreement with a recent XANES study, where the presence of Al had an ordering effect on Ca in the interlayer [29]. Moreover, at low Ca/Si ratios only Al^{IV} is present in the bridging position. However, at high Ca/Si ratios the presence of Al^{IV}, Al^V and Al^{VI} in the bridging position has been observed which provides sufficient sorption site for Al in C-S-H [45].

Solid phase analysis with TGA and XRD indicated the presence of different secondary phases at different target Ca/Si ratios. At high target Ca/Si ratios and in the presence of high NaOH concentrations, a significant amount of portlandite has been precipitated, however, at target Ca/Si ≤ 1.0 the solution was undersaturated with respect to portlandite. In the absence of NaOH, solution was undersaturated with respect to portlandite at all target Ca/Si ratios. At low Ca/Si ratios of 0.6 and 0.8 without NaOH, the presence of microcrystalline Al(OH)₃ has been observed. Furthermore, katoite was present at target Ca/Si ≥ 0.8 , although all solutions were undersaturated with respect to katoite based on the SI values.

Chapter 5 The effect of equilibration time on C-A-S-H

This chapter investigates the effect of short- and long-term equilibration time on Al uptake in C-S-H using equilibration times from 7 days to 56 days in sorption experiments and from 3 months to 3 years in co-precipitation method for C-A-S-H samples at different Ca/Si ratios, Al/Si ratio and NaOH concentrations. This chapter has been published in the Cement and Concrete Research and the information regarding the contribution of the author of this PhD thesis can be found in section 1.7.

5.1 The effect of time on secondary phases' composition

The changes in the water content of C-A-S-H and the possible presence of secondary phases with time are followed by TGA. The TGA analysis of C-A-S-H samples after different equilibration times of 7 days up to 3 years are shown in Figure 14. The water present at the surface and interlayer of C-S-H is lost over a broad temperature range up to 150 °C in agreement with different studies on C-S-H [36,79]. An additional weight loss is observed for samples after 7, 14, 28 and 56 days at ≈ 430 °C, although no crystalline phases have been detected by XRD after 3 months [58]. This weight loss has been observed previously for C-S-H in the presence of Na and Al and was tentatively assigned to an unidentified calcium sodium aluminate silicate hydrate (C-N-A-S-H) [34]. This poorly defined weight loss is absent after 2 and 3 years of equilibration and no other solids are detected by TGA and XRD [58].

The physically bound water content of C-S-H is strongly dependent on the drying procedure, duration and the relative humidity [80], resulting in some variation of the total weight loss up to 600 °C, as shown in Figure 14. Based on the TGA data the H_2O/Si ratios have been calculated and compiled in Appendix B. Despite some variation of the underlying data, the H_2O/Si ratios are around 1.05 ± 0.15 for equilibration times from 7 days up to 2 years, however, a bit lower (0.85) after 3 years equilibration.

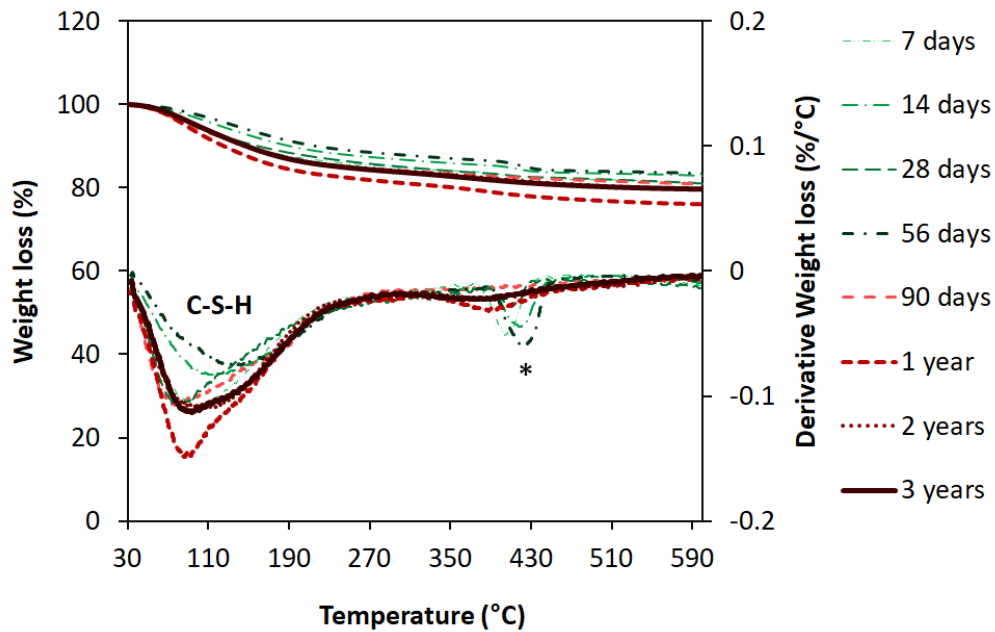
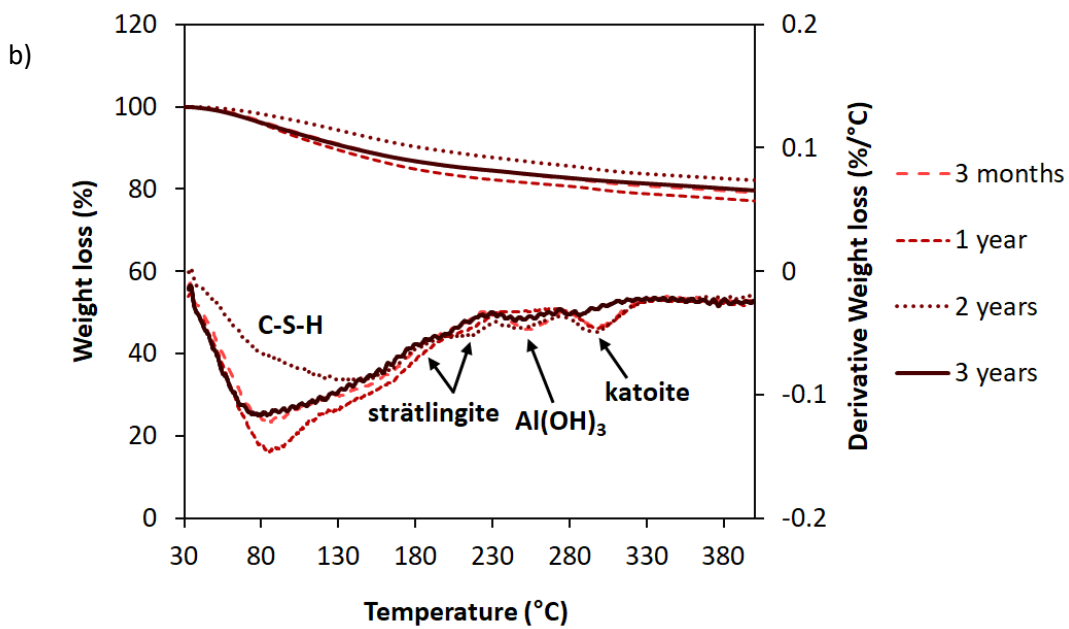
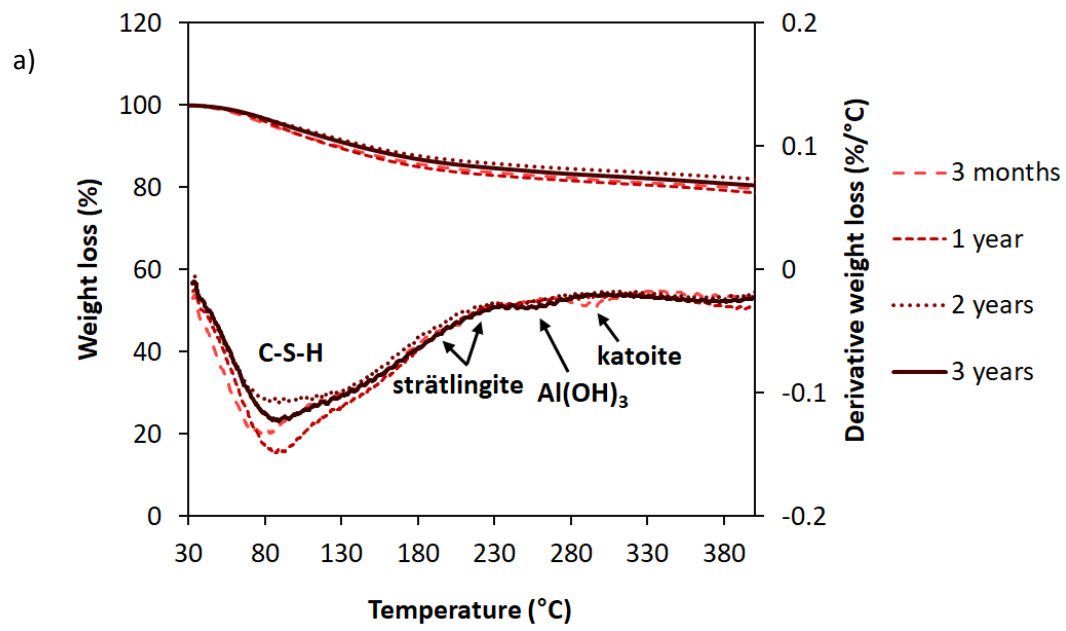


Figure 14. TGA of C-A-S-H after different equilibration times for Ca/Si = 0.8 and 1 M NaOH. (*: signals assigned to an unidentified calcium sodium aluminate silicate hydrate (C-N-A-S-H) phase [34]).

The presence of Al could also lead to the formation of secondary phases containing Al. Microcrystalline $\text{Al}(\text{OH})_3$ and strätlingite are observed by TGA mainly at low Ca/Si ratios and in the absence of NaOH, katoite mainly at higher Al contents but at all Ca/Si ratio and pH values (Appendix B). In addition, the formation of zeolites or zeolitic precursor like Ca-gismondine ($\text{CaAl}_2\text{Si}_2\text{O}_8 \cdot 4.5\text{H}_2\text{O}$) and chabazite ($\text{CaAl}_2\text{Si}_4\text{O}_{12} \cdot 6\text{H}_2\text{O}$) at low Ca/Si ratios and in the absence of alkali and OH-sodalite ($\text{Ca}_8\text{Al}_6\text{Si}_6\text{O}_{24}(\text{OH})_2 \cdot 2\text{H}_2\text{O}$) at low Ca/Si ratios and high NaOH concentrations cannot be excluded, although they are not clearly observed by TGA or XRD, as at Ca/Si = 0.6 some solutions are moderately oversaturated with respect to sodalite and at Ca/Si = 0.8 with respect to gismondine and chabazite (Appendix D). The TGA signal of the samples without alkali at Ca/Si ratio of 0.8 is also shown in Figure 15a and 15b and at Ca/Si = 1.4 in Figure 15c. While no or very little secondary phases are observed at Al/Si of 0.03 or lower, secondary phases are present at higher Al/Si ratios in agreement with the observation of L'Hopital et al. [23]. Figure 15 shows that increasing the equilibration time from 3 months to 3 years for samples with Al/Si of 0.1 and 0.2 leads to a decrease in the amount of secondary phases such as strätlingite, aluminum hydroxide and katoite. At Ca/Si = 0.8 and Al/Si = 0.1, 1.4 wt% katoite is observed after 3 months equilibration and decreased to a non-detectable level after 3 years, while the solution remains undersaturated. Similarly at Al/Si = 0.2, increasing the equilibration time from 3 months to 3 years leads also to a decrease in the amount of $\text{Al}(\text{OH})_3$ (from 1.4 wt% to 0.29 wt%) and katoite (from 2.1 wt% to 0.18 wt%) (Figure 15b). At Ca/Si of 0.8, an increase in equilibration time from 1 year to 3 years at Al/Si = 0.2 decreases the amount of strätlingite from 0.58 wt% to a non-detectable level. Also at Ca/Si ratio of 1.4 (Figure 15c), the amount of katoite decreases from 1.9 wt% after 3 months to a non-detectable level after 1 year (around 0.28 wt%).



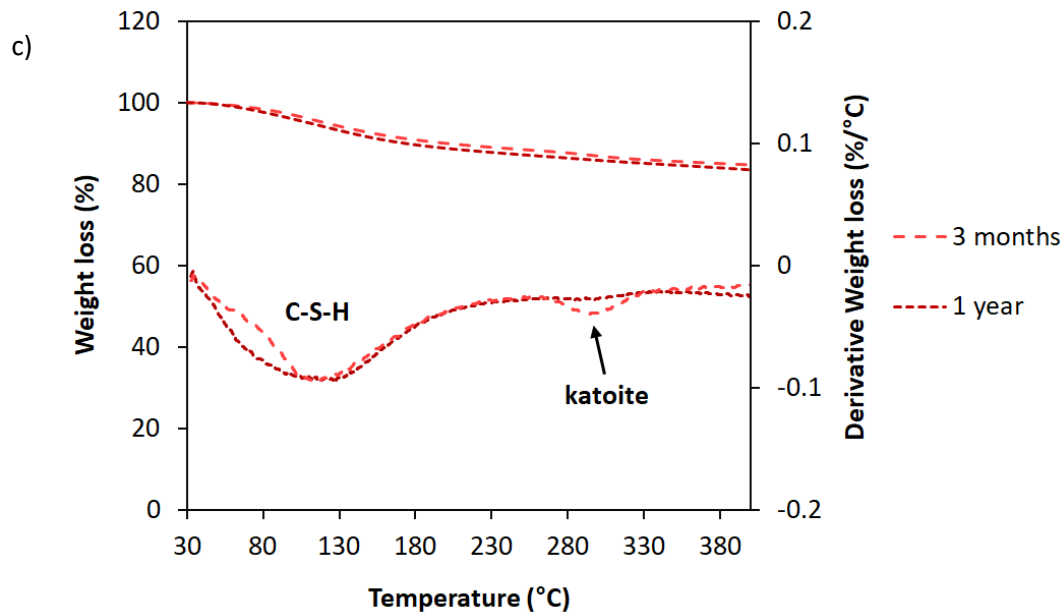


Figure 15. The effect of equilibration time on the composition of secondary phases in the absence of NaOH for a) Ca/Si = 0.8 & Al/Si = 0.1; b) Ca/Si = 0.8 & Al/Si = 0.2 and c) Ca/Si = 1.4 & Al/Si = 0.1.

The XRD pattern of C-A-S-H samples at Ca/Si = 0.8 and Al/Si = 0.1 in the absence of NaOH is shown in Figure 16. A trace of strätlingite and $\text{Al}(\text{OH})_3$ is observed only after 3 months equilibration. In addition, the presence of katoite is observed after 3 months and 1 year equilibration, however, it disappears after 2 and 3 years. The decrease in the quantity of katoite with time is in agreement with TGA results as shown in Figure 15a. L'Hopital et al. also observed katoite in addition to C-A-S-H phases after 6 months equilibration and suggested that katoite has formed initially from strongly oversaturated solutions and its quantity decreased with time for C-A-S-H at Al/Si = 0.1 as the solution was undersaturated with respect to katoite at the time studied [37]. The SI, in Appendix D, also show more negative values for strätlingite, $\text{Al}(\text{OH})_3$ and katoite with an increase in time. The SI values for a same Ca/Si and Al/Si ratio decrease with increasing the equilibration time, which is consistent with the decrease in the content of secondary phases with time. For example, for samples without alkali for Ca/Si ratio of 0.8 the SI values for $\text{Al}(\text{OH})_3$ decrease from -0.6 to -1.8 and from -0.5 to -1.8 when moving from 3 months to 1 year equilibration for Al/Si ratios of 0.1 and 0.2, respectively. The observed destabilization of $\text{Al}(\text{OH})_3$, strätlingite and katoite with time as reported in [23,37] and in the present study, indicates consistently an increased uptake of aluminum in a thermodynamically more stable C-A-S-H phase with time.

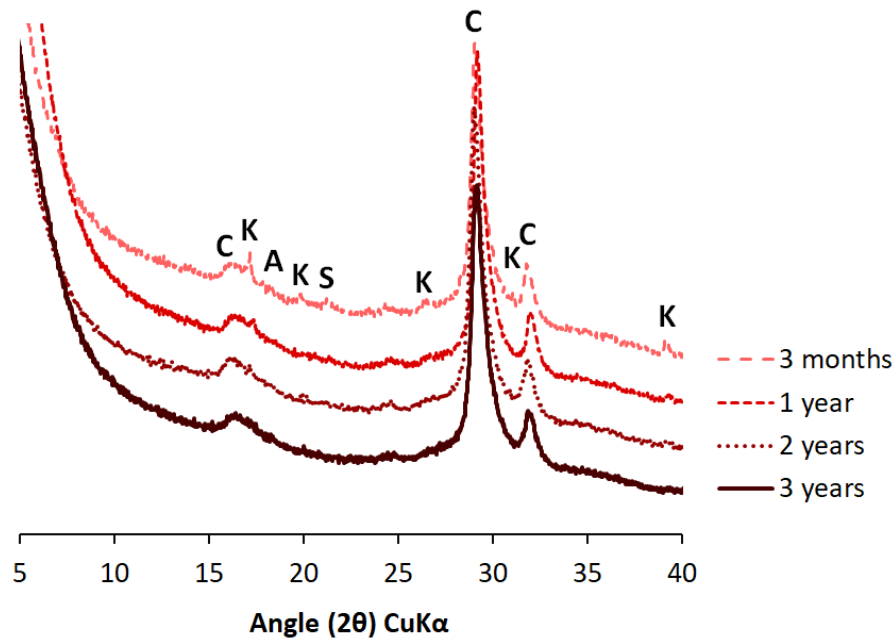


Figure 16. The XRD pattern of C-A-S-H as a function of equilibration time in the absence of NaOH for Ca/Si = 0.8 and Al/Si = 0.1 (C: C-A-S-H, K: katoite, A: Al(OH)₃, S: strätlingite).

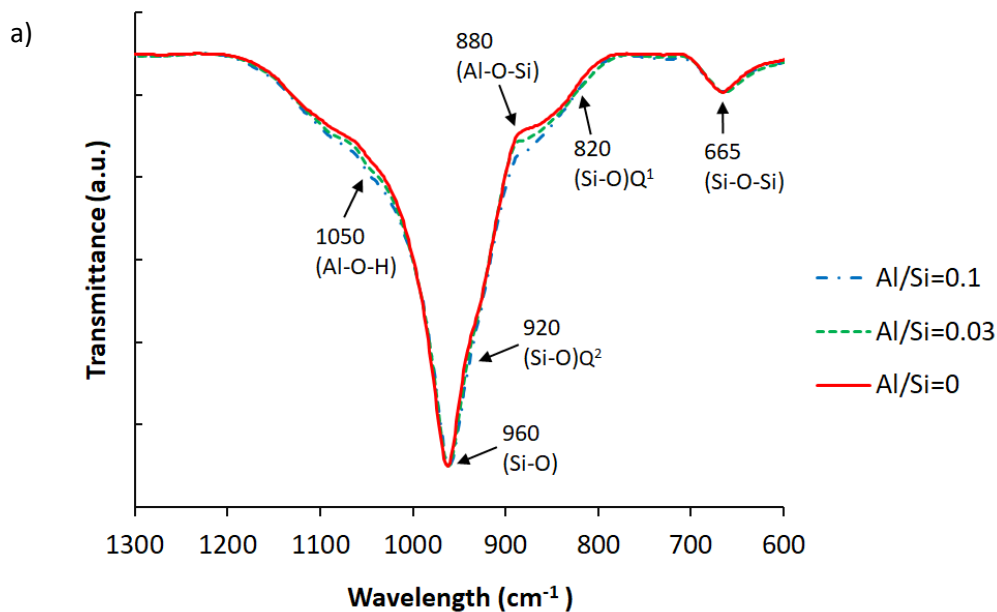
5.2 The effect of time on C-A-S-H structure

The changes in the structure of C-A-S-H are investigated by FTIR for the samples with Ca/Si ratios of 0.8 and 1.2. All the FTIR spectra show absorption bands at 1300-850 cm^{-1} , which are typical for aluminosilicates and assigned to the asymmetric and symmetric stretching vibration of Si-O-Si and Si-O-Al bonds in $[\text{SiO}_4]^{4-}$ and $[\text{AlO}_4]^{5-}$ [81–83]. The signal observed at around 665 cm^{-1} is assigned to Si-O-Si bending vibrations and water librations and shows little variations with Ca/Si [84–89]. The signal at 820 cm^{-1} is related to Si-O stretching of Q^1 tetrahedra and is more intense at high Ca/Si ratios. The main signal ranging from 900 to 1200 cm^{-1} is assigned to the stretching and deformation or bending vibration of the Si-O bands [90]. The band centered in the range of 960-970 cm^{-1} has often been attributed to Q^2 silica units of C-S-H [89,91,92]. However, a recent publication highlighted that the several bands contribute to that band at around 960 cm^{-1} [90]. Two bands at ~920 cm^{-1} and ~1060 cm^{-1} are associated with Q^2 silicate species, and a third band at ~1005 cm^{-1} is attributed to Q^1 silicate species [90]. This is also in agreement with the observation of Yu et al. [89], where a higher intensity of shoulder above 1000 cm^{-1} was established at higher Ca/Si ratios. Bands in the range of 500-750 cm^{-1} can be assigned to the stretching vibrations of Al-O bonds of the octahedrally coordinated Al, and bands in the range of 750-900 cm^{-1} to the vibrations of Al-O bond in AlO_4 units [93]. The band at about 880 cm^{-1} has been associated with the stretching vibration of Al-O-Si (terminal bond) [94]. The symmetric bending of Al-O-H have been reported in the range of 1034-1075 cm^{-1} [95–97]. The assignment of different bands is also summarized in Table 3.

Table 3. Assignment of FTIR spectra for C-A-S-H samples.

FTIR Absorption band (cm^{-1})	Assignment of Vibration	Reference
500-750	Al-O stretching vibrations of octahedrally coordinated Al	[93]
661 and 906	Al-O stretching vibrations in $\text{Al}(\text{OH})_3$	[98]
665	Si-O-Si bending vibrations	[84–89]
709, 710, 855, 860, 911, 913, 965, 970, 1016 and 1020	Si-O-Al in strätlingite	[99–101]
750-900	vibrations of Al-O bond in AlO_4 units	[93]
820	Si-O stretching of Q^1 tetrahedra	[84–89]
850-1300	asymmetric and symmetric stretching vibration of Si-O-Si and Si-O-Al bonds in $[\text{SiO}_4]^{4-}$ and $[\text{AlO}_4]^{5-}$	[81–83]
880	stretching vibration of Al-O-Si	[94]
900-1200	stretching or bending vibration of Si-O bands (Q^1 and Q^2)	[90]
914-918	OH bending vibrations in Al–OH–Al bonds (octahedral aluminum)	[84]
1034-1075	symmetric bending of Al-O-H	[95,97,98]

Figure 17 shows the FTIR spectra for samples with Ca/Si ratio of 0.8 with no Al and with 0.03 and 0.1 Al/Si ratio in the absence of NaOH. The intensity of the shoulders at 880 cm^{-1} and 1050 cm^{-1} increases with increasing Al/Si ratios indicating the presence of more Al in C-A-S-H by increasing the Al contents. Moreover, the intensity of the shoulder for Si-O stretching vibration of Q^2 sites at 920 cm^{-1} increases with increasing Al content, as is visible in Figure 17a, which could be related to the replacement of silica in the Q^2 sites by Al.



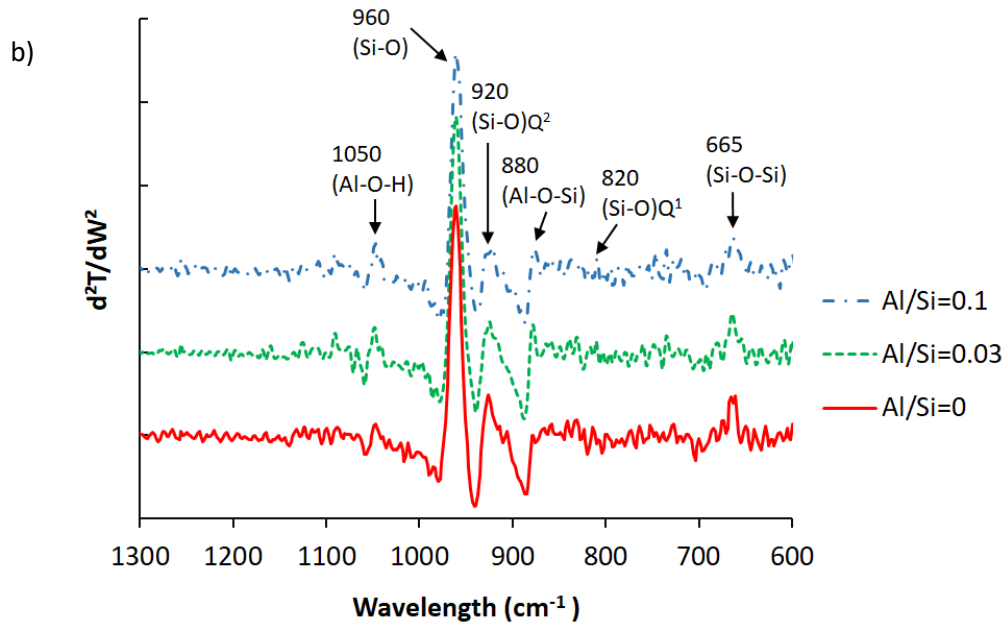
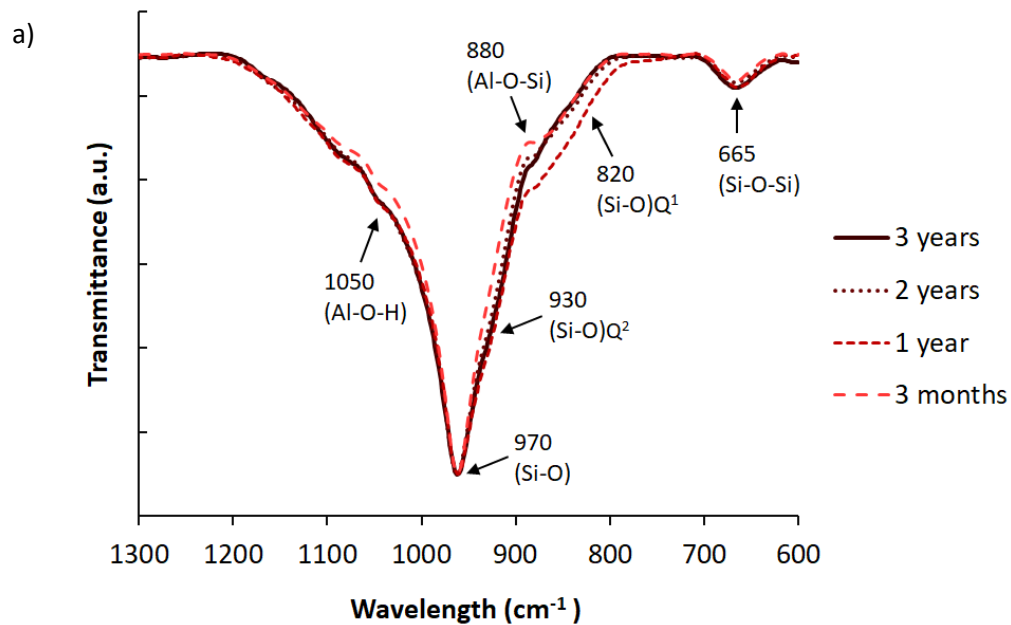


Figure 17. The FTIR spectra for C-A-S-H samples without alkali at Ca/Si = 0.8 for 2 years equilibration and different Al/Si ratios; a) transmittance (T) vs. wavelength (W) and b) 2nd derivative of the transmittance d^2T/dW^2 vs. wavelength.

The effect of equilibration time on C-A-S-H composition is represented in Figure 18 for samples without alkali for Ca/Si ratio of 0.8 and Al/Si ratio of 0.2. The main difference is observed in the intensity of the Al-O-H shoulder at around 1050 cm^{-1} which increases with longer equilibration time indicating a rearrangement of the Al over time (Figure 18a). Moreover, the intensity of Si-O stretching of Q² sites at 930 cm^{-1} increases with equilibration time, which could indicate longer silica chains with time. No clear changes are observed in the intensities of other signals.



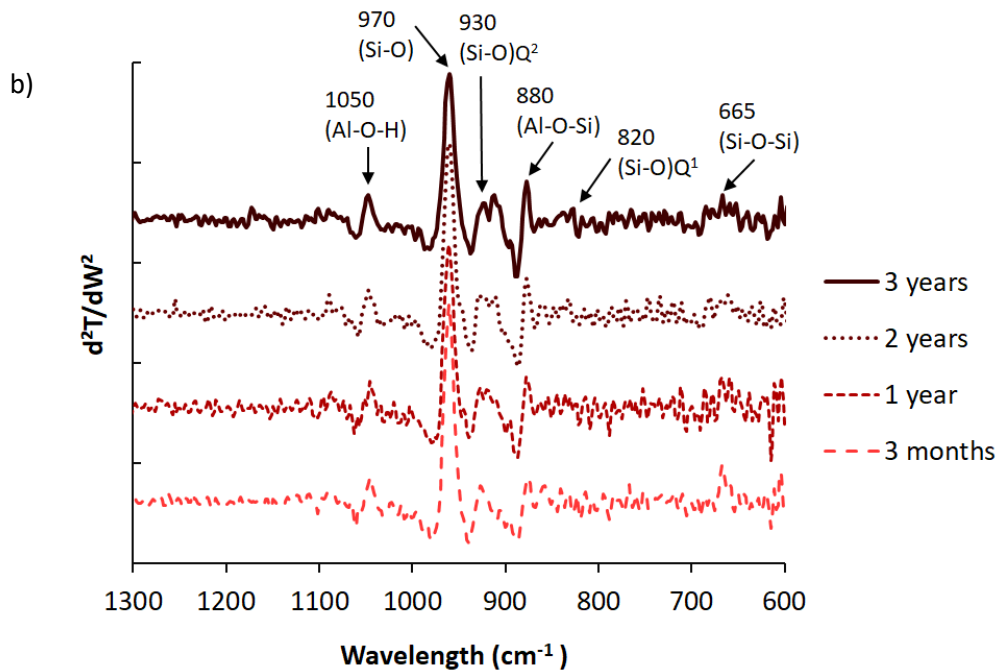
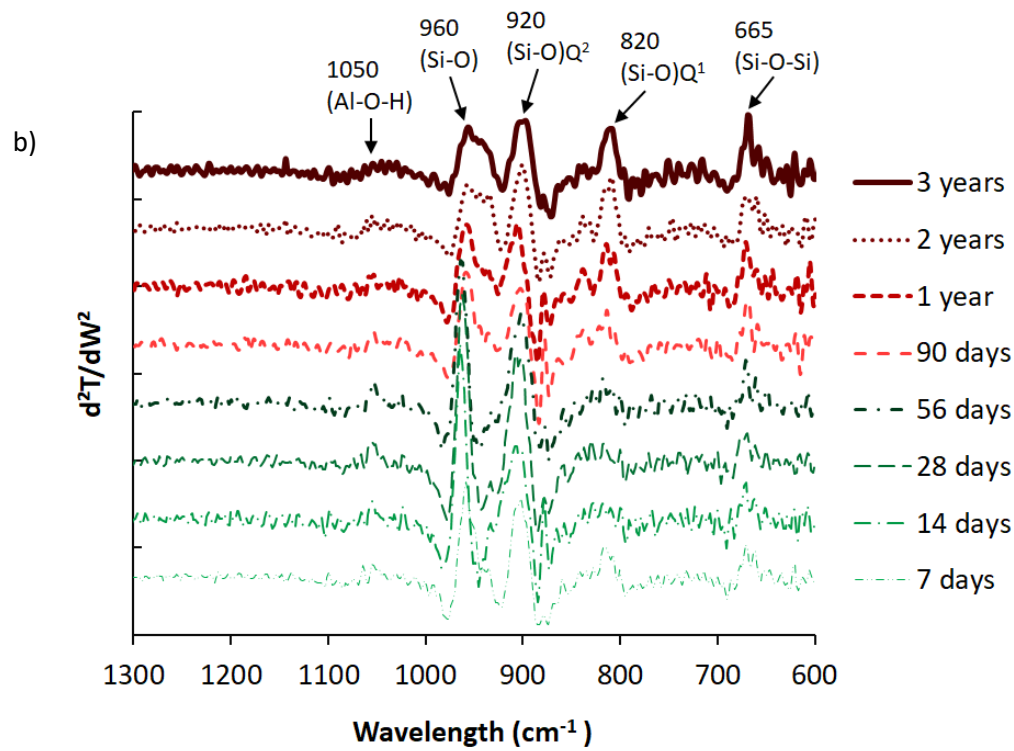
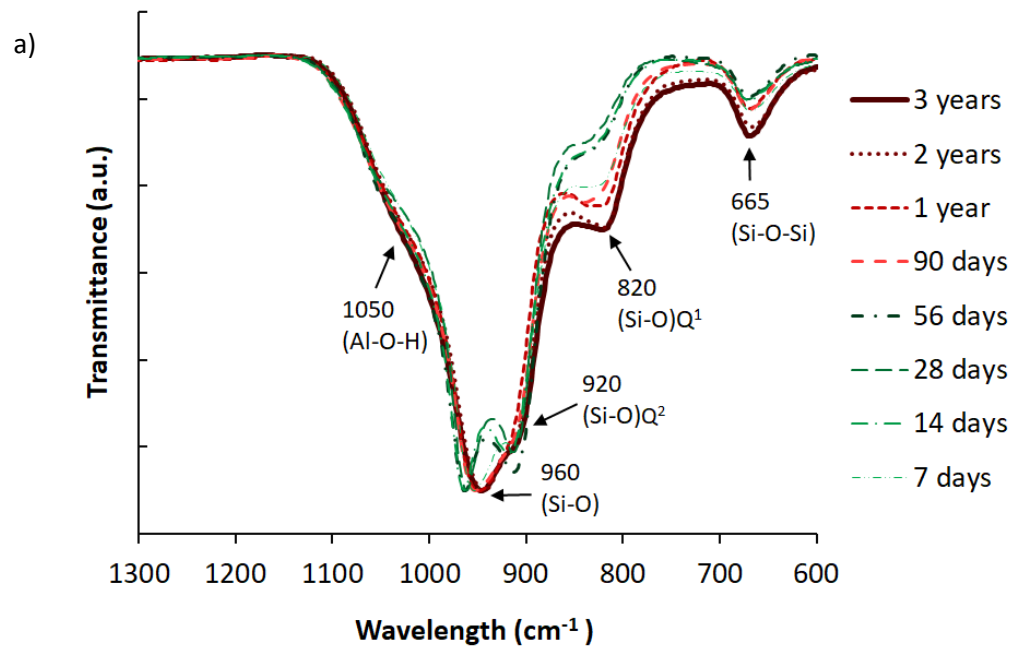


Figure 18. The FTIR spectra for C-A-S-H samples without alkali at Ca/Si = 0.8 and Al/Si = 0.2 after different equilibration times: a) transmittance (T) vs. wavelength (W) and b) 2nd derivative of the transmittance d^2T/dW^2 vs. wavelength.

Figure 19 shows the effect of equilibration time on C-A-S-H structure in the presence of 1 M NaOH for Ca/Si ratios of a, b) 0.8 and c, d) 1.2. At Ca/Si of 0.8, the intensity of (Si-O)Q¹ peak at 820 cm⁻¹ is higher than in the alkali-free samples (Figure 18) indicating the presence of more end-of-chain-SiO₂ groups and thus shorter silica chain length in the presence of high alkali hydroxide concentrations, in agreement with Si-NMR observations of similar samples [19,34,102]. At Ca/Si of 1.2, the intensity of the band at 820 cm⁻¹ is higher, consistent with the shorter silica chain length expected at higher Ca/Si ratios. For both Ca/Si ratios of 0.8 and 1.2, the intensity of (Si-O) Q¹ peak at 820 cm⁻¹ increases with an increase in equilibration time. At Ca/Si = 0.8, the signal of Si-O stretching vibration at around 960 cm⁻¹ shows a splitting into two signals at low equilibration times up to 56 days, while at later times only one signal is observed. Such a splitting of the signal can indicate a low symmetry [103]. When structural sites are present as groups of nonequivalent sites, it results in a splitting of the absorption bands indicating a low symmetry. The disappearance of this signal splitting with time indicates that environment becomes more symmetric with time, which suggests a structural rearrangement in the C-A-S-H at least up to 90 days. The Si-O stretching vibration around 960 cm⁻¹ and 920 cm⁻¹ moves to a lower wavelength with time for Ca/Si ratios of 0.8 and 1.2, respectively. Also the intensity of signal at around 665 cm⁻¹, which is related to Si-O-Si vibrations and water librations [89], decreases with time which could indicate a restructuring of the water with time in the C-A-S-H structure. Less clear changes are observed at Ca/Si = 1.2, indicating that less rearrangement occurs at higher Ca/Si ratios which is consistent with the observations in the liquid phase as discussed in section 5.4.



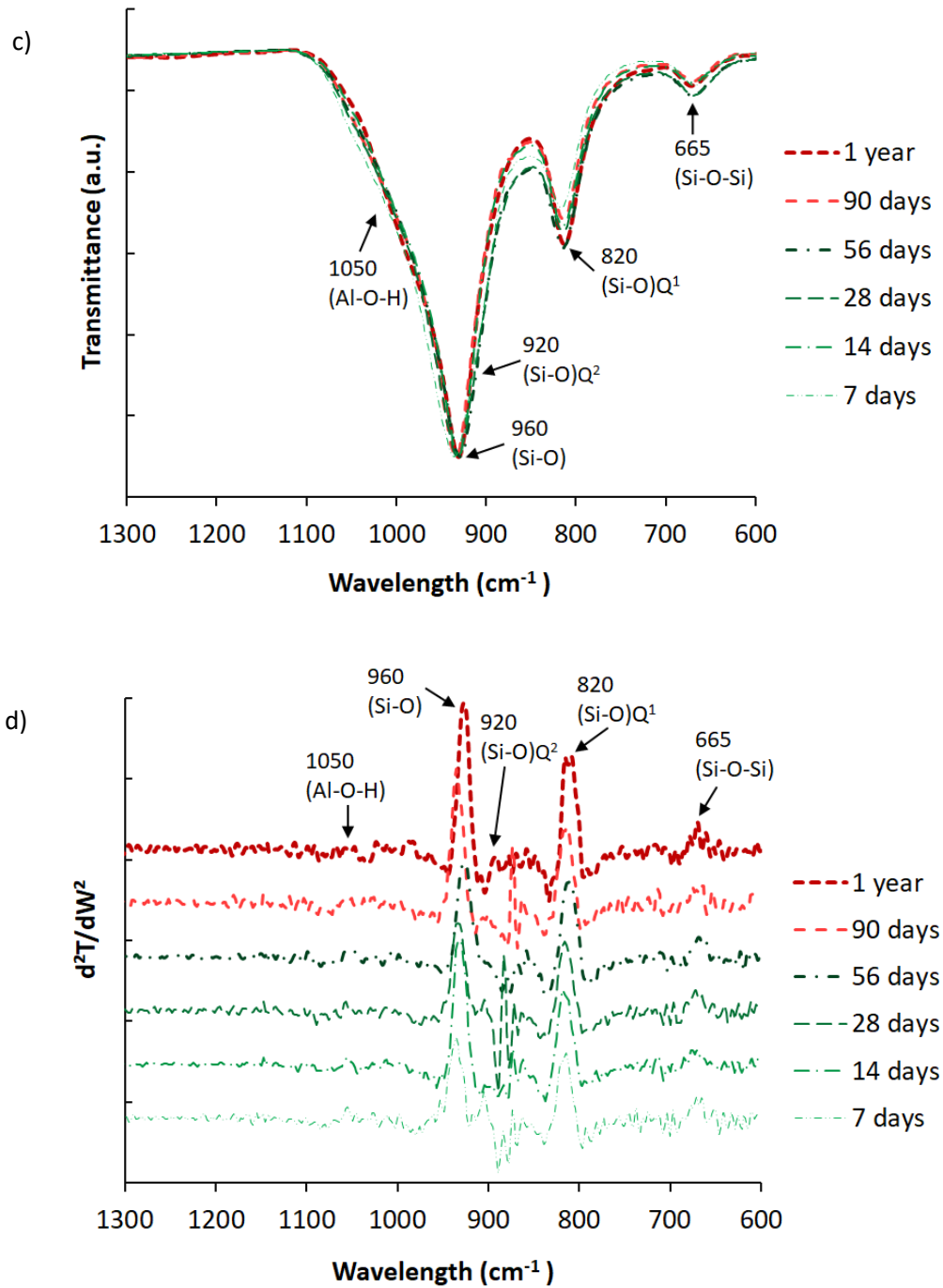


Figure 19. The FTIR spectra for C-A-S-H samples in the presence of 1 M NaOH for Al/Si = 0.03 and different equilibration times: a) transmittance (T) vs. wavelength (W) for Ca/Si = 0.8; b) 2nd derivative of the transmittance d²T/dW² vs. wavelength for Ca/Si = 0.8; c) transmittance (T) vs. wavelength (W) for Ca/Si = 1.2 and d) 2nd derivative of the transmittance d²T/dW² vs. wavelength for Ca/Si = 1.2.

5.3 The effect of time on Al uptake in C-S-H

The effect of equilibration time on Al uptake in C-S-H for Ca/Si ratios of 0.8 and 1.2 for samples containing 1 M NaOH is shown in Figure 20. For both Ca/Si ratio of 0.8 and 1.2, the Al concentrations seem quite constant between 7 to 28 days, but decrease clearly after 56 days, i.e. at the time when the FTIR spectra indicate a clear structural rearrangement as shown in Figure 19. This indicates an increase in Al uptake in C-S-H over time at both Ca/Si ratios. Little further change in Al concentrations is observed at Ca/Si = 1.2 between 3

months and 1 year equilibration time indicating that a (meta)stable equilibrium might have been reached. In contrast, for $\text{Ca/Si} = 0.8$ the Al concentrations in solution continue to decrease, albeit more slowly, up to 3 years equilibration, indicating that equilibrium is reached slower at low Ca/Si than at high Ca/Si ratios.

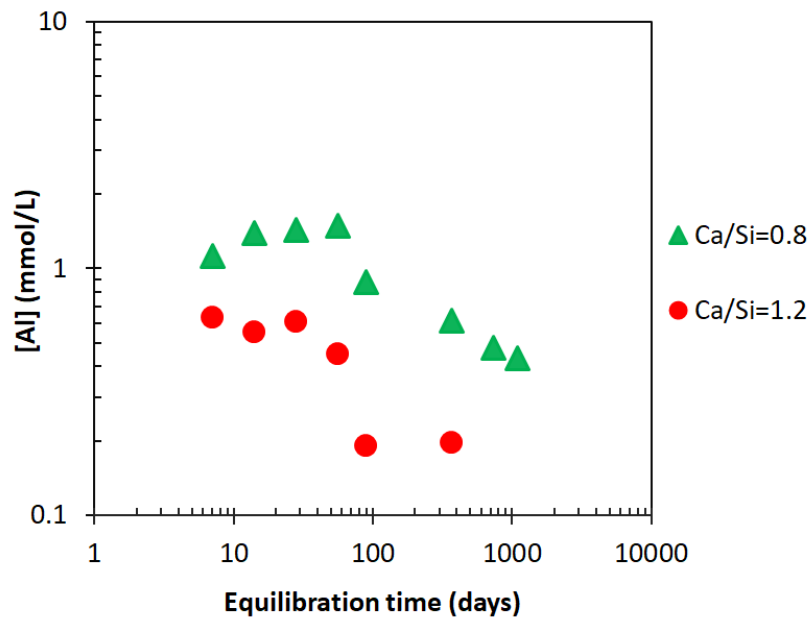
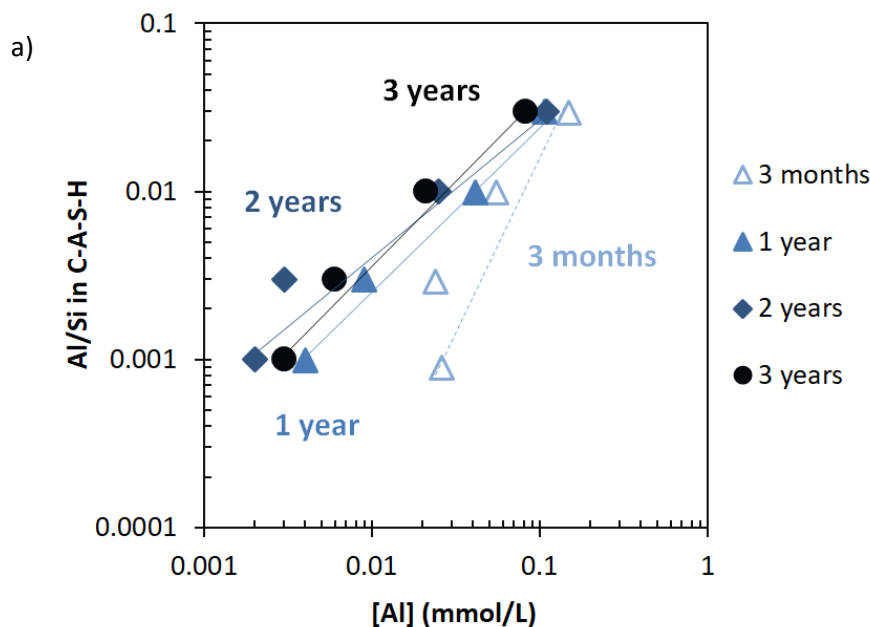


Figure 20. The effect of equilibration time on the Al concentrations in solution for Ca/Si ratios of 0.8 and 1.2 in the presence of 1 M NaOH. (The errors are smaller than the symbols' size).

This very slow ripening at low Ca/Si is visible in the presence of a) 0.1 M NaOH; b) 0.5 M NaOH and c) 1 M NaOH as shown in Figure 21, where the Al uptake in C-S-H for the Ca/Si ratio of 0.8 is plotted from 3 months to 3 years. In agreement with results discussed above, the decrease of Al concentrations and hence the uptake of Al in C-S-H accelerate over time. Increasing the equilibration time from 3 months to 1 year leads to a more distinct lowering of Al concentrations compared to the change from 1 year to 2 years. In fact, little changes in the Al concentrations are observed between 2 and 3 years equilibration indicating that the reaction of Al with C-S-H is approaching a metastable equilibrium after 2 years.



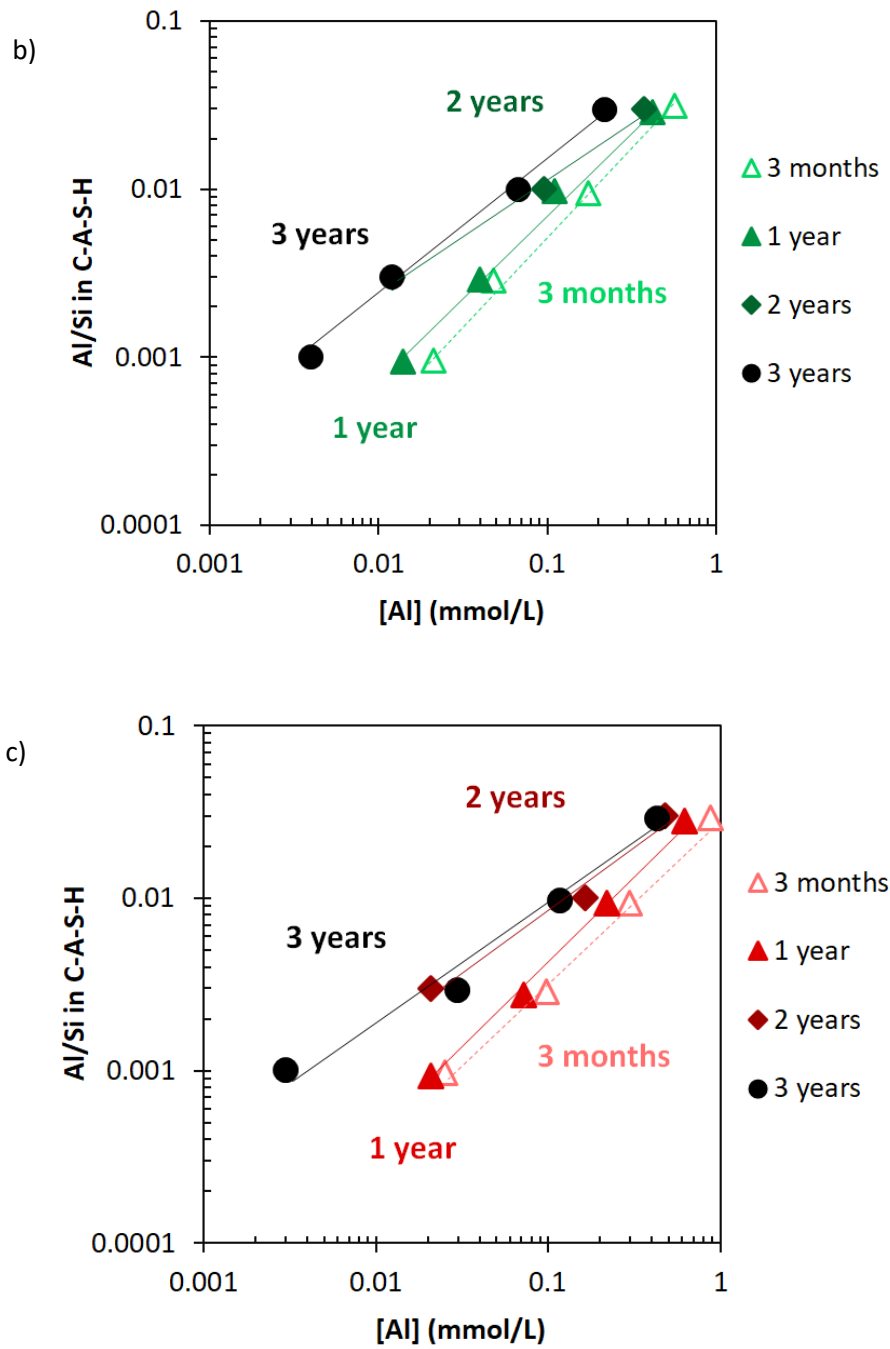
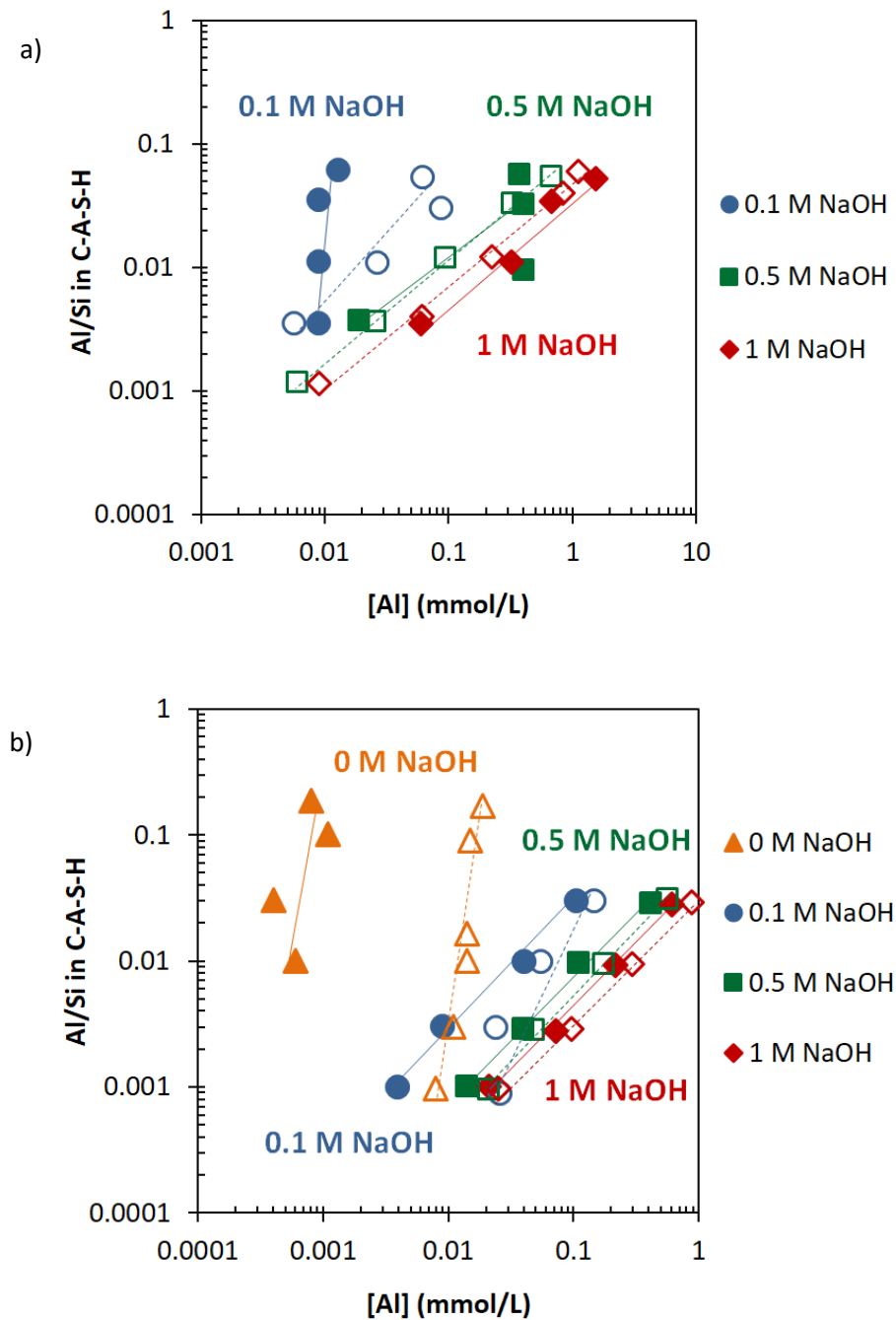


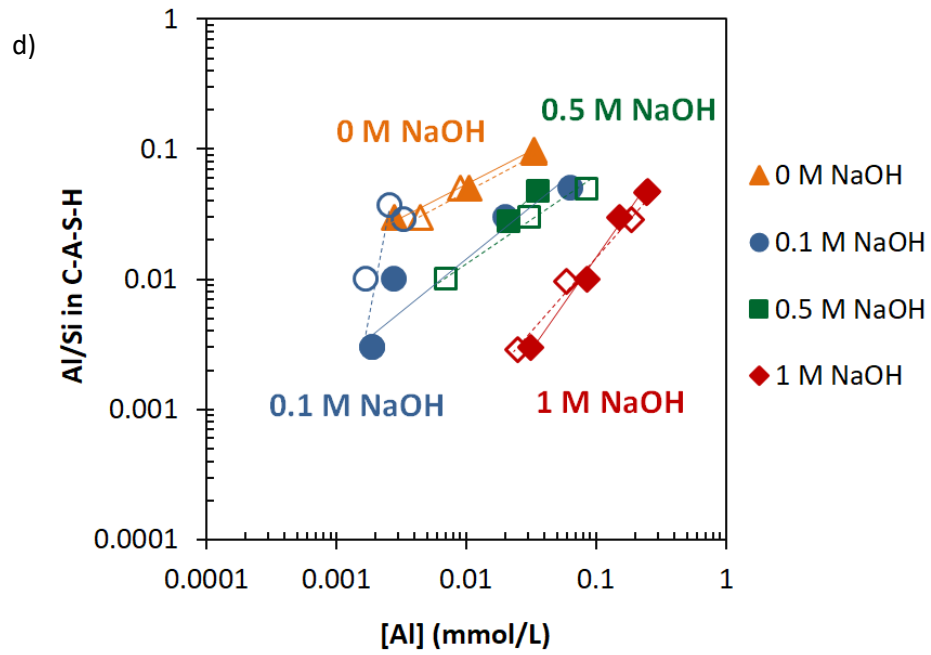
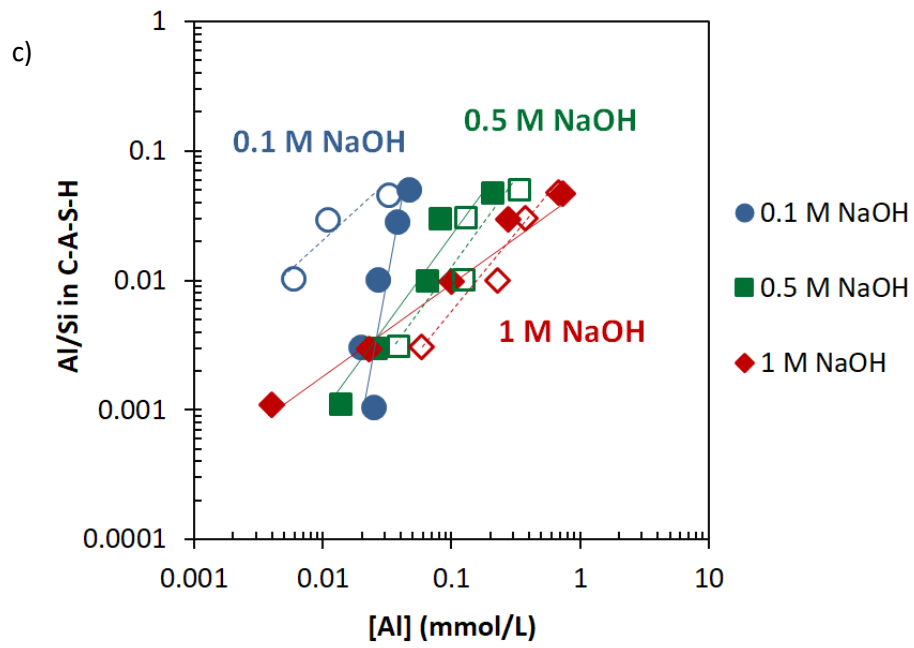
Figure 21. The Al sorption isotherm on C-A-S-H for Ca/Si = 0.8 recorded after different equilibration times for a) 0.1 M NaOH; b) 0.5 M NaOH and c) 1 M NaOH. The darkness of colors indicates an increase in equilibration time; 3 months indicated by the lightest and 3 years represented by the darkest symbols. (The lines serve as eye-guides only and the errors are smaller than the symbols' size).

5.4 The effect of NaOH, Ca/Si ratio and time on Al sorption isotherm

Figure 22 shows the effect of equilibration time on the Al uptake in C-S-H at five different Ca/Si ratios of a) 0.6; b) 0.8; c) 1.0; d) 1.2 and e) 1.4. It can be seen (Figure 22a-c) that at Ca/Si ratios of 0.6, 0.8 and 1.0, the aluminum concentrations decrease significantly with increasing the equilibration time from 3 months to 1 year. However, at higher Ca/Si ratios of 1.2 and 1.4 (Figure 22d and 22e) the Al concentrations in solution do not change significantly with time.

Moreover, the change in Al concentrations over time is more distinct at lower NaOH concentrations compared to higher concentrations. In fact, for an increase in equilibration time from 3 months to 1 year the relative decrease in Al concentrations is higher for no alkali and 0.1 M NaOH, however, it is less in the presence of 0.5 M and 1 M NaOH. Since Al concentrations in solution are higher in the presence of higher NaOH concentrations (0.5 and 1 M), the changes in the concentrations over time are less visible. The measured concentrations of Al, Ca, Si and OH^- in solution are compiled in Appendix C.





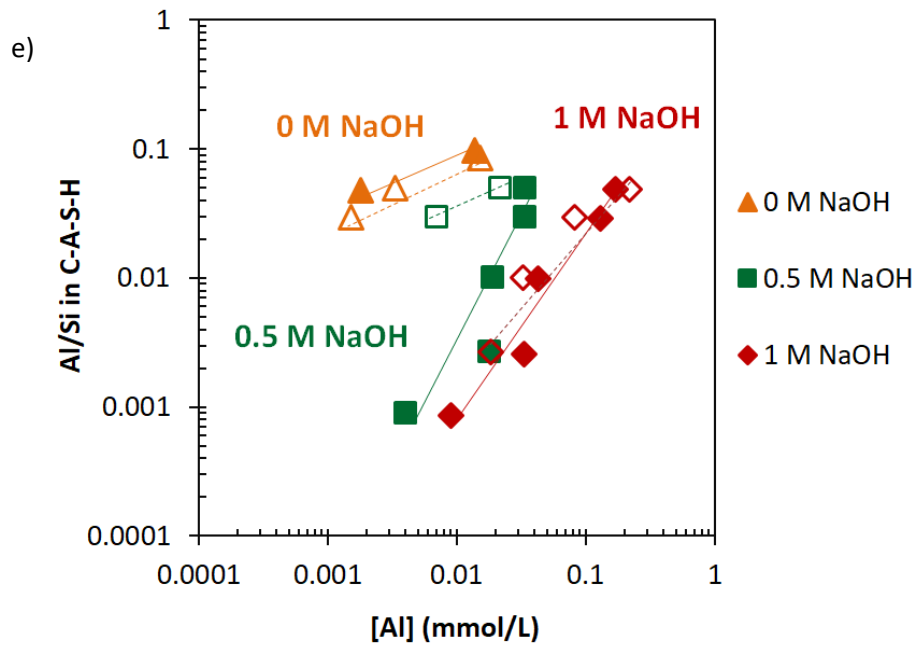


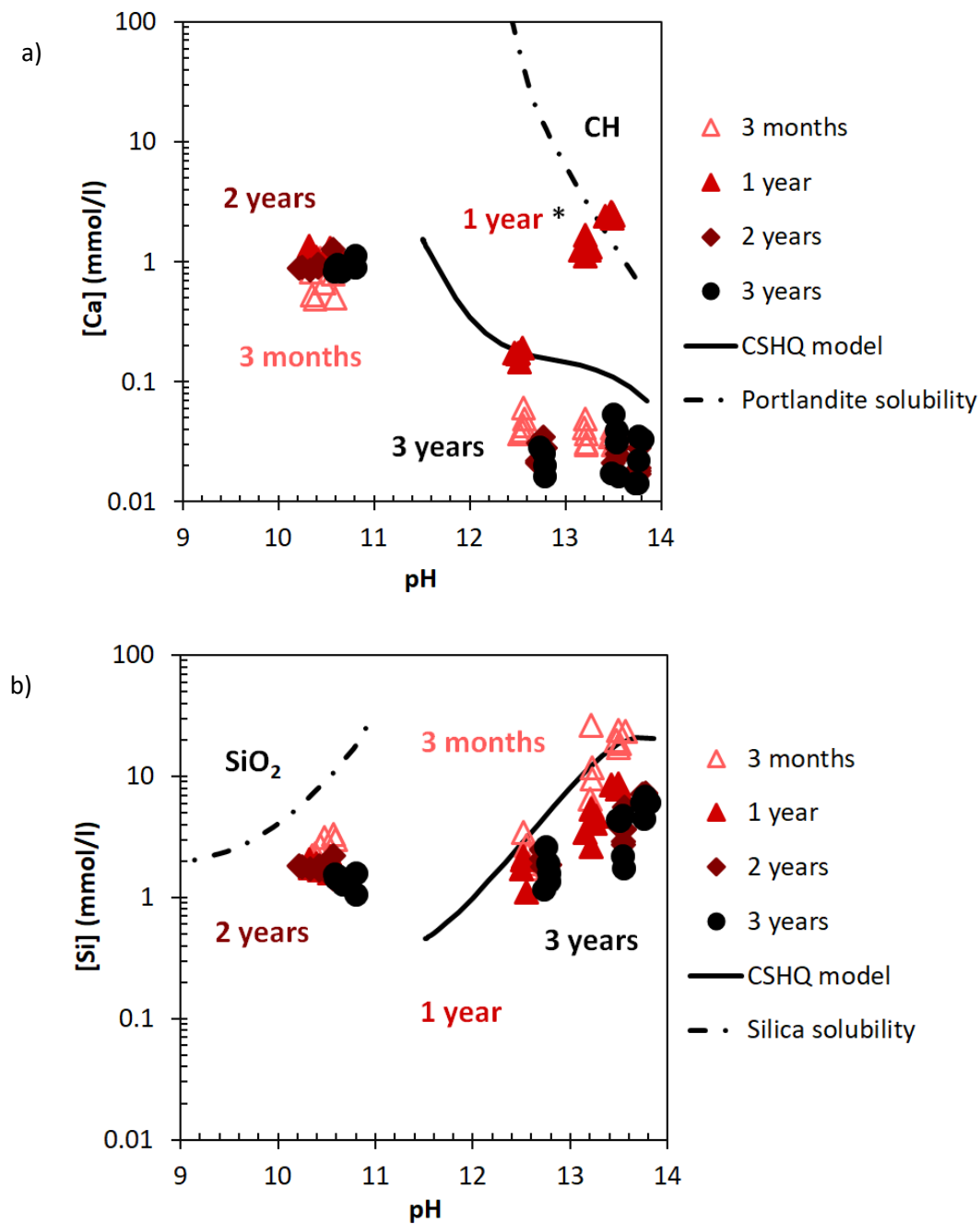
Figure 22. The effect of equilibration time on Al uptake in C-S-H for Ca/Si ratios of a) 0.6; b) 0.8; c) 1.0; d) 1.2 and e) 1.4 at 0, 0.1, 0.5 and 1 M NaOH. The 3 months samples are indicated by the empty and 1 year represented by the full symbols. (The lines serve as eye-guides only and the errors are smaller than the symbols' size).

5.5 The effect of time on aqueous phase composition

The results presented above, in particular, the disappearance of secondary Al containing phases with time and the decrease of Al concentrations in solution with time in the absence of secondary phases indicate the slow formation of thermodynamically more stable C-A-S-H phase with time. The effect of equilibration time on the concentrations of Ca and Si in solution at Ca/Si ratios of a) 0.8 and b) 1.2 is shown in Figure 23 (data for the other Ca/Si ratios are shown in Appendix G). The data measured at different Ca/Si ratios and at 0 to 0.1 Al/Si ratios are plotted as symbols as a function of pH and compared to the expected solubility of C-S-H using CSHQ model [47] indicated by lines. The measured values deviate to some extent from the modelled data, since the CSHQ model was developed based on data for alkali-free C-S-H only [47,57] and needs to be further extended to describe the changes at high pH values and the uptake of alkalis in C-S-H as discussed in L'Hopital et al. [34].

In the absence of alkali hydroxide the Si and Ca concentrations do not vary significantly with time. At low Ca/Si ratios of 0.6 (Figure 39a in Appendix G) and 0.8 (Figure 23a), no significant changes are observed in the Ca and Si concentrations in the absence of alkali hydroxide. The saturation indexes (SI) calculated from the measured concentrations indicate that the solution is near to saturation with respect to C-S-H in all cases. The solution is generally undersaturated with respect to amorphous SiO_2 (with the exception of Ca/Si = 0.6 without NaOH), microcrystalline $\text{Al}(\text{OH})_3$, katoite and strätlingite indicating that these phases will dissolve in solution if precipitated initially. The SI values for different phases are presented in Appendix D. At high alkali concentrations ($12 < \text{pH} < 14$) and at Ca/Si = 0.8, however, the Si concentrations slightly decrease in particular from 3 months to 1 year (Figure 23b). Little variation with time is observed for Ca, with the exception of the outlier values after 1 year for Ca/Si = 0.8 at 0.1, 0.5 and 1 M NaOH, where might some contaminations had occurred prior to the Ca measurements). The observed changes in Si concentrations at high alkali concentrations can be associated to the disappearance of an unidentified calcium sodium aluminate silicate hydrate (C-N-A-S-H) phase with time, which is only observed at high alkali concentrations [34].

At high Ca/Si ratios of 1.0, 1.2 and 1.4 ($\text{Ca/Si} \geq 1.0$), the changes in Si and Ca concentrations in solution are small as shown in Figure 23c and 23d (and Figure 39c-f in Appendix G). At $\text{Ca/Si} = 1.4$ and high pH values, the Ca concentrations are also limited by the possible presence of portlandite.



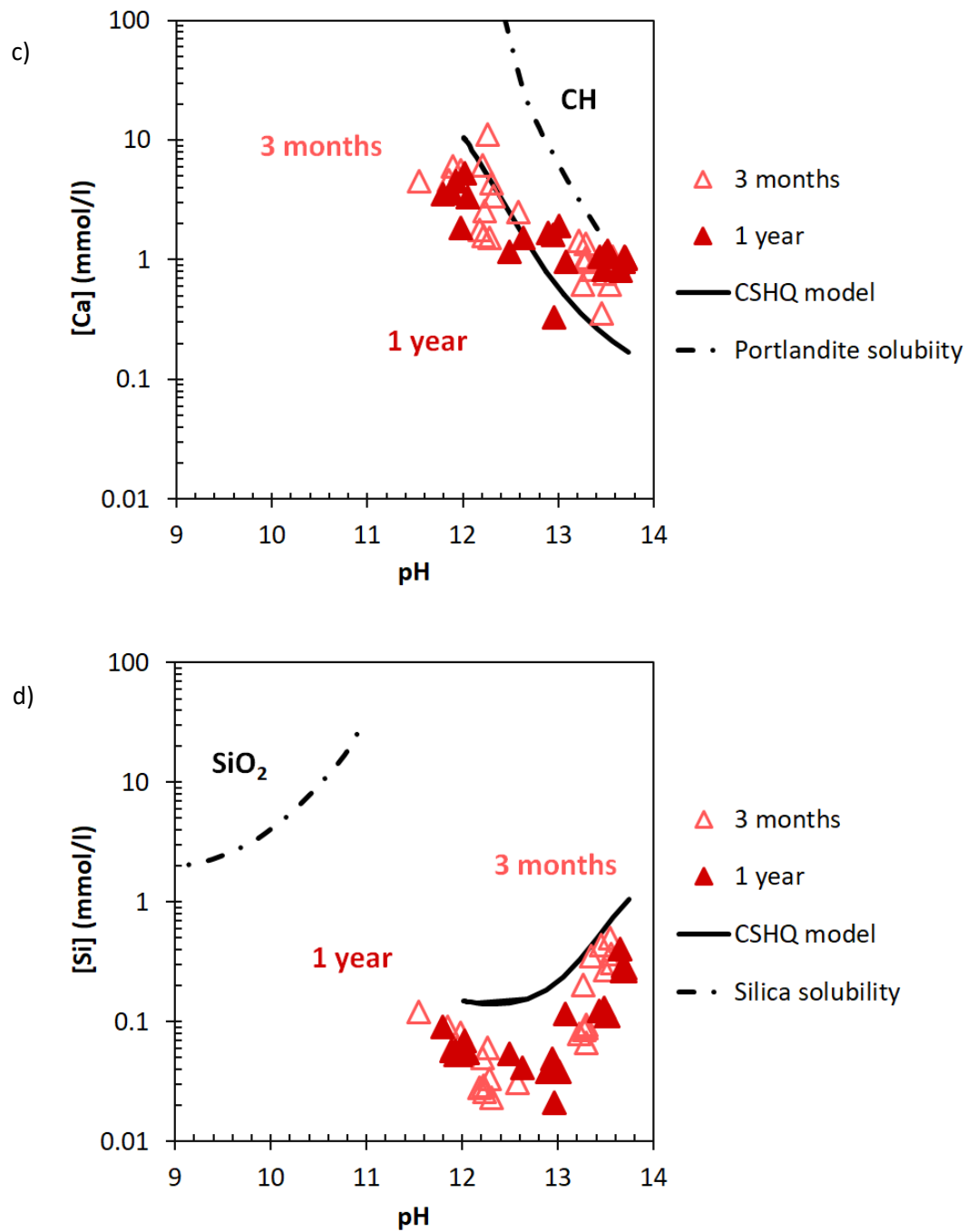


Figure 23. The effect of pH value and equilibration time on measured Ca (a,c) and Si (b,d) concentrations (symbols) and on the calculated solubility of C-S-H (using the CSHQ model [47]), portlandite and amorphous SiO₂ for Ca/Si ratios of a,b) 0.8 and c,d) 1.2 at 0, 0.1, 0.5 and 1 M NaOH. (*: outlier Ca concentrations for Ca/Si = 0.8 after 1 year equilibration). (The errors are smaller than the symbols' size).

5.6 The effect of time on C-A-S-H solubility

The solubility of C-A-S-H depends on the composition of the solid, i.e. the amount of Ca, Si and Al in the C-S-H structure, and is often described with solid solution models using different endmembers [46,47,70]. The development of such solid solution models is generally based on a large number of experimental data and is a complex and challenging task, which is not within the focus of the present study. However, the solubility of

a single composition in equilibrium with the solution can easily be calculated based on the measured elemental concentrations.

The C-A-S-H solubility with Ca/Si ratios of 0.8 and 1.2 at Al/Si = 0.03 and 1 M NaOH is calculated as detailed in Eq.3 and Eq.4, assuming a constant composition of the solid C-A-S-H and is shown in Figure 24 after different equilibration times. The solubility product of C-A-S-H with Ca/Si = 0.8 equals to $10^{-8.4 \pm 0.2}$ and does not change significantly with time indicating that the solubility is not dependent on the equilibration time. The observed decrease in Al concentrations with time due to its uptake in C-S-H is compensated by the small variations in the Ca and Si concentrations. At Ca/Si = 1.2, a solubility product of $10^{-10.5 \pm 0.3}$ is observed with a tendency to increase from $10^{-10.8}$ to $10^{-10.2}$ from 7 days to 1 year. The derived values of the solubility products of $10^{-8.4 \pm 0.2}$ for Ca/Si = 0.8 and the somewhat lower value of $10^{-10.5 \pm 0.3}$ for Ca/Si = 1.2, agree well with the changes of the solubility products with Ca/Si for C-S-H reported e.g. in [46]. The absence of any big changes in the solubility product with time despite the decrease in Al concentrations is an important result, which will help for the development of thermodynamic models for C-A-S-H.

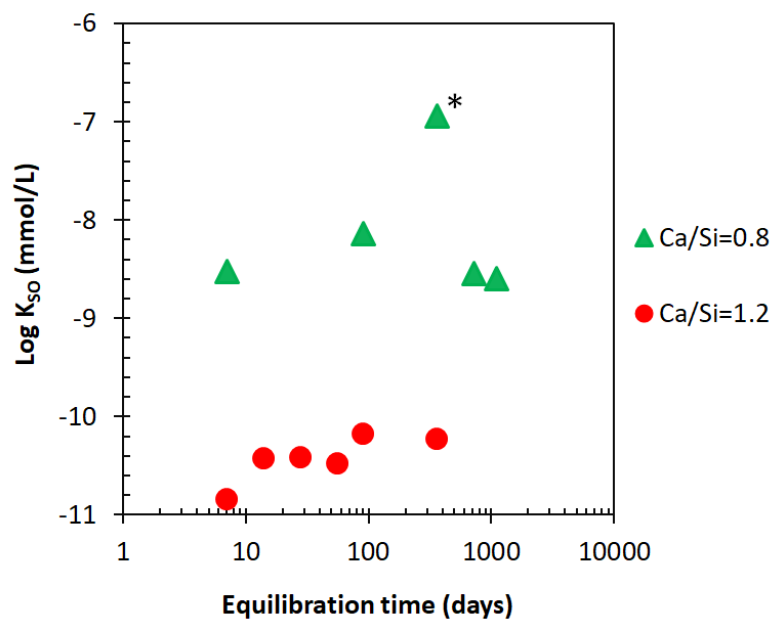


Figure 24. The effect of equilibration time on C-A-S-H solubility product with Al/Si = 0.03 and 1 M NaOH. The Ca concentrations are below the detection limit for Ca/Si = 0.8 after 14, 28 and 56 days of equilibration. (*: higher value due to the outlier Ca concentration for Ca/Si = 0.8 after 1 year equilibration).

5.7 Conclusions

The Al uptake in C-S-H was investigated after different equilibration times between 7 days to 3 years using the sorption isotherm experiments. The experiments revealed that Al uptake in C-S-H increases with equilibration time and this change over time is more distinct at low Ca/Si ratios than at high Ca/Si ratios indicating that equilibrium is reached faster at high Ca/Si ratios. At low Ca/Si ratios, the drift in Al and Si concentrations in solution were observed up to 3 years, although the changes were less important for the aged samples.

The solubility of C-A-S-H was calculated with thermodynamic modelling using the concentrations measured after different equilibration times for C-A-S-H with Ca/Si ratios of 0.8 and 1.2. The calculation indicated that the solubility of C-A-S-H with Ca/Si = 0.8 and 1.2 do not change significantly with equilibration time.

In addition to the C-A-S-H phase, also secondary phases such as strätlingite, $\text{Al}(\text{OH})_3$ and katoite formed initially, in particular at higher Al contents. Their content decreased in all cases after longer equilibration times indicating the dissolution of such secondary phases and an increase in uptake of Al in C-S-H. The FTIR analysis showed a restructuring of the C-A-S-H phase with time and this change is more significant at lower Ca/Si ratios.

Chapter 6 The effect of Al concentration on C-A-S-H

This chapter presents the effect of aluminum concentration on the amount of Al taken up in C-S-H for target Ca/Si ratio of 0.8 using the sorption isotherm experiment with equilibration times of 3 months and 1 year for different Al/Si ratios and NaOH concentrations. This chapter will be further adapted and implemented for submission and the information regarding the contribution of the author of this PhD thesis can be found in section 1.7.

6.1 C-A-S-H without NaOH

6.1.1 The effect of Al concentration on secondary phases

Figure 25 shows the effect of a) Al/Si ratios and b) equilibration time on the solid phases formed, determined from the TGA analysis of C-A-S-H samples with target Ca/Si = 0.8 in the absence of NaOH after 3 and 12 months equilibration. C-A-S-H is in all cases the main hydrate formed. At low Al/Si ratios, only C-A-S-H is present, however, at higher Al/Si ratios (≥ 0.03) secondary phases such as strätlingite, katoite, portlandite and $\text{Al}(\text{OH})_3$ precipitate. Increasing the target Al/Si ratio from 0.03 to 0.2 increases the content of aluminum hydroxide and katoite from 0.29 wt% and 1.7 wt% to 1.4 wt% and 2.1 wt%, respectively (Figure 25a). Similarly, the presence of katoite and strätlingite at target Al/Si ≥ 0.1 and $\text{Al}(\text{OH})_3$ at target Al/Si = 0.33 has been observed [23,37,58]. Details on the amounts of secondary phases are given in Appendix B.

Figure 25b illustrates how an increase in equilibration time from 3 months to 12 months results in a decrease in the content of $\text{Al}(\text{OH})_3$ and katoite. $\text{Al}(\text{OH})_3$ is only present after 3 months equilibration at target Al/Si ratios of 0.03 to 0.2. The content of katoite decreases from 1.7 wt% to a non-detectable level at target Al/Si ratio of 0.03 between 3 months and 12 months. A similar complete destabilization of $\text{Al}(\text{OH})_3$ with time is observed at target Al/Si ratios of 0.1 and 0.2; only at target Al/Si = 0.2 some katoite is still present after 12 months. The disappearance of $\text{Al}(\text{OH})_3$ and katoite with time is consistent with the undersaturation observed for these solids in the solution (Appendix D) both after 3 and 12 months, which implies an initial precipitation of these solids, which then dissolve only slowly with time. Similarly, L'Hopital et al. [37] observed the persistence of katoite in the presence of C-A-S-H phases at Ca/Si = 1.0 after 6 months equilibration although the solution were strongly undersaturated. Similar observations were made for brucite in the presence of M-S-H (Magnesium Silicate Hydrates); the kinetic hindrance of brucite dissolution was related to the presence of Si in solution [65]. It can be speculated that the Si could slow down also $\text{Al}(\text{OH})_3$ and katoite dissolution at high pH values similarly to the slowdown of quartz dissolution in the presence of Al [104], although experimental evidence is presently missing.

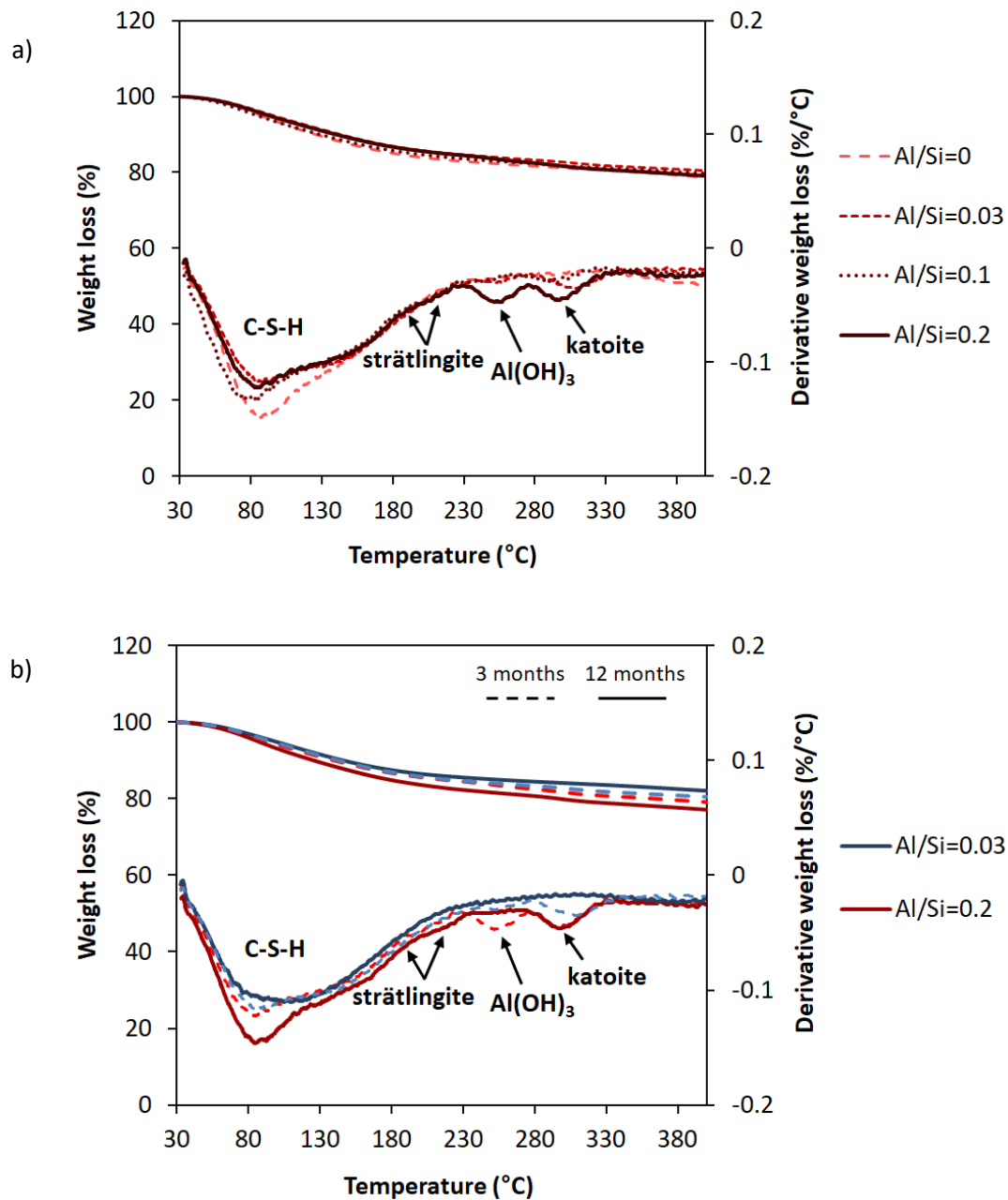


Figure 25. The effect of a) Al content at 3 months equilibration and b) equilibration time on secondary phases' content in the absence of NaOH for target Ca/Si = 0.8.

The fraction of Al in C-A-S-H and in different secondary phases such as strätlingite, Al(OH)₃ and katoite for Ca/Si = 0.8 is summarized in Table 4 and visualized in Figure 26. Table 4 shows that Al(OH)₃ and katoite are mainly present at target Al/Si \geq 0.03 and strätlingite at target Al/Si = 0.2. At all NaOH concentrations, an increase in Al/Si ratio leads to an increase in Al fraction bound in strätlingite, Al(OH)₃ and katoite. In the absence of NaOH and after 3 months equilibration, an increase in Al/Si ratio from 0.001 to 0.2 leads to an increase in the content of Al(OH)₃ and katoite from 0 to 10.7% and 6.4%, respectively. In the presence of 0.5 M NaOH, increasing the Al/Si ratio from 0.001 to 0.2 increases the Al fraction in katoite from 0 to 5.4% and 1.5% after 3 months and 15 months equilibration, respectively.

Table 4. The fraction of Al in solution, C-A-S-H and different secondary phases at different NaOH concentrations and equilibration times for target Ca/Si = 0.8.

NaOH (M)	Equilibration time (months)	Target Al/Si	% Al in solution	% Al in strätlingite	% Al in Al(OH) ₃	% Al in katoite	% Al in C-A-S-H
0	3	0.001	3.8	0	0	0	96.2
		0.003	1.8	0	0	0	98.2
		0.01	1.8	0	0	0	99.3
		0.03	0.7	0	13.1	32.9	53.8
		0.1	0.2	0	2.0	8.1	89.7
		0.2	0.1	0	10.7	6.4	82.9
0	12	0.001	<0.001	0	0	0	100
		0.003	<0.001	0	0	0	100
		0.01	0.03	0	0	0	100
		0.03	0.01	0	0	0	100
		0.1	0.01	0	0	0	100
		0.2	<0.001	1.6	0	6.4	92.0
0.1	3	0.001	12.1	0	0	0	87.9
		0.003	3.9	0	0	0	96.1
		0.01	2.6	0	0	0	97.4
		0.03	2.4	0	0	0	97.6
		0.05	1.5	0	0	0	98.5
		0.1	2.8	0	0	5.1	92.1
		0.15	2.3	0	0	4.1	93.6
		0.2	0.9	1.6	0	6.4	91.1
0.1	12	0.001	2.0	0	0	0	98.0
		0.003	1.4	0	0	0	98.6
		0.01	1.9	0	0	0	98.1
		0.03	1.7	0	0	0	98.3
	15	0.05	2.1	0	0	0	97.9
		0.1	2.4	0	0	6.1	91.5
		0.15	1.8	0	0	8.3	89.9
		0.2	2.5	4.8	0	8.5	84.2
0.5	3	0.001	9.8	0	0	0	90.2
		0.003	7.6	0	0	0	92.4
		0.01	8.3	0	0	0	91.7
		0.03	9.0	0	0	0	91.0
		0.05	1.6	0	0	4.0	94.4
		0.1	9.7	0	0	0	90.3
		0.15	9.7	0	0	5.1	85.2
		0.2	8.9	0	0	5.4	85.7

Table 4. (cont)

NaOH (M)	Equilibration time (months)	Target Al/Si	% Al in solution	% Al in strätlingite	% Al in Al(OH) ₃	% Al in katoite	% Al in C-A-S-H
0.5	12	0.001	6.7	0	0	0	93.3
		0.003	6.3	0	0	0	93.7
		0.01	5.3	0	0	0	94.7
		0.03	6.7	0	0	0	93.3
	15	0.05	6.7	0	0	0	93.3
		0.1	10.9	0	0	0	89.1
		0.15	11.8	0	0	2.8	85.4
		0.2	11.8	0	0	1.5	86.7
1	3	0.001	12.0	0	0	0	88.0
		0.003	15.3	0	0	0	84.7
		0.01	14.1	0	0	0	85.9
		0.03	14.0	0	0	0	86.0
		0.05	7.9	0	0	0	92.1
		0.1	16.5	0	0	0	83.5
		0.15	15.9	0	0	0	84.1
		0.2	25.9	0	0	1.1	73.0
1	12	0.001	9.8	0	0	0	90.2
		0.003	11.4	0	0	0	88.6
		0.01	10.4	0	0	0	89.6
		0.03	9.8	0	0	0	90.2
	15	0.05	28.3	0	0	0	71.7
		0.1	14.4	0	0	0	85.6
		0.15	19.2	0	0	0	80.8
		0.2	19.8	0	0	0.5	79.7

At low Al contents, only the C-A-S-H phase is present, however, at higher Al contents secondary phases are formed in addition to the C-A-S-H phase. Figure 26 illustrates that increasing the Al concentrations in solution leads to an increase in Al fraction in secondary phases and to a decrease in Al fraction in C-A-S-H from near 100% at low Al content to near 50%. An increase in equilibration time from 3 months to 12 months leads to a clear increase in the Al fraction in C-A-S-H and a decrease in Al in secondary phases, even at target Al/Si = 0.2 more than 90% of the Al is present in C-A-S-H after 12 months; while at lower Al/Si ratios nearly all Al is bound in C-A-S-H.

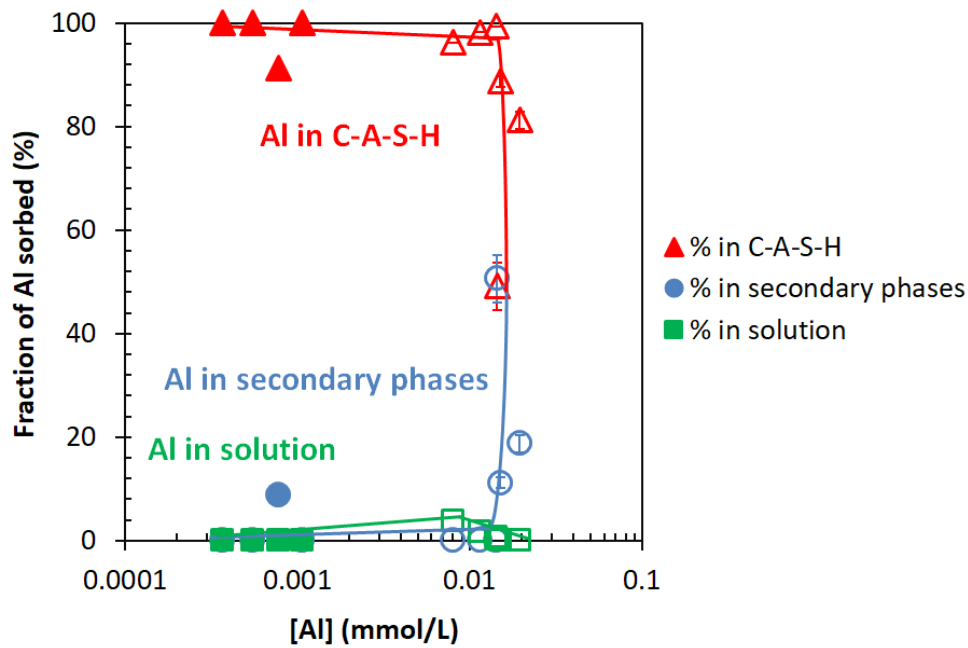


Figure 26. The Al fraction in solution, C-A-S-H and secondary phases vs measured Al concentration for target Ca/Si = 0.8 in the absence of NaOH after 3 months (empty symbols) and 12 months (filled symbols) equilibration. (The lines serve as eye-guides only).

6.1.2 The effect of Al concentration on C-A-S-H structure

The FTIR analysis has been performed in order to investigate the changes in the structure of C-A-S-H with different Al/Si ratios. Figure 27 represents the FTIR spectra for C-A-S-H samples in the absence of NaOH for a) 12 months equilibration with target Al/Si ratios from 0 to 0.2 and b) different equilibration times with target Al/Si ratios of 0.03 and 0.2. It is shown in Figure 27a that the intensity of the shoulders at 880 cm^{-1} and 1050 cm^{-1} increases with increasing Al/Si ratios indicating the presence of more Al in C-A-S-H with increasing Al contents. The intensity of the band at 665 cm^{-1} for Si-O-Si bending vibrations decreases with increasing the Al content, which could be related to the replacement of silica in the bridging position by Al. The intensity of Si-O stretching vibration of Q^1 tetrahedra at 820 cm^{-1} decreases with an increase in Al content. Richardson and co-workers used ^{27}Al and ^{29}Si MAS NMR and trimethylsilylation (TMS) and reported the absence of Q^1 sites with Al^{IV} which is also consistent with Al^{IV} occupying only the bridging tetrahedral sites of the dreierketten chains [30,105].

The FTIR spectra in Figure 27b shows that the intensity of the Al-O-Si and Al-O-H shoulders at around 880 cm^{-1} and 1050 cm^{-1} increases with longer equilibration time indicating the presence of more Al in C-A-S-H over time. The intensity of Q^2 sites of Si-O stretching vibration at 920 cm^{-1} increases significantly with equilibration time for both target Al/Si ratios of 0.03 and 0.2 indicating longer silica chain length after later ages.

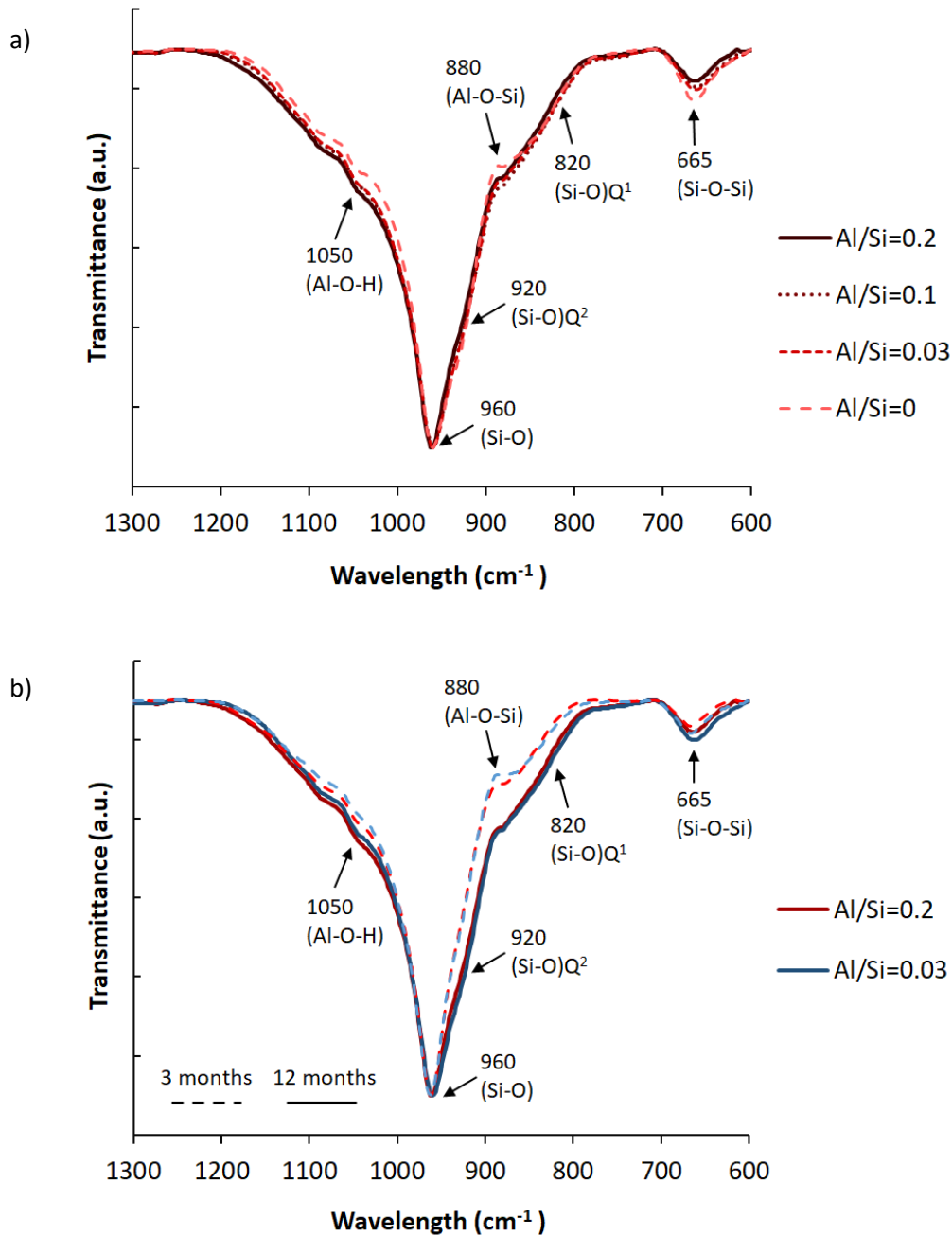


Figure 27. The FTIR spectra for C-A-S-H samples in the absence of NaOH at target Ca/Si = 0.8 for a) 12 months equilibration with different Al/Si ratios and b) different equilibration times with target Al/Si ratios of 0.03 and 0.2.

6.2 C-A-S-H with 1 M NaOH

6.2.1 The effect of Al concentration on secondary phases

Figure 28 shows that also in the presence of 1 M NaOH some katoite is present at target Al/Si ratio of 0.2, but absent at lower Al/Si, indicating the presence of less secondary phases at higher pH values, in agreement with the observations of L'Hopital et al. [34] in the presence of KOH. The amount of katoite present at target Al/Si ratio of 0.2 decreases also in the presence of 1 M NaOH with time as shown in Figure 28b, while at target Al/Si of 0.1 and below again no secondary phases are observed.

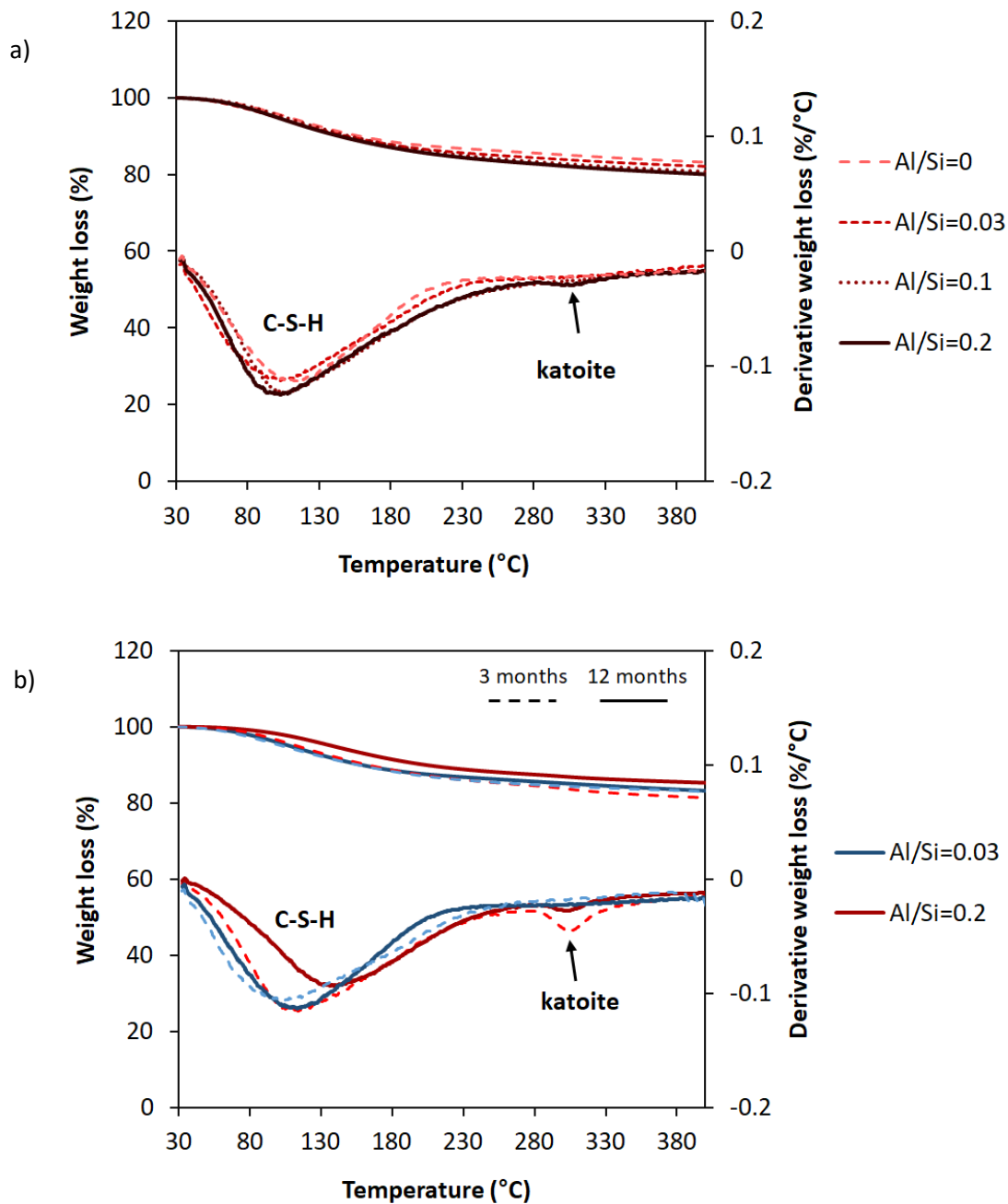


Figure 28. The effect of a) Al content at 3 months equilibration and b) equilibration time on secondary phases' content in the presence of 1 M NaOH for target Ca/Si = 0.8. (The samples at target Al/Si = 0.2 were analyzed after 15 months instead of 12 months).

Figure 29 illustrates again that virtually all Al is bound in C-AS-H at Al concentrations below 1 mmol/L. Only at high target Al/Si ratios (0.1, 0.15 and 0.2), an increase of the Al concentrations in solution is observed due to the high NaOH concentrations. At Al concentrations > 1 mmol/L, secondary phases (katoite) are present with maximum content of 1.1% after 3 months and of 0.5% after 15 months equilibration as shown in Table 4. A comparison of Figure 26 and Figure 29 indicates that the fraction of Al taken up in C-A-S-H is affected not only by the formation of Al containing secondary phases but also by the Al concentrations in solution. The fraction of Al in solution in the presence of 1 M NaOH at target Al/Si = 0.2 is 25.9% after 3 months and 19.8% after 15 months, while in the absence of NaOH, only 0.1% after 3 months and < 0.01% after 12 months of the total Al is present in solution.

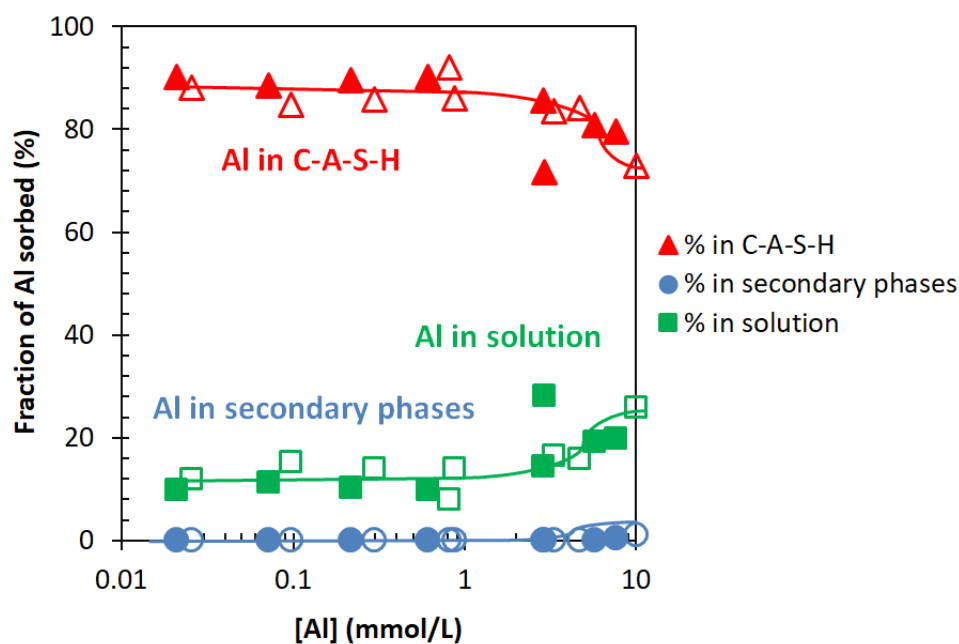


Figure 29. The Al fraction in solution, C-A-S-H and secondary phases vs measured Al concentration for target Ca/Si = 0.8 in the presence of 1 M NaOH after 3 months (empty symbols) and 15 months (filled symbols) equilibration. (The lines serve as eye-guides only and the errors are smaller than the symbols' size).

6.2.2 The effect of Al concentration on C-A-S-H structure

The FTIR spectra for C-A-S-H samples in the presence of 1 M NaOH are shown in Figure 30 for a) 15 months equilibration with target Al/Si ratios from 0 to 0.2 and b) different equilibration times with target Al/Si ratios of 0.03 and 0.2. Again, the intensity of the band at 665 cm^{-1} for Si-O-Si bending vibrations decreases with increasing the Al content. Furthermore, an additional signal around 720 cm^{-1} appears at high target Al/Si ratios of 0.1 and 0.2 which is assigned to Al-O stretching vibrations of octahedrally coordinated Al [93]. As it can be seen in Figure 30, this band is absent in the absence of Al and in the presence of low amount of Al (target Al/Si = 0.03). Moreover, the intensity of (Si-O) Q^1 peak at 820 cm^{-1} decreases significantly with an increase in Al content which indicates that the Si amount in Q^1 sites tentatively decreases and Al fills the empty bridging sites.

It is shown in Figure 30b that the intensity of the Al-O-H shoulder at around 1050 cm^{-1} does not significantly change with time compared to samples without alkali (Figure 27b) which indicates that change over time is more significant in the absence of alkali hydroxide and/or in the presence of low alkali content; in agreement with less changes in Al concentrations over time in the presence of 0.5 M and 1 M NaOH as shown in Al sorption isotherms in Figure 22. The peaks for Si-O stretching vibrations at 920 cm^{-1} and 960 cm^{-1} move to a shorter wavelength with increasing the equilibration time from 3 months to 15 months.

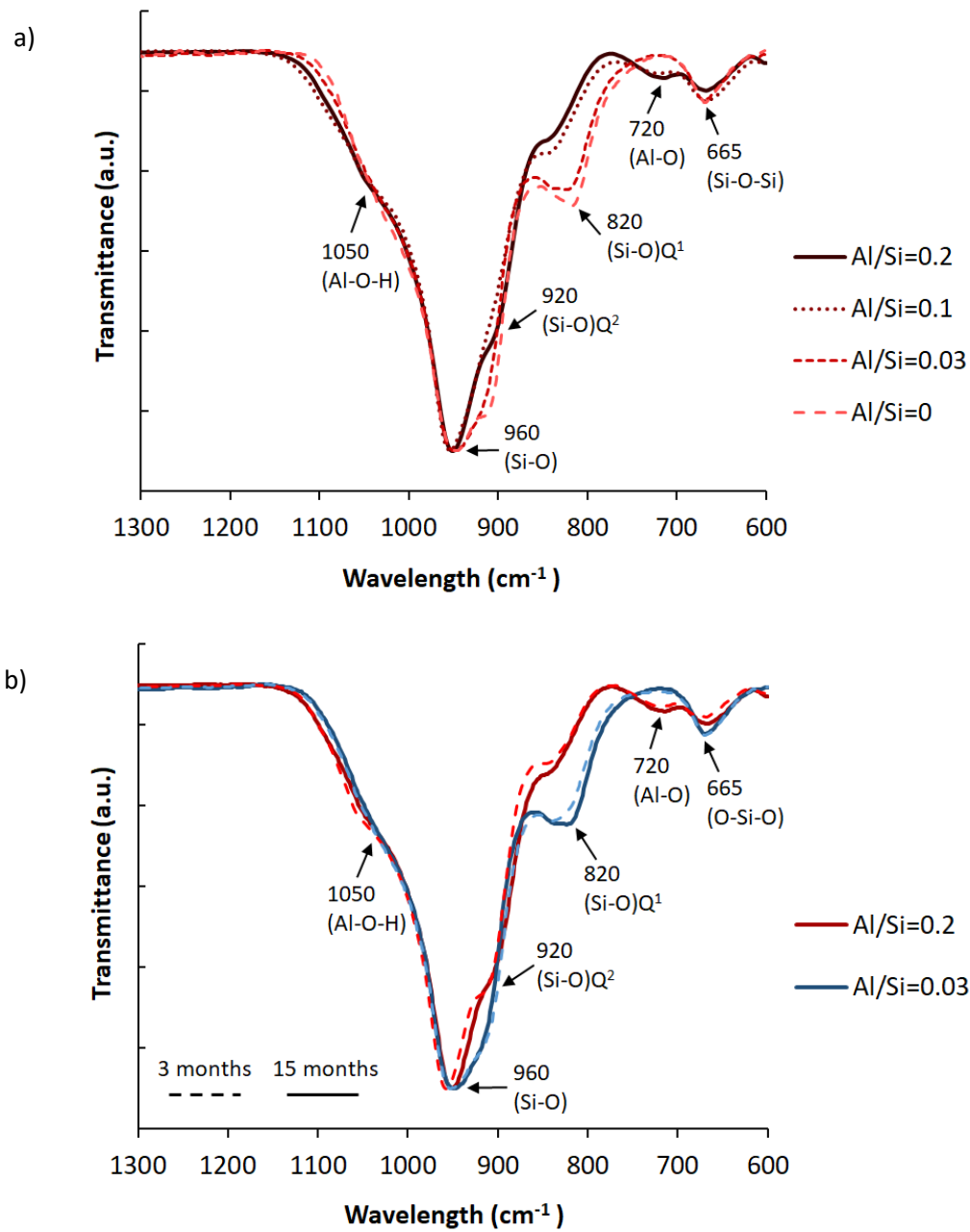


Figure 30. The FTIR spectra for C-A-S-H samples in the presence of 1 M NaOH at target Ca/Si = 0.8 for a) 15 months equilibration with different Al/Si ratios and b) different equilibration times with target Al/Si ratios of 0.03 and 0.2.

6.3 C-A-S-H with different NaOH concentrations

6.3.1 The effect of NaOH concentration on Al sorption isotherm

The Al sorption isotherms on C-A-S-H measured after 3 months and 1 year equilibration and at different NaOH concentrations are compared in Figure 31. In all cases, increasing the Al concentrations leads to higher uptake of Al in C-S-H, in agreement with previous experimental studies on Al sorption in C-S-H at relatively high Al content ($\text{Al/Si} \geq 0.05$) [23,34,37,55], as well as at low Al contents (Al/Si from 0.001 to 0.1) [58]. At low Al/Si ratios (≤ 0.03), the Al uptake in C-S-H increases with an increase in equilibration time from 3 months to 1 year. This increase is much more significant at 0 and 0.1 M than at high NaOH concentrations (0.5 and 1 M). However, at high Al/Si ratios (≥ 0.05) an increase in the Al uptake in C-S-H is observed only in samples

without alkali and with low (0.1 M) NaOH content. In the presence of 0.5 and 1 M NaOH, no increase has been observed for Al uptake in C-S-H. Since the Al concentrations are higher at high Al/Si ratios, little changes in the concentrations over time may not be obvious.

The large range studied here confirms a linear trend between the Al in solution and Al in C-A-S-H over more than 2 orders of magnitude. The linear trend points towards an Al uptake on one or several types of sorption sites, with a relative high capacity of up to $\text{Al/Si} \geq 0.2$ at target $\text{Ca/Si} = 0.8$. This continuous uptake and high sorption capacity would be consistent with an Al uptake in the bridging position of the silica chains suggested based on NMR studies [39,41]. The uptake of Al in C-S-H increases with a slope of ≈ 1 in the presence of NaOH, while a much steeper slope of ≈ 4 is observed in the absence of NaOH indicating tentatively the formation of an unidentified surface precipitate or an additional secondary phase even at those very low aluminum concentrations. Note that the solutions are clearly undersaturated with respect to Al containing hydrates such as $\text{Al}(\text{OH})_3$, strätlingite and katoite (see Appendix D) and that no secondary phases are observed at target $\text{Al/Si} \leq 0.01$ (at 3 months) and at target $\text{Al/Si} \leq 0.1$ (1 year), as shown in Table 4. Thus, either a too small amount is present to be detected or a surface precipitate might have formed; alternatively a zeolitic precursor might have formed as the alkali-free solutions are strongly oversaturated with respect to chabazite and Ca-gismondine. Note that XRD do not indicate the presence of any crystalline phases (Figure 16) and that chabazite or any zeolitic precursor present in low quantity will be visible neither by TGA (as their main weight loss will occur below 200 °C, i.e. in the range of the C-A-S-H signals) [106] nor by FTIR, where their main signals (between $\sim 900 \text{ cm}^{-1}$ to 1000 cm^{-1}) are in the same range as the C-A-S-H main signals.

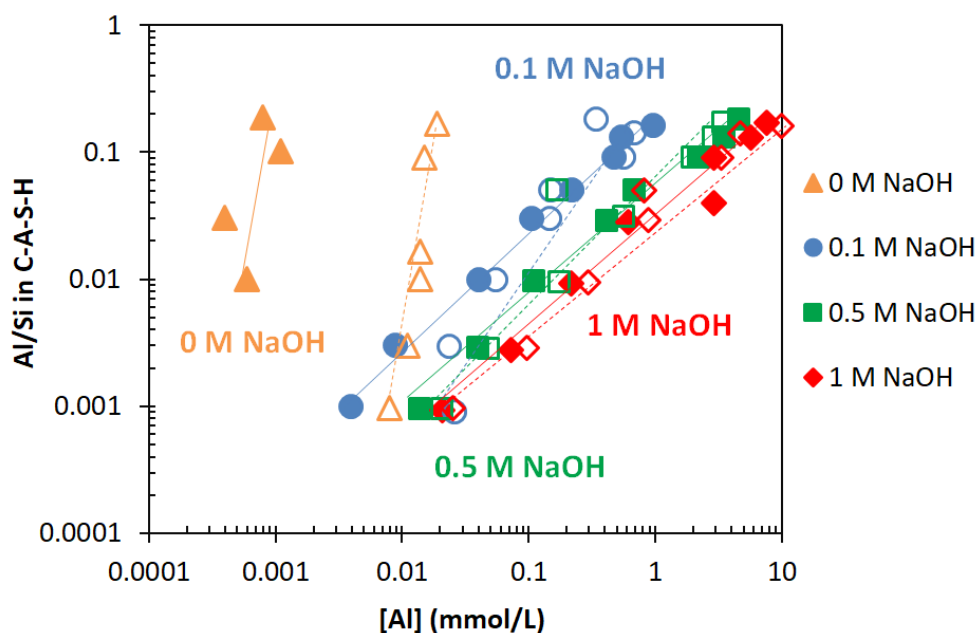


Figure 31. The Al sorption isotherm on C-A-S-H for target $\text{Ca/Si} = 0.8$ recorded after different equilibration times. The 3 months samples are indicated by empty and 1 year represented by full symbols. The samples at target $\text{Al/Si} \geq 0.05$ were analyzed after 15 months instead of 1 year. The lines indicate the slope of the increase; slopes ≤ 1 indicate sorption; slopes >1 indicate precipitation of an additional solid. (The errors are smaller than the symbols' size).

The uptake of Al into C-S-H phases can also be expressed in terms of a K_d value (distribution coefficient), which describes ratio of the quantity of Al adsorbed to the quantity of the Al remaining in the solution. The K_d values for different Al/Si ratios were calculated according to Eq. 6 and plotted versus pH values in Figure 32. The total amount of Al taken up decreases as is visible in the lowering of the K_d values from $\approx 600 \text{ m}^3/\text{kg}$ in the absence of NaOH after 1 year to $\approx 0.2 \text{ m}^3/\text{kg}$ in the presence of 1 M NaOH. The decrease

of Al uptake by C-S-H with increasing pH values (Figure 32) is comparable to the decrease of e.g. iron hydroxide complex ($\text{Fe}(\text{OH})_4^-$) uptake by TiO_2 with increasing pH [107]. The aqueous aluminum speciation depends on the pH values and negatively charged aluminum hydroxide complex $[\text{Al}(\text{OH})_4^-]$ dominates the speciation at $\text{pH} > 7$ as illustrated in Figure 7. The fraction of the $\text{Al}(\text{OH})_4^-$ species in solution increases with the pH values, which lowers the tendency of Al to be sorbed by C-S-H [58], such that the K_d values decrease with increasing the pH value. After 1 year, the 1:1 decrease of the K_d values (Figure 32) with pH confirms the important role of the solution speciation on the Al binding in C-S-H. In the absence of NaOH, the uptake is strongly influenced by the presence of secondary phases (even more so after 3 months) as discussed above, leading to a large scatter of the calculated K_d values.

The estimated K_d values of $\approx 600 \text{ m}^3/\text{kg}$ of Al in the absence of alkali are comparable to the K_d values $\approx 700 \text{ m}^3/\text{kg}$ for $\text{Fe}(\text{III})$ reported in [107], but are considerably higher than K_d values in the range of $0.1 \text{ m}^3/\text{kg}$ to $6 \text{ m}^3/\text{kg}$ observed for bivalent cations such as $\text{Fe}(\text{II})$, $\text{Ba}(\text{II})$ or $\text{Sr}(\text{II})$ [108–110].

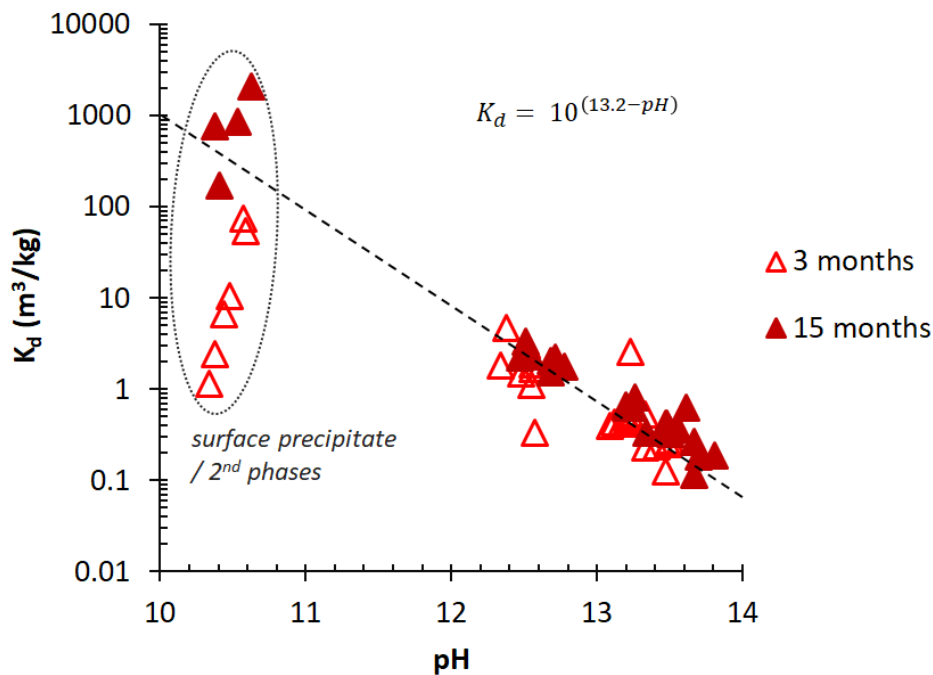


Figure 32. The pH dependence of Al sorption on C-A-S-H for target Ca/Si = 0.8. (The errors are smaller than the symbols' size).

6.3.2 The effect of NaOH concentration on secondary phases

Figure 33 shows the TGA signals for C-A-S-H samples in the absence of NaOH and presence of 1 M NaOH at target Al/Si ratios of 0.03 and 0.2 after 3 months equilibration. Increasing the NaOH concentration from 0 to 1 M leads to a decrease in the content of $\text{Al}(\text{OH})_3$ from 0.29 wt% and 1.4 wt% to a non-detectable level at target Al/Si ratios of 0.03 and 0.2, respectively. Moreover, the katoite content also decreases from 1.7 wt% and 2.1 wt% to 0 and 0.35 wt% at target Al/Si ratios of 0.03 and 0.2, respectively. In fact, the contents of secondary phases are higher at lower alkali concentrations.

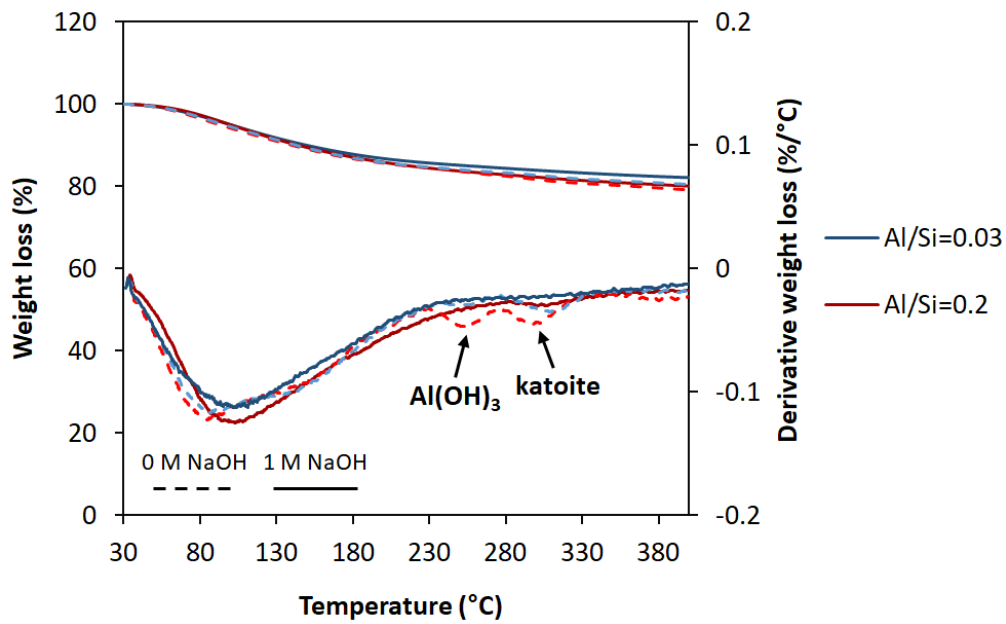


Figure 33. The effect of NaOH concentration on secondary phases' content for target Ca/Si = 0.8 with target Al/Si ratios of 0.03 and 0.2 after 3 months equilibration. The darkness of colors indicates an increase in NaOH concentration; 0 M NaOH is indicated by the dashed lines with light colors and 1 M NaOH represented by the solid lines with dark colors. (The lines serve as eye-guides only).

The sorbed Al fraction in C-A-S-H for different NaOH concentrations after 1 year equilibration is shown in Figure 34. At low NaOH concentrations, more Al is present in C-A-S-H in agreement with the higher K_d values at low pH values. At all NaOH concentrations, the fraction of Al bound in C-A-S-H decreases at higher Al concentrations due to the formation of secondary phases. High alkali concentrations lower the amount of secondary phases as shown in Figure 33, which leads to less secondary phases at lower Al concentrations and thus at intermediate Al concentrations to a higher fraction of Al bound in C-A-S-H. The Al fraction in C-A-S-H for 3 months equilibration is shown in Appendix H.

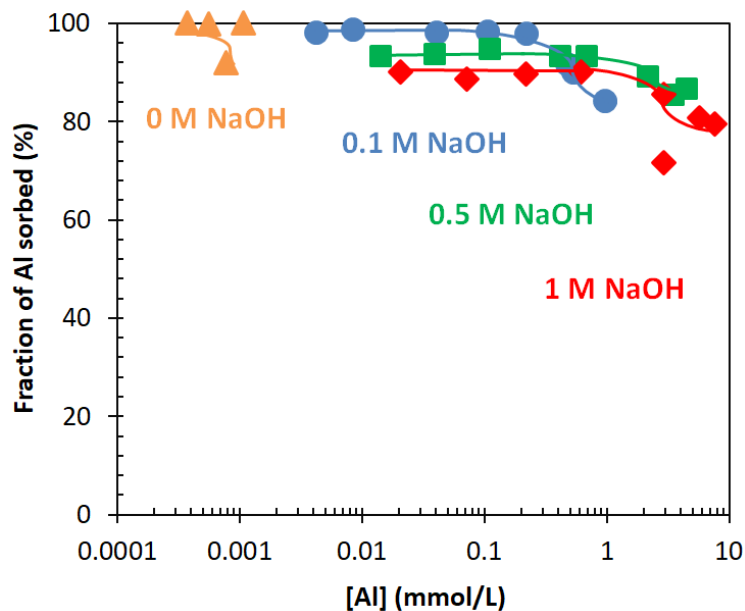


Figure 34. The Al fraction in C-A-S-H for target Ca/Si = 0.8 in the absence of NaOH and presence of 0.1, 0.5 and 1 M NaOH after 1 year equilibration. Samples at target Al/Si \geq 0.05 were analyzed after 15 months instead of 1 year. (The errors are smaller than the symbols' size).

6.3.3 The effect of NaOH concentration on C-A-S-H structure

Figure 35 shows the effect of NaOH concentration on the structure of C-A-S-H with target Al/Si ratios of 0.03 and 0.2 after 3 months equilibration. Comparing the FTIR spectra in dashed lines (no alkali) with full lines (1 M NaOH), it becomes clear that the intensity of Q¹ sites at 820 cm⁻¹ is higher in a 1 M NaOH solution than in the absence of NaOH, which indicates a shorter silica chain length in samples containing more NaOH; in agreement with the observations of [19,34,102,111] by Si NMR. At both target Al/Si ratios of 0.03 and 0.2, the intensity of Si-O stretching vibration of Q² sites at 920 cm⁻¹ increases significantly with increasing the NaOH concentrations. Both bands for Si-O at 920 cm⁻¹ and 960 cm⁻¹ move to a shorter wavelength with an increase in the NaOH concentration, which indicate a depolymerization of the silica chains [89]. Moreover, the signal for Al-O stretching vibrations of octahedrally coordinated Al appears only in the presence of 1 M NaOH. Furthermore, increasing the NaOH concentration leads to an increase in the intensity of the Al-O-H shoulder at 1050 cm⁻¹, which indicates that both the C-A-S-H structure as well the Al uptake is strongly affected by NaOH at low Ca/Si C-A-S-H studied.

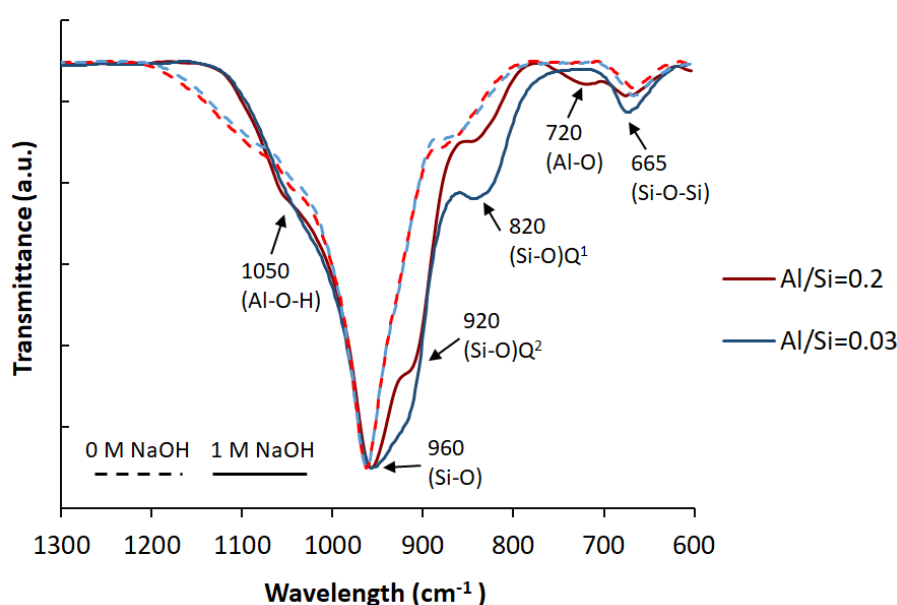


Figure 35. The FTIR spectra for C-A-S-H samples in the absence of NaOH and presence of 1 M NaOH for target Ca/Si = 0.8 with target Al/Si ratios of 0.03 and 0.2 after 3 months equilibration. The samples without NaOH are represented by dashed lines with light colors and those with 1 M NaOH are shown by solid lines with dark colors.

6.4 Conclusions

The effect of aluminum concentration on Al uptake in low Ca/Si C-S-H (Ca/Si = 0.8) was investigated using sorption isotherm experiments over a wide range of target Al/Si ratio from 0.001 to 0.2. The uptake of Al in C-S-H was confirmed by FTIR spectra, where the intensity of shoulders assigned for Al-O bands in C-A-S-H structure increased. At low Al/Si, Al was exclusively bound in C-A-S-H, while at high Al/Si ratios secondary phases containing Al such as strätlingite, Al(OH)₃ and katoite were formed in addition to the C-A-S-H phase, limiting the uptake of Al in C-A-S-H. In the absence of alkali hydroxide, secondary phases were observed by TGA at target Al/Si ≥ 0.03, while the sorption isotherms indicated the presence of traces of secondary phases even at lower Al/Si ratios.

The Al sorption isotherm at low Al/Si ratios showed more uptake of Al in C-S-H with time from 3 months to 1 year. This increase in uptake was more distinct in the absence of NaOH and at low Al concentrations than at

high Al concentrations where secondary phases were present. This indicated a slow rearrangement of C-A-S-H phases with time which increases also the Al incorporation in C-S-H. The initially low uptake might also be related to the experimental procedure used, which favors the initial formation of Al containing secondary phases leading to low Al concentrations. Over time, less Al was bound in secondary phases and a higher uptake of Al in C-S-H occurred.

The presence of NaOH progressively shifted the precipitation of secondary phases to higher Al/Si ratios; to target $\text{Al/Si} \geq 0.1$ at 0.1 M NaOH and to target $\text{Al/Si} \geq 0.2$ at 1 M NaOH. The absence of secondary phases in the presence of NaOH led to a higher fraction of Al bound in C-A-S-H at intermediate Al concentration in solution. At very low Al concentrations, however, the high pH values lowered Al uptake in C-S-H as Al had a stronger tendency to remain in solution as Al(OH)_4^- . FTIR spectra suggested a shortening of the silica chain length in samples containing NaOH, both for samples with low and high Al contents.

The Al sorption isotherm showed a linear trend between Al in solution and Al in C-A-S-H from Al/Si 0.001 up to 0.2. The linear trend pointed towards an Al uptake on one or several types of sorption sites, with a high sorption capacity, which would be consistent with an Al uptake in the bridging position of the silica chains suggested based on NMR studies [39,41]. The steep increase of Al in C-S-H in the absence of NaOH tentatively indicated the formation of a surface precipitate or of a not clearly identified secondary phase.

The decrease of the distribution coefficients, K_d values, of Al on C-S-H from $\approx 600 \text{ m}^3/\text{kg}$ in the absence of NaOH to $\approx 0.2 \text{ m}^3/\text{kg}$ in the presence of 1 M NaOH indicated a decrease of Al uptake by C-S-H with increasing the pH values. The fraction of the Al(OH)_4^- species in solution increased with the pH value, which lowered the tendency of Al to be sorbed by C-S-H.

Chapter 7 Concluding remarks

7.1 Achieved results

The understanding of the Al uptake in C-S-H is an important prerequisite for the improvement of thermodynamic models that can predict the composition of hydrated cements. However, there is a lack of experimental data available in the literature on the influence of alkali, aluminum, Ca/Si ratio as well as the short- and long-term equilibration time on the C-A-S-H solubility and structure. The objective of this PhD project was to develop a systematic experimental database of the solubility and composition of C-A-S-H in the presence and absence of alkalis. A series of experiments were carried out to investigate the solubility, structure and composition of C-A-S-H gel as a function of different parameters such as Ca/Si ratio, aluminum content, alkali concentration and equilibration time in order to obtain a better understanding of the uptake of aluminum in C-S-H. The use of ICP-OES and ICP-MS measurements in this study enabled us to record the Al uptake in C-S-H systems at very low Al concentrations, which allowed for the first time to assess the effect of pH value, Ca/Si ratio and equilibration time for Al concentrations down to 4×10^{-5} mmol/L. The sorption isotherm experiments were performed in a large range of equilibration times from 7 days up to 3 years providing a comprehensive knowledge basis about the differences in short- and long-term thermodynamic stability, chemical evolution and mechanical properties of C-A-S-H phases which is needed to facilitate the implementation of new cements associated with lower CO₂ emissions during cement manufacturing.

FTIR spectra of C-A-S-H phases confirmed the uptake of Al in C-S-H where the intensity of shoulders assigned to Al-O bands increased while the intensity of Si-O and Si-O-Si vibrations decreased. The presence of sodium hydroxide prevented aluminum hydroxide formation by increasing the pH values which led to more negative charges on C-S-H surface due to the increased deprotonation of the silanol sites, as indicated by zeta potential measurements. The increase in the fraction of the main hydroxide complex of aluminum above pH 7, $\text{Al}(\text{OH})_4^-$, limited the tendency of Al to be sorbed by C-S-H, which was in agreement with the decrease of the distribution coefficients, K_d values, of Al on C-S-H from $\approx 600 \text{ m}^3/\text{kg}$ in the absence of NaOH to $\approx 0.2 \text{ m}^3/\text{kg}$ in the presence of 1 M NaOH. The changes in the structure of C-A-S-H with NaOH addition is schematically shown in Figure 36. The replacement of Ca^{2+} ions by Na^+ ions in the interlayer at high pH values leads to less positive charge on C-A-S-H surface and thus less uptake of Al in C-S-H. The presence of alkali hydroxide progressively shifted the precipitation of secondary phases to higher Al/Si ratios and led to shorter silica chain length as indicated by FTIR spectra. The linear trend between Al uptake in C-S-H and Al in solution suggested the uptake of Al on one or several types of sorption sites, with a high sorption capacity, which was in agreement with NMR studies where Al uptake in the bridging position of the silica chains has been observed [38,39]. The steep increase of Al content in C-A-S-H in the absence of NaOH tentatively indicated the formation of a surface precipitate or of a not clearly identifiable secondary phase. At high Ca/Si ratios, the presence of more Ca^{2+} ions in the interlayer as well as the different sorption sites for Al in the silica chains led to a higher uptake of Al in C-S-H compared to that in low Ca/Si C-S-H. The parallel increase in Al and Si

concentrations in solution with increasing the pH values pointed towards the uptake of aluminum within the silica chains both at high and low Ca/Si. This was in agreement with solid state Si NMR results as well as the molecular modelling which indicated that at low Ca/Si C-S-H Al^{IV} [38,39] and at high Ca/Si C-S-H Al^{IV} , Al^{IV} and Al^{VI} are present in the bridging sites of the silica chains [45]. The Al sorption isotherm experiments after different equilibration times between 7 days to 3 years indicated a slower equilibration at low Ca/Si ratios as changes in the concentrations in solution as well as the restructuring of the C-A-S-H phase with time were more distinct. Moreover, at low Al/Si ratios and in the absence of NaOH the increase of Al uptake in C-S-H with time was more significant due to the presence of less secondary phases. At high Al/Si ratios, formation of secondary phases containing Al such as strätlingite, $\text{Al}(\text{OH})_3$ and katoite led to the uptake of Al in the secondary phases in addition to the C-A-S-H phase. Therefore, the dissolution of secondary metastable phases with time eased the uptake of Al in C-S-H.

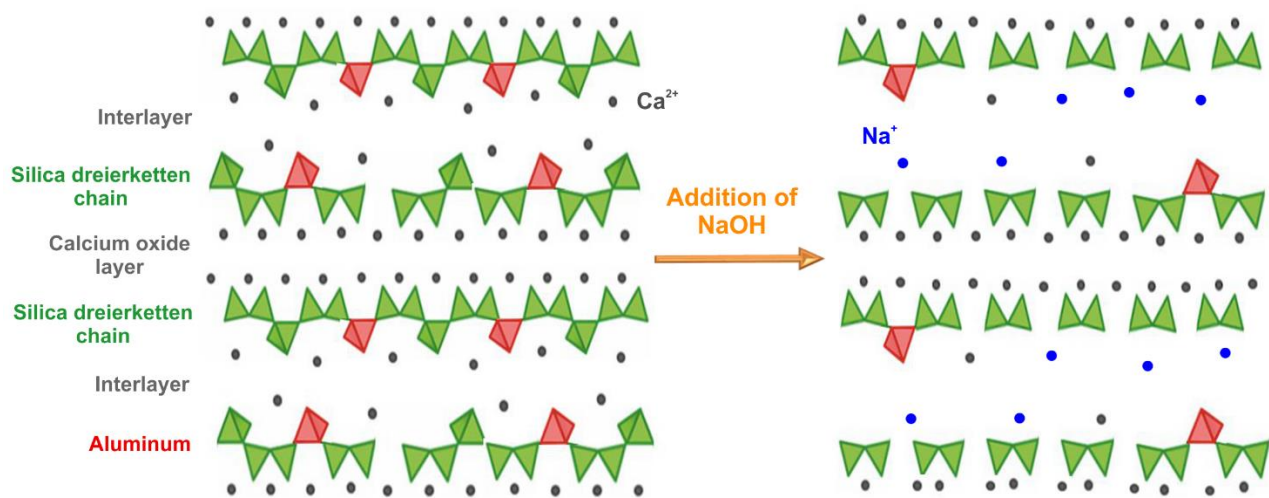


Figure 36. A schematic image representing the changes in the structure of C-A-S-H with NaOH addition. Grey circle: calcium ion; blue circle: sodium ion and red triangle: Al in the bridging position.

The solubility of C-S-H has been observed to depend on the synthesis methods [32]. The effect of different synthesis methods (co-precipitation vs sorption) has been investigated on C-A-S-H samples with Ca/Si ratios of 0.8 and 1.2 and Al/Si = 0.03 containing 1 M NaOH after 90 days equilibration using either sorption on pre-synthesized C-S-H or co-precipitation. The aqueous phase composition is shown in Figure 37 for different equilibration times from 7 days to 3 years for Ca/Si ratio of 0.8 and from 7 days to 1 year for Ca/Si ratio of 1.2. The data after 90 days equilibration indicate that for Ca/Si = 0.8, slightly lower Al, Si and Ca concentrations are observed for the sorption experiments than for the co-precipitation experiments, indicating a limited effect of the synthesis method on the aqueous phase composition. For instance, the Al concentration decreases slightly from 1.06 mmol/L to 0.88 mmol/L from sorption to co-precipitation. For Ca/Si = 1.2, the changes in the aqueous phase composition are more significant. In fact, going from sorption to co-precipitation method, the Al concentration decreases from 0.45 mmol/L to 0.19 mmol/L. The same also happens for Ca and Si concentrations in solution. Thus, at high Ca/Si ratios the Al uptake in C-S-H is more dependent on the synthesis method compared to low Ca/Si C-S-H.

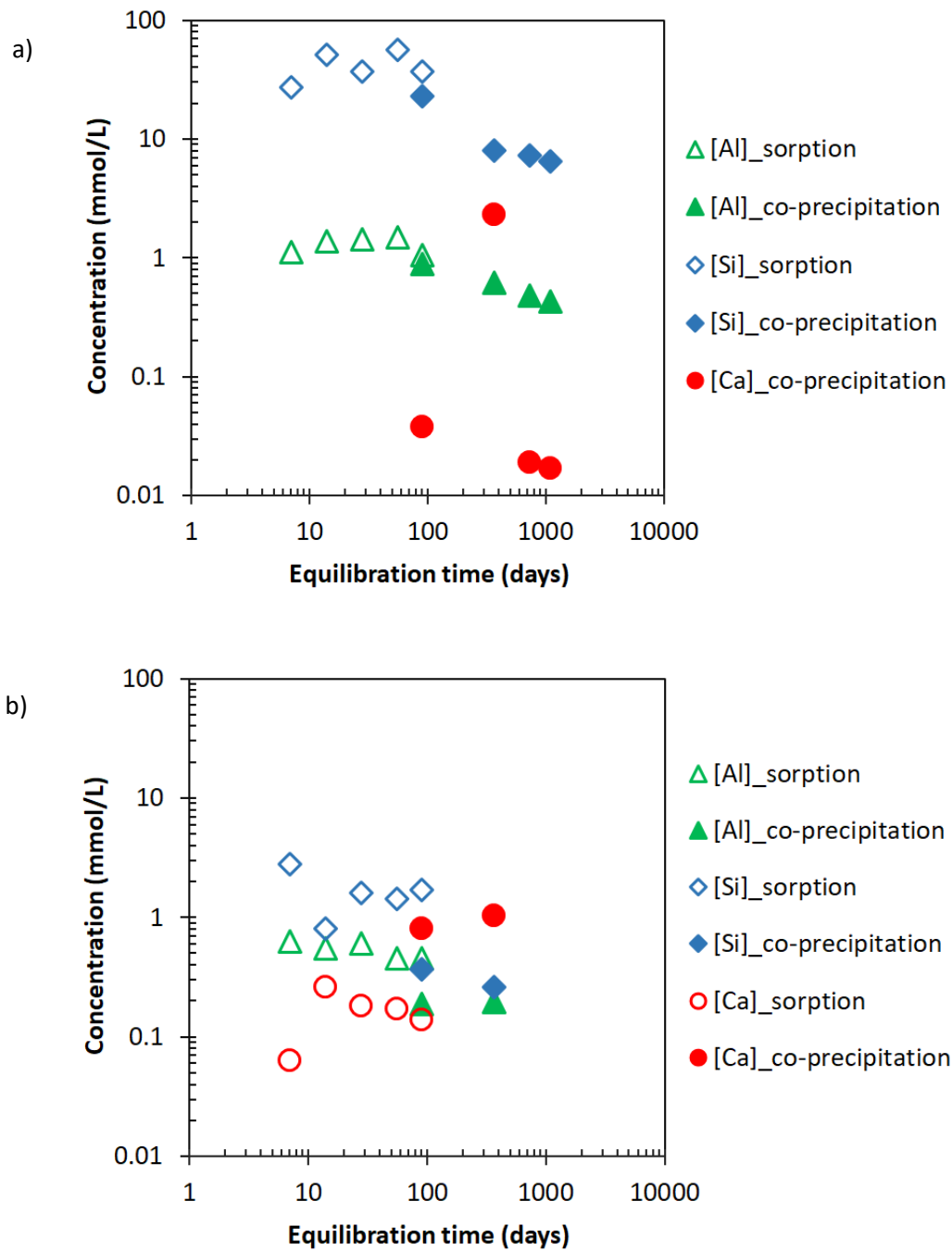


Figure 37. The effect of synthesis method (sorption: empty symbols vs co-precipitation: filled symbols) after different equilibration times for a) Ca/Si = 0.8 and b) Ca/Si = 1.2. (The Ca concentrations in sorption method are below the detection limit for Ca/Si = 0.8).

The experimental investigations using the sorption isotherm measurements indicated a low uptake of Al in C-S-H in the presence of low Al concentrations, as e.g. in the case of ordinary Portland cement (OPC). However, in the presence of higher Al concentrations such as e.g. present in the pore solution of Al-rich blended cements, much higher uptake of Al has been observed reaching values up to approximately Al/Si = 0.1. Moreover, a decrease in the content of Al containing secondary phases with time has been observed, which led to more Al uptake in C-A-S-H, which will affect also the amount and kind of secondary phases. Furthermore, supplementary cementitious materials reduce the alkalinity and pH value of the pore solution [16], leading to higher uptake of Al in C-S-H in blended cements.

Moreover, the gained fundamental knowledge on the effect of pH value, equilibration time and Al concentration on Al uptake in C-S-H phases at varying Ca/Si ratios could be used to further develop the thermodynamic modelling of C-A-S-H. Advanced thermodynamic models will help in predicting the composition and phase assemblages of blended cements, which will provide a solid scientific background for the implementation of novel cement blends with low CO₂ footprint. In order to determine the location of aluminum in the C-A-S-H phases, the structural investigations using ²⁷Al MAS NMR spectroscopy have been studied in a parallel project [112].

7.2 Future development

Although many different aspects have been investigated, a number of topics will need to be addressed in more details in the future:

The comprehensive experimental content of this thesis including the long-term data would be very helpful to define the necessary input for those who develop more sophisticated kinetic and thermodynamic models. It would be very interesting to extend the thermodynamic modelling of C-S-H to account for both short- and long-term incorporation of Al at different alkali concentrations.

The recording of different sorption isotherms for Al in C-A-S-H (dependency on alkali content, Ca/Si ratio) indicated the presence of different sorption sites for Al in C-A-S-H. An in depth investigation with ²⁷Al MAS NMR could give additional insights on the exact sorption sites for Al. Moreover, ²³Na MAS NMR might provide information regarding the alkali sorption sites.

The speciation of calcium, silicates and aluminum in the aqueous solution affects the solubility of C-A-S-H. Different dataset are available for the interactions and complex formation between different ions at low to neutral pH values, however, these data are not available for higher pH values. The existence of calcium alumino silicate complexes and their stability strongly influence the solubility of C-A-S-H. Therefore, a comprehensive study for the investigation of their existence and the quantification of their stability is needed in order to further improve the C-A-S-H thermodynamic models and to study the kinetics of C-A-S-H nucleation and growth.

And in a broader aspect, an increased uptake of Al into C-S-H lowers the availability of Al for ettringite and AFm phases formation, such that the amount of Al in C-S-H affects not only the C-S-H structure but also the amount of other phases in cement.

Appendices

Appendix A. Mixing proportions used for preparing the C-A-S-H samples.

Table 5. Mixing proportions used for preparing the C-A-S-H samples (in g per 171 mL solution) at 20 °C in long-term experiments. (Remark: for Ca/Si = 0.8 samples, 4 g of solid was suspended in 180 ml solution).

Target Ca/Si	Target Al/Si	SiO ₂ (g)	CaO.Al ₂ O ₃ (g)	CaO (g)
0.6	0	2.436	0	1.364
0.6	0.001	2.435	0.003	1.362
0.6	0.003	2.432	0.010	1.358
0.6	0.01	2.423	0.032	1.345
0.6	0.03	2.397	0.095	1.309
0.6	0.05	2.371	0.156	1.273
0.6	0.1	2.310	0.304	1.186
0.8	0	2.290	0	1.710
0.8	0.001	2.289	0.003	1.708
0.8	0.003	2.287	0.009	1.704
0.8	0.01	2.279	0.030	1.691
0.8	0.03	2.257	0.089	1.654
0.8	0.05	2.236	0.147	1.617
0.8	0.1	2.185	0.287	1.529
0.8	0.15	2.135	0.423	1.444
0.8	0.2	2.087	0.549	1.364
1.0	0	1.966	0	1.834
1.0	0.001	1.965	0.003	1.833
1.0	0.003	1.963	0.008	1.829
1.0	0.01	1.957	0.026	1.817
1.0	0.03	1.940	0.077	1.783
1.0	0.05	1.923	0.126	1.750
1.0	0.1	1.883	0.248	1.669
1.2	0	1.792	0	2.008
1.2	0.001	1.792	0.002	2.006
1.2	0.003	1.790	0.007	2.003
1.2	0.01	1.785	0.023	1.991
1.2	0.03	1.771	0.070	1.959
1.2	0.05	1.757	0.116	1.927
1.2	0.1	1.723	0.227	1.850
1.4	0	1.647	0	2.153
1.4	0.001	1.647	0.002	2.151
1.4	0.003	1.646	0.006	2.148
1.4	0.01	1.641	0.022	2.137

Table 5. (cont)

Target Ca/Si	Target Al/Si	SiO ₂ (g)	CaO.Al ₂ O ₃ (g)	CaO (g)
1.4	0.03	1.629	0.064	2.106
1.4	0.05	1.618	0.106	2.076
1.4	0.1	1.589	0.209	2.002

Table 6. Mixing proportions used for preparing the C-A-S-H samples (in g per 171 mL solution) at 20 °C in short-term experiments.

Target Ca/Si	Target Al/Si	SiO ₂ (g)	NaAlO ₂ (g)	CaO (g)
0.8	0.03	2.126	0.086	1.588
1.2	0.03	1.758	0.073	1.969

Appendix B. The solid phase composition of C-A-S-H.

Table 7. The solid phase composition after different equilibration times at 20 °C. The Ca/Si and Al/Si ratios were calculated from massbalance.

Target Ca/Si	Target Al/Si	NaOH (M)	Time (days)	strätlingite (wt%)	Al(OH) ₃ (wt%)	Katoite (wt%)	CH (wt%)	CaCO ₃ (wt%)	Ca/Si in C-A-S-H	Al/Si in C-A-S-H	Na/Si in solid	H ₂ O/Si in solid
0.6	0	0	90	n.m.	n.m.	n.m.	n.m.	n.m.	0.61	0	0	0.87
0.6	0	0	365	n.m.	n.m.	n.m.	n.m.	n.m.	0.60	0	0	0.95
0.6	0.001	0	90	n.m.	n.m.	n.m.	n.m.	n.m.	0.60	0.0010*	0	0.87
0.6	0.001	0	365	n.m.	n.m.	n.m.	n.m.	n.m.	0.60	0.0010*	0	0.95
0.6	0.003	0	90	n.o.	n.o.	n.o.	n.o.	n.o.	0.60	0.0032*	0	0.87
0.6	0.003	0	365	n.o.	n.o.	n.o.	n.o.	n.o.	0.60	0.0032*	0	0.95
0.6	0.01	0	90	n.o.	n.o.	n.o.	n.o.	n.o.	0.60	0.0102*	0	0.88
0.6	0.01	0	365	n.o.	n.o.	n.o.	n.o.	n.o.	0.60	0.0102*	0	0.95
0.6	0.03	0	90	n.o.	n.o.	n.o.	n.o.	n.o.	0.60	0.0306*	0	0.89
0.6	0.03	0	365	n.o.	n.o.	n.o.	n.o.	n.o.	0.60	0.0306*	0	0.96
0.6	0.05	0	90	n.o.	n.o.	n.o.	n.o.	n.o.	0.60	0.0508*	0	0.24
0.6	0.05	0	365	n.o.	n.o.	n.o.	n.o.	n.o.	0.60	0.0507*	0	0.97
0.6	0.1	0	90	n.o.	1.16	n.o.	n.o.	n.o.	0.60	0.0867*	0	1.02
0.6	0.1	0	365	n.o.	0.43	n.o.	n.o.	n.o.	0.60	0.0960*	0	1.00
0.6	0	0.1	90	n.m.	n.m.	n.m.	n.m.	n.m.	0.68	0	0.02	1.10
0.6	0	0.1	365	n.m.	n.m.	n.m.	n.m.	n.m.	0.68	0	0.42	1.10
0.6	0.001	0.1	90	n.m.	n.m.	n.m.	n.m.	n.m.	0.68	0.0011	-0.03	1.10
0.6	0.001	0.1	365	n.m.	n.m.	n.m.	n.m.	n.m.	0.72	0.0011*	0.44	1.17
0.6	0.003	0.1	90	n.m.	n.m.	n.m.	n.m.	n.m.	0.68	0.0035	-0.01	1.10
0.6	0.003	0.1	365	n.m.	n.m.	n.m.	n.m.	n.m.	0.68	0.0035	0.44	1.09
0.6	0.01	0.1	90	n.m.	n.m.	n.m.	n.m.	n.m.	0.66	0.0109	-0.03	1.07
0.6	0.01	0.1	365	n.m.	n.m.	n.m.	n.m.	n.m.	0.67	0.0111	0.41	1.08
0.6	0.03	0.1	90	n.o.	n.o.	0.35	n.o.	2.5	0.61	0.0300	-0.01	1.05
0.6	0.03	0.1	365	n.o.	n.o.	0.46	n.o.	1.0	0.73	0.0348	0.45	1.23
0.6	0.05	0.1	90	n.o.	n.o.	0.18	n.o.	n.o.	0.66	0.0536	0.03	1.09
0.6	0.05	0.1	365	n.o.	n.o.	n.o.	n.o.	1.1	0.72	0.0612	0.46	1.22
0.6	0	0.5	90	n.m.	n.m.	n.m.	n.m.	n.m.	1.02	0	0.29	1.49

Table 7. (cont)

Target Ca/Si	Target Al/Si	NaOH (M)	Time (days)	strätlingite (wt%)	Al(OH) ₃ (wt%)	Katoite (wt%)	CH (wt%)	CaCO ₃ (wt%)	Ca/Si in C-A-S-H	Al/Si in C-A-S-H	Na/Si in solid	H ₂ O/Si in solid
0.6	0	0.5	365	n.m.	n.m.	n.m.	n.m.	n.m.	0.74~	0	1.99	1.10
0.6	0.001	0.5	90	n.m.	n.m.	n.m.	n.m.	n.m.	0.77	0.0012	0.33	1.13
0.6	0.001	0.5	365	n.m.	n.m.	n.m.	n.m.	n.m.	0.71~	0.0011*	1.93	1.05
0.6	0.003	0.5	90	n.m.	n.m.	n.m.	n.m.	n.m.	0.72	0.0036	0.41	1.06
0.6	0.003	0.5	365	n.m.	n.m.	n.m.	n.m.	n.m.	0.74~	0.0037	2.03	1.10
0.6	0.01	0.5	90	n.m.	n.m.	n.m.	n.m.	n.m.	0.75	0.0120	0.16	1.10
0.6	0.01	0.5	365	n.m.	n.m.	n.m.	n.m.	n.m.	0.68~	0.0095	1.86	1.02
0.6	0.03	0.5	90	n.o.	n.o.	n.o.	n.o.	1.7	0.68	0.0333	0.30	1.04
0.6	0.03	0.5	365	n.o.	n.o.	n.o.	n.o.	1.2	0.68~	0.0327	1.91	1.12
0.6	0.05	0.5	90	n.o.	n.o.	n.o.	n.o.	1.6	0.68	0.0545	0.25	1.05
0.6	0.05	0.5	365	n.o.	n.o.	n.o.	n.o.	2.0	0.68~	0.0569	1.99	1.12
0.6	0	1	90	n.m.	n.m.	n.m.	n.m.	n.m.	0.79	0	0.06	1.11
0.6	0	1	365	n.m.	n.m.	n.m.	n.m.	n.m.	0.76~	0	4.04	1.12
0.6	0.001	1	90	n.m.	n.m.	n.m.	n.m.	n.m.	0.77	0.0012	0.16	1.07
0.6	0.001	1	365	n.m.	n.m.	n.m.	n.m.	n.m.	0.79~	0.0012*	4.21	1.17
0.6	0.003	1	90	n.m.	n.m.	n.m.	n.m.	n.m.	0.84	0.0040	0.41	1.18
0.6	0.003	1	365	n.m.	n.m.	n.m.	n.m.	n.m.	0.74~	0.0035	3.83	1.09
0.6	0.01	1	90	n.m.	n.m.	n.m.	n.m.	n.m.	0.80	0.0121	0.56	1.12
0.6	0.01	1	365	n.m.	n.m.	n.m.	n.m.	n.m.	0.77~	0.0112	4.16	1.15
0.6	0.03	1	90	n.o.	n.o.	n.o.	n.o.	2.5	0.87	0.0402	0.13	1.29
0.6	0.03	1	365	n.o.	n.o.	n.o.	n.o.	1.1	0.74~	0.0343	3.94	0.83
0.6	0.05	1	90	n.o.	n.o.	n.o.	n.o.	1.4	0.78	0.0600	0.52	0.87
0.6	0.05	1	365	n.o.	n.o.	n.o.	n.o.	1.7	0.71~	0.0526	3.97	1.11
0.8	0	0	90	n.m.	n.m.	n.m.	n.m.	n.m.	0.81	0	0	1.18
0.8	0	0	365	n.m.	n.m.	n.m.	n.m.	n.m.	0.80	0	0	1.18
0.8	0	0	730	n.m.	n.m.	n.m.	n.m.	n.m.	0.80	0	0	0.99
0.8	0	0	1095	n.m.	n.m.	n.m.	n.m.	n.m.	0.80	0	0	1.02
0.8	0.001	0	90	n.m.	n.m.	n.m.	n.m.	n.m.	0.80	0.0010*	0	1.18
0.8	0.001	0	365	n.m.	n.m.	n.m.	n.m.	n.m.	0.80	0.0010*	0	1.18
0.8	0.001	0	730	n.m.	n.m.	n.m.	n.m.	n.m.	0.80	0.0010*	0	0.99
0.8	0.001	0	1095	n.m.	n.m.	n.m.	n.m.	n.m.	0.80	0.0010*	0	1.02
0.8	0.003	0	90	n.m.	n.m.	n.m.	n.m.	n.m.	0.81	0.0030*	0	1.18
0.8	0.003	0	365	n.m.	n.m.	n.m.	n.m.	n.m.	0.80	0.0030*	0	1.18
0.8	0.003	0	730	n.m.	n.m.	n.m.	n.m.	n.m.	0.80	0.0030*	0	0.99
0.8	0.003	0	1095	n.m.	n.m.	n.m.	n.m.	n.m.	0.80	0.0030*	0	1.02
0.8	0.01	0	90	n.m.	n.m.	n.m.	n.m.	n.m.	0.80	0.0100	0	1.19
0.8	0.01	0	365	n.m.	n.m.	n.m.	n.m.	n.m.	0.80	0.0100	0	1.18
0.8	0.01	0	730	n.m.	n.m.	n.m.	n.m.	n.m.	0.80	0.0100*	0	1.00
0.8	0.01	0	1095	n.m.	n.m.	n.m.	n.m.	n.m.	0.80	0.0100*	0	1.02
0.8	0.03	0	90	n.o.	0.29	1.7	n.o.	n.o.	0.79	0.0160	0	1.20
0.8	0.03	0	365	n.o.	n.o.	n.o.	n.o.	n.o.	0.80	0.0300	0	1.19
0.8	0.03	0	730	n.o.	n.o.	n.o.	n.o.	n.o.	0.80	0.0300*	0	1.01
0.8	0.03	0	1095	n.o.	n.o.	n.o.	n.o.	n.o.	0.80	0.0300*	0	1.03
0.8	0.1	0	90	n.o.	0.14	1.4	n.o.	n.o.	0.80	0.0911	0	1.24
0.8	0.1	0	365	n.o.	n.o.	n.o.	n.o.	n.o.	0.80	0.1008	0	1.23

Table 7. (cont)

Target Ca/Si	Target Al/Si	NaOH (M)	Time (days)	strätlingite (wt%)	Al(OH) ₃ (wt%)	Katoite (wt%)	CH (wt%)	CaCO ₃ (wt%)	Ca/Si in C-A-S-H	Al/Si in C-A-S-H	Na/Si in solid	H ₂ O/Si in solid
0.8	0.1	0	730	n.o.	0.17	n.o.	n.o.	n.o.	0.80	0.0976*	0	1.04
0.8	0.1	0	1095	n.o.	0.29	n.o.	n.o.	n.o.	0.80	0.0964*	0	1.12
0.8	0.2	0	90	n.o.	1.4	2.1	n.o.	n.o.	0.79	0.1686	0	1.30
0.8	0.2	0	365	0.58	n.o.	2.1	n.o.	n.o.	0.78	0.1864	0	1.42
0.8	0.2	0	730	0.58	0.29	1.7	n.o.	n.o.	0.78	0.1822*	0	1.09
0.8	0.2	0	1095	n.o.	0.29	0.18	n.o.	n.o.	0.80	0.1963*	0	1.23
0.8	0	0.1	90	n.m.	n.m.	n.m.	n.m.	n.m.	0.81	0	0.19	1.18
0.8	0	0.1	365	n.m.	n.m.	n.m.	n.m.	n.m.	0.81	0	0.20	0.94
0.8	0	0.1	730	n.m.	n.m.	n.m.	n.m.	n.m.	0.80	0	0.19	0.98
0.8	0	0.1	1095	n.m.	n.m.	n.m.	n.m.	n.m.	0.81	0	0.21	0.90
0.8	0.001	0.1	90	n.m.	n.m.	n.m.	n.m.	n.m.	0.81	0.0009	0.14	1.18
0.8	0.001	0.1	365	n.m.	n.m.	n.m.	n.m.	n.m.	0.81	0.0010	0.20	0.94
0.8	0.001	0.1	730	n.m.	n.m.	n.m.	n.m.	n.m.	0.80	0.0010	0.22	0.98
0.8	0.001	0.1	1095	n.m.	n.m.	n.m.	n.m.	n.m.	0.80	0.0010	0.18	0.89
0.8	0.003	0.1	90	n.m.	n.m.	n.m.	n.m.	n.m.	0.81	0.0029	0.19	1.18
0.8	0.003	0.1	365	n.m.	n.m.	n.m.	n.m.	n.m.	0.81	0.0030	0.20	0.94
0.8	0.003	0.1	730	n.m.	n.m.	n.m.	n.m.	n.m.	0.80	0.0030	0.21	0.98
0.8	0.003	0.1	1095	n.m.	n.m.	n.m.	n.m.	n.m.	0.81	0.0030	0.19	0.89
0.8	0.01	0.1	90	n.m.	n.m.	n.m.	n.m.	n.m.	0.81	0.0098	0.19	1.18
0.8	0.01	0.1	365	n.m.	n.m.	n.m.	n.m.	n.m.	0.80	0.0099	0.19	0.94
0.8	0.01	0.1	730	n.o.	n.o.	n.o.	n.o.	0.8	0.79	0.0100	0.21	0.98
0.8	0.01	0.1	1095	n.m.	n.m.	n.m.	n.m.	n.m.	0.81	0.0100	0.20	0.90
0.8	0.03	0.1	90	n.o.	n.o.	n.o.	n.o.	1.2	0.79	0.0295	0.17	1.19
0.8	0.03	0.1	365	n.o.	n.o.	n.o.	n.o.	n.o.	0.81	0.0297	0.19	0.95
0.8	0.03	0.1	730	n.o.	n.o.	n.o.	n.o.	1.1	0.79	0.0300	0.22	0.99
0.8	0.03	0.1	1095	n.o.	n.o.	n.o.	n.o.	0.9	0.79	0.0298	0.19	0.90
0.8	0.05	0.1	90	n.o.	n.o.	n.o.	n.o.	1.4	0.82	0.051	nm	1.15
0.8	0.05	0.1	455	n.o.	n.o.	n.o.	n.o.	0.4	0.80	0.049	nm	0.77
0.8	0.1	0.1	90	n.o.	n.o.	0.88	n.o.	1.5	0.79	0.094	nm	1.15
0.8	0.1	0.1	455	n.o.	n.o.	1.1	n.o.	0.7	0.79	0.093	nm	0.96
0.8	0.15	0.1	90	n.o.	n.o.	1.1	n.o.	1.6	0.79	0.145	nm	1.19
0.8	0.15	0.1	455	n.o.	n.o.	2.1	n.o.	1.1	0.78	0.139	nm	1.25
0.8	0.2	0.1	90	0.58	n.o.	2.1	n.o.	0.9	0.81	0.192	nm	1.24
0.8	0.2	0.1	455	1.74	n.o.	2.8	n.o.	0.9	0.78	0.174	nm	1.28
0.8	0	0.5	90	n.m.	n.m.	n.m.	n.m.	n.m.	0.84	0	0.25	1.04
0.8	0	0.5	365	n.m.	n.m.	n.m.	n.m.	n.m.	0.81	0	0.48	0.95
0.8	0	0.5	730	n.m.	n.m.	n.m.	n.m.	n.m.	0.80	0	0.39	0.93
0.8	0	0.5	1095	n.m.	n.m.	n.m.	n.m.	n.m.	0.82	0	0.53	0.90
0.8	0.001	0.5	90	n.m.	n.m.	n.m.	n.m.	n.m.	0.84	0.0010	0.20	1.05
0.8	0.001	0.5	365	n.m.	n.m.	n.m.	n.m.	n.m.	0.81	0.0009	0.33	0.94
0.8	0.001	0.5	730	n.m.	n.m.	n.m.	n.m.	n.m.	0.80	0.0010*	0.43	0.93
0.8	0.001	0.5	1095	n.m.	n.m.	n.m.	n.m.	n.m.	0.81	0.0010	0.38	0.89
0.8	0.003	0.5	90	n.m.	n.m.	n.m.	n.m.	n.m.	0.82	0.0028	0.19	1.02
0.8	0.003	0.5	365	n.m.	n.m.	n.m.	n.m.	n.m.	0.82	0.0029	0.39	0.96
0.8	0.003	0.5	730	n.m.	n.m.	n.m.	n.m.	n.m.	0.80	0.0030	0.39	0.93

Table 7. (cont)

Target Ca/Si	Target Al/Si	NaOH (M)	Time (days)	strätlingite (wt%)	Al(OH) ₃ (wt%)	Katoite (wt%)	CH (wt%)	CaCO ₃ (wt%)	Ca/Si in C-A-S-H	Al/Si in C-A-S-H	Na/Si in solid	H ₂ O/Si in solid
0.8	0.003	0.5	1095	n.m.	n.m.	n.m.	n.m.	n.m.	0.81	0.0030	0.33	0.89
0.8	0.01	0.5	90	n.m.	n.m.	n.m.	n.m.	n.m.	0.82	0.0095	0.19	1.03
0.8	0.01	0.5	365	n.m.	n.m.	n.m.	n.m.	n.m.	0.81	0.0097	0.24	0.96
0.8	0.01	0.5	730	n.o.	n.o.	n.o.	n.o.	n.o.	0.80	0.0100	0.39	0.79
0.8	0.01	0.5	1095	n.o.	n.o.	n.o.	n.o.	n.o.	0.82	0.0099	0.49	0.90
0.8	0.03	0.5	90	n.o.	n.o.	n.o.	n.o.	3.7	0.86	0.0312	0.11	1.15
0.8	0.03	0.5	365	n.o.	n.o.	n.o.	n.o.	n.o.	0.81	0.0286	0.24	0.96
0.8	0.03	0.5	730	n.o.	n.o.	n.o.	n.o.	1.2	0.79	0.0300	0.44	0.98
0.8	0.03	0.5	1095	n.o.	n.o.	n.o.	n.o.	n.o.	0.82	0.0296	0.29	0.91
0.8	0.05	0.5	90	n.o.	n.o.	0.35	n.o.	2.5	0.78	0.048	nm	1.07
0.8	0.05	0.5	455	n.o.	n.o.	n.o.	n.o.	n.o.	0.81	0.047	nm	0.91
0.8	0.1	0.5	90	n.o.	n.o.	n.o.	n.o.	2.3	0.79	0.092	nm	1.10
0.8	0.1	0.5	455	n.o.	n.o.	n.o.	n.o.	0.7	0.80	0.090	nm	1.15
0.8	0.15	0.5	90	n.o.	n.o.	1.3	n.o.	1.7	0.83	0.138	nm	1.19
0.8	0.15	0.5	455	n.o.	n.o.	0.70	n.o.	n.o.	0.84	0.136	nm	0.86
0.8	0.2	0.5	90	n.o.	n.o.	1.8	n.o.	0.9	0.80	0.179	nm	1.18
0.8	0.2	0.5	455	n.o.	n.o.	0.49	n.o.	n.o.	0.83	0.181	nm	0.94
0.8	0	1	90	n.m.	n.m.	n.m.	n.m.	n.m.	0.87	0	0.15	1.14
0.8	0	1	365	n.m.	n.m.	n.m.	n.m.	n.m.	0.83	0	0.39	0.91
0.8	0	1	730	n.m.	n.m.	n.m.	n.m.	n.m.	0.80	0	0.55	0.93
0.8	0	1	1095	n.m.	n.m.	n.m.	n.m.	n.m.	0.82	0	0.58	0.83
0.8	0.001	1	90	n.m.	n.m.	n.m.	n.m.	n.m.	0.88	0.0010	-0.16	1.16
0.8	0.001	1	365	n.m.	n.m.	n.m.	n.m.	n.m.	0.82	0.0009	0.19	0.91
0.8	0.001	1	730	n.m.	n.m.	n.m.	n.m.	n.m.	0.80	0.0010	0.78	0.93
0.8	0.001	1	1095	n.m.	n.m.	n.m.	n.m.	n.m.	0.83	0.0010	0.49	0.84
0.8	0.003	1	90	n.m.	n.m.	n.m.	n.m.	n.m.	0.90	0.0029	-0.27	1.18
0.8	0.003	1	365	n.m.	n.m.	n.m.	n.m.	n.m.	0.82	0.0028	0.44	0.91
0.8	0.003	1	730	n.m.	n.m.	n.m.	n.m.	n.m.	0.80	0.0030	0.69	0.93
0.8	0.003	1	1095	n.m.	n.m.	n.m.	n.m.	n.m.	0.82	0.0029	0.49	0.83
0.8	0.01	1	90	n.m.	n.m.	n.m.	n.m.	n.m.	0.87	0.0094	0.10	1.16
0.8	0.01	1	365	n.m.	n.m.	n.m.	n.m.	n.m.	0.83	0.0094	0.49	0.92
0.8	0.01	1	730	n.o.	n.o.	n.o.	n.o.	n.o.	0.80	0.0100	0.73	0.93
0.8	0.01	1	1095	n.m.	n.m.	n.m.	n.m.	n.m.	0.82	0.0096	0.68	0.83
0.8	0.03	1	7	n.o.	n.o.	n.o.	n.o.	2.1	0.89	0.0279	0.51	1.09
0.8	0.03	1	14	n.o.	n.o.	n.o.	n.o.	3.1	0.88	0.0300	0.51	1.12
0.8	0.03	1	28	n.o.	n.o.	n.o.	n.o.	8.1	0.87	0.0277	0.51	1.16
0.8	0.03	1	56	n.o.	n.o.	n.o.	n.o.	1.8	0.88	0.0300	0.46	1.06
0.8	0.03	1	90	n.o.	n.o.	n.o.	n.o.	2.0	0.87	0.0290	0.00	1.20
0.8	0.03	1	365	n.o.	n.o.	n.o.	n.o.	n.o.	0.82	0.0281	-0.10	0.92
0.8	0.03	1	730	n.o.	n.o.	n.o.	n.o.	1.1	0.79	0.0300	0.79	0.99
0.8	0.03	1	1095	n.o.	n.o.	n.o.	n.o.	n.o.	0.82	0.0288	0.54	0.85
0.8	0.05	1	90	n.o.	n.o.	n.o.	n.o.	2.6	0.81	0.048	nm	1.12
0.8	0.05	1	455	n.o.	n.o.	n.o.	n.o.	n.o.	0.84	0.037	nm	0.95
0.8	0.1	1	90	n.o.	n.o.	n.o.	n.o.	2.8	0.79	0.086	nm	1.13
0.8	0.1	1	455	n.o.	n.o.	n.o.	n.o.	0.8	0.83	0.089	nm	1.12

Table 7. (cont)

Target Ca/Si	Target Al/Si	NaOH (M)	Time (days)	strätlingite (wt%)	Al(OH) ₃ (wt%)	Katoite (wt%)	CH (wt%)	CaCO ₃ (wt%)	Ca/Si in C-A-S-H	Al/Si in C-A-S-H	Na/Si in solid	H ₂ O/Si in solid
0.8	0.15	1	90	n.o.	n.o.	n.o.	n.o.	3.0	0.82	0.135	nm	1.20
0.8	0.15	1	455	n.o.	n.o.	n.o.	n.o.	0.6	0.83	0.128	nm	1.15
0.8	0.2	1	90	n.o.	n.o.	0.35	n.o.	3.1	0.84	0.161	nm	1.33
0.8	0.2	1	455	n.o.	n.o.	0.35	n.o.	0.4	0.84	0.168	nm	1.25
1.0	0	0	90	n.m.	n.m.	n.m.	n.m.	n.m.	1.00	0	0	1.10
1.0	0	0	365	n.m.	n.m.	n.m.	n.m.	n.m.	0.99	0	0	1.10
1.0	0.001	0	90	n.m.	n.m.	n.m.	n.m.	n.m.	1.00	0.0012*	0	1.10
1.0	0.001	0	365	n.m.	n.m.	n.m.	n.m.	n.m.	1.00	0.0012*	0	1.10
1.0	0.003	0	90	n.m.	n.m.	n.m.	n.m.	n.m.	1.00	0.0031*	0	1.10
1.0	0.003	0	365	n.m.	n.m.	n.m.	n.m.	n.m.	0.99	0.0031*	0	1.10
1.0	0.01	0	90	n.m.	n.m.	n.m.	n.m.	n.m.	1.00	0.0101	0	1.10
1.0	0.01	0	365	n.m.	n.m.	n.m.	n.m.	n.m.	0.99	0.0102*	0	1.11
1.0	0.03	0	90	n.m.	n.m.	n.m.	n.m.	n.m.	1.00	0.0302	0	1.11
1.0	0.03	0	365	n.o.	n.o.	n.o.	n.o.	n.o.	0.99	0.0302*	0	1.12
1.0	0.05	0	90	n.o.	n.o.	n.o.	n.o.	n.o.	1.00	0.0498	0	1.12
1.0	0.05	0	365	n.o.	n.o.	n.o.	n.o.	n.o.	0.99	0.0498*	0	1.17
1.0	0.1	0	90	n.o.	n.o.	0.95	n.o.	n.o.	0.99	0.0941	0	1.14
1.0	0.1	0	365	n.o.	n.o.	0.70	n.o.	n.o.	0.99	0.0957*	0	1.23
1.0	0	0.1	90	n.m.	n.m.	n.m.	n.m.	n.m.	1.00	0	0.16	1.10
1.0	0	0.1	365	n.m.	n.m.	n.m.	n.m.	n.m.	1.00	0	0.10	1.19
1.0	0.001	0.1	90	n.m.	n.m.	n.m.	n.m.	n.m.	1.00	0.0012*	0.10	1.10
1.0	0.001	0.1	365	n.m.	n.m.	n.m.	n.m.	n.m.	1.00	0.0010	0.05	1.19
1.0	0.003	0.1	90	n.m.	n.m.	n.m.	n.m.	n.m.	1.00	0.0031*	0.16	1.10
1.0	0.003	0.1	365	n.m.	n.m.	n.m.	n.m.	n.m.	1.00	0.0030	0.10	1.19
1.0	0.01	0.1	90	n.m.	n.m.	n.m.	n.m.	n.m.	1.00	0.0101	0.10	1.10
1.0	0.01	0.1	365	n.m.	n.m.	n.m.	n.m.	n.m.	1.00	0.0100	0.11	1.19
1.0	0.03	0.1	90	n.o.	n.o.	0.18	n.o.	n.o.	1.00	0.0291	0.11	1.11
1.0	0.03	0.1	365	n.o.	n.o.	0.35	n.o.	1.2	0.98	0.0278	0.05	1.20
1.0	0.05	0.1	90	n.o.	n.o.	0.70	n.o.	1.1	0.98	0.0454	0.11	1.12
1.0	0.05	0.1	365	n.o.	n.o.	n.o.	n.o.	1.2	0.98	0.0496	0.16	1.11
1.0	0	0.5	90	n.m.	n.m.	n.m.	n.m.	n.m.	1.00	0	0.47	1.10
1.0	0	0.5	365	n.m.	n.m.	n.m.	n.m.	n.m.	1.00	0	0.42	1.07
1.0	0.001	0.5	90	n.m.	n.m.	n.m.	n.m.	n.m.	1.00	0.0012*	0.31	1.10
1.0	0.001	0.5	365	n.m.	n.m.	n.m.	n.m.	n.m.	1.00	0.0011	0.31	1.07
1.0	0.003	0.5	90	n.m.	n.m.	n.m.	n.m.	n.m.	1.00	0.0031	0.47	1.08
1.0	0.003	0.5	365	n.m.	n.m.	n.m.	n.m.	n.m.	1.00	0.0030	0.47	1.07
1.0	0.01	0.5	90	n.m.	n.m.	n.m.	n.m.	n.m.	1.00	0.0101	0.37	1.15
1.0	0.01	0.5	365	n.m.	n.m.	n.m.	n.m.	n.m.	1.00	0.0098	0.47	1.07
1.0	0.03	0.5	90	n.o.	n.o.	n.o.	n.o.	3.2	0.96	0.0302	0.53	1.11
1.0	0.03	0.5	365	n.o.	n.o.	n.o.	n.o.	0.8	0.99	0.0298	0.32	1.08
1.0	0.05	0.5	90	n.o.	n.o.	n.o.	n.o.	2.7	0.97	0.0498	0.48	1.12
1.0	0.05	0.5	365	n.o.	n.o.	0.35	n.o.	1.5	0.98	0.0466	0.54	1.09
1.0	0	1	90	n.m.	n.m.	n.m.	n.m.	n.m.	1.00	0	0.63	1.10
1.0	0	1	365	n.m.	n.m.	n.m.	n.m.	n.m.	1.00	0	0.79	1.07
1.0	0.001	1	90	n.m.	n.m.	n.m.	n.m.	n.m.	1.00	0.0012*	0.05	1.10

Table 7. (cont)

Target Ca/Si	Target Al/Si	NaOH (M)	Time (days)	strätlingite (wt%)	Al(OH) ₃ (wt%)	Katoite (wt%)	CH (wt%)	CaCO ₃ (wt%)	Ca/Si in C-A-S-H	Al/Si in C-A-S-H	Na/Si in solid	H ₂ O/Si in solid
1.0	0.001	1	365	n.m.	n.m.	n.m.	n.m.	n.m.	1.00	0.0011	1.00	1.07
1.0	0.003	1	90	n.m.	n.m.	n.m.	n.m.	n.m.	1.00	0.0031	0.63	1.10
1.0	0.003	1	365	n.m.	n.m.	n.m.	n.m.	n.m.	1.00	0.0030	0.58	1.07
1.0	0.01	1	90	n.m.	n.m.	n.m.	n.m.	n.m.	1.00	0.0101	0.42	1.10
1.0	0.01	1	365	n.m.	n.m.	n.m.	n.m.	n.m.	1.01	0.0096	0.85	1.08
1.0	0.03	1	90	n.o.	n.o.	n.o.	n.o.	2.4	0.97	0.0301	0.42	0.99
1.0	0.03	1	365	n.o.	n.o.	n.o.	n.o.	0.6	0.10	0.0288	0.85	1.08
1.0	0.05	1	90	n.o.	n.o.	0.35	n.o.	3.0	0.96	0.0475	0.80	1.15
1.0	0.05	1	365	n.o.	n.o.	0.35	n.o.	3.4	0.96	0.0438	0.64	1.09
1.2	0	0	90	n.m.	n.m.	n.m.	n.m.	n.m.	1.16	0	0	1.32
1.2	0	0	365	n.m.	n.m.	n.m.	n.m.	n.m.	1.20	0	0	1.15
1.2	0.001	0	90	n.m.	n.m.	n.m.	n.m.	n.m.	1.18	0.0010	0	1.32
1.2	0.001	0	365	n.m.	n.m.	n.m.	n.m.	n.m.	1.20	0.0010*	0	1.15
1.2	0.003	0	90	n.m.	n.m.	n.m.	n.m.	n.m.	1.17	0.0030	0	1.32
1.2	0.003	0	365	n.m.	n.m.	n.m.	n.m.	n.m.	1.20	0.0030*	0	1.15
1.2	0.01	0	90	n.m.	n.m.	n.m.	n.m.	n.m.	1.14	0.0100	0	1.33
1.2	0.01	0	365	n.m.	n.m.	n.m.	n.m.	n.m.	1.20	0.0100*	0	1.16
1.2	0.03	0	90	n.o.	n.o.	n.o.	n.o.	0.9	1.16	0.0300	0	1.34
1.2	0.03	0	365	n.o.	n.o.	n.o.	n.o.	1.5	1.18	0.0300	0	1.17
1.2	0.05	0	90	n.o.	n.o.	n.o.	n.o.	1.4	1.15	0.0500	0	1.35
1.2	0.05	0	365	n.o.	n.o.	n.o.	n.o.	1.5	1.18	0.0500	0	1.18
1.2	0.1	0	90	n.o.	n.o.	0.70	n.o.	0.9	1.15	0.0949	0	1.38
1.2	0.1	0	365	n.o.	n.o.	0.35	n.o.	1.2	1.18	0.0975	0	1.20
1.2	0	0.1	90	n.m.	n.m.	n.m.	n.m.	n.m.	1.19	0	0.02	1.12
1.2	0	0.1	365	n.m.	n.m.	n.m.	n.m.	n.m.	1.20	0	-0.05	1.12
1.2	0.001	0.1	90	n.m.	n.m.	n.m.	n.m.	n.m.	1.19	0.0010	0.02	1.12
1.2	0.001	0.1	365	n.m.	n.m.	n.m.	n.m.	n.m.	1.20	0.0010*	-0.03	1.12
1.2	0.003	0.1	90	n.m.	n.m.	n.m.	n.m.	n.m.	1.19	0.0030	0.03	1.12
1.2	0.003	0.1	365	n.m.	n.m.	n.m.	n.m.	n.m.	1.20	0.0030*	-0.04	1.12
1.2	0.01	0.1	90	n.m.	n.m.	n.m.	n.m.	n.m.	1.18	0.0100	0.05	1.12
1.2	0.01	0.1	365	n.m.	n.m.	n.m.	n.m.	n.m.	1.20	0.0100*	-0.03	1.12
1.2	0.03	0.1	90	n.o.	n.o.	0.18	n.o.	1.6	1.16	0.0288	0.05	1.13
1.2	0.03	0.1	365	n.o.	n.o.	n.o.	n.o.	n.o.	1.20	0.0300	-0.06	1.13
1.2	0.05	0.1	90	n.o.	n.o.	1.9	n.o.	0.8	1.15	0.0368	0.06	1.14
1.2	0.05	0.1	365	n.o.	n.o.	n.o.	n.o.	0.8	1.19	0.0500	0.02	1.14
1.2	0	0.5	90	n.m.	n.m.	n.m.	n.m.	n.m.	1.20	0	0.06	1.27
1.2	0	0.5	365	n.m.	n.m.	n.m.	n.m.	n.m.	1.20	0	0.11	1.27
1.2	0.001	0.5	90	n.m.	n.m.	n.m.	n.m.	n.m.	1.20	0.0010	0	1.27
1.2	0.001	0.5	365	n.m.	n.m.	n.m.	n.m.	n.m.	1.20	0.0010*	0.11	1.27
1.2	0.003	0.5	90	n.m.	n.m.	n.m.	n.m.	n.m.	1.19	0.0030	0	1.27
1.2	0.003	0.5	365	n.m.	n.m.	n.m.	n.m.	n.m.	1.20	0.0030*	0.11	1.27
1.2	0.01	0.5	90	n.m.	n.m.	n.m.	n.m.	n.m.	1.19	0.0100	0.06	1.28
1.2	0.01	0.5	365	n.m.	n.m.	n.m.	n.m.	n.m.	1.20	0.0100*	0.12	1.28
1.2	0.03	0.5	90	n.o.	n.o.	n.o.	3.8	6.0	1.04	0.0298	0.17	1.07
1.2	0.03	0.5	365	n.o.	n.o.	0.35	n.o.	0.5	1.19	0.0276	0.12	1.07

Table 7. (cont)

Target Ca/Si	Target Al/Si	NaOH (M)	Time (days)	strätlingite (wt%)	Al(OH) ₃ (wt%)	Katoite (wt%)	CH (wt%)	CaCO ₃ (wt%)	Ca/Si in C-A-S-H	Al/Si in C-A-S-H	Na/Si in solid	H ₂ O/Si in solid
1.2	0.05	0.5	90	n.o.	n.o.	n.o.	0.8	2.2	1.15	0.0496	0.23	1.31
1.2	0.05	0.5	365	n.o.	n.o.	0.35	n.o.	0.7	1.19	0.0476	0.23	1.31
1.2	0	1	90	n.m.	n.m.	n.m.	n.m.	n.m.	1.20	0	0.46	1.39
1.2	0	1	365	n.m.	n.m.	n.m.	n.m.	n.m.	1.20	0	0.11	1.39
1.2	0.001	1	90	n.m.	n.m.	n.m.	n.m.	n.m.	1.20	0.0010	0.40	1.39
1.2	0.001	1	365	n.m.	n.m.	n.m.	n.m.	n.m.	1.20	0.0010	0.23	1.39
1.2	0.003	1	90	n.m.	n.m.	n.m.	n.m.	n.m.	1.20	0.0029	0.34	1.39
1.2	0.003	1	365	n.m.	n.m.	n.m.	n.m.	n.m.	1.20	0.0030	0.40	1.39
1.2	0.01	1	90	n.m.	n.m.	n.m.	n.m.	n.m.	1.20	0.0097	0.40	1.40
1.2	0.01	1	365	n.m.	n.m.	n.m.	n.m.	n.m.	1.20	0.0100	-0.06	1.39
1.2	0.03	1	7	n.o.	n.o.	n.o.	n.o.	3.7	1.17	0.0272	0.51	1.08
1.2	0.03	1	14	n.o.	n.o.	n.o.	n.o.	6.8	1.11	0.0274	0.51	1.20
1.2	0.03	1	28	n.o.	n.o.	n.o.	n.o.	4.5	1.15	0.0271	0.51	1.06
1.2	0.03	1	56	n.o.	n.o.	n.o.	n.o.	7.1	1.11	0.0280	0.46	1.20
1.2	0.03	1	90	n.o.	n.o.	n.o.	0.9	4.6	1.12	0.0290	0.29	1.41
1.2	0.03	1	365	n.o.	n.o.	n.o.	n.o.	1.7	1.18	0.0300	0.12	1.40
1.2	0.05	1	90	n.o.	n.o.	0.32	n.o.	4.0	1.14	0.0465	0.29	1.42
1.2	0.05	1	365	n.o.	n.o.	0.35	n.o.	1.8	1.17	0.0475	-0.06	1.41
1.4	0	0	90	n.m.	n.m.	n.m.	n.m.	n.m.	1.31	0	0	1.28
1.4	0	0	365	n.m.	n.m.	n.m.	n.m.	n.m.	1.32	0	0	1.32
1.4	0.0009	0	90	n.m.	n.m.	n.m.	n.m.	n.m.	1.34	0.0009*	0	1.28
1.4	0.0009	0	365	n.m.	n.m.	n.m.	n.m.	n.m.	1.32	0.0009*	0	1.32
1.4	0.0028	0	90	n.m.	n.m.	n.m.	n.m.	n.m.	1.32	0.0028*	0	1.28
1.4	0.0028	0	365	n.m.	n.m.	n.m.	n.m.	n.m.	1.32	0.0028*	0	1.32
1.4	0.01	0	90	n.m.	n.m.	n.m.	n.m.	n.m.	1.32	0.0102*	0	1.28
1.4	0.01	0	365	n.m.	n.m.	n.m.	n.m.	n.m.	1.33	0.0102*	0	1.33
1.4	0.03	0	90	n.o.	n.o.	n.o.	n.o.	n.o.	1.32	0.0299	0	1.29
1.4	0.03	0	365	n.o.	n.o.	n.o.	n.o.	n.o.	1.32	0.0299*	0	1.34
1.4	0.05	0	90	n.o.	n.o.	n.o.	n.o.	n.o.	1.33	0.0498	0	1.30
1.4	0.05	0	365	n.o.	n.o.	0.28	n.o.	n.o.	1.33	0.0477	0	1.35
1.4	0.1	0	90	n.o.	n.o.	1.9	n.o.	n.o.	1.31	0.0856	0	1.16
1.4	0.1	0	365	n.o.	n.o.	0.28	n.o.	n.o.	1.32	0.0978	0	1.24
1.4	0	0.1	90	n.m.	n.m.	n.m.	n.m.	n.m.	1.37	0	0.00	1.15
1.4	0	0.1	365	n.m.	n.m.	n.m.	n.m.	n.m.	1.38	0	0.06	1.19
1.4	0.0009	0.1	90	n.m.	n.m.	n.m.	n.m.	n.m.	1.37	0.0009*	0.12	1.15
1.4	0.0009	0.1	365	n.m.	n.m.	n.m.	n.m.	n.m.	1.38	0.0009*	0.00	1.19
1.4	0.0028	0.1	90	n.m.	n.m.	n.m.	n.m.	n.m.	1.37	0.0028*	0.00	1.16
1.4	0.0028	0.1	365	n.m.	n.m.	n.m.	n.m.	n.m.	1.38	0.0028*	0.00	1.19
1.4	0.01	0.1	90	n.m.	n.m.	n.m.	n.m.	n.m.	1.37	0.0102*	0.00	1.16
1.4	0.01	0.1	365	n.m.	n.m.	n.m.	n.m.	n.m.	1.37	0.0102*	0.06	1.19
1.4	0.03	0.1	90	n.o.	n.o.	n.o.	1.2	1.8	1.32	0.0299	0.13	1.17
1.4	0.03	0.1	365	n.o.	n.o.	n.o.	n.o.	2.2	1.35	0.0299*	0.06	1.20
1.4	0.05	0.1	90	n.o.	n.o.	n.o.	n.o.	n.o.	1.37	0.0498	0.06	1.22
1.4	0.05	0.1	365	n.o.	n.o.	n.o.	n.o.	0.4	1.38	0.0498*	0.00	1.21
1.4	0	0.5	90	n.m.	n.m.	n.m.	n.m.	n.m.	1.40	0	0.19	1.17

Table 7. (cont)

Target Ca/Si	Target Al/Si	NaOH (M)	Time (days)	strätlingite (wt%)	Al(OH) ₃ (wt%)	Katoite (wt%)	CH (wt%)	CaCO ₃ (wt%)	Ca/Si in C-A-S-H	Al/Si in C-A-S-H	Na/Si in solid	H ₂ O/Si in solid
1.4	0	0.5	365	n.m.	n.m.	n.m.	n.m.	n.m.	1.40	0	0.25	1.12
1.4	0.0009	0.5	90	n.m.	n.m.	n.m.	n.m.	n.m.	1.39	0.0009*	0.00	1.17
1.4	0.0009	0.5	365	n.m.	n.m.	n.m.	n.m.	n.m.	1.39	0.0009	0.44	1.12
1.4	0.0028	0.5	90	n.m.	n.m.	n.m.	n.m.	n.m.	1.39	0.0028*	0.25	1.17
1.4	0.0028	0.5	365	n.m.	n.m.	n.m.	n.m.	n.m.	1.39	0.0027	0.31	1.12
1.4	0.01	0.5	90	n.m.	n.m.	n.m.	n.m.	n.m.	1.39	0.0102*	0.31	1.17
1.4	0.01	0.5	365	n.m.	n.m.	n.m.	n.m.	n.m.	1.39	0.0101	0.19	1.13
1.4	0.03	0.5	90	n.o.	n.o.	n.o.	3.4	4.5	1.26	0.0298	0.13	1.18
1.4	0.03	0.5	365	n.o.	n.o.	n.o.	3.7	1.5	1.30	0.0297	0.19	1.14
1.4	0.05	0.5	90	n.o.	n.o.	n.o.	5.8	1.7	1.26	0.0497	0.13	1.06
1.4	0.05	0.5	365	n.o.	n.o.	n.o.	2.1	3.6	1.30	0.0496	0.19	1.14
1.4	0	1	90	n.m.	n.m.	n.m.	n.m.	n.m.	1.40	0	0.44	1.18
1.4	0	1	365	n.m.	n.m.	n.m.	n.m.	n.m.	1.40	0	0.81	1.13
1.4	0.0009	1	90	n.m.	n.m.	n.m.	n.m.	n.m.	1.40	0.0009*	0.31	1.18
1.4	0.0009	1	365	n.m.	n.m.	n.m.	n.m.	n.m.	1.40	0.0009	0.94	1.13
1.4	0.0028	1	90	n.m.	n.m.	n.m.	n.m.	n.m.	1.40	0.0027	0.06	1.18
1.4	0.0028	1	365	n.m.	n.m.	n.m.	n.m.	n.m.	1.40	0.0026	0.88	1.13
1.4	0.01	1	90	n.m.	n.m.	n.m.	n.m.	n.m.	1.40	0.0100	0.31	1.18
1.4	0.01	1	365	n.m.	n.m.	n.m.	n.m.	n.m.	1.40	0.0099	0.94	1.13
1.4	0.03	1	90	n.o.	n.o.	n.o.	4.0	7.2	1.22	0.0294	-0.50	1.19
1.4	0.03	1	365	n.o.	n.o.	n.o.	6.5	2.2	1.24	0.0291	0.76	1.14
1.4	0.05	1	90	n.o.	n.o.	n.o.	7.6	2.6	1.21	0.0485	6.36	1.36
1.4	0.05	1	365	n.o.	n.o.	n.o.	0.9	2.0	1.35	0.0488	0.83	1.22

*: Al concentrations in the solution are below the DL of ICP-OES and Al/Si ratios calculated considering Al concentration equals to zero.

~: Ca concentrations in the solution are below the DL of ICP-OES and Ca/Si ratios calculated considering the Ca concentration as zero.

n.m.: not measured.

n.o.: not observed.

Appendix C. Elemental concentrations in aqueous solution.

Table 8. Aqueous concentrations after different equilibration times at 20 °C.

Target Ca/Si	Target Al/Si	NaOH (M)	Time (days)	[Na] (mmol/L)	[Ca] (mmol/L)	[Si] (mmol/L)	[Al] (mmol/L)	[OH ⁻] (mmol/L)	pH
0.6	0	0	90	n.m.	0.60	3.57	<0.0004	0.06	9.76
0.6	0	0	365	n.m.	1.13	3.79	<0.0004	0.08	9.89
0.6	0.001	0	90	n.m.	1.13	3.86	<0.0004	0.07	9.84
0.6	0.001	0	365	n.m.	1.15	3.84	<0.0004	0.07	9.85
0.6	0.003	0	90	n.m.	1.12	3.86	<0.0004	0.07	9.85
0.6	0.003	0	365	n.m.	1.13	3.46	<0.0004	0.08	9.91
0.6	0.01	0	90	n.m.	1.19	3.74	<0.0004	0.09	9.94

Table 8. (cont)

Target Ca/Si	Target Al/Si	NaOH (M)	Time (days)	[Na] (mmol/L)	[Ca] (mmol/L)	[Si] (mmol/L)	[Al] (mmol/L)	[OH] (mmol/L)	pH
0.6	0.01	0	365	n.m.	1.05	3.30	<0.0004	0.07	9.87
0.6	0.03	0	90	n.m.	1.18	3.61	<0.0004	0.09	9.95
0.6	0.03	0	365	n.m.	1.17	3.61	<0.0004	0.09	9.95
0.6	0.05	0	90	n.m.	1.17	3.53	<0.0004	0.09	9.94
0.6	0.05	0	365	n.m.	1.01	3.22	<0.0004	0.09	9.97
0.6	0.1	0	90	n.m.	1.21	3.38	<0.0004	0.11	10.03
0.6	0.1	0	365	n.m.	1.07	3.39	<0.0004	0.09	9.97
0.6	0	0.1	90	90	0.04	27.7	<0.0004	15.1	12.18
0.6	0	0.1	365	50	0.01	27.9	<0.0004	19.0	12.27
0.6	0.001	0.1	90	110	0.04	28.0	<0.0004	15.1	12.18
0.6	0.001	0.1	365	50	0.02	40.1	<0.0004	19.9	12.29
0.6	0.003	0.1	90	100	0.05	28.5	0.006	16.2	12.21
0.6	0.003	0.1	365	50	0.03	27.0	0.009	20.9	12.32
0.6	0.01	0.1	90	110	0.03	21.8	0.027	20.4	12.31
0.6	0.01	0.1	365	50	0.01	24.2	0.009	24.5	12.39
0.6	0.03	0.1	90	100	0.03	15.3	0.088	21.9	12.34
0.6	0.03	0.1	365	60	0.01	46.7	0.009	20.9	12.32
0.6	0.05	0.1	90	90	0.02	21.1	0.062	16.6	12.22
0.6	0.05	0.1	365	50	0.02	42.4	0.013	9.5	11.98
0.6	0	0.5	90	460	0.006	97.1	<0.0004	229	13.36
0.6	0	0.5	365	450	<0.0002	43.8	<0.0004	309	13.49
0.6	0.001	0.5	90	440	0.004	52.9	0.006	240	13.38
0.6	0.001	0.5	365	440	<0.0002	35.8	<0.0004	282	13.44
0.6	0.003	0.5	90	420	0.005	39.8	0.026	269	13.43
0.6	0.003	0.5	365	430	<0.0002	44.0	0.019	302	13.48
0.6	0.01	0.5	90	470	0.005	47.1	0.094	263	13.42
0.6	0.01	0.5	365	450	<0.0002	28.8	0.40	331	13.52
0.6	0.03	0.5	90	440	0.004	31.9	0.32	275	13.44
0.6	0.03	0.5	365	440	<0.0002	30.5	0.40	331	13.52
0.6	0.05	0.5	90	450	0.004	31.6	0.68	263	13.42
0.6	0.05	0.5	365	430	<0.0002	34.4	0.37	331	13.52
0.6	0	1	90	990	0.004	57.5	<0.0004	457	13.66
0.6	0	1	365	950	<0.0002	49.2	<0.0004	631	13.80
0.6	0.001	1	90	970	0.005	51.6	0.009	457	13.66
0.6	0.001	1	365	960	<0.0002	57.4	<0.0004	631	13.80
0.6	0.003	1	90	930	0.005	68.2	0.06	417	13.62
0.6	0.003	1	365	1030	<0.0002	44.0	0.06	631	13.80
0.6	0.01	1	90	900	0.009	58.3	0.22	407	13.61
0.6	0.01	1	365	940	<0.0002	53.0	0.32	631	13.80
0.6	0.03	1	90	980	0.003	79.4	0.84	407	13.61
0.6	0.03	1	365	1060	<0.0002	48.2	0.68	631	13.79
0.6	0.05	1	90	910	0.007	55.0	1.11	389	13.59
0.6	0.05	1	365	960	<0.0002	40.4	1.54	661	13.81
0.8	0	0	90	n.m.	0.53	2.23	<0.0004	0.22	10.35
0.8	0	0	365	n.m.	1.34*	2.03	<0.0004	0.42	10.32

Table 8. (cont)

Target Ca/Si	Target Al/Si	NaOH (M)	Time (days)	[Na] (mmol/L)	[Ca] (mmol/L)	[Si] (mmol/L)	[Al] (mmol/L)	[OH] (mmol/L)	pH
0.8	0	0	730	n.m.	0.90	1.81	<0.0004	0.26	10.41
0.8	0	0	1095	n.m.	0.94	1.49	<0.0004	0.42	10.62
0.8	0.001	0	90	n.m.	0.82	2.13	0.008	0.22	10.34
0.8	0.001	0	365	n.m.	1.06*	1.77	<0.0004	0.21	10.33
0.8	0.001	0	730	n.m.	0.85	1.74	<0.0004	0.21	10.32
0.8	0.001	0	1095	n.m.	0.82	1.55	<0.0004	0.39	10.59
0.8	0.003	0	90	n.m.	0.49	2.28	0.011	0.24	10.38
0.8	0.003	0	365	n.m.	1.03*	1.69	<0.0004	0.26	10.41
0.8	0.003	0	730	n.m.	0.89	1.83	<0.0004	0.17	10.22
0.8	0.003	0	1095	n.m.	0.91	1.43	<0.0004	0.40	10.60
0.8	0.01	0	90	n.m.	1.08	2.68	0.014	0.28	10.44
0.8	0.01	0	365	n.m.	1.09*	1.88	0.0006	0.25	10.38
0.8	0.01	0	730	n.m.	0.91	1.78	<0.0004	0.18	10.25
0.8	0.01	0	1095	n.m.	0.90	1.40	<0.0004	0.40	10.60
0.8	0.03	0	90	n.m.	0.67	3.12	0.014	0.30	10.48
0.8	0.03	0	365	n.m.	1.07*	1.59	0.0004	0.34	10.53
0.8	0.03	0	730	n.m.	0.96	1.70	<0.0004	0.26	10.42
0.8	0.03	0	1095	n.m.	0.82	1.27	<0.0004	0.47	10.67
0.8	0.1	0	90	n.m.	0.50	3.02	0.015	0.39	10.59
0.8	0.1	0	365	n.m.	1.14*	1.56	0.0011	0.43	10.63
0.8	0.1	0	730	n.m.	0.94	1.41	<0.0004	0.37	10.57
0.8	0.1	0	1095	n.m.	0.88	1.05	<0.0004	0.65	10.81
0.8	0.2	0	90	n.m.	0.79	3.28	0.019	0.37	10.57
0.8	0.2	0	365	n.m.	1.29*	2.16	0.0008	0.35	10.54
0.8	0.2	0	730	n.m.	1.28	2.23	<0.0004	0.37	10.56
0.8	0.2	0	1095	n.m.	1.12	1.56	<0.0004	0.65	10.81
0.8	0	0.1	90	60	0.04	3.47	<0.0004	33.1	12.52
0.8	0	0.1	365	58	0.14*	2.19	<0.0004	33.1	12.51
0.8	0	0.1	730	62	0.02	2.07	<0.0004	51.3	12.70
0.8	0	0.1	1095	57	0.02	2.59	<0.0004	57.5	12.76
0.8	0.001	0.1	90	70	0.05	1.91	0.026	37.2	12.57
0.8	0.001	0.1	365	58	0.17*	2.10	0.004	29.5	12.47
0.8	0.001	0.1	730	56	0.02	2.47	0.002	51.3	12.71
0.8	0.001	0.1	1095	62	0.02	1.35	0.003	61.7	12.79
0.8	0.003	0.1	90	60	0.04	2.69	0.024	35.5	12.55
0.8	0.003	0.1	365	57	0.17*	2.06	0.009	32.4	12.51
0.8	0.003	0.1	730	59	0.03	1.85	0.003	61.7	12.79
0.8	0.003	0.1	1095	60	0.02	1.91	0.006	60.3	12.78
0.8	0.01	0.1	90	60	0.04	2.29	0.055	36.3	12.56
0.8	0.01	0.1	365	59	0.19*	1.10	0.041	35.5	12.55
0.8	0.01	0.1	730	59	0.03	1.80	0.025	52.5	12.72
0.8	0.01	0.1	1095	58	0.03	1.58	0.021	61.7	12.79
0.8	0.03	0.1	90	65	0.06	1.74	0.15	36.3	12.56
0.8	0.03	0.1	365	59	0.17*	1.72	0.11	31.6	12.50
0.8	0.03	0.1	730	58	0.03	1.74	0.11	58.9	12.76

Table 8. (cont)

Target Ca/Si	Target Al/Si	NaOH (M)	Time (days)	[Na] (mmol/L)	[Ca] (mmol/L)	[Si] (mmol/L)	[Al] (mmol/L)	[OH] (mmol/L)	pH
0.8	0.03	0.1	1095	61	0.05	1.16	0.082	55.0	12.74
0.8	0.05	0.1	90	n.m.	<0.0002	8.38	0.15	33.2	12.52
0.8	0.05	0.1	455	n.m.	0.04	1.83	0.22	48.0	12.68
0.8	0.1	0.1	90	n.m.	<0.0002	3.46	0.56	29.9	12.48
0.8	0.1	0.1	455	n.m.	0.03	2.53	0.48	59.7	12.78
0.8	0.15	0.1	90	n.m.	<0.0002	5.85	0.68	22.0	12.34
0.8	0.15	0.1	455	n.m.	0.01	4.60	0.54	51.7	12.71
0.8	0.2	0.1	90	n.m.	<0.0002	9.15	0.34	24.0	12.38
0.8	0.2	0.1	455	n.m.	0.01	4.93	0.97	47.9	12.68
0.8	0	0.5	90	450	0.03	9.55	<0.0004	166	13.22
0.8	0	0.5	365	400	1.26*	3.46	<0.0004	141	13.15
0.8	0	0.5	730	440	0.02	3.89	<0.0004	316	13.50
0.8	0	0.5	1095	390	0.02	4.24	<0.0004	324	13.51
0.8	0.001	0.5	90	460	0.03	11.7	0.021	166	13.22
0.8	0.001	0.5	365	430	1.68*	2.65	0.014	162	13.21
0.8	0.001	0.5	730	430	0.02	2.87	<0.0004	347	13.53
0.8	0.001	0.5	1095	420	0.04	1.72	0.004	363	13.56
0.8	0.003	0.5	90	460	0.04	5.61	0.048	166	13.22
0.8	0.003	0.5	365	420	1.12*	5.36	0.040	162	13.20
0.8	0.003	0.5	730	440	0.03	2.73	0.012	347	13.53
0.8	0.003	0.5	1095	430	0.03	2.19	0.012	347	13.54
0.8	0.01	0.5	90	460	0.04	6.45	0.17	158	13.20
0.8	0.01	0.5	365	450	1.33*	4.66	0.11	182	13.26
0.8	0.01	0.5	730	440	0.02	3.65	0.09	363	13.56
0.8	0.01	0.5	1095	400	0.02	4.72	0.07	347	13.54
0.8	0.03	0.5	90	480	0.05	26.1	0.57	162	13.21
0.8	0.03	0.5	365	450	1.24*	4.09	0.42	178	13.25
0.8	0.03	0.5	730	430	0.02	5.52	0.37	363	13.55
0.8	0.03	0.5	1095	440	0.01	4.32	0.22	309	13.49
0.8	0.05	0.5	90	n.m.	<0.0002	2.14	0.17	169	13.23
0.8	0.05	0.5	455	n.m.	0.03	2.56	0.69	409	13.61
0.8	0.1	0.5	90	n.m.	<0.0002	3.83	1.96	147	13.17
0.8	0.1	0.5	455	n.m.	0.03	2.40	2.21	367	13.56
0.8	0.15	0.5	90	n.m.	<0.0002	14.3	2.89	122	13.09
0.8	0.15	0.5	455	n.m.	0.01	10.9	3.51	313	13.50
0.8	0.2	0.5	90	n.m.	<0.0002	17.6	3.44	132	13.12
0.8	0.2	0.5	455	n.m.	0.02	7.65	4.57	220	13.34
0.8	0	1	90	970	0.04	17.2	<0.0004	309	13.49
0.8	0	1	365	920	2.40*	8.52	<0.0004	263	13.42
0.8	0	1	730	930	0.02	7.13	<0.0004	550	13.74
0.8	0	1	1095	880	0.03	6.05	<0.0004	550	13.74
0.8	0.001	1	90	1030	0.03	19.9	0.025	295	13.47
0.8	0.001	1	365	960	2.57*	7.85	0.021	302	13.47
0.8	0.001	1	730	880	0.03	5.82	<0.0004	589	13.76
0.8	0.001	1	1095	900	0.03	6.72	0.003	589	13.77

Table 8. (cont)

Target Ca/Si	Target Al/Si	NaOH (M)	Time (days)	[Na] (mmol/L)	[Ca] (mmol/L)	[Si] (mmol/L)	[Al] (mmol/L)	[OH] (mmol/L)	pH
0.8	0.003	1	90	1050	0.04	23.8	0.097	309	13.49
0.8	0.003	1	365	910	2.44*	8.07	0.072	316	13.50
0.8	0.003	1	730	900	0.02	6.50	0.021	589	13.77
0.8	0.003	1	1095	900	0.01	6.02	0.030	646	13.81
0.8	0.01	1	90	980	0.03	18.7	0.30	316	13.50
0.8	0.01	1	365	900	2.52*	8.73	0.22	309	13.49
0.8	0.01	1	730	890	0.02	7.11	0.16	589	13.77
0.8	0.01	1	1095	860	0.02	4.40	0.12	575	13.76
0.8	0.03	1	7	900	0.01	27.2	1.12	537	13.73
0.8	0.03	1	14	900	<0.0002	51.7	1.39	537	13.73
0.8	0.03	1	28	900	<0.0002	37.2	1.43	589	13.77
0.8	0.03	1	56	930	<0.0002	56.2	1.49	617	13.79
0.8	0.03	1	90	1000	0.04	23.3	0.88	372	13.57
0.8	0.03	1	365	1020	2.32*	8.06	0.61	309	13.48
0.8	0.03	1	730	880	0.02	7.34	0.48	589	13.77
0.8	0.03	1	1095	890	0.02	6.44	0.43	589	13.77
0.8	0.05	1	90	n.m.	<0.0002	8.99	0.81	216	13.33
0.8	0.05	1	455	n.m.	0.02	8.80	2.92	469	13.67
0.8	0.1	1	90	n.m.	<0.0002	6.09	3.32	216	13.33
0.8	0.1	1	455	n.m.	0.02	8.96	2.90	469	13.67
0.8	0.15	1	90	n.m.	<0.0002	12.4	4.72	260	13.41
0.8	0.15	1	455	n.m.	0.03	9.19	5.71	652	13.81
0.8	0.2	1	90	n.m.	<0.0002	17.4	10.0	296	13.47
0.8	0.2	1	455	n.m.	0.02	11.1	7.65	496	13.70
1.0	0	0	90	n.m.	3.29	0.06	<0.0004	7.6	11.88
1.0	0	0	365	n.m.	0.97	0.04	<0.0004	13.5	12.13
1.0	0.001	0	90	n.m.	3.39	0.03	<0.0004	10.2	12.01
1.0	0.001	0	365	n.m.	0.90	0.03	<0.0004	13.2	12.12
1.0	0.003	0	90	n.m.	3.38	0.04	<0.0004	9.3	11.97
1.0	0.003	0	365	n.m.	1.07	0.05	<0.0004	12.0	12.08
1.0	0.01	0	90	n.m.	3.21	0.04	0.004	7.9	11.90
1.0	0.01	0	365	n.m.	1.13	0.06	<0.0004	11.0	12.04
1.0	0.03	0	90	n.m.	3.90	0.04	0.009	6.3	11.80
1.0	0.03	0	365	n.m.	1.07	0.07	<0.0004	10.2	12.01
1.0	0.05	0	90	n.m.	1.17	0.02	0.012	6.9	11.84
1.0	0.05	0	365	n.m.	1.16	0.07	<0.0004	10.5	12.02
1.0	0.1	0	90	n.m.	1.85	0.04	0.015	7.1	11.85
1.0	0.1	0	365	n.m.	1.20	0.08	<0.0004	9.1	11.95
1.0	0	0.1	90	70	0.30	0.16	<0.0004	74.1	12.87
1.0	0	0.1	365	80	0.24	0.23	<0.0004	100	13.00
1.0	0.001	0.1	90	80	0.48	0.08	<0.0004	75.9	12.88
1.0	0.001	0.1	365	90	0.48	0.14	0.025	97.7	12.98
1.0	0.003	0.1	90	70	0.75	0.17	<0.0004	77.6	12.89
1.0	0.003	0.1	365	80	0.37	0.13	0.020	77.6	12.88
1.0	0.01	0.1	90	80	0.43	0.10	0.006	91.2	12.96

Table 8. (cont)

Target Ca/Si	Target Al/Si	NaOH (M)	Time (days)	[Na] (mmol/L)	[Ca] (mmol/L)	[Si] (mmol/L)	[Al] (mmol/L)	[OH] (mmol/L)	pH
1.0	0.01	0.1	365	80	0.48	0.16	0.027	107	13.02
1.0	0.03	0.1	90	80	0.43	0.13	0.011	70.8	12.85
1.0	0.03	0.1	365	90	0.47	0.14	0.038	74.1	12.86
1.0	0.05	0.1	90	80	0.28	0.18	0.033	79.4	12.90
1.0	0.05	0.1	365	70	0.25	0.28	0.047	72.4	12.85
1.0	0	0.5	90	410	0.16	0.36	<0.0004	295	13.52
1.0	0	0.5	365	420	0.16	0.43	<0.0004	316	13.49
1.0	0.001	0.5	90	440	0.25	0.22	<0.0004	316	13.56
1.0	0.001	0.5	365	440	0.18	0.43	0.01	324	13.50
1.0	0.003	0.5	90	410	0.20	0.23	0.04	331	13.56
1.0	0.003	0.5	365	410	0.17	0.49	0.03	324	13.51
1.0	0.01	0.5	90	430	0.20	0.47	0.12	355	13.58
1.0	0.01	0.5	365	410	0.19	0.48	0.07	380	13.57
1.0	0.03	0.5	90	400	0.18	0.51	0.13	363	13.56
1.0	0.03	0.5	365	440	0.18	0.46	0.081	398	13.59
1.0	0.05	0.5	90	410	0.12	0.53	0.34	372	13.58
1.0	0.05	0.5	365	400	0.15	0.62	0.21	398	13.59
1.0	0	1	90	880	0.25	0.46	<0.0004	631	13.80
1.0	0	1	365	850	0.24	0.49	<0.0004	589	13.77
1.0	0.001	1	90	1000	0.29	0.36	<0.0004	575	13.76
1.0	0.001	1	365	810	0.16	0.73	0.004	646	13.81
1.0	0.003	1	90	880	0.23	0.41	0.061	562	13.75
1.0	0.003	1	365	890	0.13	0.87	0.021	646	13.81
1.0	0.01	1	90	920	0.31	0.22	0.23	562	13.75
1.0	0.01	1	365	840	0.11	1.23	0.10	617	13.79
1.0	0.03	1	90	910	0.13	0.94	0.38	562	13.75
1.0	0.03	1	365	840	0.13	0.88	0.28	589	13.76
1.0	0.05	1	90	850	0.16	0.63	0.67	589	13.77
1.0	0.05	1	365	880	0.10	0.53	0.74	589	13.77
1.2	0	0	90	n.m.	6.15	0.14	<0.0004	16.2	12.21
1.2	0	0	365	n.m.	3.58	0.06	<0.0004	7.8	11.89
1.2	0.001	0	90	n.m.	3.39	0.16	0.0005	20.9	12.32
1.2	0.001	0	365	n.m.	4.56	0.06	<0.0004	8.5	11.93
1.2	0.003	0	90	n.m.	6.01	0.03	0.0007	7.9	11.90
1.2	0.003	0	365	n.m.	3.33	0.05	<0.0004	11.2	12.04
1.2	0.01	0	90	n.m.	11.1	0.04	0.0005	18.2	12.26
1.2	0.01	0	365	n.m.	5.25	0.07	<0.0004	10.5	12.02
1.2	0.03	0	90	n.m.	5.62	0.01	0.004	9.5	11.98
1.2	0.03	0	365	n.m.	1.86	0.05	0.003	9.5	11.98
1.2	0.05	0	90	n.m.	4.59	0.04	0.009	7.1	11.85
1.2	0.05	0	365	n.m.	1.80	0.05	0.011	8.5	11.93
1.2	0.1	0	90	n.m.	4.51	0.03	0.033	3.5	11.54
1.2	0.1	0	365	n.m.	3.52	0.09	0.033	6.2	11.79
1.2	0	0.1	90	96	1.57	0.02	<0.0004	16.6	12.22
1.2	0	0.1	365	108	1.61	0.05	<0.0004	87	12.95

Table 8. (cont)

Target Ca/Si	Target Al/Si	NaOH (M)	Time (days)	[Na] (mmol/L)	[Ca] (mmol/L)	[Si] (mmol/L)	[Al] (mmol/L)	[OH] (mmol/L)	pH
1.2	0.001	0.1	90	96	1.79	0.02	0.0009	15.1	12.18
1.2	0.001	0.1	365	105	1.92	0.04	<0.0004	102	13.02
1.2	0.003	0.1	90	95	1.51	0.02	0.002	19.1	12.28
1.2	0.003	0.1	365	107	1.67	0.04	0.002	78	12.89
1.2	0.01	0.1	90	91	4.32	0.02	0.002	20.0	12.30
1.2	0.01	0.1	365	105	0.33	0.02	0.003	91	12.96
1.2	0.03	0.1	90	91	2.55	0.02	0.003	17.0	12.23
1.2	0.03	0.1	365	111	1.53	0.04	0.020	43	12.64
1.2	0.05	0.1	90	89	2.51	0.02	0.003	38.0	12.58
1.2	0.05	0.1	365	96	1.17	0.05	0.064	31	12.49
1.2	0	0.5	90	470	0.97	0.06	<0.0004	186	13.27
1.2	0	0.5	365	490	0.96	0.12	<0.0004	120	13.08
1.2	0.001	0.5	90	480	0.97	0.06	0.003	195	13.29
1.2	0.001	0.5	365	500	0.83	0.13	<0.0004	302	13.47
1.2	0.003	0.5	90	470	1.36	0.05	0.002	195	13.29
1.2	0.003	0.5	365	500	1.06	0.12	<0.0004	269	13.43
1.2	0.01	0.5	90	470	1.05	0.07	0.007	195	13.29
1.2	0.01	0.5	365	490	1.19	0.11	<0.0004	331	13.52
1.2	0.03	0.5	90	470	1.45	0.06	0.031	166	13.22
1.2	0.03	0.5	365	470	1.13	0.11	0.021	316	13.49
1.2	0.05	0.5	90	460	0.61	0.15	0.085	182	13.26
1.2	0.05	0.5	365	460	1.05	0.12	0.036	302	13.47
1.2	0	1	90	920	0.36	0.16	<0.0004	282	13.45
1.2	0	1	365	980	1.01	0.28	<0.0004	501	13.70
1.2	0.001	1	90	930	0.77	0.08	0.008	309	13.49
1.2	0.001	1	365	960	0.81	0.40	0.007	447	13.65
1.2	0.003	1	90	940	0.82	0.08	0.025	224	13.35
1.2	0.003	1	365	930	0.97	0.27	0.032	468	13.66
1.2	0.01	1	90	930	0.62	0.08	0.059	347	13.54
1.2	0.01	1	365	1010	0.97	0.29	0.085	479	13.69
1.2	0.03	1	7	900	0.06	2.8	0.63	631	13.80
1.2	0.03	1	14	900	0.26	0.8	0.55	631	13.80
1.2	0.03	1	28	900	0.18	1.6	0.61	646	13.81
1.2	0.03	1	56	930	0.17	1.4	0.45	692	13.84
1.2	0.03	1	90	950	0.84	0.12	0.19	363	13.56
1.2	0.03	1	365	980	1.04	0.26	0.15	501	13.69
1.2	0.05	1	90	950	1.06	0.12	0.25	372	13.57
1.2	0.05	1	365	1010	1.06	0.28	0.25	490	13.69
1.4	0	0	90	n.m.	13.8	0.02	<0.0004	26.9	12.43
1.4	0	0	365	n.m.	12.2	0.006	<0.0004	55.0	12.73
1.4	0.001	0	90	n.m.	10.2	0.02	<0.0004	31.6	12.50
1.4	0.001	0	365	n.m.	12.1	0.006	<0.0004	31.6	12.50
1.4	0.003	0	90	n.m.	13.0	0.02	<0.0004	33.1	12.52
1.4	0.003	0	365	n.m.	12.1	0.006	<0.0004	38.0	12.58
1.4	0.01	0	90	n.m.	12.3	0.02	<0.0004	39.8	12.60

Table 8. (cont)

Target Ca/Si	Target Al/Si	NaOH (M)	Time (days)	[Na] (mmol/L)	[Ca] (mmol/L)	[Si] (mmol/L)	[Al] (mmol/L)	[OH] (mmol/L)	pH
1.4	0.01	0	365	n.m.	12.0	0.006	<0.0004	52.5	12.72
1.4	0.03	0	90	n.m.	12.0	0.02	0.001	39.8	12.60
1.4	0.03	0	365	n.m.	12.2	0.003	<0.0004	33.1	12.51
1.4	0.05	0	90	n.m.	11.5	0.02	0.003	39.8	12.60
1.4	0.05	0	365	n.m.	10.0	0.004	0.002	32.4	12.51
1.4	0.1	0	90	n.m.	10.1	0.03	0.015	22.4	12.35
1.4	0.1	0	365	n.m.	11.3	0.005	0.014	32.4	12.50
1.4	0	0.1	90	100	4.39	0.01	<0.0004	83.2	12.92
1.4	0	0.1	365	90	4.01	0.01	<0.0004	83.2	12.92
1.4	0.001	0.1	90	80	4.06	0.01	<0.0004	97.7	12.99
1.4	0.001	0.1	365	100	3.97	0.01	<0.0004	95.5	12.98
1.4	0.003	0.1	90	90	4.12	0.01	<0.0004	100	13.00
1.4	0.003	0.1	365	100	3.63	0.01	<0.0004	97.7	12.99
1.4	0.01	0.1	90	100	4.79	0.01	<0.0004	95.5	12.98
1.4	0.01	0.1	365	90	4.13	0.01	<0.0004	97.7	12.99
1.4	0.03	0.1	90	80	4.88	0.02	0.001	95.5	12.98
1.4	0.03	0.1	365	90	3.48	0.01	<0.0004	97.7	12.98
1.4	0.05	0.1	90	90	5.16	0.01	0.003	105	13.02
1.4	0.05	0.1	365	100	1.77	0.01	<0.0004	110	13.04
1.4	0	0.5	90	470	0.94	0.07	<0.0004	380	13.58
1.4	0	0.5	365	460	0.89	0.06	<0.0004	417	13.61
1.4	0.001	0.5	90	500	1.11	0.06	<0.0004	398	13.60
1.4	0.001	0.5	365	430	0.92	0.08	0.004	447	13.64
1.4	0.003	0.5	90	460	1.00	0.06	<0.0004	417	13.62
1.4	0.003	0.5	365	450	1.02	0.07	0.018	468	13.66
1.4	0.01	0.5	90	450	1.01	0.08	<0.0004	417	13.62
1.4	0.01	0.5	365	470	0.97	0.07	0.019	490	13.68
1.4	0.03	0.5	90	480	1.05	0.07	0.007	407	13.61
1.4	0.03	0.5	365	470	1.02	0.09	0.034	324	13.50
1.4	0.05	0.5	90	480	1.05	0.06	0.022	295	13.47
1.4	0.05	0.5	365	470	1.05	0.08	0.034	380	13.57
1.4	0	1	90	930	0.59	0.23	<0.0004	389	13.59
1.4	0	1	365	870	0.54	0.24	<0.0004	676	13.83
1.4	0.001	1	90	950	0.51	0.27	<0.0004	457	13.66
1.4	0.001	1	365	850	0.52	0.25	0.009	661	13.82
1.4	0.003	1	90	990	0.51	0.24	0.018	603	13.78
1.4	0.003	1	365	860	0.52	0.23	0.033	550	13.74
1.4	0.01	1	90	950	0.59	0.26	0.033	550	13.74
1.4	0.01	1	365	850	0.52	0.27	0.043	589	13.77
1.4	0.03	1	90	1080	0.60	0.25	0.081	603	13.78
1.4	0.03	1	365	880	0.55	0.24	0.13	631	13.80
1.4	0.05	1	90	880	0.59	0.24	0.22	661	13.82
1.4	0.05	1	365	870	0.54	0.23	0.17	661	13.82

*: Ca concentrations for Ca/Si = 0.8 after 1 year equilibration are outliers.

Appendix D. Saturation Indexes for different solid phases.

Table 9. The calculated saturation indexes (SI) values for strätlingite, microcrystalline Al(OH)₃, katoite, CSHQ, amorphous silica, portlandite, Ca-gismondine, chabazite and OH-sodalite.

Target Ca/Si	Target Al/Si	NaOH (M)	Time (days)	Strätling ite	Al(OH) ₃	Katoite	CSHQ	Amorpho us Silica	Portlan dite	Gismondi ne	Chabazite	Sodalite
0.6	0	0	90	n.c.	n.c.	n.c.	-0.2	0	-6.6	n.c.	n.c.	n.c.
0.6	0	0	365	n.c.	n.c.	n.c.	0.1	-0.1	-6.1	n.c.	n.c.	n.c.
0.6	0.001	0	90	n.c.	n.c.	n.c.	0.1	0	-6.1	n.c.	n.c.	n.c.
0.6	0.001	0	365	n.c.	n.c.	n.c.	0.1	0	-6.1	n.c.	n.c.	n.c.
0.6	0.003	0	90	n.c.	n.c.	n.c.	0.1	0	-6.1	n.c.	n.c.	n.c.
0.6	0.003	0	365	n.c.	n.c.	n.c.	0	-0.1	-6.1	n.c.	n.c.	n.c.
0.6	0.01	0	90	n.c.	n.c.	n.c.	0.1	-0.1	-6.0	n.c.	n.c.	n.c.
0.6	0.01	0	365	n.c.	n.c.	n.c.	0	-0.1	-6.1	n.c.	n.c.	n.c.
0.6	0.03	0	90	n.c.	n.c.	n.c.	0.1	-0.1	-5.9	n.c.	n.c.	n.c.
0.6	0.03	0	365	n.c.	n.c.	n.c.	0.1	-0.1	-6.0	n.c.	n.c.	n.c.
0.6	0.05	0	90	n.c.	n.c.	n.c.	-0.1	-0.1	-6.0	n.c.	n.c.	n.c.
0.6	0.05	0	365	n.c.	n.c.	n.c.	0	-0.2	-6.0	n.c.	n.c.	n.c.
0.6	0.1	0	90	n.c.	n.c.	n.c.	0.1	-0.2	-5.8	n.c.	n.c.	n.c.
0.6	0.1	0	365	n.c.	n.c.	n.c.	0.1	-0.2	-6.0	n.c.	n.c.	n.c.
0.6	0	0.1	90	n.c.	n.c.	n.c.	0.1	-1.5	-4.4	n.c.	n.c.	n.c.
0.6	0	0.1	365	n.c.	n.c.	n.c.	-0.5	-1.6	-5.0	n.c.	n.c.	n.c.
0.6	0.001	0.1	90	n.c.	n.c.	n.c.	-0.2	-1.5	-4.4	n.c.	n.c.	n.c.
0.6	0.001	0.1	365	n.c.	n.c.	n.c.	-0.3	-1.6	-4.7	n.c.	n.c.	n.c.
0.6	0.003	0.1	90	-6.5	-2.9	-15	-0.1	-1.6	-4.3	-1.7	-2.3	-5.1
0.6	0.003	0.1	365	-6.6	-2.8	-15	-0.3	-1.6	-4.4	-1.8	-2.6	-6.4
0.6	0.01	0.1	90	-5.7	-2.3	-14	-0.3	-1.7	-4.4	-1.0	-2.0	-1.7
0.6	0.01	0.1	365	-7.6	-2.9	-17	-0.5	-1.7	-4.8	-2.5	-3.5	-6.9
0.6	0.03	0.1	90	-4.5	-1.8	-13	-0.3	-1.9	-4.2	-0.1	-1.4	0.4
0.6	0.03	0.1	365	-7.7	-2.8	-17	-0.5	-1.6	-5.0	-2.3	-2.9	-5.7
0.6	0.05	0.1	90	-5.1	-1.9	-14	-0.3	-1.6	-4.6	-0.1	-0.8	0.4
0.6	0.05	0.1	365	-6.4	-2.3	-16	-0.3	-1.2	-5.0	-0.6	-0.5	-3.6
0.6	0	0.5	90	n.c.	n.c.	n.c.	-0.3	-2.9	-3.8	n.c.	n.c.	n.c.
0.6	0	0.5	365	n.c.	n.c.	n.c.	-0.4	-3.3	-5.6	n.c.	n.c.	n.c.
0.6	0.001	0.5	90	n.c.	n.c.	n.c.	-0.3	-3.0	-3.8	n.c.	n.c.	n.c.
0.6	0.001	0.5	365	n.c.	n.c.	n.c.	-0.4	-3.3	-5.6	n.c.	n.c.	n.c.
0.6	0.003	0.5	90	-8.3	-3.7	-15	-0.3	-3.2	-3.6	-5.9	-9.9	-5.7
0.6	0.003	0.5	365	-13	-3.9	-21	-0.4	-3.3	-5.6	-8.5	-13	-7.0
0.6	0.01	0.5	90	-7.3	-3.2	-14	-0.3	-3.1	-3.7	-4.7	-8.5	-1.6
0.6	0.01	0.5	365	-10	-2.6	-18	-0.4	-3.5	-5.4	-6.1	-11	0.1
0.6	0.03	0.5	90	-6.1	-2.6	-13	-0.3	-3.3	-3.6	-3.8	-7.9	0.7
0.6	0.03	0.5	365	-10	-2.6	-18	-0.4	-3.5	-5.4	-6.1	-11	0.2
0.6	0.05	0.5	90	-5.6	-2.2	-14	-0.3	-3.3	-3.7	-3.2	-7.3	2.8
0.6	0.05	0.5	365	-10	-2.6	-18	-0.4	-3.5	-5.5	-6.1	-11	0
0.6	0	1	90	n.c.	n.c.	n.c.	-0.1	-3.5	-3.3	n.c.	n.c.	n.c.
0.6	0	1	365	n.c.	n.c.	n.c.	-0.2	-3.9	-5.0	n.c.	n.c.	n.c.
0.6	0.001	1	90	n.c.	n.c.	n.c.	-0.1	-3.6	-3.2	n.c.	n.c.	n.c.
0.6	0.001	1	365	n.c.	n.c.	n.c.	-0.2	-3.8	-5.0	n.c.	n.c.	n.c.
0.6	0.003	1	90	-8.2	-3.7	-14	-0.1	-3.4	-3.4	-6.2	-10	-2.8

Table 9. (cont)

Target Ca/Si	Target Al/Si	NaOH (M)	Time (days)	Strätling ite	Al(OH) ₃	Katoite	CSHQ	Amorpho us Silica	Portlan dite	Gismondi ne	Chabazite	Sodalite
0.6	0.003	1	365	-12	-3.9	-19	-0.2	-3.9	-5.0	-9.1	-14	-5.1
0.6	0.01	1	90	-6.4	-3.1	-12	-0.1	-3.4	-3.1	-4.7	-9.1	0.4
0.6	0.01	1	365	-11	-3.2	-18	-0.2	-3.8	-5.0	-7.6	-13	-0.8
0.6	0.03	1	90	-6.4	-2.6	-13	-0.1	-3.3	-3.6	-4.0	-8.3	4.2
0.6	0.03	1	365	-10	-2.8	-17.1	-0.2	-3.9	-5.0	-6.9	-12	1.5
0.6	0.05	1	90	-5.1	-2.4	-11	-0.1	-3.4	-3.2	-3.3	-7.7	4.8
0.6	0.05	1	365	-9.2	-2.4	-16	-0.2	-3.9	-4.9	-6.3	-11	2.9
0.8	0	0	90	n.c.	n.c.	n.c.	-0.1	-0.5	-5.9	n.c.	n.c.	n.c.
0.8	0	0	365	n.c.	n.c.	n.c.	0.1	-0.5	-5.5	n.c.	n.c.	n.c.
0.8	0	0	730	n.c.	n.c.	n.c.	0	-0.6	-5.5	n.c.	n.c.	n.c.
0.8	0	0	1095	n.c.	n.c.	n.c.	0	-0.9	-5.1	n.c.	n.c.	n.c.
0.8	0.001	0	90	-3.4	-0.6	-15	0	-0.5	-5.7	3.7	5.3	-88
0.8	0.001	0	365	n.c.	n.c.	n.c.	0	-0.6	-5.6	n.c.	n.c.	n.c.
0.8	0.001	0	730	n.c.	n.c.	n.c.	-0.1	-0.6	-5.7	n.c.	n.c.	n.c.
0.8	0.001	0	1095	n.c.	n.c.	n.c.	0	-0.8	-5.2	n.c.	n.c.	n.c.
0.8	0.003	0	90	-3.5	-0.5	-15	-0.1	-0.5	-5.8	3.7	5.4	-87
0.8	0.003	0	365	n.c.	n.c.	n.c.	0	-0.7	-5.5	n.c.	n.c.	n.c.
0.8	0.003	0	730	n.c.	n.c.	n.c.	-0.1	-0.5	-5.9	n.c.	n.c.	n.c.
0.8	0.003	0	1095	n.c.	n.c.	n.c.	0	-0.9	-5.1	n.c.	n.c.	n.c.
0.8	0.01	0	90	-2.5	-0.5	-13	0.2	-0.5	-5.4	4.3	5.9	-86
0.8	0.01	0	365	-5.4	-1.8	-16	0.1	-0.6	-5.5	1.4	2.8	-95
0.8	0.01	0	730	n.c.	n.c.	n.c.	-0.1	-0.5	-5.8	n.c.	n.c.	n.c.
0.8	0.01	0	1095	n.c.	n.c.	n.c.	0	-0.9	-5.1	n.c.	n.c.	n.c.
0.8	0.03	0	90	-2.8	-0.5	-14	0.2	-0.5	-5.5	4.2	5.9	-86
0.8	0.03	0	365	-5.7	-2.1	-16	0.1	-0.8	-5.2	0.6	1.7	-97
0.8	0.03	0	730	n.c.	n.c.	n.c.	0	-0.7	-5.4	n.c.	n.c.	n.c.
0.8	0.03	0	1095	n.c.	n.c.	n.c.	0	-1.0	-5.1	n.c.	n.c.	n.c.
0.8	0.1	0	90	-2.9	-0.6	-14	0.1	-0.6	-5.5	3.9	5.4	-86
0.8	0.1	0	365	-4.7	-1.8	-15	0.1	-0.9	-5.0	1.3	2.2	-95
0.8	0.1	0	730	n.c.	n.c.	n.c.	0	-0.9	-5.2	n.c.	n.c.	n.c.
0.8	0.1	0	1095	n.c.	n.c.	n.c.	0	-1.2	-4.7	n.c.	n.c.	n.c.
0.8	0.2	0	90	-2.3	-0.5	-13	0.3	-0.5	-5.3	4.4	6.0	-85
0.8	0.2	0	365	-4.8	-1.8	-15	0.2	-0.7	-5.1	1.5	2.8	-94
0.8	0.2	0	730	n.c.	n.c.	n.c.	0.3	-0.7	-5.1	n.c.	n.c.	n.c.
0.8	0.2	0	1095	n.c.	n.c.	n.c.	0.1	-1.1	-4.6	n.c.	n.c.	n.c.
0.8	0	0.1	90	n.c.	n.c.	n.c.	-0.5	-2.5	-3.8	n.c.	n.c.	n.c.
0.8	0	0.1	365	n.c.	n.c.	n.c.	-0.1	-2.7	-3.0	n.c.	n.c.	n.c.
0.8	0	0.1	730	n.c.	n.c.	n.c.	-0.6	-2.9	-3.6	n.c.	n.c.	n.c.
0.8	0	0.1	1095	n.c.	n.c.	n.c.	-0.7	-2.9	-3.7	n.c.	n.c.	n.c.
0.8	0.001	0.1	90	-4.6	-2.4	-11	-0.4	-2.8	-3.3	-2.1	-5.2	-8.8
0.8	0.001	0.1	365	n.c.	n.c.	n.c.	-3.1	-12.1	-2.4	n.c.	n.c.	n.c.
0.8	0.001	0.1	730	-7.6	-3.6	-14	-0.6	-2.9	-3.6	-4.9	nc	-16
0.8	0.001	0.1	1095	-7.7	-3.6	-13	-0.6	-3.3	-3.2	-3.3	nc	-5.2
0.8	0.003	0.1	90	-4.9	-2.4	-12	-0.4	-2.7	-3.6	-2.1	-4.7	-8.5
0.8	0.003	0.1	365	-7.0	-3.0	-13	-0.1	-2.7	-2.9	-2.3	-5.1	-12

Table 9. (cont)

Target Ca/Si	Target Al/Si	NaOH (M)	Time (days)	Strätling ite	Al(OH) ₃	Katoite	CSHQ	Amorpho us Silica	Portlan dite	Gismondi ne	Chabazite	Sodalite
0.8	0.003	0.1	730	-7.0	-3.5	-13	-0.6	-3.1	-3.2	-5.0	-8.6	-16
0.8	0.003	0.1	1095	-6.7	-3.3	-13	-0.7	-3.1	-3.5	-3.1	-7.9	-4.4
0.8	0.01	0.1	90	-4.1	-2.1	-11	-0.5	-2.7	-3.5	-1.4	-4.2	-6.7
0.8	0.01	0.1	365	-2.9	-2.2	-8.5	-0.1	-3.1	-2.6	-1.4	-5.0	-9.6
0.8	0.01	0.1	730	-5.1	-2.5	-11	-0.6	-3.0	-3.3	-2.8	-6.2	-10
0.8	0.01	0.1	1095	-5.3	-2.7	-11	-0.6	-3.2	-3.2	-3.2	-7.0	-3.3
0.8	0.03	0.1	90	-2.9	-1.6	-9.3	-0.4	-2.8	-3.3	-0.5	-3.6	-4.6
0.8	0.03	0.1	365	-2.2	-1.7	-8.4	-0.1	-2.8	-2.9	-0.2	-3.2	-5.6
0.8	0.03	0.1	730	-3.7	-1.9	-9.9	-0.5	-3.1	-3.2	-1.6	-5.1	-6.8
0.8	0.03	0.1	1095	-3.5	-2.1	-9.2	-0.5	-3.3	-2.9	-3.3	-5.6	-1.9
0.8	0.05	0.1	90	n.c.	-1.6	n.c.	-1.0	-2.1	n.c.	n.c.	n.c.	n.c.
0.8	0.05	0.1	455	-3.0	-1.6	-9.3	-0.5	-3.0	-3.3	-0.8	-4.1	-3.0
0.8	0.1	0.1	90	nc	-1.0	nc	-1.1	-2.5	nc	nc	nc	nc
0.8	0.1	0.1	455	-2.7	-1.4	-9.1	-0.5	-3.0	-3.4	-0.4	-3.7	-0.7
0.8	0.15	0.1	90	n.c.	-0.8	n.c.	-1.0	-2.1	n.c.	n.c.	n.c.	n.c.
0.8	0.15	0.1	455	-3.7	-1.2	-11.3	-0.7	-2.6	-4.2	-0.2	-2.8	1.6
0.8	0.2	0.1	90	nc	-1.1	nc	-1.0	-1.9	nc	nc	nc	nc
0.8	0.2	0.1	455	-3.2	-1.0	-10.9	-0.7	-2.6	-4.2	0.4	-2.1	3.5
0.8	0	0.5	90	n.c.	n.c.	n.c.	-0.4	-3.2	-3.1	n.c.	n.c.	n.c.
0.8	0	0.5	365	n.c.	n.c.	n.c.	0.8	-3.6	-1.1	n.c.	n.c.	n.c.
0.8	0	0.5	730	n.c.	n.c.	n.c.	-0.4	-4.0	-2.4	n.c.	n.c.	n.c.
0.8	0	0.5	1095	n.c.	n.c.	n.c.	-0.4	-4.0	-2.6	n.c.	n.c.	n.c.
0.8	0.001	0.5	90	-6.1	-3.3	-12	-0.3	-3.1	-3.1	-4.2	-7.8	-4.3
0.8	0.001	0.5	365	-2.5	-3.4	-5.4	0.9	-3.9	-0.8	-3.7	-8.9	-10
0.8	0.001	0.5	730	n.c.	n.c.	n.c.	-0.4	-4.2	-2.2	n.c.	n.c.	n.c.
0.8	0.001	0.5	1095	-6.9	-4.3	-10	-0.4	-4.3	-1.8	-4.5	-14	-7.7
0.8	0.003	0.5	90	-5.0	-2.9	-10	-0.3	-3.4	-2.8	-3.7	-7.9	-3.8
0.8	0.003	0.5	365	-2.1	-2.9	-5.9	0.8	-3.5	-1.2	-2.4	-6.7	-5.0
0.8	0.003	0.5	730	-6.3	-3.7	-10	-0.4	-4.2	-2.1	-6.5	-12	-12
0.8	0.003	0.5	1095	-6.2	-3.8	-9.9	-0.4	-4.4	-2.0	-4.4	-13	-6.7
0.8	0.01	0.5	90	-3.8	-2.3	-9.4	-0.3	-3.3	-2.8	-2.4	-6.4	0
0.8	0.01	0.5	365	-1.0	-2.5	-4.4	0.9	-3.7	-1.0	-1.8	-6.4	-3.1
0.8	0.01	0.5	730	-4.7	-2.9	-8.8	-0.4	-4.2	-2.2	-4.8	-11	-6.2
0.8	0.01	0.5	1095	-5.4	-3.0	-10	-0.4	-4.2	-2.5	-4.0	-10	-5.0
0.8	0.03	0.5	90	-3.3	-1.9	-9.8	-0.3	-2.8	-3.2	-0.9	-3.8	5.9
0.8	0.03	0.5	365	0.1	-1.9	-3.3	0.9	-3.7	-1.0	-0.7	-5.5	0.1
0.8	0.03	0.5	730	-3.9	-2.3	-8.5	-0.4	-4.0	-2.5	-3.5	-8.9	-1.7
0.8	0.03	0.5	1095	-4.5	-2.5	-9.2	-0.4	-4.0	-2.6	-4.0	-9.3	-3.9
0.8	0.05	0.5	90	n.c.	-2.3	n.c.	-0.6	-3.9	n.c.	n.c.	n.c.	n.c.
0.8	0.05	0.5	455	-2.8	-2.1	-6.3	-0.3	-4.4	-1.9	-3.3	-9.6	-2.1
0.8	0.1	0.5	90	n.c.	-1.2	n.c.	-0.6	-3.5	n.c.	n.c.	n.c.	n.c.
0.8	0.1	0.5	455	-1.7	-1.5	-5.4	-0.4	-4.4	-2.0	-2.2	-8.4	1.0
0.8	0.15	0.5	90	n.c.	-1.0	n.c.	-0.5	-2.8	n.c.	n.c.	n.c.	n.c.
0.8	0.15	0.5	455	-2.7	-1.3	-8.2	-0.4	-3.6	-3.1	-1.3	-6.0	6.4
0.8	0.2	0.5	90	n.c.	-1.0	n.c.	-0.5	-2.8	n.c.	n.c.	n.c.	n.c.

Table 9. (cont)

Target Ca/Si	Target Al/Si	NaOH (M)	Time (days)	Strätling ite	Al(OH) ₃	Katoite	CSHQ	Amorpho us Silica	Portlan dite	Gismondi ne	Chabazite	Sodalite
0.8	0.2	0.5	455	-1.7	-1.0	-7.2	-0.3	-3.5	-2.9	-0.4	-4.8	7.8
0.8	0	1	90	n.c.	n.c.	n.c.	-0.1	-3.5	-2.7	n.c.	n.c.	n.c.
0.8	0	1	365	n.c.	n.c.	n.c.	1.3	-3.8	-0.6	n.c.	n.c.	n.c.
0.8	0	1	730	n.c.	n.c.	n.c.	-0.2	-4.3	-2.2	n.c.	n.c.	n.c.
0.8	0	1	1095	n.c.	n.c.	n.c.	-0.2	-4.4	-1.9	n.c.	n.c.	n.c.
0.8	0.001	1	90	-6.3	-3.6	-12	-0.1	-3.4	-2.7	-5.0	-9.1	-2.9
0.8	0.001	1	365	-2.1	-3.5	-4.7	1.3	-3.9	-0.4	-3.6	-8.8	-6.0
0.8	0.001	1	730	n.c.	n.c.	n.c.	-0.2	-4.4	-1.9	n.c.	n.c.	n.c.
0.8	0.001	1	1095	-7.7	-4.7	-11	-0.2	-4.4	-1.9	-4.4	-14	-8.3
0.8	0.003	1	90	-5.1	-3.0	-10	-0.1	-3.3	-2.7	-3.8	-7.8	0.8
0.8	0.003	1	365	-1.1	-3.0	-3.7	1.3	-3.9	-0.4	-2.7	-7.9	-3.1
0.8	0.003	1	730	-6.5	-3.8	-10	-0.2	-4.4	-2.1	-6.9	-13	-8.9
0.8	0.003	1	1095	-6.4	-3.7	-10	-0.3	-4.5	-2.1	-4.5	-13	-6.9
0.8	0.01	1	90	-4.2	-2.5	-9.6	-0.1	-3.5	-2.7	-3.0	-7.3	3.0
0.8	0.01	1	365	-0.1	-2.5	-2.8	1.3	-3.9	-0.5	-1.6	-6.7	0
0.8	0.01	1	730	-4.8	-2.9	-8.7	-0.2	-4.3	-2.2	-5.1	-11	-3.4
0.8	0.01	1	1095	-4.8	-3.0	-8.2	-0.3	-4.6	-1.9	-4.6	-12	-5.4
0.8	0.03	1	7	-4.3	-2.2	-9.5	-0.2	-3.7	-2.9	-3.1	-8.0	4.4
0.8	0.03	1	14	-10	-2.3	-19	-0.2	-3.5	-5.9	-5.7	-10	5.8
0.8	0.03	1	28	-9.8	-2.2	-18	-0.2	-3.7	-5.7	-5.8	-10	5.1
0.8	0.03	1	56	-10	-2.3	-18	-0.2	-3.5	-5.8	-5.9	-10	5.5
0.8	0.03	1	90	-3.2	-2.1	-8.4	-0.1	-3.5	-2.6	-2.2	-6.6	5.5
0.8	0.03	1	365	0.7	-2.1	-1.9	1.3	-3.9	-0.5	-0.8	-6.0	3.0
0.8	0.03	1	730	-3.8	-2.5	-7.6	-0.2	-4.3	-2.1	-4.1	-10	-0.2
0.8	0.03	1	1095	-4.0	-2.5	-7.8	-0.3	-4.4	-2.1	-4.4	-10	-4.3
0.8	0.05	1	90	n.c.	-1.8	n.c.	-0.4	-3.5	n.c.	n.c.	n.c.	n.c.
0.8	0.05	1	455	-2.2	-1.6	-6.5	-0.2	-4.1	-2.3	-2.1	-7.7	5.8
0.8	0.1	1	90	n.c.	-1.1	n.c.	-0.4	-3.7	n.c.	n.c.	n.c.	n.c.
0.8	0.1	1	455	-2.2	-1.6	-6.5	-0.2	-4.1	-2.3	-2.1	-7.7	5.8
0.8	0.15	1	90	n.c.	-1.1	n.c.	-0.3	-3.5	n.c.	n.c.	n.c.	n.c.
0.8	0.15	1	455	-1.3	-1.4	-4.9	-0.2	-4.4	-1.9	-1.9	-8.0	6.1
0.8	0.2	1	90	n.c.	-0.9	n.c.	-0.3	-3.0	n.c.	n.c.	n.c.	n.c.
0.8	0.2	1	455	-1.4	-1.2	-5.7	-0.2	-4.1	-2.3	-1.3	-6.9	8.3
1.0	0	0	90	n.c.	n.c.	n.c.	-0.5	-4.0	-2.1	n.c.	n.c.	n.c.
1.0	0	0	365	n.c.	n.c.	n.c.	-0.7	-4.0	-2.2	n.c.	n.c.	n.c.
1.0	0.001	0	90	-6.2	-3.9	-9.7	-0.6	-4.5	-1.8	-4.5	-13	-7.0
1.0	0.001	0	365	n.c.	n.c.	n.c.	-0.8	-4.2	-2.2	n.c.	n.c.	n.c.
1.0	0.003	0	90	-6.2	-3.9	-9.8	-0.6	-4.3	-1.9	-4.3	-13	-6.6
1.0	0.003	0	365	n.c.	n.c.	n.c.	-0.7	-4.1	-2.2	n.c.	n.c.	n.c.
1.0	0.01	0	90	-3.5	-2.5	-7.5	-0.6	-4.2	-2.0	-4.2	-9.5	-3.8
1.0	0.01	0	365	n.c.	n.c.	n.c.	-0.6	-4.0	-2.3	n.c.	n.c.	n.c.
1.0	0.03	0	90	-2.8	-2.1	-7.0	-0.6	-4.1	-2.2	-4.0	-8.2	-2.7
1.0	0.03	0	365	n.c.	n.c.	n.c.	-0.5	-3.8	-2.3	n.c.	n.c.	n.c.
1.0	0.05	0	90	-3.4	-2.0	-8.0	-1.0	-4.1	-2.6	-4.1	-8.6	-3.0
1.0	0.05	0	365	n.c.	n.c.	n.c.	-0.5	-3.8	-2.3	n.c.	n.c.	n.c.

Table 9. (cont)

Target Ca/Si	Target Al/Si	NaOH (M)	Time (days)	Strätling ite	Al(OH) ₃	Katoite	CSHQ	Amorpho us Silica	Portlan dite	Gismondi ne	Chabazite	Sodalite
1.0	0.1	0	90	-1.8	-1.9	-7.4	0.1	-2.9	-2.4	-2.9	-3.6	-0.4
1.0	0.1	0	365	n.c.	n.c.	n.c.	-0.5	-3.7	-2.4	n.c.	n.c.	n.c.
1.0	0	0.1	90	n.c.	n.c.	n.c.	-0.3	-4.4	-1.6	n.c.	n.c.	n.c.
1.0	0	0.1	365	n.c.	n.c.	n.c.	-0.2	-4.4	-1.5	n.c.	n.c.	n.c.
1.0	0.001	0.1	90	-7.4	-4.8	-9.9	-0.4	-4.9	-1.3	-4.9	-16	-9.0
1.0	0.001	0.1	365	-3.0	-2.8	-5.5	-0.2	-4.7	-1.2	-4.8	-12	-4.7
1.0	0.003	0.1	90	-6.8	-4.8	-9.4	-0.0	-4.6	-1.1	-4.6	-15	-8.4
1.0	0.003	0.1	365	-3.4	-2.8	-6.3	-0.3	-4.6	-1.4	-4.6	-11	-4.6
1.0	0.01	0.1	90	-4.5	-3.4	-6.9	-0.3	-4.9	-1.2	-4.9	-13	-6.2
1.0	0.01	0.1	365	-2.9	-2.8	-5.4	-0.1	-4.7	-1.1	-4.8	-12	-4.7
1.0	0.03	0.1	90	-3.8	-3.1	-6.8	-0.3	-4.6	-1.4	-4.6	-11	-5.0
1.0	0.03	0.1	365	-2.6	-2.5	-5.6	-0.2	-4.5	-1.4	-4.6	-10	-3.9
1.0	0.05	0.1	90	-3.1	-2.6	-6.3	-0.2	-4.4	-1.6	-4.4	-10	-4.0
1.0	0.05	0.1	365	-2.7	-2.4	-6.4	-0.2	-4.1	-1.7	-4.1	-8.8	-3.2
1.0	0	0.5	90	n.c.	n.c.	n.c.	-0.2	-5.1	-1.1	n.c.	n.c.	n.c.
1.0	0	0.5	365	n.c.	n.c.	n.c.	-0.1	-5.0	-1.0	n.c.	n.c.	n.c.
1.0	0.001	0.5	90	-8.2	-5.5	-9.8	-0.2	-5.4	-0.8	-5.4	-19	-11
1.0	0.001	0.5	365	-4.6	-3.6	-6.6	-0.1	-5.0	-1.0	-5.1	-14	-6.8
1.0	0.003	0.5	90	-5.2	-3.2	-9.0	-0.4	-4.4	-2.1	-4.4	-12	-5.6
1.0	0.003	0.5	365	-4.1	-3.4	-6.1	-0.1	-5.0	-1.0	-5.0	-14	-6.2
1.0	0.01	0.5	90	-5.3	-2.8	-10	-0.5	-4.1	-2.7	-4.1	-10	-4.7
1.0	0.01	0.5	365	-3.2	-3.1	-5.0	-0.1	-5.1	-0.9	-5.1	-13	-5.6
1.0	0.03	0.5	90	-2.6	-2.7	-4.6	-0.1	-5.1	-0.9	-5.1	-12	-4.9
1.0	0.03	0.5	365	-3.1	-2.9	-4.8	-0.1	-5.2	-0.9	-5.2	-13	-5.5
1.0	0.05	0.5	90	-2.2	-2.3	-4.2	-0.2	-5.1	-1.1	-5.1	-12	-4.3
1.0	0.05	0.5	365	-2.3	-2.5	-4.4	0	-5.0	-1.0	-5.0	-12	-4.5
1.0	0	1	90	n.c.	n.c.	n.c.	0	-5.7	-0.4	n.c.	n.c.	n.c.
1.0	0	1	365	n.c.	n.c.	n.c.	0	-5.7	-0.5	n.c.	n.c.	n.c.
1.0	0.001	1	90	-8.3	-5.8	-9.0	0	-5.7	-0.4	-5.7	-20	-12
1.0	0.001	1	365	-6.0	-4.5	-7.2	-0.1	-5.4	-0.6	-5.4	-17	-8.9
1.0	0.003	1	90	-3.5	-3.3	-4.4	0	-5.6	-0.5	-5.6	-15	-6.7
1.0	0.003	1	365	-4.6	-3.7	-6.0	-0.1	-5.3	-0.7	-5.4	-15	-7.3
1.0	0.01	1	90	-2.3	-2.7	-2.8	-0.1	-5.9	-0.4	-5.9	-15	-5.9
1.0	0.01	1	365	-3.4	-3.1	-5.2	-0.1	-5.1	-0.9	-5.2	-14	-5.8
1.0	0.03	1	90	-2.2	-2.5	-3.8	-0.1	-5.2	-0.8	-5.2	-13	-4.6
1.0	0.03	1	365	-2.4	-2.6	-4.0	-0.1	-5.3	-0.8	-5.3	-13	-5.0
1.0	0.05	1	90	-1.6	-2.2	-2.9	-0.1	-5.4	-0.7	-5.4	-13	-4.4
1.0	0.05	1	365	-1.7	-2.2	-3.4	-0.1	-5.2	-0.9	-5.2	-12	-4.1
1.2	0	0	90	n.c.	n.c.	n.c.	-0.3	-4.8	-1.3	n.c.	n.c.	n.c.
1.2	0	0	365	n.c.	n.c.	n.c.	-0.4	-4.1	-2.0	n.c.	n.c.	n.c.
1.2	0.001	0	90	n.c.	n.c.	n.c.	-0.4	-4.1	-2.0	n.c.	n.c.	n.c.
1.2	0.001	0	365	n.c.	n.c.	n.c.	-0.4	-4.2	-1.8	n.c.	n.c.	n.c.
1.2	0.003	0	90	-4.7	-3.3	-8.4	-0.4	-4.2	-1.9	-5.1	-11	-114
1.2	0.003	0	365	n.c.	n.c.	n.c.	-0.4	-4.3	-1.8	n.c.	n.c.	n.c.
1.2	0.01	0	90	-4.7	-3.8	-6.8	-0.2	-5.0	-1.0	-6.9	-14	-119

Table 9. (cont)

Target Ca/Si	Target Al/Si	NaOH (M)	Time (days)	Strätlingite	Al(OH) ₃	Katoite	CSHQ	Amorphous Silica	Portlandite	Gismondine	Chabazite	Sodalite
1.2	0.01	0	365	n.c.	n.c.	n.c.	-0.3	-4.3	-1.6	n.c.	n.c.	n.c.
1.2	0.03	0	90	-3.0	-2.5	-6.6	-0.3	-4.2	-1.7	-3.5	-9.3	-109
1.2	0.03	0	365	-4.0	-2.7	-8.1	-0.6	-4.0	-2.1	-4.0	-9.5	-109
1.2	0.05	0	90	-2.4	-2.1	-6.6	-0.3	-3.9	-2.0	-2.3	-7.5	-105
1.2	0.05	0	365	-2.5	-2.1	-6.4	-0.5	-4.1	-1.9	-2.8	-8.5	-106
1.2	0.1	0	90	-1.2	-1.2	-6.7	-0.3	-3.2	-2.6	0.1	-3.8	-98
1.2	0.1	0	365	-1.3	-1.5	-6.0	-0.4	-3.7	-2.2	-0.9	-5.7	-101
1.2	0	0.1	90	n.c.	n.c.	n.c.	-0.8	-4.5	-2.0	n.c.	n.c.	n.c.
1.2	0	0.1	365	n.c.	n.c.	n.c.	-0.2	-5.4	-0.6	n.c.	n.c.	n.c.
1.2	0.001	0.1	90	-5.8	-3.5	-9.5	-0.8	-4.5	-2.1	-6.4	-13	-27
1.2	0.001	0.1	365	n.c.	n.c.	n.c.	-0.2	-5.7	-0.4	n.c.	n.c.	n.c.
1.2	0.003	0.1	90	-5.2	-3.3	-8.7	-0.7	-4.6	-1.9	-5.9	-12	-26
1.2	0.003	0.1	365	-5.0	-3.8	-6.3	-0.3	-5.5	-0.7	-7.8	-16	-30
1.2	0.01	0.1	90	-4.8	-3.3	-7.3	-0.6	-5.0	-1.4	-6.5	-14	-29
1.2	0.01	0.1	365	-5.9	-3.7	-7.8	-0.8	-5.5	-1.3	-8.2	-16	-28
1.2	0.03	0.1	90	-4.5	-3.0	-7.7	-0.7	-4.7	-1.8	-5.5	-12	-25
1.2	0.03	0.1	365	-3.0	-2.6	-5.3	-0.4	-5.0	-1.2	-4.9	-12	-21
1.2	0.05	0.1	90	-4.6	-3.4	-6.6	-0.5	-5.2	-1.1	-6.7	-15	-28
1.2	0.05	0.1	365	-2.0	-1.9	-5.1	-0.5	-4.6	-1.6	-3.1	-9.7	-16
1.2	0	0.5	90	n.c.	n.c.	n.c.	-0.1	-5.6	-0.6	n.c.	n.c.	n.c.
1.2	0	0.5	365	n.c.	n.c.	n.c.	-0.1	-5.1	-0.9	n.c.	n.c.	n.c.
1.2	0.001	0.5	90	-5.1	-4.1	-6.1	-0.1	-5.6	-0.5	-8.2	-17	-22
1.2	0.001	0.5	365	n.c.	n.c.	n.c.	0.1	-5.7	-0.3	n.c.	n.c.	n.c.
1.2	0.003	0.5	90	-5.3	-4.3	-6.0	-0.1	-5.8	-0.4	-8.8	-18	-26
1.2	0.003	0.5	365	n.c.	n.c.	n.c.	0.1	-5.7	-0.2	n.c.	n.c.	n.c.
1.2	0.01	0.5	90	-4.3	-3.7	-5.3	-0.1	-5.6	-0.5	-7.4	-16	-21
1.2	0.01	0.5	365	n.c.	n.c.	n.c.	0.2	-5.9	-0.1	n.c.	n.c.	n.c.
1.2	0.03	0.5	90	-2.8	-3.0	-3.8	0	-5.6	-0.5	-6.1	-14	-17
1.2	0.03	0.5	365	-3.3	-3.4	-3.6	0.1	-5.8	-0.1	-7.1	-16	-20
1.2	0.05	0.5	90	-2.2	-2.6	-4.0	0	-5.1	-0.8	-4.6	-12	-12
1.2	0.05	0.5	365	-2.8	-3.2	-3.3	0.1	-5.7	-0.2	-6.5	-15	-18
1.2	0	1	90	n.c.	n.c.	n.c.	0	-5.1	-0.8	n.c.	n.c.	n.c.
1.2	0	1	365	n.c.	n.c.	n.c.	0.4	-5.8	0.1	n.c.	n.c.	n.c.
1.2	0.001	1	90	-4.2	-3.9	-5.2	0.2	-5.4	-0.4	-7.3	-16	-17
1.2	0.001	1	365	n.c.	n.c.	n.c.	0.4	-5.5	-0.1	n.c.	n.c.	n.c.
1.2	0.003	1	90	-3.0	-3.3	-4.6	0.2	-5.1	-0.6	-6.7	-13	-15
1.2	0.003	1	365	-2.9	-3.4	-3.2	0.3	-5.7	-0.0	-5.5	-16	-12
1.2	0.01	1	90	-2.5	-3.1	-3.8	0.3	-5.2	-0.4	-5.9	-13	-12
1.2	0.01	1	365	-2.0	-3.0	-2.3	0.4	-5.7	0.0	-5.3	-15	-11
1.2	0.03	1	7	-2.3	-2.3	-4.8	-0.1	-4.8	-1.3	-3.9	-11	-2.4
1.2	0.03	1	14	-1.3	-2.4	-2.4	0.1	-5.4	-0.4	-4.3	-13	-6.1
1.2	0.03	1	28	-1.4	-2.3	-3.1	0.1	-5.1	-0.7	-3.9	-12	-4.0
1.2	0.03	1	56	-1.8	-2.5	-3.3	0.1	-5.2	-0.6	-4.4	-12	-5.3
1.2	0.03	1	90	-1.3	-2.6	-2.2	0.3	-5.4	-0.2	-4.5	-13	-8.8
1.2	0.03	1	365	-1.5	-2.8	-1.7	0.4	-5.8	0.1	-5.5	-15	-12

Table 9. (cont)

Target Ca/Si	Target Al/Si	NaOH (M)	Time (days)	Strätling ite	Al(OH) ₃	Katoite	CSHQ	Amorpho us Silica	Portlan dite	Gismondi ne	Chabazite	Sodalite
1.2	0.05	1	90	-1.0	-2.5	-1.6	0.4	-5.5	-0.1	-4.5	-13	-8.8
1.2	0.05	1	365	-1.1	-2.6	-1.2	0.4	-5.8	0.1	-5.0	-14	-10
1.4	0	0	90	n.c.	n.c.	n.c.	0	-5.4	-0.6	n.c.	n.c.	n.c.
1.4	0	0	365	n.c.	n.c.	n.c.	-0.6	-6.8	-0.1	n.c.	n.c.	n.c.
1.4	0.001	0	90	n.c.	n.c.	n.c.	-0.4	-5.9	-0.5	n.c.	n.c.	n.c.
1.4	0.001	0	365	n.c.	n.c.	n.c.	-0.7	-6.5	-0.4	n.c.	n.c.	n.c.
1.4	0.003	0	90	n.c.	n.c.	n.c.	-0.4	-6.1	-0.4	n.c.	n.c.	n.c.
1.4	0.003	0	365	n.c.	n.c.	n.c.	-0.7	-6.6	-0.3	n.c.	n.c.	n.c.
1.4	0.01	0	90	n.c.	n.c.	n.c.	-0.3	-6.1	-0.3	n.c.	n.c.	n.c.
1.4	0.01	0	365	n.c.	n.c.	n.c.	-0.6	-6.8	-0.1	n.c.	n.c.	n.c.
1.4	0.03	0	90	-4.4	-3.7	-4.6	-0.3	-6.2	-0.3	-8.3	-18	-122
1.4	0.03	0	365	n.c.	n.c.	n.c.	-0.9	-6.8	-0.4	n.c.	n.c.	n.c.
1.4	0.05	0	90	-3.6	-3.3	-4.0	-0.3	-6.1	-0.3	-7.5	-17	-120
1.4	0.05	0	365	-4.8	-3.5	-4.9	-0.9	-6.6	-0.5	-9.1	-20	-125
1.4	0.1	0	90	-2.1	-2.4	-3.6	-0.3	-5.4	-0.8	-4.8	-13	-112
1.4	0.1	0	365	-2.9	-2.6	-3.0	-0.8	-6.5	-0.5	-7.1	-18	-119
1.4	0	0.1	90	n.c.	n.c.	n.c.	-0.5	-6.4	-0.3	n.c.	n.c.	n.c.
1.4	0	0.1	365	n.c.	n.c.	n.c.	-0.4	-6.3	-0.3	n.c.	n.c.	n.c.
1.4	0.001	0.1	90	n.c.	n.c.	n.c.	-0.4	-6.4	-0.2	n.c.	n.c.	n.c.
1.4	0.001	0.1	365	n.c.	n.c.	n.c.	-0.4	-6.4	-0.2	n.c.	n.c.	n.c.
1.4	0.003	0.1	90	n.c.	n.c.	n.c.	-0.4	-6.5	-0.2	n.c.	n.c.	n.c.
1.4	0.003	0.1	365	n.c.	n.c.	n.c.	-0.4	-6.4	-0.3	n.c.	n.c.	n.c.
1.4	0.01	0.1	90	n.c.	n.c.	n.c.	-0.4	-6.5	-0.2	n.c.	n.c.	n.c.
1.4	0.01	0.1	365	n.c.	n.c.	n.c.	-0.4	-6.5	-0.2	n.c.	n.c.	n.c.
1.4	0.03	0.1	90	-5.2	-4.2	-5.0	-0.3	-6.4	-0.1	-9.6	-20	-37
1.4	0.03	0.1	365	n.c.	n.c.	n.c.	-0.4	-6.4	-0.3	n.c.	n.c.	n.c.
1.4	0.05	0.1	90	-4.5	-3.8	-4.0	-0.3	-6.6	-0.0	-9.2	-20	-36
1.4	0.05	0.1	365	n.c.	n.c.	n.c.	-0.6	-6.4	-0.4	n.c.	n.c.	n.c.
1.4	0	0.5	90	n.c.	n.c.	n.c.	0	-6.2	-0.1	n.c.	n.c.	n.c.
1.4	0	0.5	365	n.c.	n.c.	n.c.	0	-6.2	-0.0	n.c.	n.c.	n.c.
1.4	0.001	0.5	90	n.c.	n.c.	n.c.	0	-6.3	0.0	n.c.	n.c.	n.c.
1.4	0.001	0.5	365	-5.1	-4.3	-4.9	0	-6.2	0.0	-9.5	-19	-27
1.4	0.003	0.5	90	n.c.	n.c.	n.c.	0	-6.3	0.0	n.c.	n.c.	n.c.
1.4	0.003	0.5	365	-3.8	-3.7	-3.4	0	-6.3	0.1	-8.3	-18	-23
1.4	0.01	0.0	90	n.c.	n.c.	n.c.	0.1	-6.2	0.0	n.c.	n.c.	n.c.
1.4	0.01	0.5	365	-3.8	-3.7	-3.4	0	-6.3	0.1	-8.4	-19	-23
1.4	0.03	0.5	90	-4.6	-4.1	-4.4	0	-6.2	0.0	-8.9	-19	-25
1.4	0.03	0.5	365	-3.0	-3.2	-3.3	0	-5.9	-0.1	-6.9	-16	-19
1.4	0.05	0.5	90	-3.6	-3.4	-3.8	-0.1	-6.1	-0.2	-7.5	-17	-21
1.4	0.05	0.5	365	-3.1	-3.3	-3.0	0.1	-6.1	-0.0	-7.3	-17	-20
1.4	0	1	90	n.c.	n.c.	n.c.	0.1	-5.6	-0.3	n.c.	n.c.	n.c.
1.4	0	1	365	n.c.	n.c.	n.c.	0.1	-6.0	-0.0	n.c.	n.c.	n.c.
1.4	0.001	1	90	n.c.	n.c.	n.c.	0.1	-5.7	-0.3	n.c.	n.c.	n.c.
1.4	0.001	1	365	-4.6	-4.1	-4.7	0.1	-5.9	-0.0	-8.7	-18	-20
1.4	0.003	1	90	-4.0	-3.8	-4.3	0.1	-5.9	-0.1	-7.9	-17	-18

Table 9. (cont)

Target Ca/Si	Target Al/Si	NaOH (M)	Time (days)	Strätlingite	Al(OH) ₃	Katoite	CSHQ	Amorphous Silica	Portlandite	Gismondine	Chabazite	Sodalite
1.4	0.003	1	365	-3.5	-3.5	-3.8	0.1	-5.8	-0.1	-7.3	-16	-16
1.4	0.01	1	90	-3.4	-3.5	-3.7	0.2	-5.8	-0.1	-7.1	-16	-16
1.4	0.01	1	365	-3.2	-3.4	-3.5	0.1	-5.8	-0.1	-7.0	-16	-16
1.4	0.03	1	90	-2.6	-3.2	-2.8	0.2	-5.9	-0.0	-6.6	-16	-13
1.4	0.03	1	365	-2.3	-2.9	-2.4	0.1	-5.9	-0.0	-6.3	-16	-13
1.4	0.05	1	90	-1.8	-2.8	-1.8	0.2	-6.0	0.0	-5.9	-15	-12
1.4	0.05	1	365	-2.1	-2.8	-2.1	0.1	-6.0	-0.0	-6.2	-16	-13

n.c.: not calculated as the Al and/or Ca concentrations were below the DL of ICP-OES.

Appendix E. The error calculations for solid phase composition.

Table 10. The calculated molar Al/Si and Ca/Si ratios in C-A-S-H and the corresponding errors.

Target Ca/Si	Target Al/Si	NaOH (M)	Time (days)	Ca/Si in C-A-S-H	Error of Ca/Si in C-A-S-H	Al/Si in C-A-S-H	Error of Al/Si in C-A-S-H
0.6	0	0	90	0.61	<0.0001	0	---
0.6	0	0	365	0.60	<0.0001	0	---
0.6	0.001	0	90	0.60	<0.0001	0.0010*	<0.00001
0.6	0.001	0	365	0.60	<0.0001	0.0010*	<0.00001
0.6	0.003	0	90	0.60	<0.0001	0.0032*	<0.00001
0.6	0.003	0	365	0.60	<0.0001	0.0032*	<0.00001
0.6	0.01	0	90	0.60	<0.0001	0.0102*	<0.00001
0.6	0.01	0	365	0.60	<0.0001	0.0102*	<0.00001
0.6	0.03	0	90	0.60	<0.0001	0.0306*	<0.00001
0.6	0.03	0	365	0.60	<0.0001	0.0306*	<0.00001
0.6	0.05	0	90	0.60	<0.0001	0.0508*	<0.00001
0.6	0.05	0	365	0.60	<0.0001	0.0507*	<0.00001
0.6	0.1	0	90	0.60	<0.0001	0.0867*	0.001
0.6	0.1	0	365	0.60	<0.0001	0.0960*	0.0006
0.6	0	0.1	90	0.68	<0.0001	0	---
0.6	0	0.1	365	0.68	<0.0001	0	---
0.6	0.001	0.1	90	0.68	<0.0001	0.0011	<0.00001
0.6	0.001	0.1	365	0.72	<0.0001	0.0011*	<0.00001
0.6	0.003	0.1	90	0.68	<0.0001	0.0035	<0.00001
0.6	0.003	0.1	365	0.68	<0.0001	0.0035	<0.00001
0.6	0.01	0.1	90	0.66	<0.0001	0.0109	0.0002
0.6	0.01	0.1	365	0.67	<0.0001	0.0111	<0.00001
0.6	0.03	0.1	90	0.61	0.003	0.0300	0.0001
0.6	0.03	0.1	365	0.73	0.002	0.0348	0.0003
0.6	0.05	0.1	90	0.66	0.0002	0.0536	0.03
0.6	0.05	0.1	365	0.72	0.001	0.0612	<0.00001
0.6	0	0.5	90	1.02	<0.0001	0	---
0.6	0	0.5	365	0.74~	<0.0001	0	---
0.6	0.001	0.5	90	0.77	<0.0001	0.0012	<0.00001
0.6	0.001	0.5	365	0.71~	<0.0001	0.0011*	<0.00001
0.6	0.003	0.5	90	0.72	<0.0001	0.0036	<0.00001

Table 10. (cont)

Target Ca/Si	Target Al/Si	NaOH (M)	Time (days)	Ca/Si in C-A-S-H	Error of Ca/Si in C-A-S-H	Al/Si in C-A-S-H	Error of Al/Si in C-A-S-H
0.6	0.003	0.5	365	0.74~	<0.0001	0.0037	<0.00001
0.6	0.01	0.5	90	0.75	<0.0001	0.0120	<0.00001
0.6	0.01	0.5	365	0.68~	<0.0001	0.0095	<0.00001
0.6	0.03	0.5	90	0.68	0.002	0.0333	<0.00001
0.6	0.03	0.5	365	0.68~	0.001	0.0327	<0.00001
0.6	0.05	0.5	90	0.68	0.002	0.0545	<0.00001
0.6	0.05	0.5	365	0.68~	0.002	0.0569	<0.00001
0.6	0	1	90	0.79	<0.0001	0	---
0.6	0	1	365	0.76~	<0.0001	0	---
0.6	0.001	1	90	0.77	<0.0001	0.0012	<0.00001
0.6	0.001	1	365	0.79~	<0.0001	0.0012*	<0.00001
0.6	0.003	1	90	0.84	<0.0001	0.0040	<0.00001
0.6	0.003	1	365	0.74~	<0.0001	0.0035	<0.00001
0.6	0.01	1	90	0.80	<0.0001	0.0121	<0.00001
0.6	0.01	1	365	0.77~	<0.0001	0.0112	<0.00001
0.6	0.03	1	90	0.87	0.004	0.0402	<0.00001
0.6	0.03	1	365	0.74~	0.001	0.0343	<0.00001
0.6	0.05	1	90	0.78	0.002	0.0600	<0.00001
0.6	0.05	1	365	0.71~	0.002	0.0526	<0.00001
0.8	0	0	90	0.81	<0.0001	0	---
0.8	0	0	365	0.80	<0.0001	0	---
0.8	0	0	730	0.80	<0.0001	0	---
0.8	0	0	1095	0.80	<0.0001	0	---
0.8	0.001	0	90	0.80	<0.0001	0.0010*	<0.00001
0.8	0.001	0	365	0.80	<0.0001	0.0010*	<0.00001
0.8	0.001	0	730	0.80	<0.0001	0.0010*	<0.00001
0.8	0.001	0	1095	0.80	<0.0001	0.0010*	<0.00001
0.8	0.003	0	90	0.81	<0.0001	0.0030*	<0.00001
0.8	0.003	0	365	0.80	<0.0001	0.0030*	<0.00001
0.8	0.003	0	730	0.80	<0.0001	0.0030*	<0.00001
0.8	0.003	0	1095	0.80	<0.0001	0.0030*	<0.00001
0.8	0.01	0	90	0.80	<0.0001	0.0100	<0.00001
0.8	0.01	0	365	0.80	<0.0001	0.0100	<0.00001
0.8	0.01	0	730	0.80	<0.0001	0.0100*	<0.00001
0.8	0.01	0	1095	0.80	<0.0001	0.0100*	<0.00001
0.8	0.03	0	90	0.79	0.002	0.0160	0.001
0.8	0.03	0	365	0.80	<0.0001	0.0300	<0.00001
0.8	0.03	0	730	0.80	<0.0001	0.0300*	<0.00001
0.8	0.03	0	1095	0.80	1.03	0.0300*	<0.00001
0.8	0.1	0	90	0.80	0.001	0.0911	0.001
0.8	0.1	0	365	0.80	<0.0001	0.1008	<0.00001
0.8	0.1	0	730	0.80	<0.0001	0.0976*	0.0002
0.8	0.1	0	1095	0.80	1.12	0.0964*	0.0004
0.8	0.2	0	90	0.79	0.002	0.1686	0.003
0.8	0.2	0	365	0.78	0.002	0.1864	0.002

Table 10. (cont)

Target Ca/Si	Target Al/Si	NaOH (M)	Time (days)	Ca/Si in C-A-S-H	Error of Ca/Si in C-A-S-H	Al/Si in C-A-S-H	Error of Al/Si in C-A-S-H
0.8	0.2	0	730	0.78	0.002	0.1822*	0.002
0.8	0.2	0	1095	0.80	0.0002	0.1963*	0.0005
0.8	0	0.1	90	0.80	<0.0001	0	---
0.8	0	0.1	365	0.80	<0.0001	0	---
0.8	0	0.1	730	0.80	<0.0001	0	---
0.8	0	0.1	1095	0.80	<0.0001	0	---
0.8	0.001	0.1	90	0.81	<0.0001	0.0009	<0.00001
0.8	0.001	0.1	365	0.81	<0.0001	0.0010	<0.00001
0.8	0.001	0.1	730	0.80	<0.0001	0.0010	<0.00001
0.8	0.001	0.1	1095	0.80	<0.0001	0.0010	<0.00001
0.8	0.003	0.1	90	0.81	<0.0001	0.0029	<0.00001
0.8	0.003	0.1	365	0.81	<0.0001	0.0030	<0.00001
0.8	0.003	0.1	730	0.80	<0.0001	0.0030	<0.00001
0.8	0.003	0.1	1095	0.81	<0.0001	0.0030	<0.00001
0.8	0.01	0.1	90	0.81	<0.0001	0.0098	<0.00001
0.8	0.01	0.1	365	0.80	<0.0001	0.0099	<0.00001
0.8	0.01	0.1	730	0.79	0.0008	0.0100	<0.00001
0.8	0.01	0.1	1095	0.81	<0.0001	0.0100	<0.00001
0.8	0.03	0.1	90	0.79	0.001	0.0295	<0.00001
0.8	0.03	0.1	365	0.81	<0.0001	0.0297	<0.00001
0.8	0.03	0.1	730	0.79	0.001	0.0300	<0.00001
0.8	0.03	0.1	1095	0.79	0.001	0.0298	<0.00001
0.8	0.05	0.1	90	0.82	0.001	0.051	0.0005
0.8	0.05	0.1	455	0.80	0.0007	0.049	<0.00001
0.8	0.1	0.1	90	0.79	0.003	0.094	0.0006
0.8	0.1	0.1	455	0.79	0.002	0.093	0.0006
0.8	0.15	0.1	90	0.79	0.003	0.145	0.002
0.8	0.15	0.1	455	0.78	0.004	0.139	0.001
0.8	0.2	0.1	90	0.81	0.003	0.192	0.0002
0.8	0.2	0.1	455	0.78	0.005	0.174	0.003
0.8	0	0.5	90	0.84	<0.0001	0	---
0.8	0	0.5	365	0.81	<0.0001	0	---
0.8	0	0.5	730	0.80	<0.0001	0	---
0.8	0	0.5	1095	0.82	<0.0001	0	---
0.8	0.001	0.5	90	0.84	<0.0001	0.0010	<0.00001
0.8	0.001	0.5	365	0.81	<0.0001	0.0009	<0.00001
0.8	0.001	0.5	730	0.80	<0.0001	0.0010*	<0.00001
0.8	0.001	0.5	1095	0.81	<0.0001	0.0010	<0.00001
0.8	0.003	0.5	90	0.82	<0.0001	0.0028	<0.00001
0.8	0.003	0.5	365	0.82	<0.0001	0.0029	<0.00001
0.8	0.003	0.5	730	0.80	<0.0001	0.0030	<0.00001
0.8	0.003	0.5	1095	0.81	<0.0001	0.0030	<0.00001
0.8	0.01	0.5	90	0.82	<0.0001	0.0095	<0.00001
0.8	0.01	0.5	365	0.81	<0.0001	0.0097	<0.00001
0.8	0.01	0.5	730	0.80	<0.0001	0.0100	<0.00001

Table 10. (cont)

Target Ca/Si	Target Al/Si	NaOH (M)	Time (days)	Ca/Si in C-A-S-H	Error of Ca/Si in C-A-S-H	Al/Si in C-A-S-H	Error of Al/Si in C-A-S-H
0.8	0.01	0.5	1095	0.82	<0.0001	0.0099	<0.00001
0.8	0.03	0.5	90	0.86	0.004	0.0312	<0.00001
0.8	0.03	0.5	365	0.81	<0.0001	0.0286	<0.00001
0.8	0.03	0.5	730	0.79	0.001	0.0300	<0.00001
0.8	0.03	0.5	1095	0.82	<0.0001	0.0296	<0.00001
0.8	0.05	0.5	90	0.78	0.003	0.048	0.0002
0.8	0.05	0.5	455	0.81	<0.0001	0.047	<0.00001
0.8	0.1	0.5	90	0.79	0.002	0.092	<0.00001
0.8	0.1	0.5	455	0.80	0.0008	0.090	<0.00001
0.8	0.15	0.5	90	0.83	0.003	0.138	0.0008
0.8	0.15	0.5	455	0.84	0.0007	0.136	0.0004
0.8	0.2	0.5	90	0.80	0.003	0.179	0.001
0.8	0.2	0.5	455	0.83	0.0005	0.181	0.0003
0.8	0	1	90	0.87	<0.0001	0	---
0.8	0	1	365	0.83	<0.0001	0	---
0.8	0	1	730	0.80	<0.0001	0	---
0.8	0	1	1095	0.82	<0.0001	0	---
0.8	0.001	1	90	0.88	<0.0001	0.0010	<0.00001
0.8	0.001	1	365	0.82	<0.0001	0.0009	<0.00001
0.8	0.001	1	730	0.80	<0.0001	0.0010	<0.00001
0.8	0.001	1	1095	0.83	<0.0001	0.0010	<0.00001
0.8	0.003	1	90	0.90	<0.0001	0.0029	<0.00001
0.8	0.003	1	365	0.82	<0.0001	0.0028	<0.00001
0.8	0.003	1	730	0.80	<0.0001	0.0030	<0.00001
0.8	0.003	1	1095	0.82	<0.0001	0.0029	<0.00001
0.8	0.01	1	90	0.87	<0.0001	0.0094	<0.00001
0.8	0.01	1	365	0.83	<0.0001	0.0094	<0.00001
0.8	0.01	1	730	0.80	<0.0001	0.0100	<0.00001
0.8	0.01	1	1095	0.82	<0.0001	0.0096	<0.00001
0.8	0.03	1	7	0.89	0.003	0.0279	<0.00001
0.8	0.03	1	14	0.88	0.005	0.0300	<0.00001
0.8	0.03	1	28	0.87	0.01	0.0277	<0.00001
0.8	0.03	1	56	0.88	0.002	0.0300	<0.00001
0.8	0.03	1	90	0.87	0.003	0.0290	<0.00001
0.8	0.03	1	365	0.82	<0.0001	0.0281	<0.00001
0.8	0.03	1	730	0.79	0.001	0.0300	<0.00001
0.8	0.03	1	1095	0.82	<0.0001	0.0288	<0.00001
0.8	0.05	1	90	0.81	0.004	0.048	<0.00001
0.8	0.05	1	455	0.84	<0.0001	0.037	<0.00001
0.8	0.1	1	90	0.79	0.003	0.086	<0.00001
0.8	0.1	1	455	0.83	0.0009	0.089	<0.00001
0.8	0.15	1	90	0.82	0.003	0.135	<0.00001
0.8	0.15	1	455	0.83	0.001	0.128	<0.00001
0.8	0.2	1	90	0.84	0.003	0.161	0.0002
0.8	0.2	1	455	0.84	0.0009	0.168	0.0002

Table 10. (cont)

Target Ca/Si	Target Al/Si	NaOH (M)	Time (days)	Ca/Si in C-A-S-H	Error of Ca/Si in C-A-S-H	Al/Si in C-A-S-H	Error of Al/Si in C-A-S-H
1.0	0	0	90	1.00	<0.0001	0	---
1.0	0	0	365	0.99	<0.0001	0	---
1.0	0.001	0	90	1.00	<0.0001	0.0012*	<0.00001
1.0	0.001	0	365	1.00	<0.0001	0.0012*	<0.00001
1.0	0.003	0	90	1.00	<0.0001	0.0031*	<0.00001
1.0	0.003	0	365	0.99	<0.0001	0.0031*	<0.00001
1.0	0.01	0	90	1.00	<0.0001	0.0101	<0.00001
1.0	0.01	0	365	0.99	<0.0001	0.0102*	<0.00001
1.0	0.03	0	90	1.00	<0.0001	0.0302	<0.00001
1.0	0.03	0	365	0.99	<0.0001	0.0302*	<0.00001
1.0	0.05	0	90	1.00	<0.0001	0.0498	<0.00001
1.0	0.05	0	365	0.99	<0.0001	0.0498*	<0.00001
1.0	0.1	0	90	0.99	0.001	0.0941	0.0006
1.0	0.1	0	365	0.99	0.0007	0.0957*	0.0004
1.0	0	0.1	90	1.00	<0.0001	0	---
1.0	0	0.1	365	1.00	<0.0001	0	---
1.0	0.001	0.1	90	1.00	<0.0001	0.0012*	<0.00001
1.0	0.001	0.1	365	1.00	<0.0001	0.0010	<0.00001
1.0	0.003	0.1	90	1.00	<0.0001	0.0031*	<0.00001
1.0	0.003	0.1	365	1.00	<0.0001	0.0030	<0.00001
1.0	0.01	0.1	90	1.00	<0.0001	0.0101	<0.00001
1.0	0.01	0.1	365	1.00	<0.0001	0.0100	<0.00001
1.0	0.03	0.1	90	1.00	0.0002	0.0291	0.0001
1.0	0.03	0.1	365	0.98	0.002	0.0278	0.0002
1.0	0.05	0.1	90	0.98	0.002	0.0454	0.0004
1.0	0.05	0.1	365	0.98	0.002	0.0496	<0.00001
1.0	0	0.5	90	1.00	<0.0001	0	---
1.0	0	0.5	365	1.00	<0.0001	0	---
1.0	0.001	0.5	90	1.00	<0.0001	0.0012*	<0.00001
1.0	0.001	0.5	365	1.00	<0.0001	0.0011	<0.00001
1.0	0.003	0.5	90	1.00	<0.0001	0.0031	<0.00001
1.0	0.003	0.5	365	1.00	<0.0001	0.0030	<0.00001
1.0	0.01	0.5	90	1.00	<0.0001	0.0101	<0.00001
1.0	0.01	0.5	365	1.00	<0.0001	0.0098	<0.00001
1.0	0.03	0.5	90	0.96	0.004	0.0302	<0.00001
1.0	0.03	0.5	365	0.99	0.001	0.0298	<0.00001
1.0	0.05	0.5	90	0.97	0.003	0.0498	<0.00001
1.0	0.05	0.5	365	0.98	0.002	0.0466	0.0002
1.0	0	1	90	1.00	<0.0001	0	---
1.0	0	1	365	1.00	<0.0001	0	---
1.0	0.001	1	90	1.00	<0.0001	0.0012*	<0.00001
1.0	0.001	1	365	1.00	<0.0001	0.0011	<0.00001
1.0	0.003	1	90	1.00	<0.0001	0.0031	<0.00001
1.0	0.003	1	365	1.00	<0.0001	0.0030	<0.00001
1.0	0.01	1	90	1.00	<0.0001	0.0101	<0.00001

Table 10. (cont)

Target Ca/Si	Target Al/Si	NaOH (M)	Time (days)	Ca/Si in C-A-S-H	Error of Ca/Si in C-A-S-H	Al/Si in C-A-S-H	Error of Al/Si in C-A-S-H
1.0	0.01	1	365	1.01	<0.0001	0.0096	<0.00001
1.0	0.03	1	90	0.97	0.003	0.0301	<0.00001
1.0	0.03	1	365	0.10	0.0008	0.0288	<0.00001
1.0	0.05	1	90	0.96	0.004	0.0475	<0.00001
1.0	0.05	1	365	0.96	0.005	0.0438	0.0002
1.2	0	0	90	1.16	<0.0001	0	---
1.2	0	0	365	1.20	<0.0001	0	---
1.2	0.001	0	90	1.18	<0.0001	0.0010	<0.00001
1.2	0.001	0	365	1.20	<0.0001	0.0010*	<0.00001
1.2	0.003	0	90	1.17	<0.0001	0.0030	<0.00001
1.2	0.003	0	365	1.20	<0.0001	0.0030*	<0.00001
1.2	0.01	0	90	1.14	<0.0001	0.0100	<0.00001
1.2	0.01	0	365	1.20	<0.0001	0.0100*	<0.00001
1.2	0.03	0	90	1.16	0.001	0.0300	<0.00001
1.2	0.03	0	365	1.18	0.002	0.0300	<0.00001
1.2	0.05	0	90	1.15	0.002	0.0500	<0.00001
1.2	0.05	0	365	1.18	0.002	0.0500	<0.00001
1.2	0.1	0	90	1.15	0.002	0.0949	0.0005
1.2	0.1	0	365	1.18	0.002	0.0975	0.0002
1.2	0	0.1	90	1.19	<0.0001	0	---
1.2	0	0.1	365	1.20	<0.0001	0	---
1.2	0.001	0.1	90	1.19	<0.0001	0.0010	<0.00001
1.2	0.001	0.1	365	1.20	<0.0001	0.0010*	<0.00001
1.2	0.003	0.1	90	1.19	<0.0001	0.0030	<0.00001
1.2	0.003	0.1	365	1.20	<0.0001	0.0030*	<0.00001
1.2	0.01	0.1	90	1.18	<0.0001	0.0100	<0.00001
1.2	0.01	0.1	365	1.20	<0.0001	0.0100*	<0.00001
1.2	0.03	0.1	90	1.16	0.002	0.0288	0.0001
1.2	0.03	0.1	365	1.20	0.002	0.0300	<0.00001
1.2	0.05	0.1	90	1.15	0.003	0.0368	0.001
1.2	0.05	0.1	365	1.19	0.001	0.0500	<0.00001
1.2	0	0.5	90	1.20	<0.0001	0	---
1.2	0	0.5	365	1.20	<0.0001	0	---
1.2	0.001	0.5	90	1.20	<0.0001	0.0010	<0.00001
1.2	0.001	0.5	365	1.20	<0.0001	0.0010*	<0.00001
1.2	0.003	0.5	90	1.19	<0.0001	0.0030	<0.00001
1.2	0.003	0.5	365	1.20	<0.0001	0.0030*	<0.00001
1.2	0.01	0.5	90	1.19	<0.0001	0.0100	<0.00001
1.2	0.01	0.5	365	1.20	<0.0001	0.0100*	<0.00001
1.2	0.03	0.5	90	1.04	0.01	0.0298	<0.00001
1.2	0.03	0.5	365	1.19	0.001	0.0276	0.0002
1.2	0.05	0.5	90	1.15	0.004	0.0496	<0.00001
1.2	0.05	0.5	365	1.19	0.001	0.0476	0.0002
1.2	0	1	90	1.20	<0.0001	0	---
1.2	0	1	365	1.20	<0.0001	0	---

Table 10. (cont)

Target Ca/Si	Target Al/Si	NaOH (M)	Time (days)	Ca/Si in C-A-S-H	Error of Ca/Si in C-A-S-H	Al/Si in C-A-S-H	Error of Al/Si in C-A-S-H
1.2	0.001	1	90	1.20	<0.0001	0.0010	<0.00001
1.2	0.001	1	365	1.20	<0.0001	0.0010	<0.00001
1.2	0.003	1	90	1.20	<0.0001	0.0029	<0.00001
1.2	0.003	1	365	1.20	<0.0001	0.0030	<0.00001
1.2	0.01	1	90	1.20	<0.0001	0.0097	<0.00001
1.2	0.01	1	365	1.20	<0.0001	0.0100	<0.00001
1.2	0.03	1	7	1.17	0.005	0.0272	<0.00001
1.2	0.03	1	14	1.11	0.009	0.0274	<0.00001
1.2	0.03	1	28	1.15	0.006	0.0271	<0.00001
1.2	0.03	1	56	1.11	0.01	0.0280	<0.00001
1.2	0.03	1	90	1.12	0.008	0.0290	<0.00001
1.2	0.03	1	365	1.18	0.002	0.0300	<0.00001
1.2	0.05	1	90	1.14	0.006	0.0465	0.0002
1.2	0.05	1	365	1.17	0.003	0.0475	0.0002
1.4	0	0	90	1.31	<0.0001	0	---
1.4	0	0	365	1.32	<0.0001	0	---
1.4	0.0009	0	90	1.34	<0.0001	0.0009*	<0.00001
1.4	0.0009	0	365	1.32	<0.0001	0.0009*	<0.00001
1.4	0.0028	0	90	1.32	<0.0001	0.0028*	<0.00001
1.4	0.0028	0	365	1.32	<0.0001	0.0028*	<0.00001
1.4	0.01	0	90	1.32	<0.0001	0.0102*	<0.00001
1.4	0.01	0	365	1.33	<0.0001	0.0102*	<0.00001
1.4	0.03	0	90	1.32	<0.0001	0.0299	<0.00001
1.4	0.03	0	365	1.32	<0.0001	0.0299*	<0.00001
1.4	0.05	0	90	1.33	<0.0001	0.0498	<0.00001
1.4	0.05	0	365	1.33	0.0003	0.0477	0.0002
1.4	0.1	0	90	1.31	0.002	0.0856	0.001
1.4	0.1	0	365	1.32	0.0003	0.0978	0.0002
1.4	0	0.1	90	1.37	<0.0001	0	---
1.4	0	0.1	365	1.38	<0.0001	0	---
1.4	0.0009	0.1	90	1.37	<0.0001	0.0009*	<0.00001
1.4	0.0009	0.1	365	1.38	<0.0001	0.0009*	<0.00001
1.4	0.0028	0.1	90	1.37	<0.0001	0.0028*	<0.00001
1.4	0.0028	0.1	365	1.38	<0.0001	0.0028*	<0.00001
1.4	0.01	0.1	90	1.37	<0.0001	0.0102*	<0.00001
1.4	0.01	0.1	365	1.37	<0.0001	0.0102*	<0.00001
1.4	0.03	0.1	90	1.32	0.005	0.0299	<0.00001
1.4	0.03	0.1	365	1.35	0.002	0.0299*	<0.00001
1.4	0.05	0.1	90	1.37	0.01	0.0498	<0.00001
1.4	0.05	0.1	365	1.38	0.0006	0.0498*	<0.00001
1.4	0	0.5	90	1.40	<0.0001	0	---
1.4	0	0.5	365	1.40	<0.0001	0	---
1.4	0.0009	0.5	90	1.39	<0.0001	0.0009*	<0.00001
1.4	0.0009	0.5	365	1.39	<0.0001	0.0009	<0.00001
1.4	0.0028	0.5	90	1.39	<0.0001	0.0028*	<0.00001

Table 10. (cont)

Target Ca/Si	Target Al/Si	NaOH (M)	Time (days)	Ca/Si in C-A-S-H	Error of Ca/Si in C-A-S-H	Al/Si in C-A-S-H	Error of Al/Si in C-A-S-H
1.4	0.0028	0.5	365	1.39	<0.0001	0.0027	<0.00001
1.4	0.01	0.5	90	1.39	<0.0001	0.0102*	<0.00001
1.4	0.01	0.5	365	1.39	<0.0001	0.0101	<0.00001
1.4	0.03	0.5	90	1.26	0.01	0.0298	<0.00001
1.4	0.03	0.5	365	1.30	0.009	0.0297	<0.00001
1.4	0.05	0.5	90	1.26	0.01	0.0497	<0.00001
1.4	0.05	0.5	365	1.30	0.01	0.0496	<0.00001
1.4	0	1	90	1.40	<0.0001	0	---
1.4	0	1	365	1.40	<0.0001	0	---
1.4	0.0009	1	90	1.40	<0.0001	0.0009*	<0.00001
1.4	0.0009	1	365	1.40	<0.0001	0.0009	<0.00001
1.4	0.0028	1	90	1.40	<0.0001	0.0027	<0.00001
1.4	0.0028	1	365	1.40	<0.0001	0.0026	<0.00001
1.4	0.01	1	90	1.40	<0.0001	0.0100	<0.00001
1.4	0.01	1	365	1.40	<0.0001	0.0099	<0.00001
1.4	0.03	1	90	1.22	0.02	0.0294	<0.00001
1.4	0.03	1	365	1.24	0.01	0.0291	<0.00001
1.4	0.05	1	90	1.21	0.02	0.0485	<0.00001
1.4	0.05	1	365	1.35	0.004	0.0488	<0.00001

*: Al concentrations in the solution are below the DL of ICP-OES and Al/Si ratios calculated considering Al concentration equals to zero.

~: Ca concentrations in the solution are below the DL of ICP-OES and Ca/Si ratios calculated considering the Ca concentration as zero.

Table 11. The calculated K_d values and the corresponding errors.

Target Ca/Si	Target Al/Si	NaOH (M)	Time (days)	K_d (m ³ /kg)	Error of K_d (m ³ /kg)
0.8	0.001	0	90	1.1	<0.0001
0.8	0.001	0	365	nm	<0.0001
0.8	0.003	0	90	2.4	<0.0001
0.8	0.003	0	365	nm	<0.0001
0.8	0.01	0	90	6.6	<0.0001
0.8	0.01	0	365	170	<0.0001
0.8	0.03	0	90	10.5	0.90
0.8	0.03	0	365	760	<0.0001
0.8	0.1	0	90	54.3	0.62
0.8	0.1	0	365	845	<0.0001
0.8	0.2	0	90	73.8	1.5
0.8	0.2	0	365	2053	17.8
0.8	0.001	0.1	90	0.33	<0.0001
0.8	0.001	0.1	365	2.2	<0.0001
0.8	0.003	0.1	90	1.1	<0.0001
0.8	0.003	0.1	365	3.3	<0.0001

Table 11. (cont)

Target Ca/Si	Target Al/Si	NaOH (M)	Time (days)	K _d (m ³ /kg)	Error of K _d (m ³ /kg)
0.8	0.01	0.1	90	1.7	<0.0001
0.8	0.01	0.1	365	2.3	<0.0001
0.8	0.03	0.1	90	1.9	<0.0001
0.8	0.03	0.1	365	2.6	<0.0001
0.8	0.05	0.1	90	3.0	<0.0001
0.8	0.05	0.1	455	2.0	<0.0001
0.8	0.1	0.1	90	1.5	0.008
0.8	0.1	0.1	455	1.7	0.012
0.8	0.15	0.1	90	1.8	0.008
0.8	0.15	0.1	455	2.2	0.021
0.8	0.2	0.1	90	4.7	0.041
0.8	0.2	0.1	455	1.5	0.024
0.8	0.001	0.5	90	0.42	<0.0001
0.8	0.001	0.5	365	0.62	<0.0001
0.8	0.003	0.5	90	0.55	<0.0001
0.8	0.003	0.5	365	0.67	<0.0001
0.8	0.01	0.5	90	0.50	<0.0001
0.8	0.01	0.5	365	0.81	<0.0001
0.8	0.03	0.5	90	0.45	<0.0001
0.8	0.03	0.5	365	0.63	<0.0001
0.8	0.05	0.5	90	2.6	0.01
0.8	0.05	0.5	455	0.63	<0.0001
0.8	0.1	0.5	90	0.42	<0.0001
0.8	0.1	0.5	455	0.37	<0.0001
0.8	0.15	0.5	90	0.39	0.002
0.8	0.15	0.5	455	0.33	0.001
0.8	0.2	0.5	90	0.43	0.003
0.8	0.2	0.5	455	0.33	0.001
0.8	0.001	1	90	0.33	<0.0001
0.8	0.001	1	365	0.41	<0.0001
0.8	0.003	1	90	0.25	<0.0001
0.8	0.003	1	365	0.35	<0.0001
0.8	0.01	1	90	0.27	<0.0001
0.8	0.01	1	365	0.39	<0.0001
0.8	0.03	1	90	0.28	<0.0001
0.8	0.03	1	365	0.41	<0.0001
0.8	0.05	1	90	0.53	<0.0001
0.8	0.05	1	455	0.11	<0.0001
0.8	0.1	1	90	0.23	<0.0001
0.8	0.1	1	455	0.27	<0.0001
0.8	0.15	1	90	0.24	<0.0001
0.8	0.15	1	455	0.19	<0.0001
0.8	0.2	1	90	0.13	<0.0001
0.8	0.2	1	455	0.18	<0.0001

nm: not measured as the Al concentrations were below the DL of ICP-OES.

Appendix F. Further details about ICP-MS and ICP-OES measurements discussed in chapter 2.

Because of the relatively high concentration of Si in the samples, the effect of measuring Si at m/z 28 on Al at m/z 27 was evaluated. To do that, Si and Al single standard solutions were separately prepared in the same range of the expected concentration in the samples to be measured (0-4 mg/L for Si and 0-50 µg/L for Al). 2-min transient signals of 27Al and 28Si for each standard solution were acquired by the same ICP-MS instrument used for the whole analysis and the calibration curves of Si and Al were made using the averaged values of these intensities. The ICP-MS sensitivities of Al and Si were 270.2 and 1032.0 cps/ppb, respectively. The acquired signals on m/z 27, when Si standard solutions were measured, were quantified using the Al calibration data. Figure 38 shows the quantified effect of Si on the m/z 27. The slope of this curve presents the m/z ratio 27 to 28 due to the effect of Si. The results showed a negligible influence of Si on the signal attributed to Al; the presence of Si contributed to 0.12 % to the signal measured at m/z 27. Therefore, for the multi-standard solutions (containing Al and Si at equal amounts) used for calibration, the effect of Si is negligible. However, for the samples which contained much lower Al concentrations than Si, the effect of Si was corrected and the net intensity of Al (used to determine the corresponding concentration) was calculated by subtracting the measured intensity from that of the sample having the same pH value and containing no Al.

Table 12. Optimized parameters used for the ICP-MS and ICP-OES analysis.

	ICP-MS			ICP-OES		
Power / W	1350			1250		
Flow of carrier gas (Ar) / L/min	1.04			0.86		
Sampling depth / mm	10			-		
He flow (Collision gas) mL/min	2			-		
Torch configuration	-			Axial		
Measured Elements	Al	Ca	Si	Al	Ca	Si
Measured isotopes/lines	m/z 27	m/z 44	m/z 28	396.152 nm	393.366 nm	212.412 nm
LOD (ppb)	0.15	3.09	4.02	5.46	0.15	32.4
Sensitivity (cps/ppb)	1032	35.9	270.2	66.2	8899.1	8.5
R ²	>0.999	>0.999	>0.999	>0.999	>0.999	>0.999

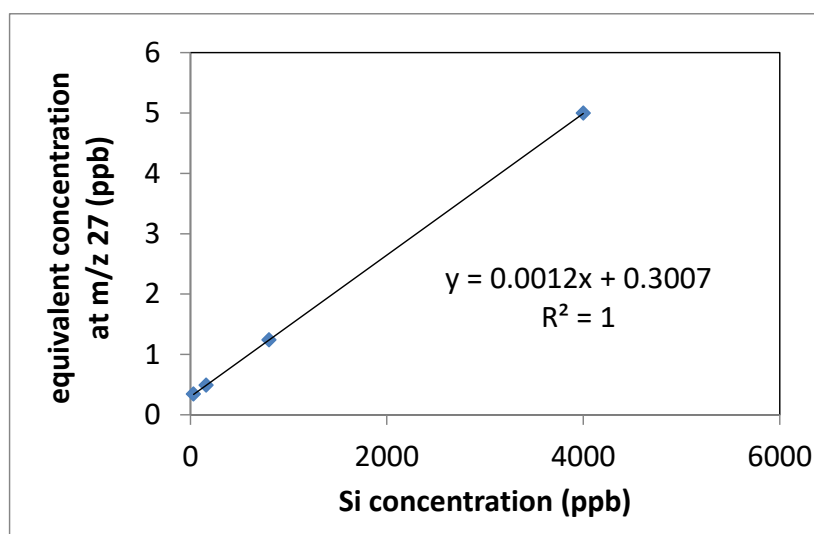
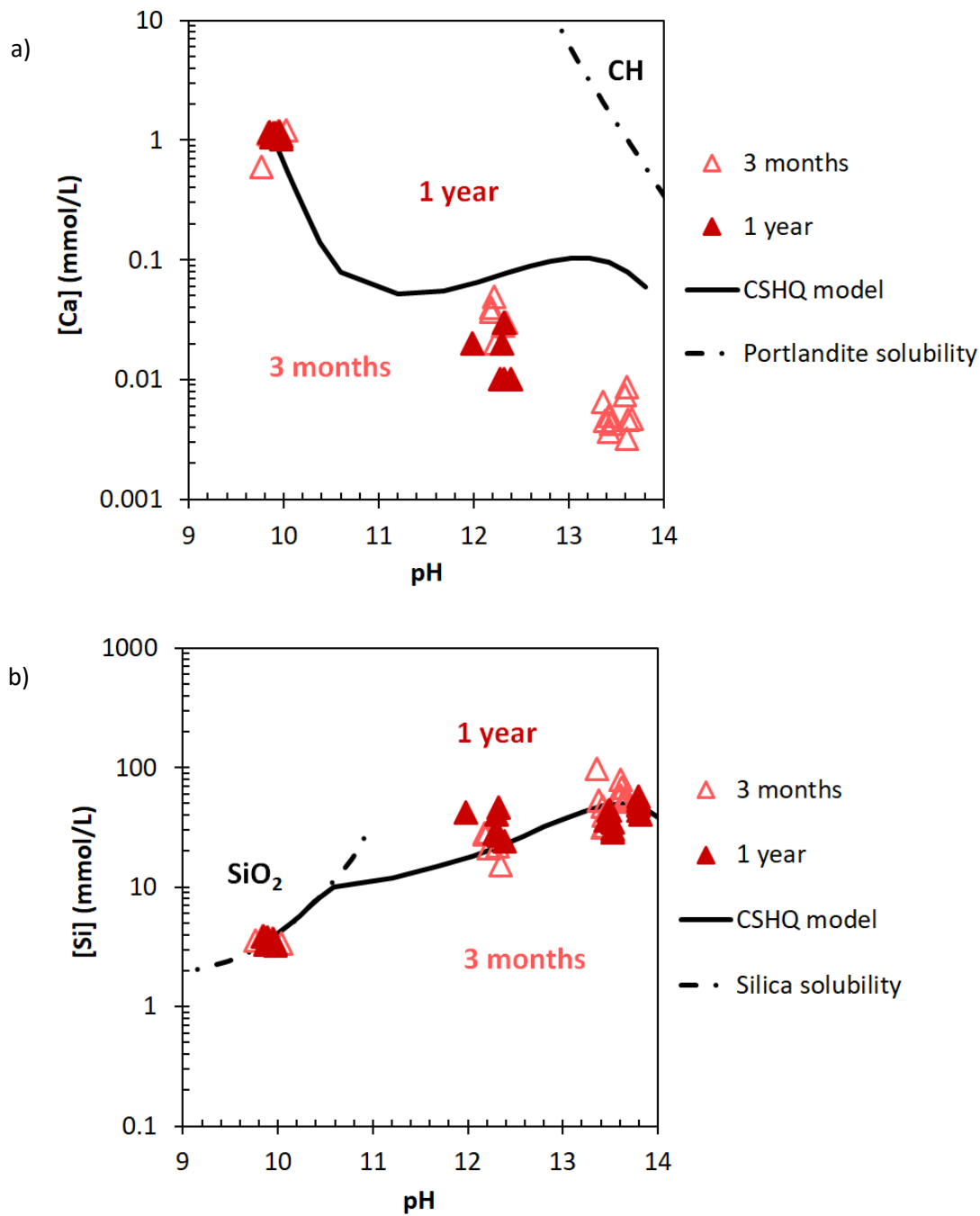
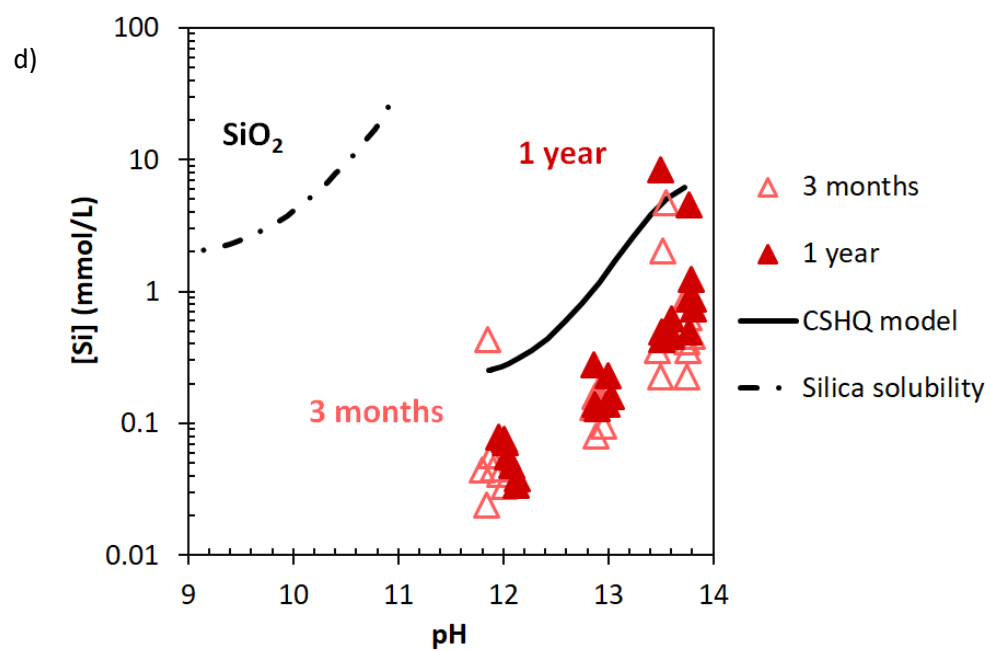
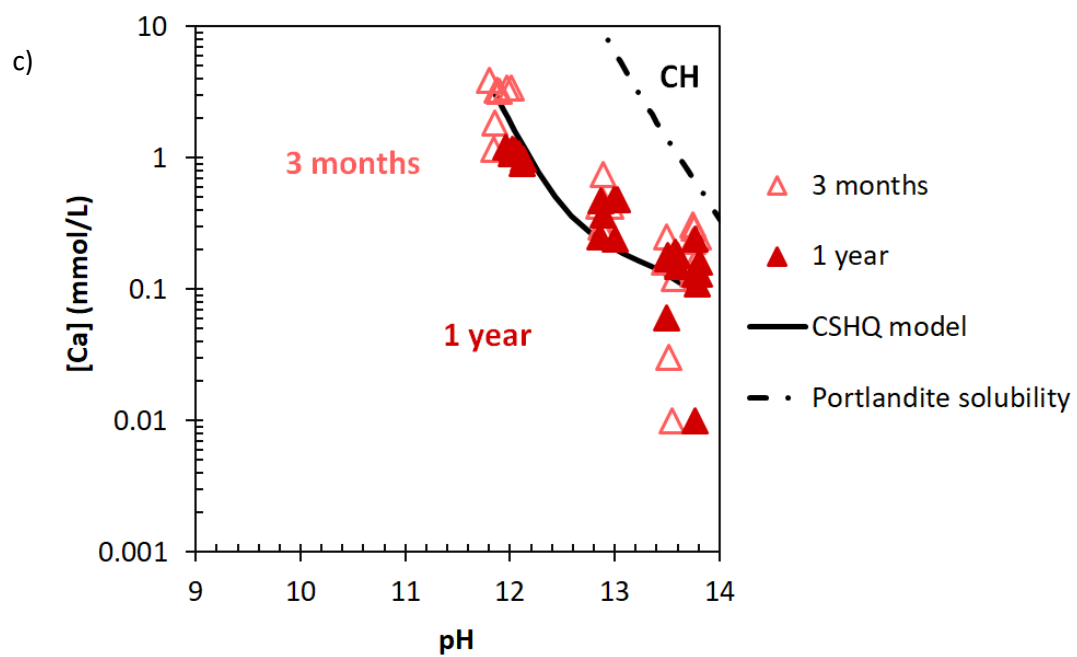


Figure 38. The quantified effect of Si on m/z 27.

Appendix G. The effect of equilibration time on Ca and Si concentrations for Ca/Si ratios of 0.6, 1.0 and 1.4 discussed in section 5.5 of chapter 5.





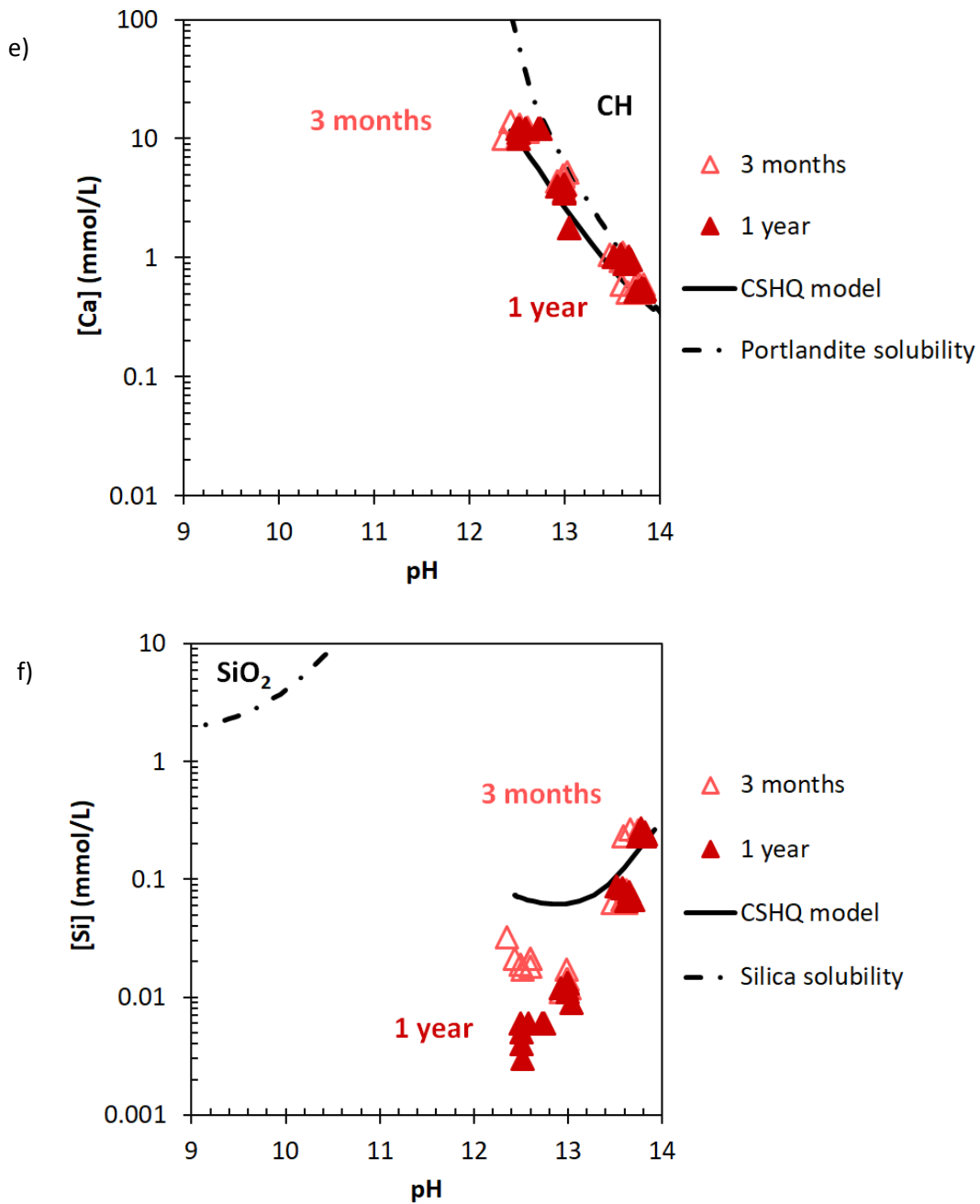


Figure 39. The effect of pH value and equilibration time on measured Ca (a,c,e) and Si (b,d,f) concentrations (symbols) and on the calculated solubility of C-S-H (using the CSHQ model [47]), portlandite and amorphous SiO₂ for Ca/Si ratios of a,b) 0.6; c,d) 1.0 and e,f) 14.

Appendix H. The Al fraction in C-A-S-H for Ca/Si = 0.8 after 3 months equilibration discussed in section 6.3.2 of chapter 6.

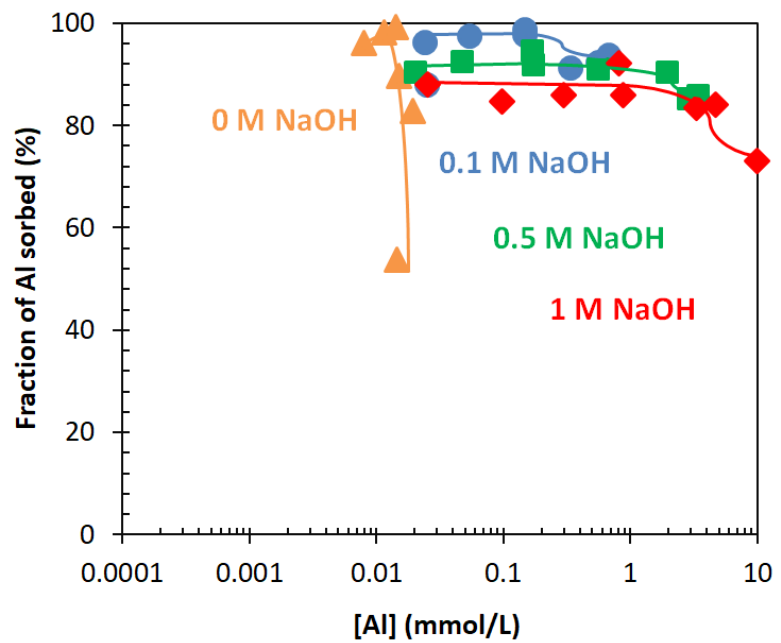


Figure 40. The Al fraction in C-A-S-H for target Ca/Si = 0.8 in the absence of NaOH and presence of 0.1, 0.5 and 1 M NaOH after 3 months equilibration.

References

- [1] S.A. Miller, R.J. Myers, Environmental Impacts of Alternative Cement Binders, *Environ. Sci. Technol.* 54 (2020) 677–686. <https://doi.org/10.1021/acs.est.9b05550>.
- [2] E. Gartner, Industrially interesting approaches to “low-CO₂” cements, *Cem. Concr. Res.* 34 (2004) 1489–1498. <https://doi.org/10.1016/j.cemconres.2004.01.021>.
- [3] H.F.W. Taylor, *Cement chemistry*, 2nd ed., Thomas Telford Publishing, London, 1997. <https://doi.org/10.1680/cc.25929>.
- [4] M. Glavind, Sustainability of cement, concrete and cement replacement materials in construction, in: *Sustain. Constr. Mater.*, Woodhead Publishing Limited, 2014: pp. 120–147. <https://doi.org/10.1533/9781845695842.120>.
- [5] K.L. Scrivener, V.M. John, E.M. Gartner, Eco-efficient cements: Potential economically viable solutions for a low-CO₂ cement-based materials industry, *Cem. Concr. Res.* 114 (2018) 2–26. <https://doi.org/10.1016/j.cemconres.2018.03.015>.
- [6] L.D. Ellis, A.F. Badel, M.L. Chiang, R.J.-Y. Park, Y.-M. Chiang, Toward electrochemical synthesis of cement—An electrolyzer-based process for decarbonating CaCO₃ while producing useful gas streams, *Proc. Natl. Acad. Sci.* (2019) 201821673. <https://doi.org/10.1073/pnas.1821673116>.
- [7] J. Li, G. Geng, W. Zhang, Y.S. Yu, D.A. Shapiro, P.J.M. Monteiro, The hydration of β - and α' H - dicalcium silicates: an X-ray spectromicroscopic study, *ACS Sustain. Chem. Eng.* 7 (2019) 2316–2326. <https://doi.org/10.1021/acssuschemeng.8b05060>.
- [8] M. Thomas, L. Barcelo, B. Blair, K. Cail, A. Delagrave, K. Kazanis, Lowering the carbon footprint of concrete by reducing clinker content of cement, *Transp. Res. Rec.* (2012) 99–104. <https://doi.org/10.3141/2290-13>.
- [9] P.J.M. Monteiro, S.A. Miller, A. Horvath, Towards sustainable concrete, *Nat. Mater.* 16 (2017) 698–699. <https://doi.org/10.1038/nmat4930>.
- [10] IEA, WBCSD, *Technology Roadmap: Low-Carbon Transition in the Cement Industry 2060*, 2018. <https://www.wbcd.org/Sector-Projects/Cement-Sustainability-Initiative/Resources/Technology-Roadmap-Low-Carbon-Transition-in-the-Cement-Industry>.
- [11] B. Lothenbach, K. Scrivener, R.D. Hooton, Supplementary cementitious materials, *Cem. Concr. Res.* 41 (2011) 1244–1256. <https://doi.org/10.1016/j.cemconres.2010.12.001>.
- [12] J. Li, W. Zhang, C. Li, P.J.M. Monteiro, Green concrete containing diatomaceous earth and limestone: Workability, mechanical properties, and life-cycle assessment, *J. Clean. Prod.* 223 (2019) 662–679. <https://doi.org/10.1016/j.jclepro.2019.03.077>.
- [13] I. Baur, C. Ludwig, C.A. Johnson, The leaching behavior of cement stabilized air pollution control residues: A comparison of field and laboratory investigations, *Environ. Sci. Technol.* 35 (2001) 2817–2822. <https://doi.org/10.1021/es000243r>.
- [14] C. Ludwig, C.A. Johnson, M. Käppeli, A. Ulrich, S. Riediker, Hydrological and geochemical factors controlling the leaching of cemented MSWI air pollution control residues: A lysimeter field study, *J. Contam. Hydrol.* 42 (2000) 253–272. [https://doi.org/10.1016/S0169-7722\(99\)00083-2](https://doi.org/10.1016/S0169-7722(99)00083-2).
- [15] H.M. Saleh, S.B. Eskander, Innovative cement-based materials for environmental protection and restoration, in: *New Mater. Civ. Eng.*, Butterworth Heinemann, 2020: pp. 613–641.

<https://doi.org/10.1016/b978-0-12-818961-0.00018-1>.

- [16] J. Duchesne, M.A. Bérubé, Effect of supplementary cementing materials on the composition of cement hydration products, *Adv. Cem. Based Mater.* 2 (1995) 43–52.
<https://doi.org/10.3989/revmetalm.2003.v39.iextra.1127>.
- [17] R. Shahrin, C.P. Bobko, Characterizing strength and failure of calcium silicate hydrate aggregates in cement paste under micropillar compression, *J. Nanomechanics Micromechanics.* 7 (2017) 1–6.
[https://doi.org/10.1061/\(ASCE\)NM.2153-5477.0000137](https://doi.org/10.1061/(ASCE)NM.2153-5477.0000137).
- [18] I.G. Richardson, The nature of C-S-H in hardened cements, 29 (1999) 1131–1147.
[https://doi.org/10.1016/S0008-8846\(99\)00168-4](https://doi.org/10.1016/S0008-8846(99)00168-4).
- [19] B. Lothenbach, A. Nonat, Calcium silicate hydrates: Solid and liquid phase composition, *Cem. Concr. Res.* 78 (2015) 57–70. <https://doi.org/10.1016/j.cemconres.2015.03.019>.
- [20] M. Antoni, J. Rossen, F. Martirena, K. Scrivener, Cement substitution by a combination of metakaolin and limestone, *Cem. Concr. Res.* 42 (2012) 1579–1589.
<https://doi.org/10.1016/j.cemconres.2012.09.006>.
- [21] C. Li, H. Zhu, M. Wu, K. Wu, Z. Jiang, Pozzolanic reaction of fly ash modified by fluidized bed reactor-vapor deposition, *Cem. Concr. Res.* 92 (2017) 98–109.
<https://doi.org/10.1016/j.cemconres.2016.11.016>.
- [22] C. Li, M. Wu, Q. Chen, Z. Jiang, Chemical and mineralogical alterations of concrete subjected to chemical attacks in complex underground tunnel environments during 20–36 years, *Cem. Concr. Compos.* 86 (2018) 139–159. <https://doi.org/10.1016/j.cemconcomp.2017.11.007>.
- [23] E. L'Hôpital, B. Lothenbach, D.A. Kulik, K. Scrivener, Influence of calcium to silica ratio on aluminium uptake in calcium silicate hydrate, *Cem. Concr. Res.* 85 (2016) 111–121.
<https://doi.org/10.1016/j.cemconres.2016.01.014>.
- [24] L. Irbe, R.E. Beddoe, D. Heinz, The role of aluminium in C-A-S-H during sulfate attack on concrete, *Cem. Concr. Res.* 116 (2019) 71–80. <https://doi.org/10.1016/j.cemconres.2018.11.012>.
- [25] J.E. Rossen, Composition and morphology of C-A-S-H in pastes of alite and cement blended with supplementary cementitious materials, 2014.
- [26] G.L. Kalousek, Crystal chemistry of hydrous calcium silicates: I, Substitution of aluminum in lattice of tobermorite, *J. Am. Ceram. Soc.* 40 (1957) 74–80.
- [27] J. Haas, A. Nonat, From C-S-H to C-A-S-H: Experimental study and thermodynamic modelling, *Cem. Concr. Res.* 68 (2015) 124–138. <https://doi.org/10.1016/j.cemconres.2014.10.020>.
- [28] E. Bonaccorsi, S. Merlino, A.R. Kampf, The crystal structure of tobermorite 14 Å (plombierite), a C-S-H phase, *J. Am. Ceram. Soc.* 88 (2005) 505–512. <https://doi.org/10.1111/j.1551-2916.2005.00116.x>.
- [29] J. Li, G. Geng, R. Myers, Y.S. Yu, D. Shapiro, C. Carraro, R. Maboudian, P.J.M. Monteiro, The chemistry and structure of calcium (alumino) silicate hydrate: A study by XANES, ptychographic imaging, and wide- and small-angle scattering, *Cem. Concr. Res.* 115 (2019) 367–378.
<https://doi.org/10.1016/j.cemconres.2018.09.008>.
- [30] I.G. Richardson, A.R. Brough, R. Brydson, G.W. Groves, C.M. Dobson, Location of aluminium in substituted calcium silicate hydrate (C-S-H) gels as determined by Si-29 and Al-27 NMR and EELS, *J. Am. Ceram. Soc.* 76 (1993) 2285–2288. <https://doi.org/10.1111/j.1151-2916.1993.tb07765.x>.

- [31] S. Ortaboy, J. Li, G. Geng, R.J. Myers, P.J.M. Monteiro, R. Maboudian, C. Carraro, Effects of CO₂ and temperature on the structure and chemistry of C-(A-)S-H investigated by Raman spectroscopy, *RSC Adv.* 7 (2017) 48925–48933. <https://doi.org/10.1039/c7ra07266j>.
- [32] J.J. Chen, J.J. Thomas, H.F.W. Taylor, H.M. Jennings, Solubility and structure of calcium silicate hydrate, *Cem. Concr. Res.* 34 (2004) 1499–1519. <https://doi.org/10.1016/j.cemconres.2004.04.034>.
- [33] P. Faucon, A. Delagrave, J.C. Petit, C. Richet, J.M. Marchand, H. Zanni, Aluminum incorporation in calcium silicate hydrates (C–S–H) depending on their Ca/Si ratio, *J. Phys. Chem. B.* 103 (1999) 7796–7802. <https://doi.org/10.1021/jp990609q>.
- [34] E.L. Hôpital, B. Lothenbach, K. Scrivener, D.A. Kulik, Alkali uptake in calcium alumina silicate hydrate (C-A-S-H), *Cem. Concr. Res.* 85 (2016) 122–136. <https://doi.org/10.1016/j.cemconres.2016.03.009>.
- [35] R.J. Myers, E. L'Hôpital, J.L. Provis, B. Lothenbach, Composition-solubility-structure relationships in calcium (alkali) aluminosilicate hydrate (C-(N,K-)A-S-H), *Dalt. Trans.* 44 (2015) 13530–13544. <https://doi.org/10.1039/c5dt01124h>.
- [36] R.J. Myers, E. L'Hôpital, J.L. Provis, B. Lothenbach, Effect of temperature and aluminium on calcium (alumino)silicate hydrate chemistry under equilibrium conditions, *Cem. Concr. Res.* 68 (2015) 83–93. <https://doi.org/10.1016/j.cemconres.2014.10.015>.
- [37] E. L'Hôpital, B. Lothenbach, G. Le Saout, D. Kulik, K. Scrivener, Incorporation of aluminium in calcium-silicate-hydrates, *Cem. Concr. Res.* 75 (2015) 91–103. <https://doi.org/10.1016/j.cemconres.2015.04.007>.
- [38] X. Pardal, F. Brunet, T. Charpentier, I. Pochard, A. Nonat, ²⁷Al and ²⁹Si solid-state NMR characterization of calcium-aluminosilicate-hydrate, *Inorg. Chem.* 51 (2012) 1827–1836. <https://doi.org/10.1021/ic202124x>.
- [39] G. Renaudin, J. Russias, F. Leroux, C. Cau-dit-Coumes, F. Frizon, Structural characterization of C-S-H and C-A-S-H samples—Part II: Local environment investigated by spectroscopic analyses, *J. Solid State Chem.* 182 (2009) 3320–3329. <https://doi.org/10.1016/j.jssc.2009.09.024>.
- [40] M.D. Andersen, H.J. Jakobsen, J. Skibsted, A new aluminium-hydrate species in hydrated Portland cements characterized by ²⁷Al and ²⁹Si MAS NMR spectroscopy, *Cem. Concr. Res.* 36 (2006) 3–17. <https://doi.org/10.1016/j.cemconres.2005.04.010>.
- [41] G.K. Sun, J.F. Young, R.J. Kirkpatrick, The role of Al in C-S-H: NMR, XRD, and compositional results for precipitated samples, *Cem. Concr. Res.* 36 (2006) 18–29. <https://doi.org/10.1016/j.cemconres.2005.03.002>.
- [42] P. Faucon, J.F. Jacquinet, J.M. Delaue, J. Virlet, Molecular dynamics simulation of Al³⁺ and Na⁺ substitutions in the tobermorite structure, *Philos. Mag. B.* 75 (1997) 769–783. <https://doi.org/10.1080/13642819708202353>.
- [43] M.J. Abdolhosseini Qomi, F.J. Ulm, R.J.M. Pellenq, Evidence on the dual nature of aluminum in the calcium-silicate-hydrates based on atomistic simulations, *J. Am. Ceram. Soc.* 95 (2012) 1128–1137. <https://doi.org/10.1111/j.1551-2916.2011.05058.x>.
- [44] L. Pegado, C. Labbez, S. V. Churakov, Mechanism of aluminium incorporation into C-S-H from ab initio calculations, *J. Mater. Chem. A.* 2 (2014) 3477–3483. <https://doi.org/10.1039/c3ta14597b>.
- [45] A. Kunhi Mohamed, P. Moutzouri, P. Berruyer, B.J. Walder, J. Siramanont, M. Harris, M. Negroni, S.C. Galmarini, S.C. Parker, K.L. Scrivener, L. Emsley, P. Bowen, The atomic-level structure of

cementitious calcium aluminate silicate hydrate, *J. Am. Chem. Soc.* 142 (2020) 11060–11071. <https://doi.org/10.1021/jacs.0c02988>.

- [46] C.S. Walker, S. Sutou, C. Oda, M. Mihara, A. Honda, Calcium silicate hydrate (C-S-H) gel solubility data and a discrete solid phase model at 25 °C based on two binary non-ideal solid solutions, *Cem. Concr. Res.* 79 (2016) 1–30. <https://doi.org/10.1016/j.cemconres.2015.07.006>.
- [47] D.A. Kulik, Improving the structural consistency of C-S-H solid solution thermodynamic models, *Cem. Concr. Res.* 41 (2011) 477–495. <https://doi.org/10.1016/j.cemconres.2011.01.012>.
- [48] K. Fujii, W. Kondo, Heterogeneous equilibrium of calcium silicate hydrate in water at 30 °C, *J. Chem. Soc. Dalt. Trans.* (1981) 645–651.
- [49] E.P. Flint, L.S. Wells, Study of the system CaO-SiO₂-H₂O at 30 °C and of the reaction of water on the anhydrous calcium silicates, *Bur. Stand. J. Res.* 12 (1934) 751–783. <https://doi.org/10.6028/jres.012.060>.
- [50] S.A. Greenberg, T.N. Chang, Investigation of the colloidal hydrated calcium silicates. II. Solubility relationships in the calcium oxide-silica-water system at 25°, *J. Phys. Chem.* 69 (1965) 182–188. <https://doi.org/10.1021/j100885a027>.
- [51] H.F.W. Taylor, Hydrated calcium silicates. Part I. Compound formation at ordinary temperatures, *J. Chem. Soc. London.* 276 (1950) 3682–3690.
- [52] P.S. Roller, G.J. Ervin, The system calcium oxide-silica-water at 30°. The association of silicate* ion in dilute alkaline solution, *J. Am. Ceram. Soc.* 62 (1940) 461–471. <https://doi.org/10.1097/00007611-192203000-00016>.
- [53] G. Renaudin, J. Russias, F. Leroux, F. Frizon, C. Cau-dit-Coumes, Structural characterization of C-S-H and C-A-S-H samples-Part I: Long-range order investigated by Rietveld analyses, *J. Solid State Chem.* 182 (2009) 3312–3319. <https://doi.org/10.1016/j.jssc.2009.09.026>.
- [54] R.J. Myers, S.A. Bernal, R. San Nicolas, J.L. Provis, Generalized structural description of calcium-sodium aluminosilicate hydrate gels: The cross-linked substituted tobermorite model, *Langmuir.* 29 (2013) 5294–5306. <https://doi.org/10.1021/la4000473>.
- [55] X. Pardal, I. Pochard, A. Nonat, Experimental study of Si-Al substitution in calcium-silicate-hydrate (C-S-H) prepared under equilibrium conditions, *Cem. Concr. Res.* 39 (2009) 637–643. <https://doi.org/10.1016/j.cemconres.2009.05.001>.
- [56] I.G. Richardson, J. Skibsted, L. Black, R.J. Kirkpatrick, Characterisation of cement hydrate phases by TEM, NMR and Raman spectroscopy, *Adv. Cem. Res.* 22 (2010) 233–248. <https://doi.org/10.1680/adcr.2010.22.4.233>.
- [57] T. Wagner, D.A. Kulik, F.F. Hingerl, S. V. Dmytrieva, GEM-Selektor geochemical modeling package: TSolMod library and data interface for multicomponent phase models, *Can. Mineral.* 50 (2012) 1173–1195. <https://doi.org/10.3749/canmin.50.5.1173>.
- [58] S. Barzgar, B. Lothenbach, M. Tarik, A. Di Giacomo, C. Ludwig, The effect of sodium hydroxide on Al uptake by calcium silicate hydrates (C-S-H), *J. Colloid Interface Sci.* 572 (2020) 246–256. <https://doi.org/10.1016/j.jcis.2020.03.057>.
- [59] S. Barzgar, M. Tarik, C. Ludwig, B. Lothenbach, The effect of equilibration time on Al uptake in C-S-H, *Cem. Concr. Res.* 144 (2021) 106438. <https://doi.org/10.1016/j.cemconres.2021.106438>.
- [60] A. Vollpracht, B. Lothenbach, R. Snellings, J. Haufe, The pore solution of blended cements: a review,

Mater. Struct. Constr. 49 (2016) 3341–3367. <https://doi.org/10.1617/s11527-015-0724-1>.

- [61] B. Lothenbach, F. Winnefeld, Thermodynamic modelling of the hydration of Portland cement, *Cem. Concr. Res.* 36 (2006) 209–226. <https://doi.org/10.1016/j.cemconres.2005.03.001>.
- [62] B. Traynor, H. Uvegi, E. Olivetti, B. Lothenbach, R.J. Myers, Methodology for pH measurement in high alkali cementitious systems, *Cem. Concr. Res.* 135 (2020) 106122. <https://doi.org/10.1016/j.cemconres.2020.106122>.
- [63] R.W. O’Brien, D.W. Cannon, W.N. Rowlands, Electroacoustic determination of particle size and zeta potential, *J. Colloid Interface Sci.* 173 (1995) 406–418. <https://doi.org/10.1006/jcis.1995.1341>.
- [64] B. Lothenbach, P. Durdziński, K. De Weerd, Thermogravimetric analysis (TGA), in: *A Pract. Guid. to Microstruct. Anal. Cem. Mater.*, 1st ed., CRC Press, 2016: pp. 178–208. <https://doi.org/10.1201/b19074-5>.
- [65] E. Bernard, B. Lothenbach, D. Rentsch, I. Pochard, A. Dauzères, Formation of magnesium silicate hydrates (M-S-H), *Phys. Chem. Earth.* 99 (2017) 142–157. <https://doi.org/10.1016/j.pce.2017.02.005>.
- [66] T. Thoenen, W. Hummel, U. Berner, E. Curti, The PSI/Nagra chemical thermodynamic database 12/07, Villigen PSI, 2014. https://www.psi.ch/sites/default/files/import/les/DatabaseEN/PSI-Bericht%252014-04_final_druckerei.pdf.
- [67] B. Lothenbach, D.A. Kulik, T. Matschei, M. Balonis, L. Baquerizo, B. Dilnesa, G.D. Miron, R.J. Myers, Cemdata18: A chemical thermodynamic database for hydrated Portland cements and alkali-activated materials, *Cem. Concr. Res.* 115 (2019) 472–506. <https://doi.org/10.1016/j.cemconres.2018.04.018>.
- [68] H.C. Helgeson, D.H. Kirkham, G.G. Flowers, Theoretical prediction of the thermodynamic behavior of aqueous electrolytes at high pressure and temperature: IV. Calculation of activity coefficients, osmotic coefficients, and apparent molal and standard and relative partial molal properties to 600°C a, *Am. J. Sci.* 281 (1981) 1249–1516.
- [69] B.J. Merkel, B. Planer-Friedrich, *Groundwater Geochemistry: A Practical Guide to Modeling of Natural and Contaminated Aquatic Systems*, 2nd ed., Springer, Berlin, 2008. <https://doi.org/10.1007/b138774>.
- [70] R.J. Myers, S.A. Bernal, J.L. Provis, A thermodynamic model for C-(N)-A-S-H gel: CNASH-ss. Derivation and validation, *Cem. Concr. Res.* 66 (2014) 27–47. <https://doi.org/10.1016/j.cemconres.2014.07.005>.
- [71] R.J. Myers, B. Lothenbach, S.A. Bernal, J.L. Provis, Thermodynamic modelling of alkali-activated slag cements, *Appl. Geochemistry.* 61 (2015) 233–247. <https://doi.org/10.1016/j.apgeochem.2015.06.006>.
- [72] W. Stumm, J.J. Morgan, *Chemical Equilibria and Rates in Natural Waters*, *Aquat. Chem.* (1996) 1022.
- [73] M. James, R.J. Hunter, R.W. O’Brien, Effect of Particle Size Distribution and Aggregation on Electroacoustic Measurements of ζ Potential, *Langmuir.* 8 (1992) 420–423. <https://doi.org/10.1021/la00038a017>.
- [74] P. Sipos, The structure of Al(III) in strongly alkaline aluminate solutions - A review, *J. Mol. Liq.* 146 (2009) 1–14. <https://doi.org/10.1016/j.molliq.2009.01.015>.
- [75] R.F. Giese, W. Wu, C.J. Van Oss, Surface and electrokinetic properties of clays and other mineral

particles, untreated and treated with organic or inorganic cations, *J. Dispers. Sci. Technol.* 17 (1996) 527–547. <https://doi.org/10.1080/01932699608943521>.

- [76] S. V. Churakov, C. Labbez, L. Pegado, M. Sulpizi, Intrinsic acidity of surface sites in calcium silicate hydrates and its implication to their electrokinetic properties, *J. Phys. Chem. C* 118 (2014) 11752–11762. <https://doi.org/10.1021/jp502514a>.
- [77] D.E. Macphee, K. Luke, F.P. Glasser, E.E. Lachowski, Solubility and aging of calcium silicate hydrates in alkaline solutions at 25 °C, *J. Am. Ceram. Soc.* 54 (1989) 646–654.
- [78] G.L. Kalousek, Studies of portions of the quaternary system soda-lime-silica-water at 25 degrees C, *J. Res. Natl. Bur. Stand.* (1934). 32 (2012) 285. <https://doi.org/10.6028/jres.032.015>.
- [79] A.C.A. Muller, K.L. Scrivener, A.M. Gajewicz, P.J. McDonald, Use of bench-top NMR to measure the density, composition and desorption isotherm of C-S-H in cement paste, *Microporous Mesoporous Mater.* 178 (2013) 99–103. <https://doi.org/10.1016/j.micromeso.2013.01.032>.
- [80] P. Suwanmaneechot, A. Aili, I. Maruyama, Creep behavior of C-S-H under different drying relative humidities: Interpretation of microindentation tests and sorption measurements by multi-scale analysis, *Cem. Concr. Res.* 132 (2020) 106036. <https://doi.org/10.1016/j.cemconres.2020.106036>.
- [81] E. Kapeluszna, Ł. Kotwica, A. Różycka, Ł. Gołek, Incorporation of Al in C-A-S-H gels with various Ca/Si and Al/Si ratio: Microstructural and structural characteristics with DTA/TG, XRD, FTIR and TEM analysis, *Constr. Build. Mater.* 155 (2017) 643–653. <https://doi.org/10.1016/j.conbuildmat.2017.08.091>.
- [82] A. Adamczyk, E. Długoń, The FTIR studies of gels and thin films of Al₂O₃-TiO₂ and Al₂O₃-TiO₂-SiO₂ systems, *Spectrochim. Acta - Part A Mol. Biomol. Spectrosc.* 89 (2012) 11–17. <https://doi.org/10.1016/j.saa.2011.12.018>.
- [83] W. Mozgawa, M. Król, T. Bajda, IR spectra in the studies of anion sorption on natural sorbents, *J. Mol. Struct.* 993 (2011) 109–114. <https://doi.org/10.1016/j.molstruc.2010.11.070>.
- [84] C.A. Ríos, C.D. Williams, M.A. Fullen, Hydrothermal synthesis of hydrogarnet and tobermorite at 175 °C from kaolinite and metakaolinite in the CaO-Al₂O₃-SiO₂-H₂O system: A comparative study, *Appl. Clay Sci.* 43 (2009) 228–237. <https://doi.org/10.1016/j.clay.2008.09.014>.
- [85] S. Wang, X. Peng, L. Tang, L. Zeng, C. Lan, Influence of inorganic admixtures on the 11 Å-tobermorite formation prepared from steel slags: XRD and FTIR analysis, *Constr. Build. Mater.* 60 (2014) 42–47. <https://doi.org/10.1016/j.conbuildmat.2014.03.002>.
- [86] N.Y. Mostafa, A.A. Shaltout, H. Omar, S.A. Abo-El-Enein, Hydrothermal synthesis and characterization of aluminium and sulfate substituted 1.1 nm tobermorites, *J. Alloys Compd.* 467 (2009) 332–337. <https://doi.org/10.1016/j.jallcom.2007.11.130>.
- [87] H. Maeda, E.H. Ishida, T. Kasuga, Hydrothermal preparation of tobermorite incorporating phosphate species, *Mater. Lett.* 68 (2012) 382–384. <https://doi.org/10.1016/j.matlet.2011.11.017>.
- [88] E.I. Al-Wakeel, S.A. El-Korashy, Reaction mechanism of the hydrothermally treated CaO-SiO₂-Al₂O₃ and CaO-SiO₂-Al₂O₃-CaSO₄ systems, *J. Mater. Sci.* 31 (1996) 1909–1913. <https://doi.org/10.1007/BF00372207>.
- [89] P. Yu, R.J. Kirkpatrick, B. Poe, P.F. McMillan, X. Cong, Structure of calcium silicate hydrate (C-S-H): Near-, mid-, and far-infrared spectroscopy, 82 (1999) 742–748.
- [90] J. Higl, D. Hinder, C. Rathgeber, B. Ramming, M. Lindén, Detailed in situ ATR-FTIR spectroscopy study

of the early stages of C-S-H formation during hydration of monoclinic C3S, *Cem. Concr. Res.* 142 (2021) 106367. <https://doi.org/10.1016/j.cemconres.2021.106367>.

- [91] L. Fernandez, C. Alonso, A. Hidalgo, C. Andrade, The role of magnesium during the hydration of C3S and C-S-H formation. Scanning electron microscopy and mid-infrared studies, *Adv. Cem. Res.* 17 (2005) 9–21. <https://doi.org/10.1680/adcr.2005.17.1.9>.
- [92] L. Fernández-Carrasco, D. Torrens-Martín, L.M. Morales, S. Martínez-Ramírez, Infrared Spectroscopy in the Analysis of Building and Construction Materials, in: *Infrared Spectrosc. - Mater. Sci. Eng. Technol.*, INTECH, 2012: pp. 369–382. <https://doi.org/10.5772/36186>.
- [93] P. Padmaja, G.M. Anilkumar, P. Mukundan, G. Aruldas, K.G.K. Warriar, Characterisation of stoichiometric sol-gel mullite by fourier transform infrared spectroscopy, *Int. J. Inorg. Mater.* 3 (2001) 693–698. [https://doi.org/10.1016/S1466-6049\(01\)00189-1](https://doi.org/10.1016/S1466-6049(01)00189-1).
- [94] J. Partyka, M. Leśniak, Raman and infrared spectroscopy study on structure and microstructure of glass-ceramic materials from SiO₂-Al₂O₃-Na₂O-K₂O-CaO system modified by variable molar ratio of SiO₂/Al₂O₃, *Spectrochim. Acta - Part A Mol. Biomol. Spectrosc.* 152 (2016) 82–91. <https://doi.org/10.1016/j.saa.2015.07.045>.
- [95] K. Djebaili, Z. Mekhalif, A. Boumaza, A. Djelloul, XPS, FTIR, EDX, XRD analysis of Al₂O₃ scales grown on Pm2000 alloy, *J. Spectrosc.* 2015 (2015) 1–16. <https://doi.org/10.1155/2015/868109>.
- [96] C. Liu, K. Shih, Y. Gao, F. Li, L. Wei, Dechlorinating transformation of propachlor through nucleophilic substitution by dithionite on the surface of alumina, *J. Soils Sediments.* 12 (2012) 724–733. <https://doi.org/10.1007/s11368-012-0506-0>.
- [97] S. Vasudevan, B.S. Kannan, J. Lakshmi, S. Mohanraj, G. Sozhan, Effects of alternating and direct current in electrocoagulation process on the removal of fluoride from water, *J. Chem. Technol. Biotechnol.* 86 (2011) 428–436. <https://doi.org/10.1002/jctb.2534>.
- [98] L. Zhu, S. Pu, F. Lu, K. Liu, T. Zhu, J. Li, J. Li, Preparation of dispersed aluminum hydroxide nanoparticles via non-aqueous route and surface modification, *Mater. Chem. Phys.* 135 (2012) 979–984. <https://doi.org/10.1016/j.matchemphys.2012.06.002>.
- [99] J.F. Zapata, H.A. Colorado, M.A. Gomez, Effect of high temperature and additions of silica on the microstructure and properties of calcium aluminate cement pastes, *J. Sustain. Cem. Mater.* 0 (2020) 1–27. <https://doi.org/10.1080/21650373.2020.1737593>.
- [100] M.U. Okoronkwo, F.P. Glasser, Strätlingite: Compatibility with sulfate and carbonate cement phases, *Mater. Struct.* 49 (2016) 3569–3577. <https://doi.org/10.1617/s11527-015-0740-1>.
- [101] Ș. Marincea, D.G. Dumitraș, C. Ghineț, A.M. Fransolet, F. Hatert, M. Rondeaux, Gehlenite from three occurrences of high-temperature skarns, Romania: New mineralogical data, *Can. Mineral.* 49 (2011) 1001–1014. <https://doi.org/10.3749/canmin.49.4.1001>.
- [102] N. Garg, V.O. Özçelik, J. Skibsted, C.E. White, Nanoscale Ordering and Depolymerization of Calcium Silicate Hydrates in the Presence of Alkalis, *J. Phys. Chem. C.* 123 (2019) 24873–24883. <https://doi.org/10.1021/acs.jpcc.9b06412>.
- [103] N. V. Chukanov, *Infrared Spectra of Mineral Species*, Springer Netherlands, 2014. <http://link.springer.com/10.1007/978-94-007-7128-4>.
- [104] B.R. Bickmore, K.L. Nagy, A.K. Gray, A.R. Brinkerhoff, The effect of Al(OH)₄⁻ on the dissolution rate of quartz, *Geochim. Cosmochim. Acta.* 70 (2006) 290–305. <https://doi.org/10.1016/j.gca.2005.09.017>.

- [105] I.G. Richardson, J.G. Cabrera, Nature of C-S-H in model slag-cements, *Cem. Concr. Compos.* 22 (2000) 259–266. [https://doi.org/10.1016/S0958-9465\(00\)00022-6](https://doi.org/10.1016/S0958-9465(00)00022-6).
- [106] B. Ma, B. Lothenbach, Thermodynamic study of cement/rock interactions using experimentally generated solubility data of zeolites, *Cem. Concr. Res.* 135 (2020) 106–149. <https://doi.org/10.1016/j.cemconres.2020.106149>.
- [107] A. Mancini, E. Wieland, G. Geng, R. Dähn, J. Skibsted, B. Wehrli, B. Lothenbach, Fe(III) uptake by calcium silicate hydrates, *Appl. Geochemistry*. 113 (2019). <https://doi.org/10.1016/j.apgeochem.2019.104460>.
- [108] A. Mancini, E. Wieland, G. Geng, B. Lothenbach, B. Wehrli, R. Dähn, Fe (II) interaction with cement phases : Method development , wet chemical studies and X-ray absorption spectroscopy, *J. Colloid Interface Sci.* 588 (2020) 692–704. <https://doi.org/10.1016/j.jcis.2020.11.085>.
- [109] T. Missana, M. García-Gutiérrez, M. Mingarro, U. Alonso, Analysis of barium retention mechanisms on calcium silicate hydrate phases, *Cem. Concr. Res.* 93 (2017) 8–16. <https://doi.org/10.1016/j.cemconres.2016.12.004>.
- [110] J. Tits, E. Wieland, C.J. Müller, C. Landesman, M.H. Bradbury, Strontium binding by calcium silicate hydrates, *J. Colloid Interface Sci.* 300 (2006) 78–87. <https://doi.org/10.1016/j.jcis.2006.03.043>.
- [111] R.J. Myers, S.A. Bernal, J.D. Gehman, J.S.J. Van Deventer, J.L. Provis, The role of al in cross-linking of alkali-Activated slag cements, *J. Am. Ceram. Soc.* 98 (2015) 996–1004. <https://doi.org/10.1111/jace.13360>.
- [112] F.S. Yang, Structural Characterization of Calcium Alumino-Silicate Hydrate (C-A-S-H) Phases by Solid-State NMR Spectroscopy, Aarhus University, 2021.

Curriculum Vitae

SONYA BARZGAR

Phone: (+41)787178682
sonya.barzgar@empa.ch
sonya.barzgar@epfl.ch

Luegislandstrasse 368
8051, Zurich, Switzerland

EDUCATION

PhD

Environmental Engineering

Swiss Federal Laboratories for Materials Science and Technology (Empa), Switzerland

Paul Scherrer Institute (PSI), Switzerland

École polytechnique fédérale de Lausanne (EPFL), Switzerland

Dissertation: "The effect of alkali hydroxides and equilibration time on Al uptake by calcium silicate hydrates (C-S-H)"

Advisors: Prof. Christian Ludwig, Prof. Barbara Lothenbach

May 2017 - July 2021

M.Sc.

Environmental Engineering; GPA: 3.90/4.00

University of Calgary, Calgary, Canada

Thesis: "Investigating the inhibitory effect of acidic pHs on methane biofiltration technology"

Advisor: Prof. Joseph Patrick Hettiaratchi

Jan 2015 - Feb 2017

B.Sc.

Chemical Engineering; GPA: 17.86/20.00

Sharif University of Technology, Tehran, Iran

Sep 2009 - Sep 2013

HONOURS AND AWARDS

- Ranked 1st among class of 2015 graduate students of Environmental Engineering, M.Sc. graduate.
- Ranked 3rd among 140 students of the class of 2009 in Chemical Engineering, B.Sc. graduate.
- Excellent high school diploma award for highest GPA in class of mathematics and physics, June 2008, Iran.

PUBLICATIONS

- Barzgar, S., Yan, Y., Tarik, M., Ludwig, C., & Lothenbach, B., The effect of Al concentration on Al uptake in C-S-H, *to be submitted*.
- Barzgar, S., Tarik, M., Ludwig, C., & Lothenbach, B., (2021), The effect of equilibration time on Al uptake in C-S-H, *Cement and Concrete Research*, 144, 106438.
- Barzgar, S., Tarik, M., Lothenbach, B., & Ludwig, C., (2020), The effect of sodium hydroxide on Al uptake by calcium silicate hydrates (C-S-H), *Journal of Colloid and Interface Science*, 572, 246-256. (featured as cover page article)
- Barzgar, S., Hettiaratchi, J. P., Pearce, L., & Kumar S. (2017), Inhibitory effects of acidic pH and confounding effects of moisture content on methane biofiltration, *Bioresource Technology*, 245, 633-640.

CONFERENCES

- "The effect of alkali hydroxide and equilibration time on Al uptake by calcium silicate hydrates (C-S-H)", oral presentation, 3rd International Conference on the Chemistry of the Construction Materials (ICCCM), Mar 2021, Karlsruhe, Germany.
- "The effect of pH, Ca/Si ratio and equilibration time on Al uptake in C-S-H", oral presentation, ERICA-CASH II conference, Jan 2021, Heidelberg, Germany.
- "The effect of pH, Ca/Si ratio and equilibration time on Al uptake in calcium silicate hydrates (C-S-H)", poster presentation, 3rd Doctoral Colloquium Bioenergy, Sep 2020, Leipzig, Germany.
- "The effect of pH and Ca/Si ratio on Al uptake in C-S-H", oral presentation, 39th Cement and Concrete Science Conference (39 CCS), Sep 2019, Bath, United kingdom.
- "Effect of aluminum on C-S-H structure, stability and solubility", poster presentation, 15th International Congress on the Chemistry of Cement (ICCC), Sep 2019, Prague, Czech Republic.
- "Effect of aluminum on C-S-H structure, stability and solubility", poster presentation, Empa PhD Symposium, Nov 2018, Dübendorf, Switzerland.
- "Effect of Hydrogen Sulfide (H₂S) on Methane Oxidation in a Biofilter", poster presentation, The Air and Waste Management Association - CPANS 8th Conference, May 2016, Calgary, Canada.

WORKSHOPS

- "Thermodynamic Modelling of Cementitious Systems", June 2019, Empa, Dübendorf, Switzerland.
- "GEM-Selektor training workshop", Jan 2019, Paul Scherrer Institute (PSI), Villigen, Switzerland.
- "2nd WORKSHOP Calcium-Silicate Hydrates Containing Aluminium: C-A-S-H II", April 2018, Empa, Dübendorf, Switzerland.

CERTIFICATION COURSES

- CCMX Advanced Course - Inorganic Particle Synthesis by Precipitation: From Nanoparticles to Self-organised Mesocrystals and from Theory to Practice, EPFL, Lausanne, Oct 2020.
- Limestone-Calcined Clay-Cement: Characterization Methods, EPFL, Lausanne, Feb 2020.
- CCMX Advanced Course - Advanced X-ray Diffraction Methods for Coatings: strain, defects and deformation analysis of thin films, Empa, Dübendorf, Jan 2020.

TEACHING EXPERIENCE

- "Project Management I course", Jan 2016, University of Calgary, Canada.